

R-0 7/77

2/14

NASA CR-134891

11-15-77

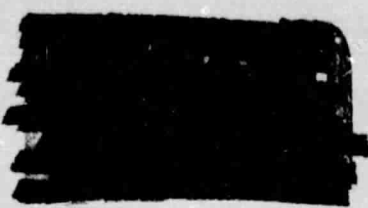
2-78

5-78

6-78

8-78

10-78



# Acoustic Analysis of Aft Noise Reduction Techniques Measured on a Subsonic Tip Speed 50.8 cm (Twenty Inch) Diameter Fan

by

D. Stimpert  
A. Clemons

GENERAL ELECTRIC COMPANY

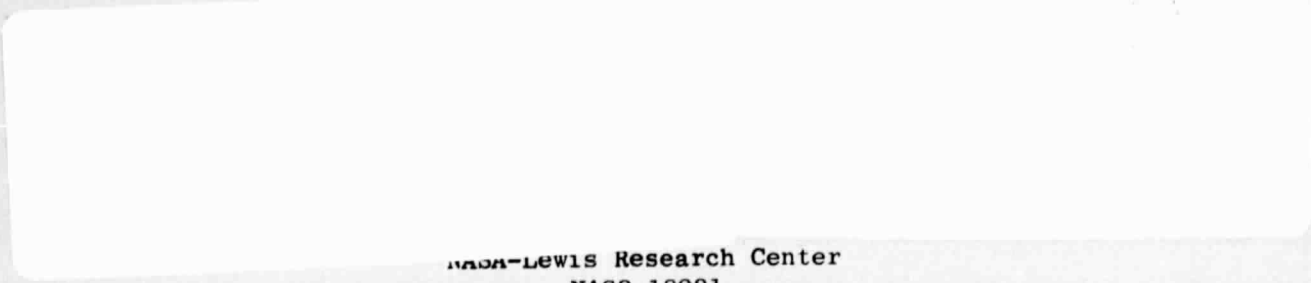
(NASA-CR-134891) ACOUSTIC ANALYSIS OF AFT NOISE REDUCTION TECHNIQUES MEASURED ON A SUBSONIC TIP SPEED 50.8 cm (TWENTY INCH) DIAMETER FAN (General Electric Co.) 149 p  
HC A07/MP A01 CSCL 21E G3/07

N80-15102

Unclas  
33484

Prepared For

National Aeronautics and Space Administration



NASA-Lewis Research Center  
NAS3-18021

1. Report No. NASA CR-134891	2. Government Accession No.	3. Recipient's Catalog No.	
4. Title and Subtitle Acoustic Analysis of Aft Noise Reduction Techniques Measured on a Subsonic Tip Speed 50.8 cm (Twenty Inch) Diameter Fan		5. Report Date January 1977	
		6. Performing Organization Code	
7. Author(s) D.L. Stimpert, A. Clemons		8. Performing Organization Report No. R75AEG368	
		10. Work Unit No.	
9. Performing Organization Name and Address General Electric Company Aircraft Engine Group Cincinnati, Ohio 45215		11. Contract or Grant No. NAS3-18021	
		13. Type of Report and Period Covered Contractor Report	
		14. Sponsoring Agency Code	
12. Sponsoring Agency Name and Address National Aeronautics and Space Administration Washington, D.C. 20546			
16. Supplementary Notes Test Report, Project Manager: CC Ciepluch, QCSEE Project Office Technical Advisor: DA Sagerser NASA Lewis Research Center Cleveland, Ohio 44135			
18. Abstract <p>This report is an analysis of sound data which were obtained during tests of a 50.8 cm (20 inch) diameter, subsonic tip speed, low pressure ratio fan. The test matrix was divided into two major investigations - source noise reduction techniques and aft duct noise reduction with acoustic treatment. Source noise reduction techniques which were investigated include minimizing second harmonic noise by varying vane/blade ratio, variation in spacing, and lowering the Mach number through the vane row to lower fan broadband noise. Investigations conducted with treatment in the aft duct include flow noise effects, faceplate porosity, rotor-OGV treatment, slant cell treatment, splitter simulation with variable depth on the outer wall and constant thickness treatment on the inner wall, and variable boundary conditions such as variation in treatment panel thickness and orientation, and mixed porosity combined with variable thickness. Additional technology development study results are reported, including test results and analysis of sound separation probes, modal propagation and attenuation based upon in-duct modal measurements, and analysis of rotor wake characteristics.</p>			
17. Key Words (Suggested by Author(s)) Short-Haul Aircraft Noise Aft Fan Noise Fan Noise Noise			
19. Security Classif. (of this report) Unclassified	20. Security Classif. (of this page) Unclassified	21. No. of Pages	22. Price

## FOREWORD

The analyses presented in this report were conducted by the following General Electric Company personnel:

Vane/Blade Ratio Effects	R. Mani D.L. Stimpert
Spacing Effects and Low-Mach Vanes	B.M. Gahn D.L. Stimpert R.K. Matta
Aft Treatment Results	A. Clemons
Sound Separation Probe	M.T. Moore
Rotor Wake Analysis	B.M. Gahn
Radial Modal Measurements	R.E. Kraft J.W. Zwick

Test Engineers for the tests which were conducted at General Electric Company's Research and Development Center were K. Bekofske, R. Sheer, and R. Warren.

## TABLE OF CONTENTS

<u>Section</u>	<u>Page</u>	
I	SUMMARY	1
II	INTRODUCTION	2
III	SOURCE NOISE REDUCTION TECHNIQUES	9
	A. Vane/Blade Ratio Effects	9
	B. Rotor-Stator Spacing Effects	13
	C. Low-Mach Vanes	17
IV	AFT SUPPRESSION TESTS	21
	A. Porosity Effects	21
	B. Variable Boundary Conditions	28
	C. Treatment Area Effectiveness	33
	D. Splitter Simulation	37
	E. Rotor-OGV Treatment	45
	F. Variable Depth Treatment Orientation	48
	G. Slant Cell Treatment	48
	H. Treatment Regenerated Noise	56
V	IN-DUCT MEASUREMENTS	60
	A. Sound Separation Probe	60
	B. Modal Measurements	69
	1. Theory of Modal Measurement	69
	2. Experimental Results	76
	3. Data Analysis	76
	4. The Use of Modal Measurements in Prediction of Suppression	92
	C. Rotor Wake Analysis	110
	1. Basics of Hot Film Anemometry	110
	2. Probe Calibration	111
	3. Data Acquisition	117
	4. Data Filtering	117
	5. Reduction to Velocity	117
	6. Modulation	121
	7. Summary and Conclusions	130
VI	CONCLUSIONS	133
VII	NOMENCLATURE	135
VIII	REFERENCES	138

## LIST OF ILLUSTRATIONS

<u>Figure</u>		<u>Page</u>
1.	Schematic of General Electric Company Anechoic Chamber.	3
2.	Scale Model Fan Test Vehicle Schematic.	4
3.	Installed Test Vehicle.	5
4.	Predicted Second Harmonic PWL Decrease as a Function of Vane Number.	10
5.	Measured Second Harmonic Narrowband SPL's as a Function of Vane/Blade Ratio.	11
6.	Peak Sideline SPL's as a Function of Vane Number.	12
7.	PWL Change at 2000 to 6300 Hz as a Function of Rotor-Stator Spacing.	14
8.	Predicted PWL Change with Spacing.	15
9.	Summation of Rotor Turbulence and Rotor/Stator Noise.	16
10.	Model Fan Flowpaths.	18
11.	Comparison of Baseline and Low-Mach Vane Exhaust Noise Levels.	19
12.	Comparison of Baseline and Low-Mach Inlet Probe SPL's.	20
13.	Measured Suppression Vs. Porosity for Constant-Depth Liner.	22
14.	Measured Suppression Vs. Porosity for Variable-Depth Liner.	24
15.	Variable-Depth, Constant-Porosity and Variable-Depth, Variable-Porosity Configurations.	25
16.	Measured Suppression with Constant Vs. Variable Porosity.	26
17.	Suppression Spectra for Individual Panels Vs. $H/\lambda_0$ .	27
18.	Measured Suppression Spectra at Two Fan Speeds, 12% Porosity.	29
19.	Measured Suppression Spectra at Two Fan Speeds, 27% Porosity.	30

LIST OF ILLUSTRATIONS (Continued)

<u>Figure</u>		<u>Page</u>
20.	Constant-Depth and Variable-Depth Treatment Configurations.	31
21.	Measured Suppression Spectra for Constant Vs. Variable Panel Depth.	32
22.	Predicted Vs. Measured Suppression Spectra, Constant Depth, 12% Porosity Panels.	34
23.	Predicted Vs. Measured Suppression Spectra, Variable Depth, Mixed Porosity Panels.	35
24.	Predicted Vs. Measured Suppression Spectra - Splitter Simulation, 12% Porosity Panels.	36
25.	Configurations with and without Reduced Treatment Area.	38
26.	Suppressed and Unsuppressed Spectra for Different Treatment Areas.	39
27.	Predicted Vs. Measured Suppression Loss Resulting from Reduced Treatment Area.	40
28.	Suppression Vs. L/H (Actual).	41
29.	Variable-Depth Treatment and Splitter Simulation Configurations.	42
30.	Splitter Simulation Vs. Constant-Depth Wall Treatment.	43
31.	Splitter Simulation Compared to Treatment with Variable Depth on Both Walls.	44
32.	Measured Suppression for Rotor-OGV Treatment.	46
33.	Measured Suppression of Fully Treated Fan Exhaust with and without Rotor-OGV Treatment.	47
34.	Thin/Thick Vs. Thick/Thin Variable-Depth Treatment Configurations.	49
35.	Effect of Treatment Orientation on Suppression.	50
36.	Suppression Spectra for Thin/Thick Vs. Thick/Thin Treatment.	51

LIST OF ILLUSTRATIONS (Continued)

<u>Figure</u>		<u>Page</u>
37.	Straight Cell and Slant Cell Treatment Configurations.	53
38.	Suppression Spectra for Slant Cell and 2.54 cm (1 in.) Straight Cell.	54
39.	Suppression Spectra for Slant Cell and 3.8 cm (1.5 in.) Straight Cell.	55
40.	Treatment Regenerated Flow Noise Configurations.	57
41.	Aft Suppression Spectra Change with Duct Mach Number Change.	58
42.	Sound Separation Probe.	61
43.	Frequency Response of Sensors in Sound Separation Probe.	62
44.	Typical Cross Correlation of Signals from the Sound Separation Probe.	63
45.	Tone Removal by Interpolation of Cross Spectrum.	64
46.	Correlations from Sound Separation Probe - Hardwall Configuration (18).	66
47.	Correlations from Sound Separation Probe - 12 Percent Thin-To-Thick Configuration (7).	67
48.	Correlations from Sound Separation Probe - 27 Percent Thin-To-Thick Configuration (8).	68
49.	Total Broadband Level 0 - 5000 Hz (Tones Removed).	70
50.	Separated Broadband Level 0 - 5000 Hz (Tones Removed).	71
51.	Illustration of Characteristic Duct Modes.	73
52.	Schematic of Modal Measurement Apparatus in Rotor 55 Vehicle.	75
53.	Relative Logarithmic Magnitude of Cross-Spectrum for Downstream Probe; Hardwall Configuration 75-1F, 70% Speed, Immersion 4.4 cm (1.715 in.).	77

LIST OF ILLUSTRATIONS (Continued)

<u>Figure</u>		<u>Page</u>
54.	Cross-Spectrum for Downstream Probe; Hardwall Configuration 75-1F, 70% Speed, Immersion of 4.4 cm (1.715 in.).	78
55.	Relative Logarithmic Magnitude of Cross-Spectrum for Downstream Probe; Hardwall Configuration 75-1F, 100% Speed, Immersion 4.4 cm (1.715 in.).	80
56.	Cross-Spectrum for Downstream Probe; Hardwall Configuration 75-1F, 100% Speed, Immersion of 4.4 cm (1.715 in.).	81
57.	Complex Acoustic Pressure Profile for Hardwall Configuration 75-1F; 1320 Hz, 70% Speed.	83
58.	Complex Acoustic Pressure Profile for Hardwall Configuration 75-1F; 2640 Hz, 70% Speed.	84
59.	Complex Acoustic Pressure Profile for Hardwall Configuration 75-1F; 4000 Hz, 70% Speed.	85
60.	Complex Acoustic Pressure Profile for Hardwall Configuration 75-1F; 5280 Hz, 70% Speed.	86
61.	Complex Acoustic Pressure Profile for Hardwall Configuration 75-1F; 1920 Hz, 100% Speed.	87
62.	Complex Acoustic Pressure Profile for Hardwall Configuration 75-1F; 3800 Hz, 100% Speed.	88
63.	Complex Acoustic Pressure Profile for Hardwall Configuration 75-1F; 5860 Hz, 100% Speed.	89
64.	Complex Acoustic Pressure Profile for Hardwall Configuration 75-1F; 7640 Hz, 100% Speed.	90
65.	Relative Modal Participation for Hardwall Configuration 75-1F; 70% Speed, 1320 Hz.	93
66.	Relative Modal Participation for Hardwall Configuration 75-1F; 70% Speed, 2640 Hz.	94
67.	Relative Modal Participation for Hardwall Configuration 75-1F; 70% Speed, 4000 Hz.	95
68.	Relative Modal Participation for Hardwall Configuration 75-1F; 70% Speed, 5280 Hz.	96



LIST OF ILLUSTRATIONS (Concluded)

<u>Figure</u>		<u>Page</u>
69.	Relative Modal Participation for Hardwall Configuration 75-1F; 100% Speed, 1920 Hz.	97
70.	Relative Modal Participation for Hardwall Configuration 75-1F; 100% Speed, 3800 Hz.	98
71.	Relative Modal Participation for Hardwall Configuration 75-1F; 100% Speed, 5800 Hz.	99
72.	Relative Modal Participation for Hardwall Configuration 75-1F; 100% Speed, 7640 Hz.	100
73.	Reexpansion of Complex Acoustic Pressure Profile; 1320 Hz, 70% Speed.	101
74.	Reexpansion of Complex Acoustic Pressure Profile; 1920 Hz, 100% Speed.	102
75.	Designation of Configurations Used for Analytical Predictions.	103
76.	Velocity-Sensitive, Hot Film Probe.	112
77.	Basic Operation of Hot Film Probe.	113
78.	Hot Film Probe Calibration.	114
79.	Hot Film Probe Calibration for Rotor 55 Wake Survey.	115
80.	Directionality Calibration.	116
81.	Rotor 55 Hot Film Probe Measurement Points.	118
82.	Hot Film Wake Data, Filtered at 12800 Hz.	119
83.	Typical Rotor Exit Velocity Triangle.	120
84.	Design Velocity Triangle and Probe Orientation.	122
85.	Rotor 55 Hot Film Wake Survey Data.	123
86.	Rotor 55 Wake Trace.	127
87.	Comparison of Experimental Mathematical Wake Shapes.	131

## LIST OF TABLES

<u>Table</u>		<u>Page</u>
I.	Source Noise Test Configurations.	6
II.	Aft Suppression Test Configurations.	7
III.	Rotor 55 Modal Analysis.	91
IV.	Calculated $\Delta$ PWL Suppressions, Rotor 55.	104
V.	Measured 1/3-Octave $\Delta$ PWL Suppressions, Rotor 55.	105
VI.	Measured Narrowband $\Delta$ PWL Suppressions, Rotor 55.	106
VII.	Comparison of Measured and Calculated Suppression Effectiveness Rankings of Rotor 55 Treatment Configurations, 70% Speed.	108
VIII.	Comparison of Measured and Calculated Suppression Effectiveness Rankings of Rotor 55 Treatment Configurations, 100% Speed.	109

## SECTION I

### SUMMARY

A test program was conducted to investigate aft radiated noise reduction techniques. Both reduction of noise at the source and suppression in the aft duct were studied. Source noise reduction techniques included the effects of rotor-stator spacing, the effect of vane/blade ratio on second harmonic tone propagation, and the effect of axial Mach number through the vane row. Aft suppression tests included a number of variations in treatment design such as variable depth treatment, frame treatment between the rotor and OGV, slanted cells in the treatment cavity, panel resistance as a function of tuning frequency, and flow-regenerated noise effects.

The noise source for these investigations was a low pressure ratio, subsonic tip speed, scale model fan which had a diameter of 50.8 cm (20 inches). Aft radiated noise data, as determined by free-field measurements in the General Electric Company anechoic chamber, are presented and analyzed. Additional technology development study results are reported including test results and analysis of sound separation probes, modal propagation and attenuation based upon in-duct modal measurements, and analysis of rotor wake characteristics.

At close spacing (0.5 true rotor tip chords) it was demonstrated that second harmonic sound pressure level tended to minimize at a vane/blade ratio of 1.87. No significant reduction in fan broadband noise levels was observed by decreasing the Mach number through the vanes; however, this may be due to the levels at wide (1.5 true rotor chords) spacing being controlled by rotor-turbulence noise and not rotor-stator noise. Tests of acoustic treatment panels with various porosities and backing depths showed that to increase suppression, variable depth treatment panels should be used with porosities that optimize the acoustic resistance for each panel.

Analysis of two-axis, hot film data taken between the rotor and outlet guide vanes showed the wake data to contain large amounts of wake amplitude modulation and only small period (wake spacing) modulation.

## SECTION II

### INTRODUCTION

General Electric Company is currently engaged in the Quiet Clean Short-Haul Experimental Engine (QCSEE) Program under NASA Contract NAS3-18021. A major objective of this program is to develop and demonstrate the technology required to achieve the stringent noise goals required for commercial turbofan short-haul aircraft. More details of the QCSEE objectives and design rationale are available in References 1 and 2.

As part of the effort to meet these goals, a component test program was conducted to investigate techniques for reduction of source noise and aft radiated noise by exhaust duct treatment. The test series, designated the Scale Model Fan Test Program, was conducted in the General Electric Company Anechoic Chamber located at Schenectady, New York. Aft radiated noise level effects were measured with the noise source provided by a low tip speed, low pressure ratio, 50.8 cm (20 inch) diameter NASA-Lewis Research Center Fan (designated Rotor 55). Rotor 55 is a variable pitch fan with a design pressure ratio of 1.2 and a tip speed of 213 meters per second (700 feet per second), and was designed by Hamilton Standard. Aerodynamic performance of the fan is documented in Reference 3, while acoustic performance of the six foot diameter fan designated QF9 (of which Rotor 55 was a direct scale model) is given in Reference 4.

The test chamber and its sound field are shown schematically in Figure 1 while Figure 2 presents the test vehicle schematically. A photograph of the installed vehicle is shown in Figure 3, with the location of the duct probes identified. Test results along with more details of the test facility, test vehicle, data acquisition system, and data reduction system may be found in Reference 5. This report is intended to provide an in-depth analysis of the test results.

The test matrix was divided into two major investigations: source noise reduction techniques, and aft duct noise reduction with acoustic treatment. Source noise reduction techniques which were investigated include minimizing second harmonic noise by varying vane/blade ratio, variation in rotor-OGV spacing, and lowering the Mach number through the vane row to lower fan broadband noise. The entire source noise test matrix is shown in Table I.

Investigations conducted with treatment in the aft duct include face-plate porosity, treatment placed between the rotor and OGV, slant cell treatment, splitter simulation with variable-depth treatment on the outer wall and constant-thickness treatment on the inner wall, and various combinations of wall treatment, such as thin-to-thick, thick-to-thin, mixed porosity combined with mixed thickness, and flow noise effects. All aft suppression configurations are summarized in Table II. On selected configurations, radial modal measurements were made to determine the mode structure seen by the treatment.

ORIGINAL PAGE IS  
OF POOR QUALITY

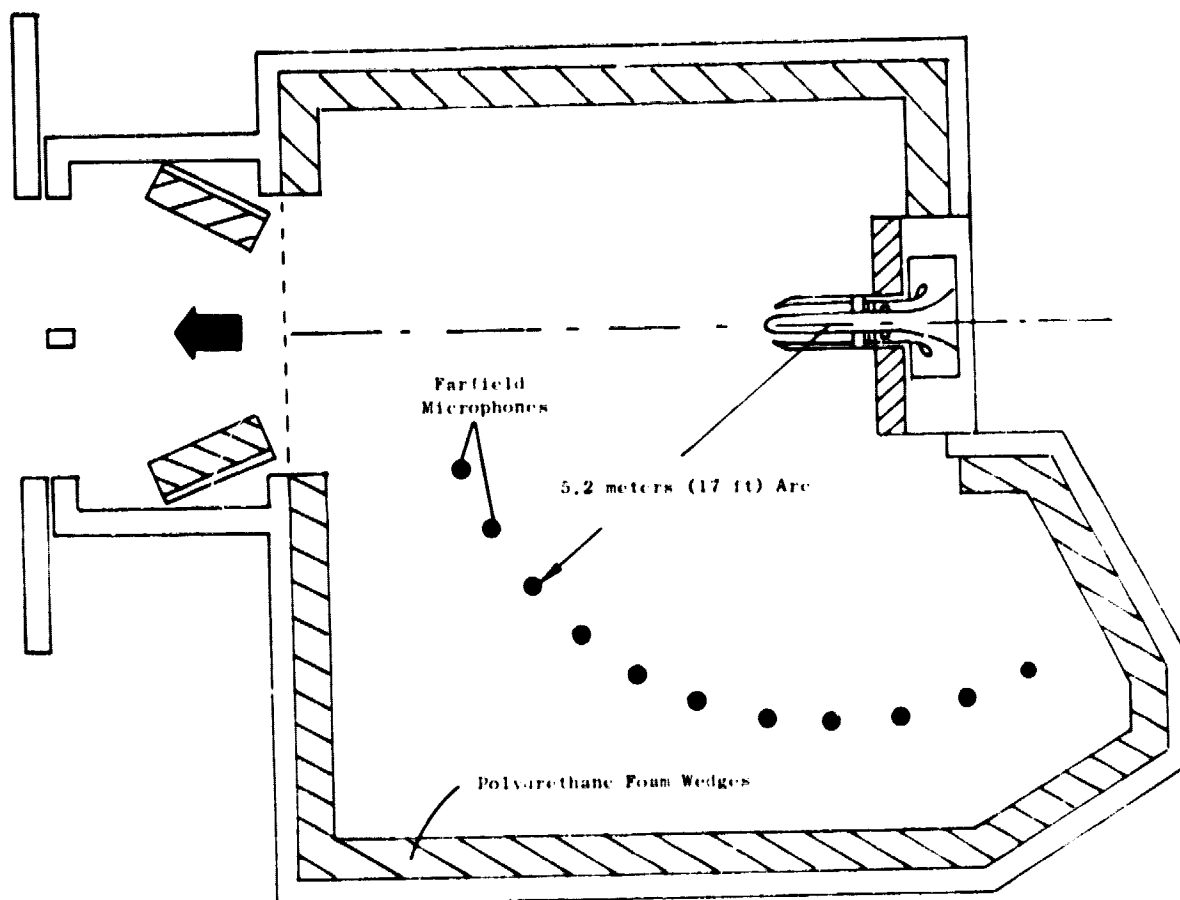


Figure 1. Schematic of General Electric Company Anechoic Chamber.

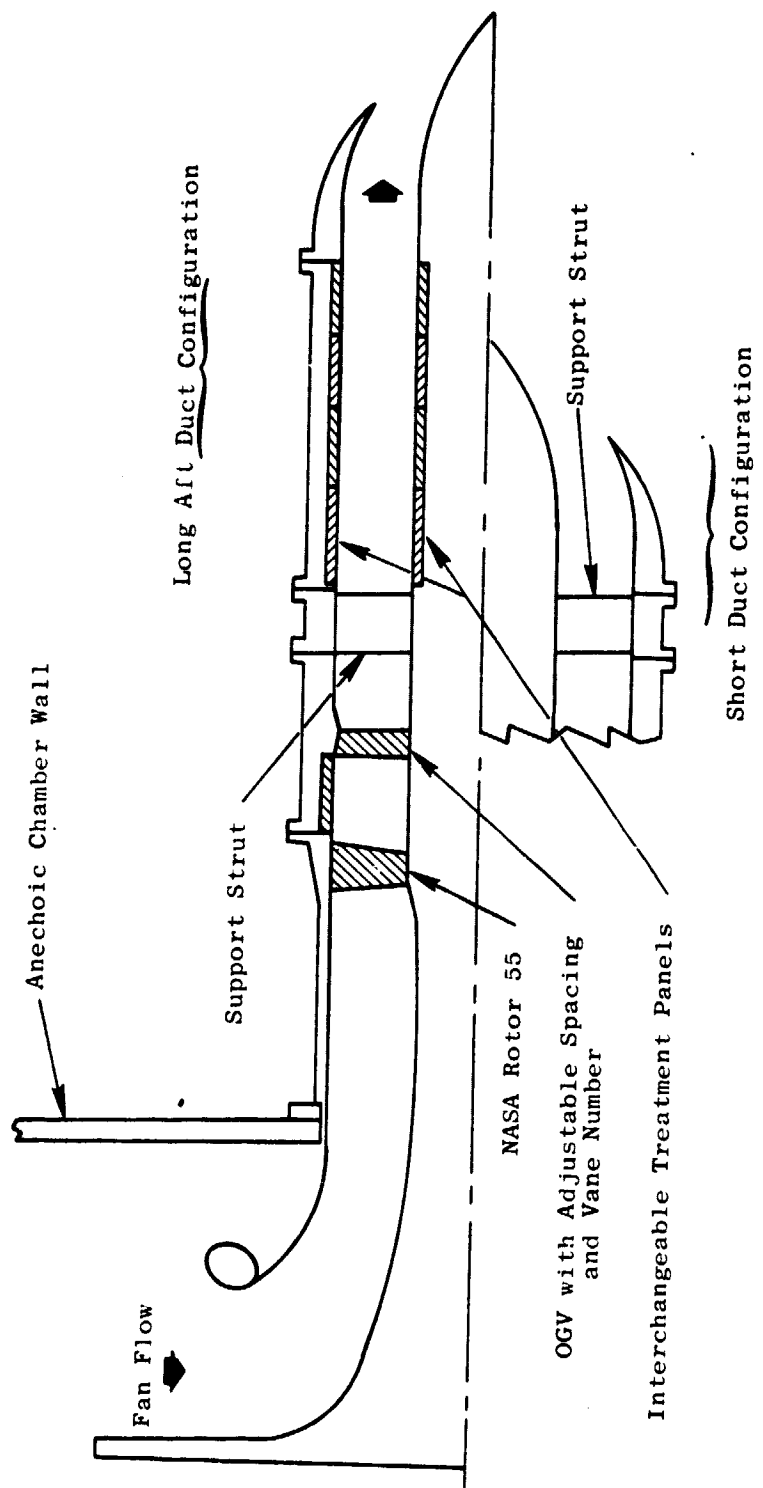


Figure 2. Scale Model Fan Test Vehicle Schematic.

ORIGINAL PAGE IS  
OF POOR QUALITY

ORIGINAL PAGE IS  
OF POOR QUALITY

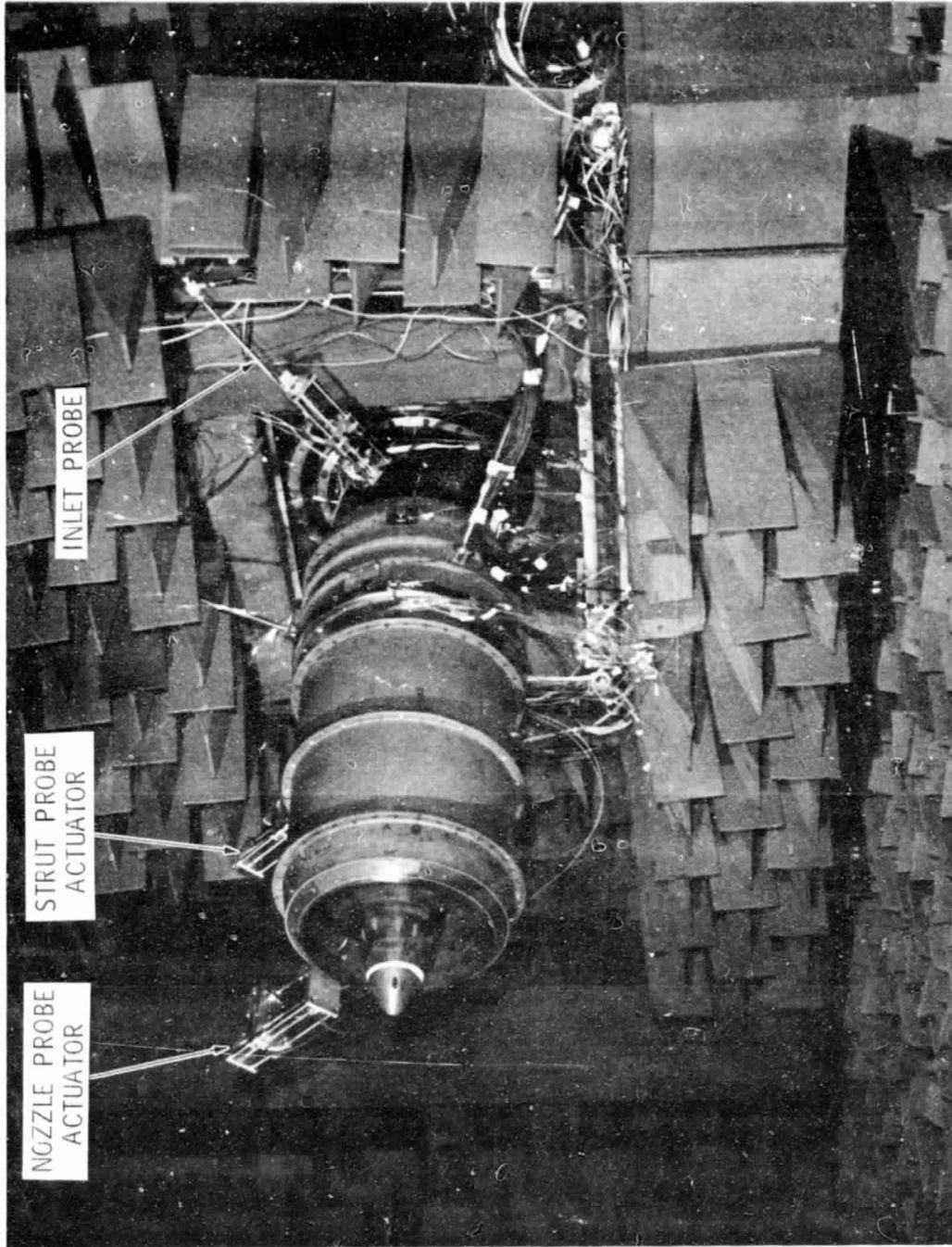
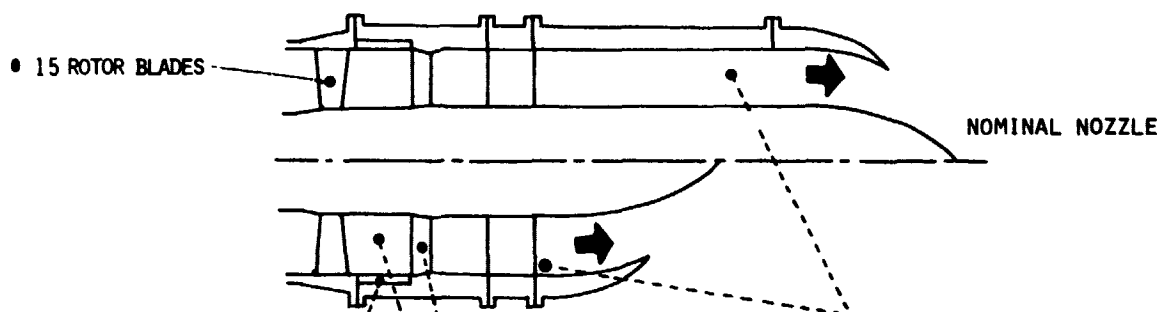


Figure 3. Installed Test Vehicle (C27414).

Table I. Source Noise Test Configurations.

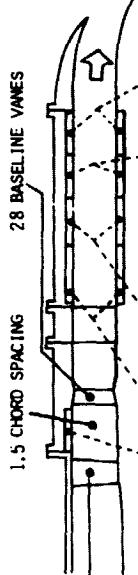


CONFIGURATION	ROTOR-OGV TREATMENT	SPACING	VANE NUMBER	VANE/BLADE RATIO	DUCT LENGTH	COMMENTS
1B	NO	1.5	11	0.73	LONG	STAGE 55 VANES
2	YES	1.5	28	1.87	SHORT	BASELINE VANES
3A	↓	1.5	31	2.07	↓	BASELINE VANES
4B	↓	1.5	31	2.07	↓	LOW MACH VANES
5	↓	1.0	28	1.87	↓	BASELINE VANES
6	↓	1.5	28	1.87	LONG	↓
12	↓	1.5	26	1.73	SHORT	
13	↓	1.5	27	1.80	↓	
14A	↓	2.0	28	1.87	↓	
18	NO	1.5	28	1.87	LONG	
19	YES	1.5	25	1.67	SHORT	
20	↓	1.5	29	1.93	↓	
21	↓	1.5	30	2.00	↓	
22	↓	1.5	28	1.87	↓	
27	NO	0.5	31	2.07	↓	
28	↓	↓	30	2.00	↓	
29	↓	↓	29	1.93	↓	
30	↓	↓	28	1.87	↓	
31	↓	↓	27	1.80	↓	
32	↓	↓	26	1.73	↓	
33	↓	↓	25	1.67	↓	

(REPEAT OF CONFIG. 2)



Table II. Aft Suppression Test Configurations.



• 15 ROTOR BLADES  
1.5 CHORD SPACING  
28 BASELINE VANES

\*INNER AND OUTER PANELS ARE THE SAME DEPTH AND POROSITY UNLESS OTHERWISE NOTED BY (1) AND (0).  
\*\*R DENOTES AERODYNAMIC RAMES IN FRONT OF THE ROTOR.

CONFIGURATION	ROTOR-OGV TREATMENT	DEPTH POROSITY		DEPTH POROSITY		DEPTH POROSITY		DEPTH POROSITY		NOZZLE	COMMENTS
		IN. (CM.)	%	IN. (CM.)	%	IN. (CM.)	%	IN. (CM.)	%		
6	YES	0	0	0	0	0	0	0	0	NOMINAL	
7, 7R	NO	.25(.64)	12	.50(1.27)	12	.75(1.91)	12	1.5(3.81)	12	→	
8, 8R		.25(.64)	27	.50(1.27)	27	.75(1.91)	27	1.5(3.81)	27	→	
9, 9R		.50(1.27)	27	.25(.64)	27	.75(1.91)	27	1.5(3.81)	27	→	
10, 10R		.50(1.27)	27	.25(.64)	27	.75(1.91)	27	1.5(3.81)	27	→	
16, 16R		.25(.64)	27	.50(1.27)	27	.75(1.91)	27	1.0(2.54)	27	→	
17		.75(1.91)	27	.75(1.91)	27	.75(1.91)	27	.75(1.91)	27	→	
18, 18R		0	0	0	0	0	0	0	0	→	
23		0	0	0	0	0	0	0	0	→	
24		(0).25(.64)	27	.50(1.27)	27	.75(1.91)	27	1.5(3.81)	27	→	
		(1).75(1.91)	27	.75(1.91)	27	.75(1.91)	27	.75(1.91)	27	→	
25		(0).25(.64)	27	.50(1.27)	27	.75(1.91)	27	1.0(2.54)	27	→	
		(1).25(.64)	27	.50(1.27)	27	.75(1.91)	27	1.5(3.81)	27	→	
26		1.5(3.81)	12	.75(1.91)	12	.50(1.27)	12	.25(.64)	12	→	
75-1A		0	0	0	0	0	0	.25(.64)	12	→	
75-1B								.50(1.27)	12	→	
75-1C								.75(1.91)	12	→	
75-1D								1.5(3.81)	12	→	
75-1E								1.0(2.54)	27	→	
75-1F								0	0	→	

WITH 0.6 IN. (1.52 CM) SPLITTER

SLANT CELL - LAST OUTER PANEL

SLANT CELL

Table II. Aft Suppression Test Configurations (Concluded).

\* INNER AND OUTER PANELS ARE THE SAME DEPTH AND POROSITY UNLESS OTHERWISE NOTED BY (1) AND (10).

CONFIGURATION	ROTOR-OGV TREATMENT	DEPTH POROSITY		DEPTH POROSITY		DEPTH POROSITY		DEPTH POROSITY		NOZZLE	COMMENTS
		IN.(CM.)	%	IN.(CM.)	%	IN.(CM.)	%	IN.(CM.)	%		
75-16	NO	0	0	0	0	0	0	0	0	NOMINAL	
75-1H	↓	↓	↓	↓	↓	↓	↓	↓	↓		
75-1I	↓	↓	↓	↓	↓	↓	↓	↓	↓		
75-1J	↓	↓	↓	↓	↓	↓	↓	↓	↓		
75-1K	↓	↓	↓	↓	↓	↓	↓	↓	↓		
75-2	YES	.25(.64)	12	.50(1.27)	12	.75(1.91)	12	.75(1.91)	12		
75-3	NO	.75(1.91)	12	.75(1.91)	12	.75(1.91)	12	.75(1.91)	12		
75-4	{(0), .25(.64)	12	.50(1.27)	12	.50(1.27)	12	.75(1.91)	12	1.5(3.81)		
75-5	{(1), .75(1.91)	12	.75(1.91)	12	.75(1.91)	12	.75(1.91)	12	.75(1.91)		
75-6A	1.5(3.81)	27	.75(1.91)	27	.75(1.91)	12	.50(1.27)	27	.25(.64)		
75-6B	.75(1.91)	12	.75(1.91)	12	.75(1.91)	12	.75(1.91)	12	.75(1.91)		
75-6C	0	0	0	0	0	0	0	0	0		
75-6D	1.5(3.81)	27	0	0	0	0	0	0	0		
75-7	0	0	.75(1.91)	27	.75(1.91)	12	.50(1.27)	12	1.5(3.81)		
75-8	.25(.64)	12	.75(1.91)	12	.75(1.91)	12	.25(.64)	12	1.5(3.81)		
75-9	.25(.64)	12	.50(1.27)	12	.75(1.91)	12	.75(1.91)	12	1.5(3.81)		TREATMENT L/H = 3.68

} STAGE 55 VANES

## SECTION III

### SOURCE NOISE REDUCTION TECHNIQUES

#### A. Vane/Blade Ratio Effects

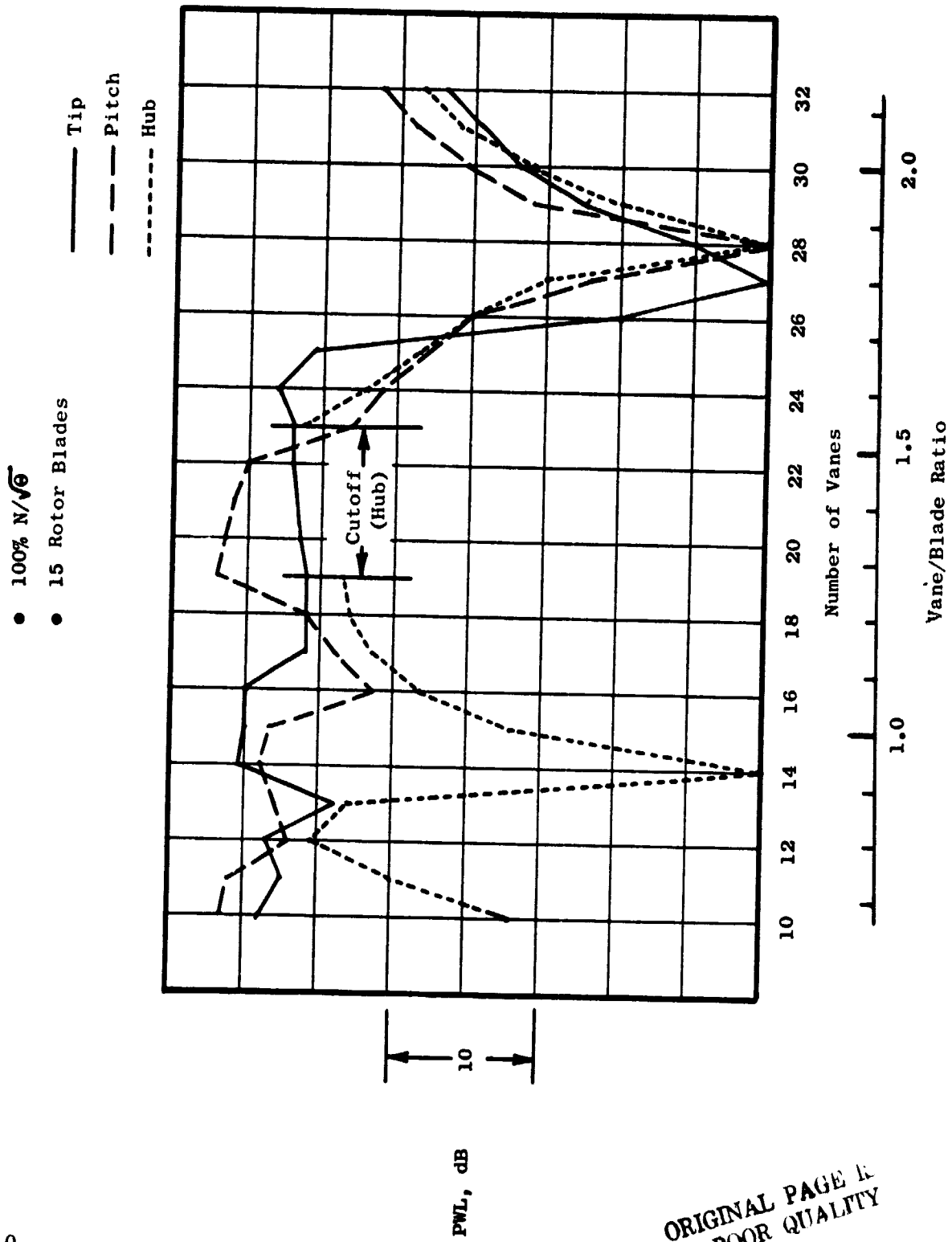
A well-established technique for the reduction of blade passing frequency noise in axial flow jet engines, caused by interaction between the rotor and stator rows, is to employ a vane/blade ratio (V/B) such that the tone is cut off. A convenient approximation is that cutoff begins when V/B exceeds  $n(1 + M_t)$ , where  $M_t$  denotes the fan tip Mach number, and  $n$  denotes the harmonic number of the tone one desires to eliminate. This phenomenon is generally applied to the fundamental tone, which is the most critical source of noise on most fans. For low tip speed, low blade number fans, however, the second harmonic can be more critical than the fundamental to PNL levels. There is a technique that can be applied to second harmonic tone reduction and which was investigated in this test program. When considering noise generated above "cutoff", it can be shown (Reference 6) that a favorable orientation of the spiral wave generating the noise, relative to the orientation of the unsteady blade forces (ultimately responsible for the noise), can create a mismatch between the dipole orientation and the propagating mode that will reduce the radiated noise. The technique works only for subsonic tip speeds (as indeed does the "cutoff" effect) and also works only for a particular direction, i.e., either aft or forward radiated noise.

Calculations using the method described in Reference 6 were carried out for Rotor 55. The results in Figure 4 show that as the vane number was varied from 25 to 31, the vane number of 28 (V/B = 1.87) would demonstrate the second harmonic tone reduction.

Measured narrowband second harmonic levels are presented in Figure 5 for two aft angles. The levels at 1.5 chord spacing show no distinct minimum, as predicted, at 28 vanes. This may be due to a second noise source such as rotor turbulence controlling at the wide spacing of 1.5 chords. However, decreasing the spacing to 0.5 chord results in a minimum appearing for 27 vanes at 1.88 radians (108 degrees), and 28 vanes at 2.06 radians (118 degrees).

Figure 6 presents the 1/3-octave band, 0.5 chord spacing data which have been extrapolated to 61 m (200 ft) sideline. Here the peak sideline SPL's for fan speeds of 70, 80, 90, and 100%  $N\sqrt{\theta}$  tend to minimize at a vane number of 28.

These results indicate that the second harmonic can be successfully minimized in accordance with the analysis in Reference 6. Further, the apparent lack of success at wider spacings may be caused by rotor turbulence noise being dominant. Thus, this technique has the potential for a noise reduction in the in-flight regime where low inlet turbulence levels would be expected.



ORIGINAL PAGE 1  
OF POOR QUALITY

Figure 4. Predicted Second Harmonic PWL Decrease as a Function of Vane Number.

ORIGINAL PAGE IS  
OF POOR QUALITY

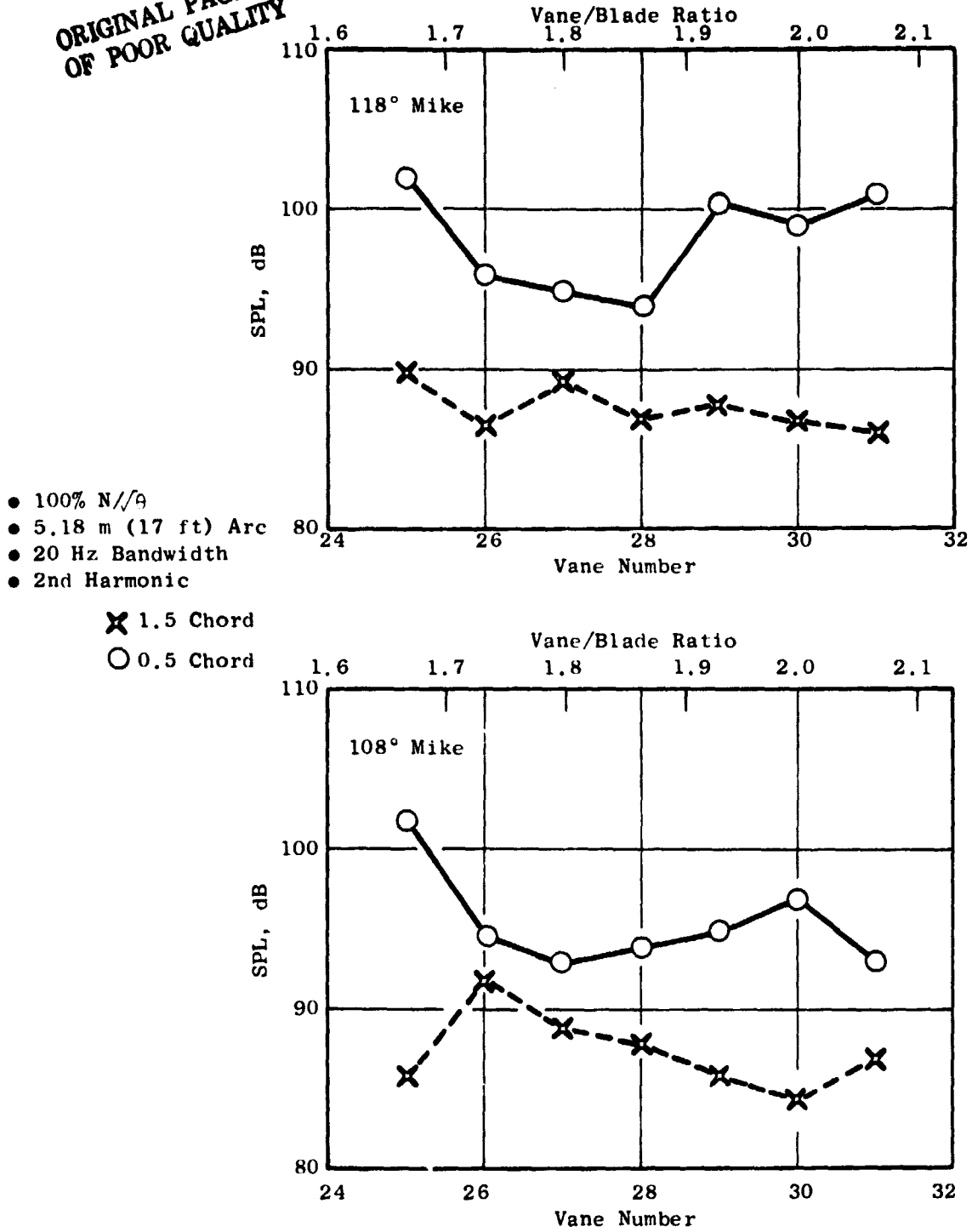


Figure 5. Measured Second Harmonic, Narrowband SPL's as a Function of Vane/Blade Ratio.

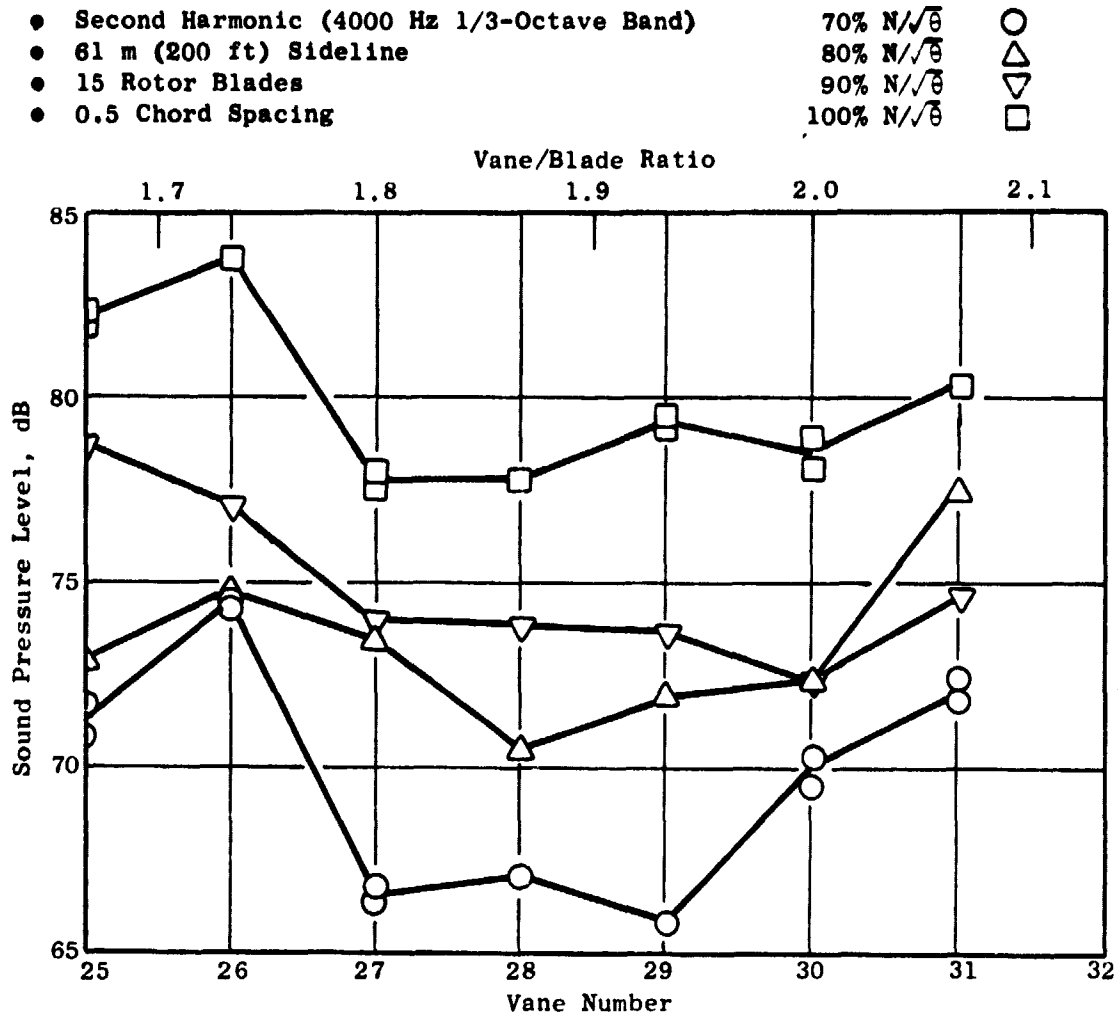


Figure 6. Peak Sideline SPL's as a Function of Vane Number.

## B. Rotor-Stator Spacing

The effect of rotor-stator spacing at the optimum vane/blade ratio (1.87) for minimizing second harmonic tone propagation was investigated at four values of spacing, expressed in multiples of true rotor tip chords. The four spacings were 0.5, 1.0, 1.5, and 2.0.

One-third octave band PWL data for frequencies of 2000 to 6300 Hz are presented in Figure 7. These data show little or no change at the lower frequencies with spacing; however, as the 1/3-octave band center frequencies increase, the effect of rotor-stator spacing becomes more pronounced. It appears that a second noise source is controlling at the wide spacings and lower frequencies and that at higher frequencies this noise source is not as evident.

Various investigators, References 6 and 7, have shown how interaction of inlet disturbances such as turbulence eddies, ground vortices, wall boundary layer fluctuations, and thermal gradients results in noise generation by the rotor. Generally, the turbulence eddies form the dominant noise generation mechanism, Reference 8. The noise spectrum generated by rotor turbulence interaction is controlled by the incoming turbulence spectrum; however, both discrete frequency and broadband noise may result (References 6 and 8). It has been found that the turbulence spectrum normally peaks at the low frequencies and falls off rapidly at the higher frequencies. Correspondingly the noise spectrum was also found to decay with frequency. These results are consistent with the data which are presented in Figure 7.

If we examine the curve at 4000 Hz, the 1/3-octave band which contains the second harmonic, a definite decrease with spacing can be seen. The decrease with spacing is not as marked as our current prediction of viscous wake spacing, shown in Figure 8, which uses the Silverstein wake model from Reference 9. As spacing increases to 2 chords, it appears that a second source such as rotor-turbulence noise is controlling. Spacing would not be expected to have an effect on rotor-turbulence noise levels; therefore, it can be assumed that the rotor-turbulence level is 130 dB and that this value is constant with spacing. Then at 0.5 chord, the sum of rotor-stator noise and rotor-turbulence noise (130 dB) must add to give the measured level of 133.5 dB. Figure 9 shows the relative levels of rotor-turbulence noise and rotor-stator noise at each value of spacing with the Silverstein model applied to the rotor-stator noise calculated at 0.5 chord. The sum of the two sources is in good agreement with the measured data.

The above exercise indicates that at the wide spacings such as 2.0 and 1.5 chords, a second noise source may be contributing. There is still a potential benefit from the wide spacings of 1.5 and 2.0 in actual flight where rotor-turbulence noise should be greatly reduced.

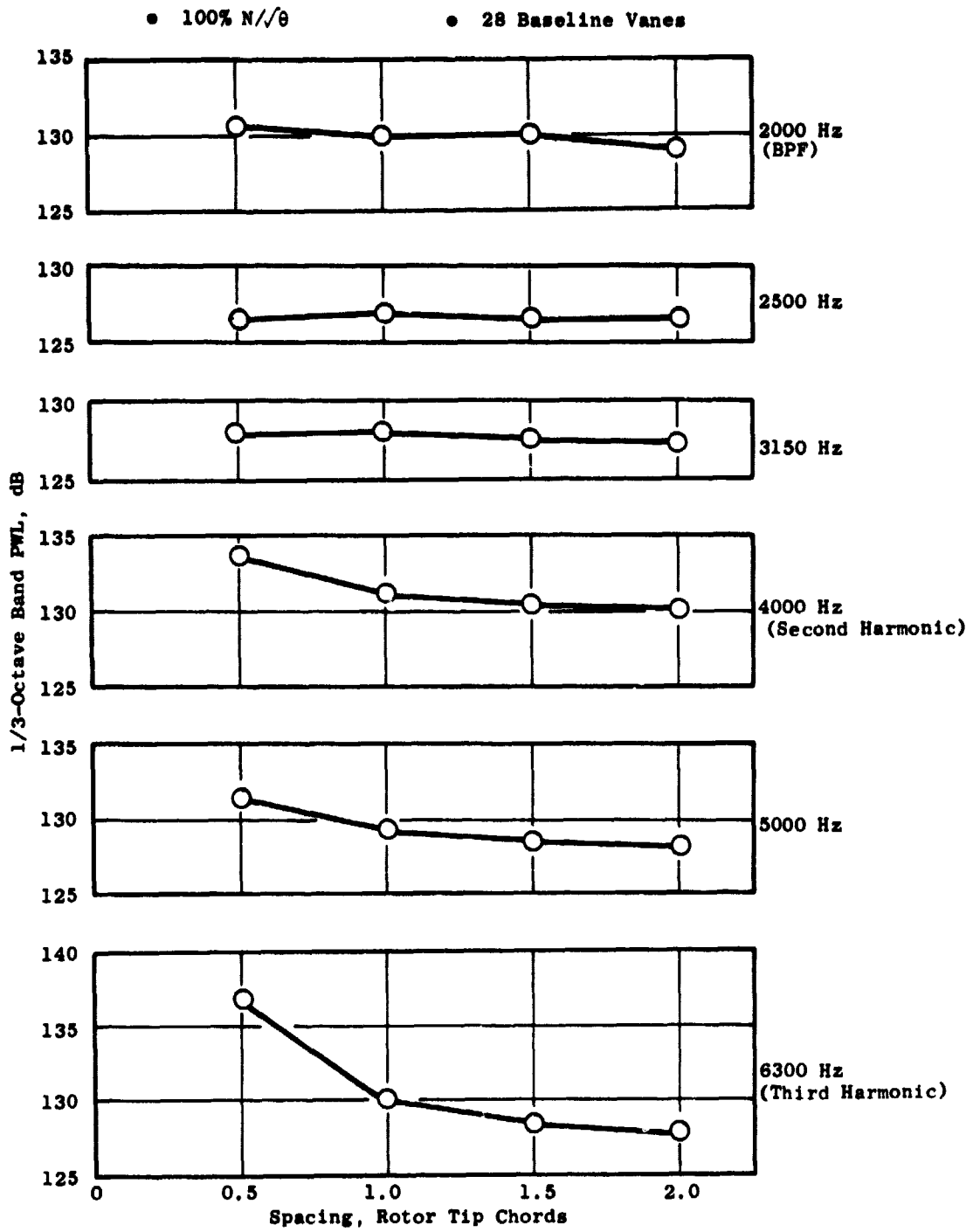


Figure 7. PWL Change at 2000 to 6300 Hz as a Function of Vane Spacing.



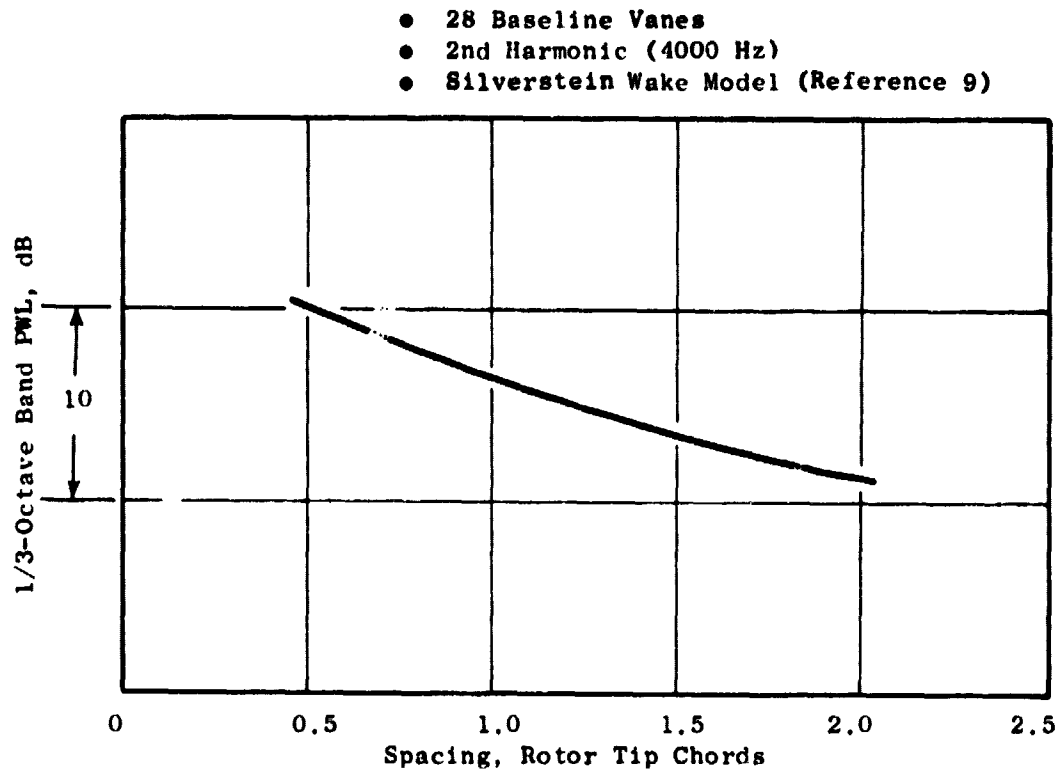


Figure 8. Predicted PWL Change with Spacing.

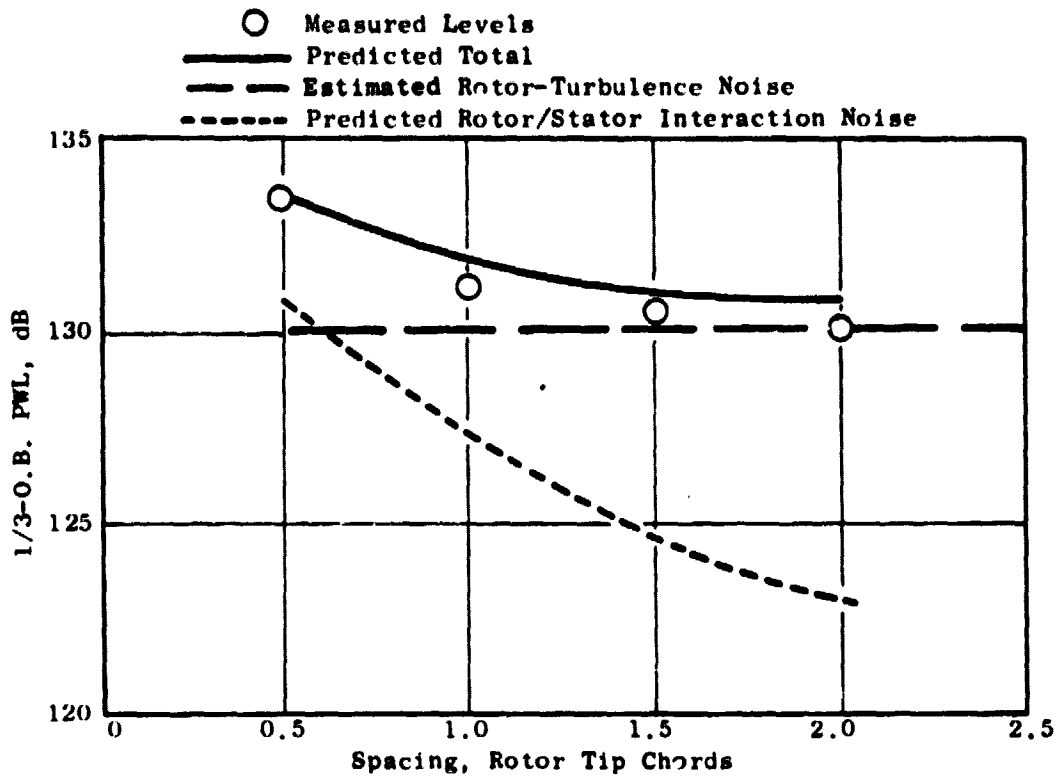


Figure 9. Summation of Rotor-Turbulence and Rotor/Stator Noise.

### C. Low-Mach Vanes

One of the source noise reduction techniques investigated in this test program involved increasing the annulus area through the vane row. This annulus area increase (shown in Figure 10) of 11% resulted in about a 10% decrease in the axial Mach number through the vane row. Hanson's fan noise prediction method (Reference 10) was reviewed to determine the relation between axial velocity and sound power level. It was found that the approximate change in generated noise power due to a change in axial velocity is given by  $30 \log$  (axial velocity ratio). For a 10 percent decrease in axial Mach number through the vane row, one would estimate 1.4 dB reduction in stator-generated broadband noise. Although not a significant effect for an unsuppressed engine, with a highly suppressed fan duct this could translate to 1.0 to 1.4 PNdB suppression if broadband noise were the dominant source left after suppression.

Measured data indicate no significant change in the broadband noise of far-field SPL's. This is seen in Figure 11 which compares 1.88 radian (108 degree) narrowband spectra.

There are two possible reasons for the lack of noise reductions with this technique. The first is poor aerodynamic performance and the second is that another noise source is masking any benefit due to the low-Mach vanes. However, the aerodynamic performance (discussed in more detail in Reference 5) shows only a slight decrease in the low-Mach vane total pressure recovery and airflow when compared to the baseline vanes. There appears to be no performance basis for the lack of noise reduction. Similar results are evident for probe data taken upstream of the rotor. A narrowband comparison at one immersion is presented in Figure 12. This comparison shows that the low-Mach vanes may have increased the forward radiated noise by 1 or 2 dB.

Previous sections, particularly those dealing with the vane/blade ratio results, have given strong indication that rotor inlet turbulence levels are controlling the aft radiated noise at 1.5 chord spacing. This could conceivably be the reason for the lack of positive results from the low-Mach vanes. However, it should be noted that this does not mean low-Mach vanes should not be investigated further as a means of reducing noise in flight, but rather they should be evaluated in a test where the levels and eddy sizes of inlet turbulence can be controlled.

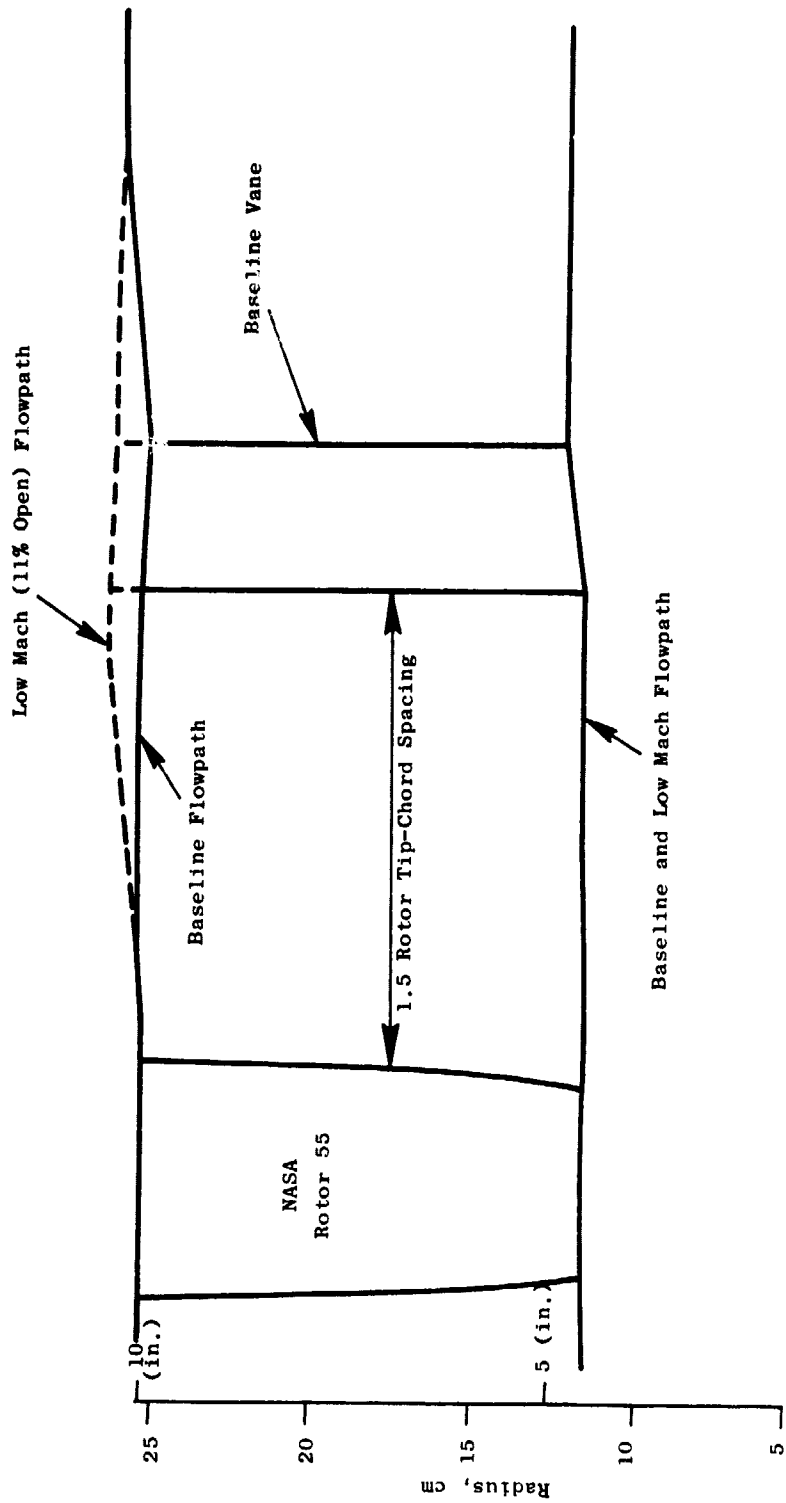


Figure 10. Model Fan Flowpaths.

ORIGINAL PAGE IS  
OF POOR QUALITY

- 5.18 m (17 ft) Arc
- 20 Hz Bandwidth
- 108 Degrees
- 100%  $N/\theta$

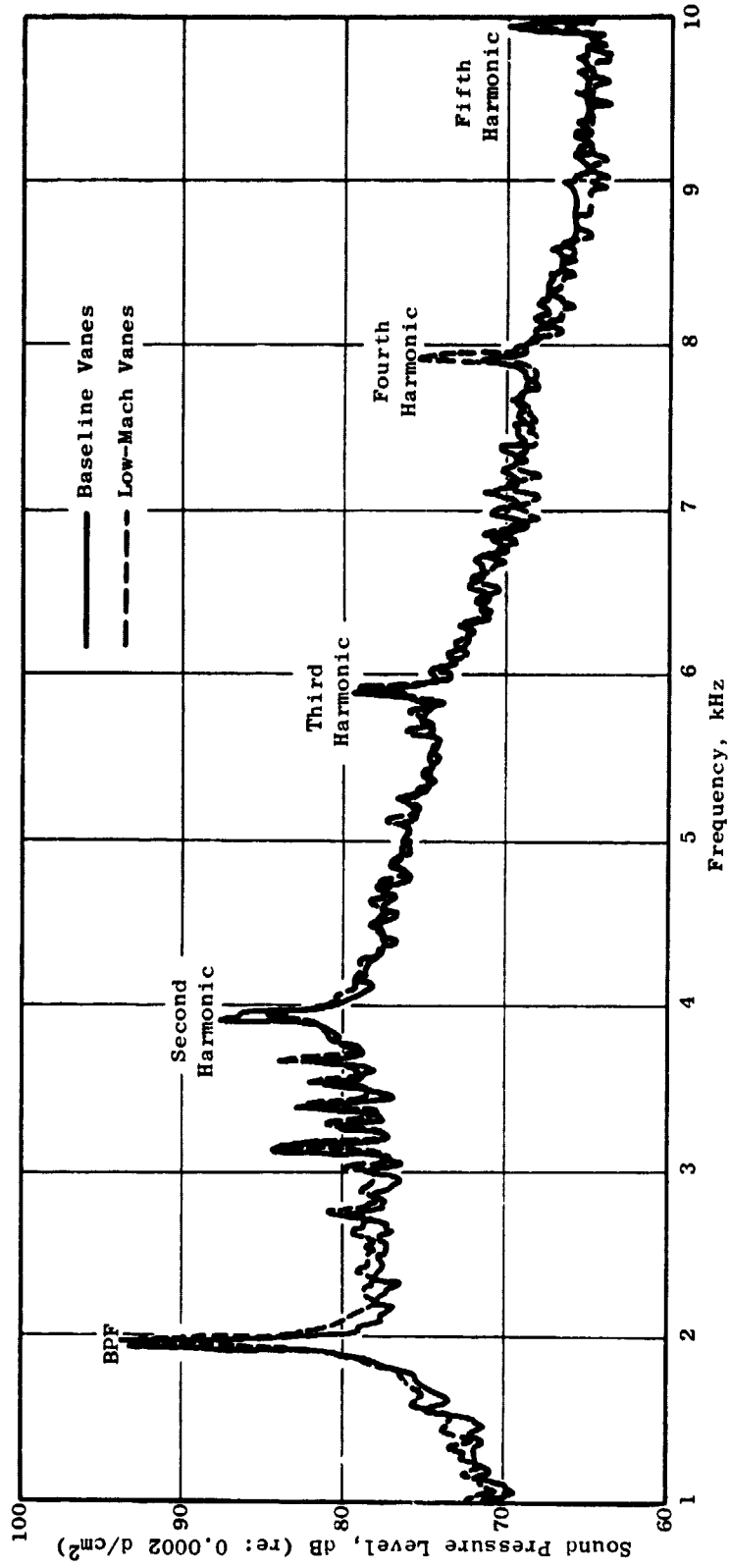


Figure 11. Comparison of Baseline and Low-Mach Vane Exhaust Noise Levels.

- 5.18 m (17 ft) Arc
- 20 Hz Bandwidth
- Inlet Probe (Not Corrected for Probe Response)
- 100%  $N/\theta$
- Immersion = 6.1 cm (2.4 in.)

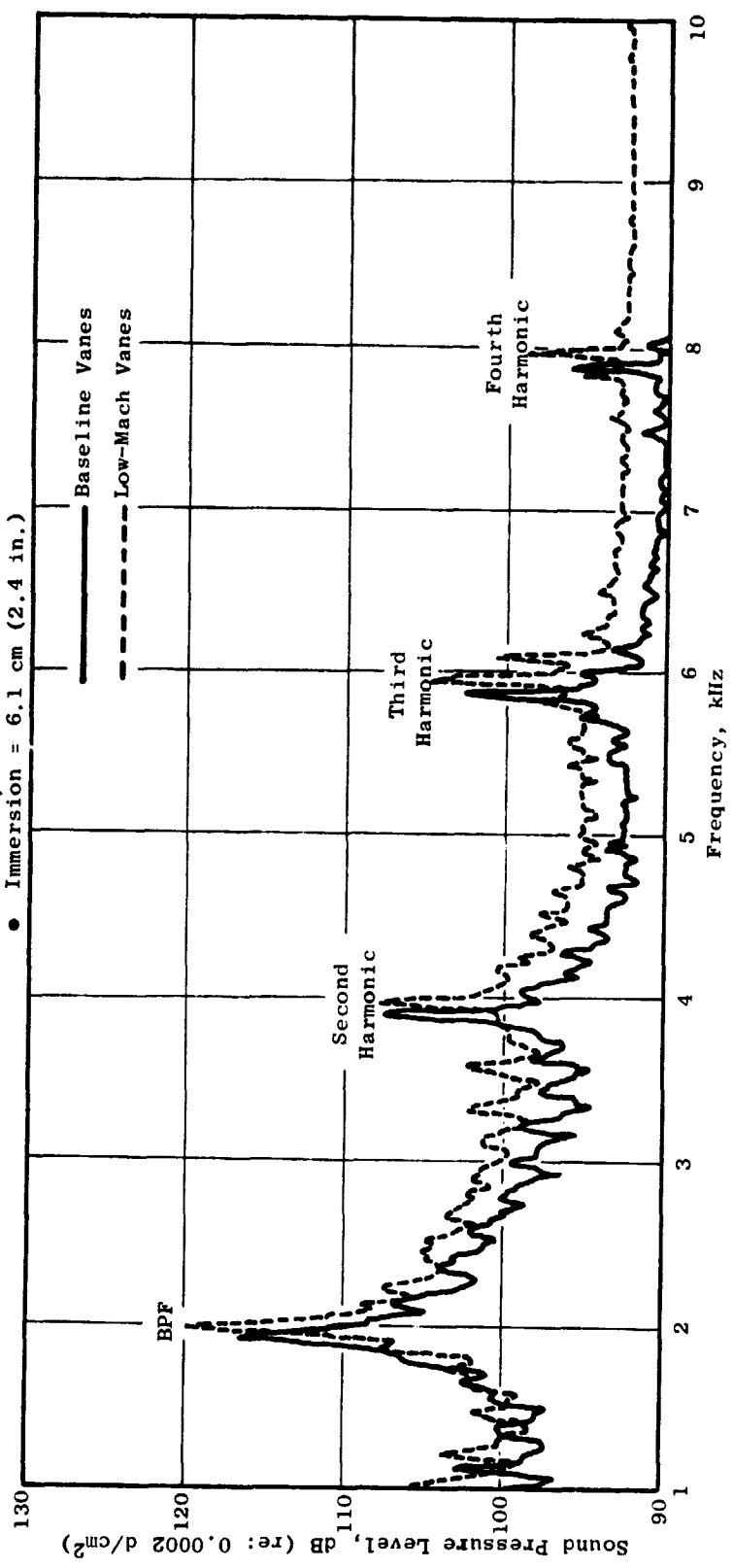


Figure 12. Comparison of Baseline and Low-Mach Inlet Probe SPL's.

## SECTION IV

### AFT SUPPRESSION TESTS

#### A. Porosity Effects

The aft duct treatment configurations tested had faceplate porosities of 12% and 27%. The selection of the two constant porosities was based on acoustic duct data.

The variable-depth treatment designs have four different sections of treatment. Each of these sections is designed to a different tuning frequency which produces a variation in the acoustic parameter  $H/\lambda_0$ . Theoretically, the optimum acoustic resistance varies with this parameter. Thick acoustic liners tuned to low frequencies give low  $(H/\lambda_0)$  values and require low resistance. Thus, a higher porosity value is required for the thick panel relative to a thinner panel.

Various treatment depth combinations were evaluated at 12% and 27% porosities. All had a treated L/H value of 4.6 made up of four treatment panels. The different combinations of thickness,  $t$ , and porosity,  $\sigma$ , which were tested and which are relevant to this discussion are as follows:

<u>Configuration</u>	<u>Treatment Panel</u>											
	t	$\frac{1}{\sigma}$	$\sigma$	t	$\frac{2}{\sigma}$	$\sigma$	t	$\frac{3}{\sigma}$	$\sigma$	t	$\frac{4}{\sigma}$	$\sigma$
Constant Depth (75-3)	1.9cm (0.75 in.)		12%	1.9cm (0.75 in.)		12%	1.9cm (0.75 in.)		12%	1.9cm (0.75 in.)		12%
Constant Depth (17)	1.9cm (0.75 in.)		27%	1.9cm (0.75 in.)		27%	1.9cm (0.75 in.)		27%	1.9cm (0.75 in.)		27%
Variable-Depth Panels (7)	0.6cm (0.25 in.)		12%	1.2cm (0.50 in.)		12%	1.9cm (0.75 in.)		12%	3.8cm (1.5 in.)		12%
Variable-Depth Panels (8)	0.6cm (0.25 in.)		27%	1.2cm (0.50 in.)		27%	1.9cm (0.75 in.)		27%	3.8cm (1.5 in.)		27%
Variable Depth and Mixed Porosity (75-8)	1.27cm (0.50 in.)		12%	1.9cm (0.75 in.)		12%	0.635cm (0.25 in.)		12%	3.8cm (1.5 in.)		27%

The measured 1/3-octave band suppression for a configuration with a 1.9cm (0.75 in.) constant panel depth is shown in Figure 13 for porosities of 12% and 27%. The configuration is also shown in the figure. The data were taken at the maximum aft acoustic angle for fan speeds of 70% and 100%  $N/\sqrt{\theta}$ .

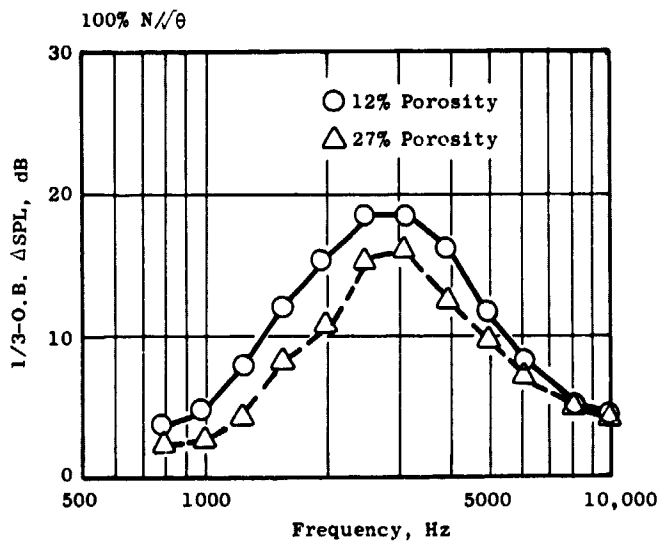
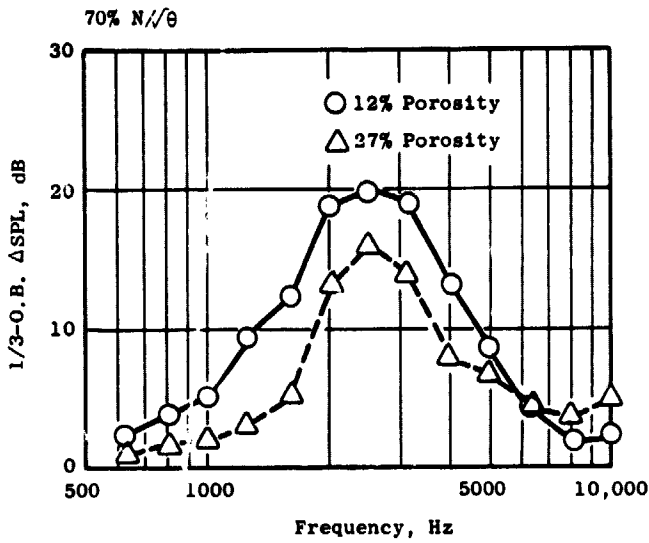
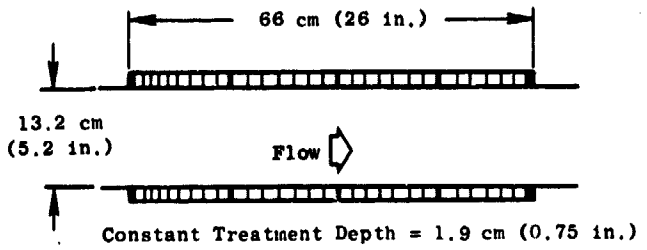


Figure 13. Measured Suppression Vs. Porosity for Constant Depth Liner.



The treatment with 12% porosity gives a higher level of suppression over the frequency range indicated. This suggests that the acoustic resistance of 12% porosity face sheet is nearer the optimum value for the subjected conditions. The duct Mach number at 70%  $N/\sqrt{\theta}$  is 0.3 and 0.42 at 100%  $N/\sqrt{\theta}$ .

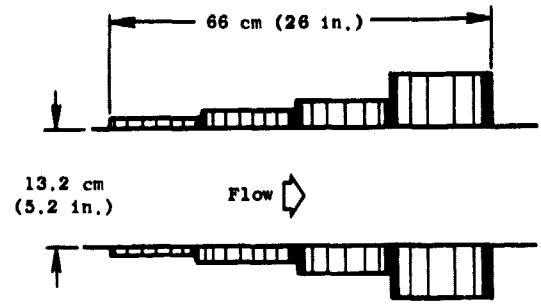
Figure 14 gives suppression spectra for the variable-depth treatment design indicated in the figure. The data are for fan speeds of 70% and 100%  $N/\sqrt{\theta}$  at the maximum aft acoustic angle. The 12% porosity gives more suppression at the higher frequencies (3150 Hz to 8000 Hz), with the 27% porosity configuration offering more peak suppression by an amount of 2 dB to 3 dB at 100%  $N/\sqrt{\theta}$ . The 12% porosity gives more suppression for all frequencies at 70%  $N/\sqrt{\theta}$ .

The two treatment configurations shown in Figure 15 have variable-depth panels with one having a constant 12% faceplate porosity and the other having panels with 12% and 27% porosity. The configuration with the mixed porosity is also different in that the 3.81cm (1.5 in.) and the 1.27cm (0.50 in.) panel positions are interchanged.

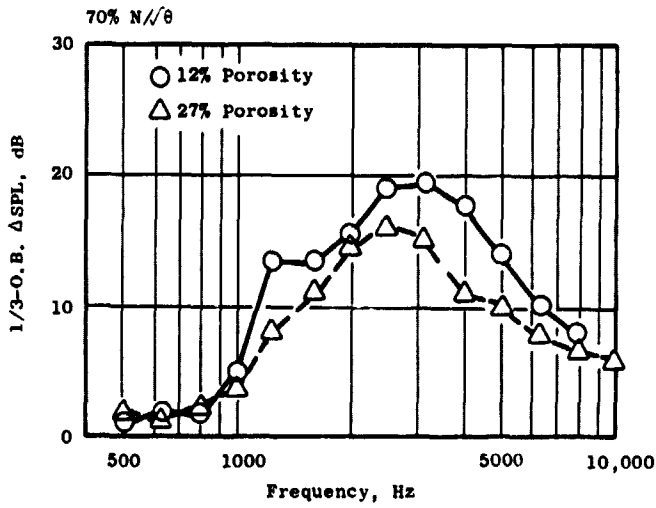
Suppression spectra for the two configurations are shown in Figure 16. The suppression is given for fan speeds of 70%  $N/\sqrt{\theta}$  and 100%  $N/\sqrt{\theta}$  at the maximum aft acoustic angle. Suppression comparison for the two configurations shows little difference at the higher frequency values. The 100%  $N/\sqrt{\theta}$  data show the mixed porosity configuration to give higher peak attenuation, and also show more suppression for most of the frequencies below the peak attenuation frequency. This increase in suppression is probably a result of having changed the thick panel porosity from 12% to 27%, which gives a lower acoustic resistance value. Theoretically, a lower resistance is required for the thicker panel since it is tuned to a lower frequency and has a smaller  $H/\lambda_0$  value.

The four treatment panels that make up the variable-depth treatment configurations as just shown were evaluated separately. The panels were evaluated with 12% and 27% faceplate porosities. The data obtained enable an evaluation to be made of each individual panel's suppression performance, and also give data showing the suppression level variation with  $H/\lambda_0$  versus faceplate porosity.

Figure 17 gives suppression data as measured for the single panels with a treated L/H of 1.15. The suppression spectra given are for 100%  $N/\sqrt{\theta}$  at the maximum aft acoustic angle. The four liner depths give four tuning frequencies which enable a comparison of peak suppression versus the acoustic parameter ( $H/\lambda_0$ ). The results show that for  $H/\lambda_0$  values of 1.94, 1.22, and 0.97, the 12% porosity gives more peak suppression. However, as the  $H/\lambda_0$  value is reduced to 0.78 with the 3.81cm (1.5 in.) panel, the 27% porosity has the higher peak suppression. This result is strong evidence that for the lower  $H/\lambda_0$ 's a lower resistance value is required for suppression optimization. This does not suggest that 27% porosity is optimum, but that relative to 12% the resulting acoustic resistance is nearer optimum for these  $H/\lambda_0$  and L/H values.



Panel Depth { 0.6 cm 1.2 cm 1.9 cm 3.5 cm  
 (0.25 in.) (0.5 in.) (0.75 in.) (1.5 in.)



● Maximum Aft Angle

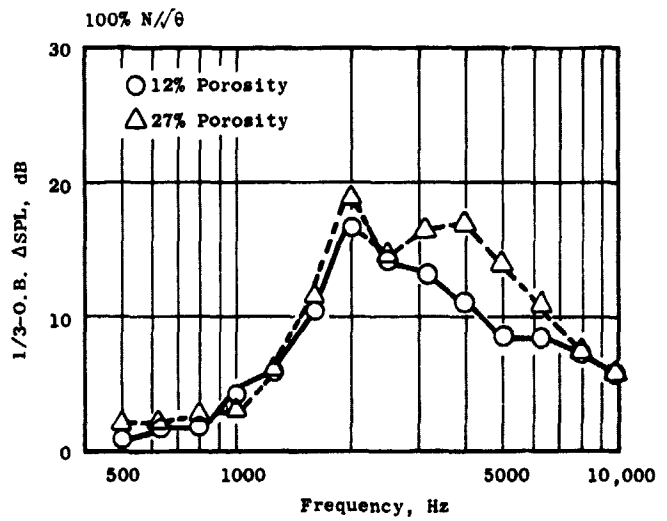
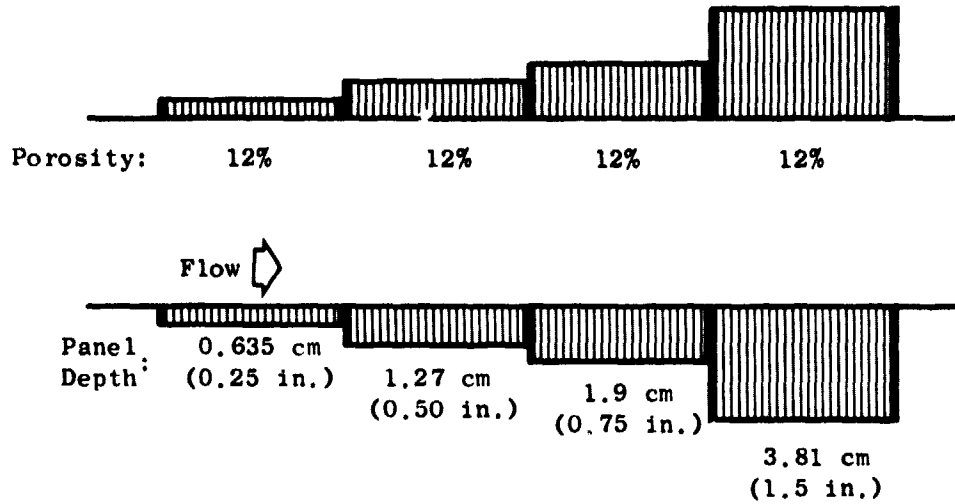


Figure 14. Measured Suppression Vs. Porosity for Variable-Depth Liner.

ORIGINAL PAGE IS  
OF POOR QUALITY

● Configuration 7

- Variable Depth
- 12% Porosity



● Configuration 75-8

- Variable Depth
- Mixed Porosity

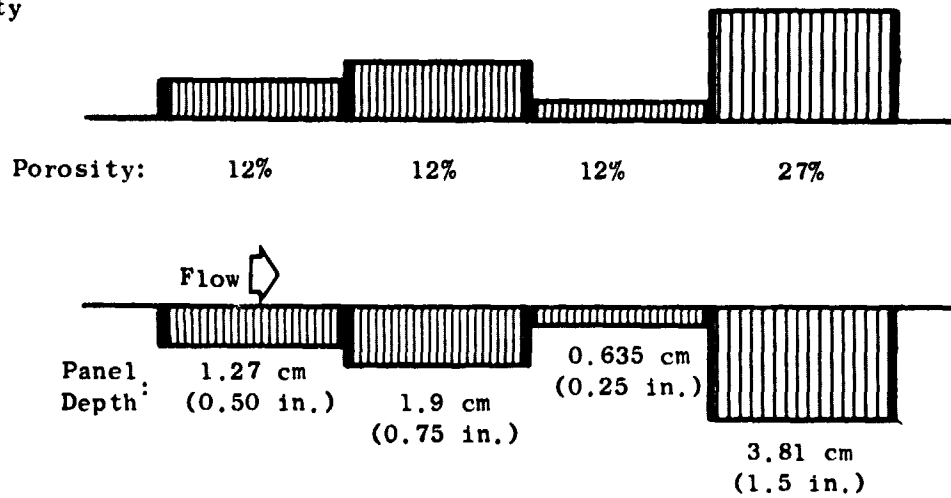


Figure 15. Variable-Depth, Constant-Porosity and Variable-Depth, Variable-Porosity Configurations.

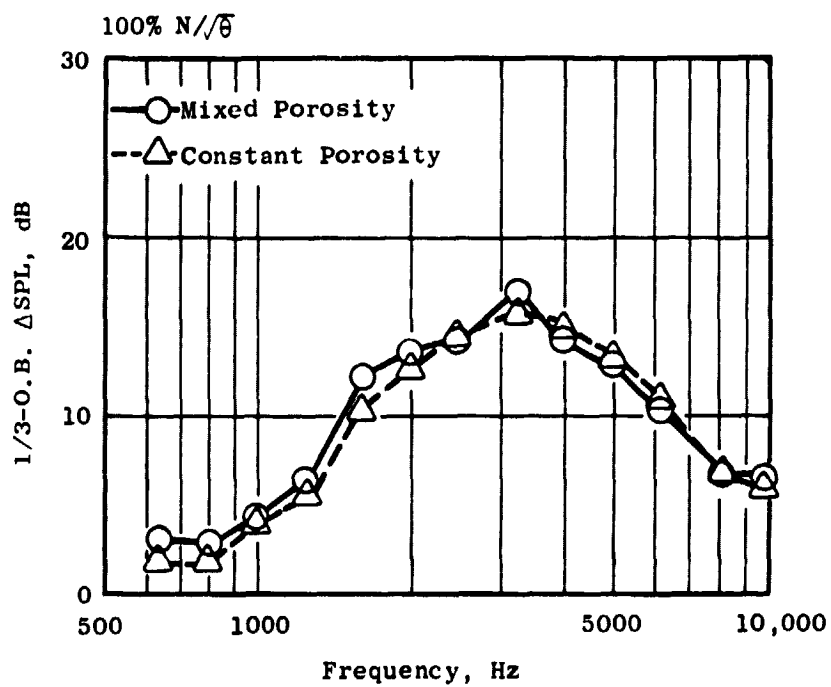
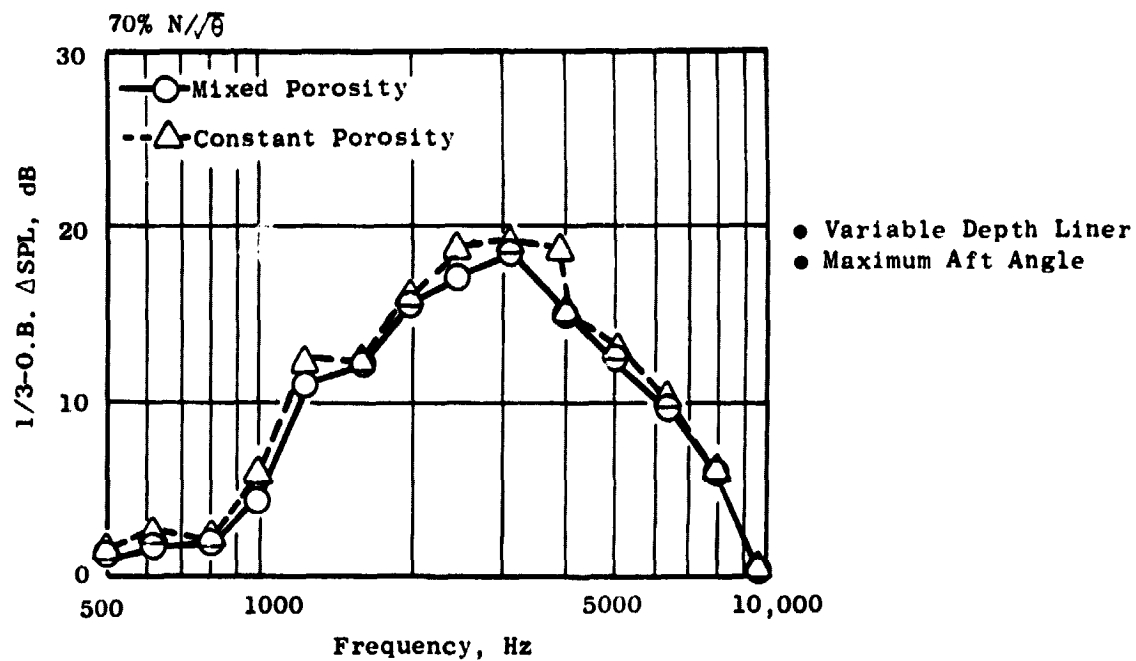


Figure 16. Measured Suppression with Constant Vs. Variable Porosity.

ORIGINAL PAGE IS  
OF POOR QUALITY

- 100%  $N/\sqrt{\epsilon}$ , Max. Aft Angle
- Single Panels,  $L/H = 1.15$

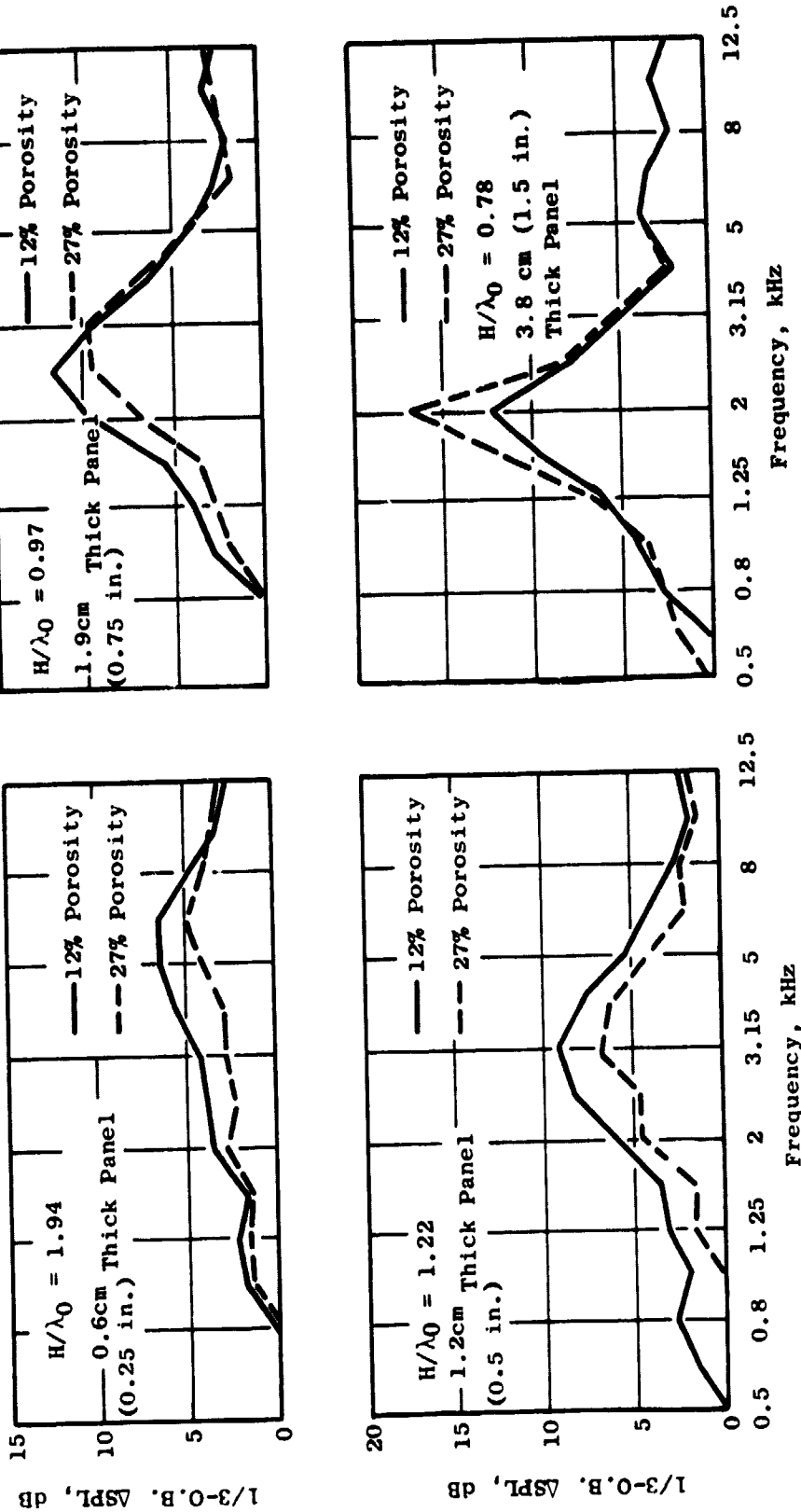


Figure 17. Suppression Spectra for Individual Panels Vs.  $H/\lambda_0$ .

The suppression spectra shown in Figures 18 and 19 are for the constant-depth 1.91 cm (0.75 in.) treatment with porosity values of 12% and 27%. The data provide a comparison of suppression versus duct Mach number, which gives a corresponding acoustic resistance variation. The Mach numbers for 70%  $N/\sqrt{\theta}$  and 100%  $N/\sqrt{\theta}$  are 0.3 and 0.42, respectively.

Figure 18 gives the suppression for the configuration having 12% porosity at the two fan speed points. The peak suppression decreases by as much as 3 dB as the fan speed is increased from 70% to 100%  $N/\sqrt{\theta}$ . The reduced suppression indicates that as the duct Mach number increases the acoustic resistance for the 12% porosity liner is also increased, giving a higher resistance, which is farther removed from the optimum values.

Figure 19 gives the same type of data comparison for the configuration with 27% faceplate porosity. Here, the peak suppression increases as the fan speed is increased from 70%  $N/\sqrt{\theta}$  to 100%  $N/\sqrt{\theta}$ . This indicates that at 70%  $N/\sqrt{\theta}$  the 27% porosity faceplate acoustic resistance is below the optimum value. However, as the duct Mach number increases from 0.3 to 0.42, with the corresponding increase in fan speed, the resistance is also increased. The higher suppression noted in the data comparison is a result of now having a resistance value nearer the optimum resistance requirement.

The overall result of the comparisons for changes in duct Mach number is that neither the 12% nor the 27% porosity have the optimum acoustic resistance at 100%  $N/\sqrt{\theta}$  for all panels. Thus, a configuration with variable-depth treatment must also have mixed porosities for design optimization.

#### B. Variable Boundary Conditions

Suppression characteristics for treatment configurations having constant-porosity, constant-depth treatment; constant-porosity, variable-depth treatment; and mixed-porosity, variable-depth treatment are discussed in this section. These variations in the treatment design were included to enable the identification of a design with improved peak attenuation and suppression bandwidth characteristics.

Two treatment configurations are shown in Figure 20. The first configuration has variable treatment depths with the second having constant-depth treatment. A 12% faceplate porosity was used for the two configurations.

Figure 21 gives a comparison of the suppression for the constant versus variable-depth treatment at 100%  $N/\sqrt{\theta}$ . The variable-depth treatment shows a wider suppression bandwidth, with the constant-depth treatment giving more peak suppression. These suppression characteristics are expected since the variable-depth treatment gives four different tuning frequencies, spreading the suppression out over a broader frequency range. The constant-depth treatment has one design frequency which gives a higher suppression level at that design frequency.

ORIGINAL PAGE IS  
OF POOR QUALITY

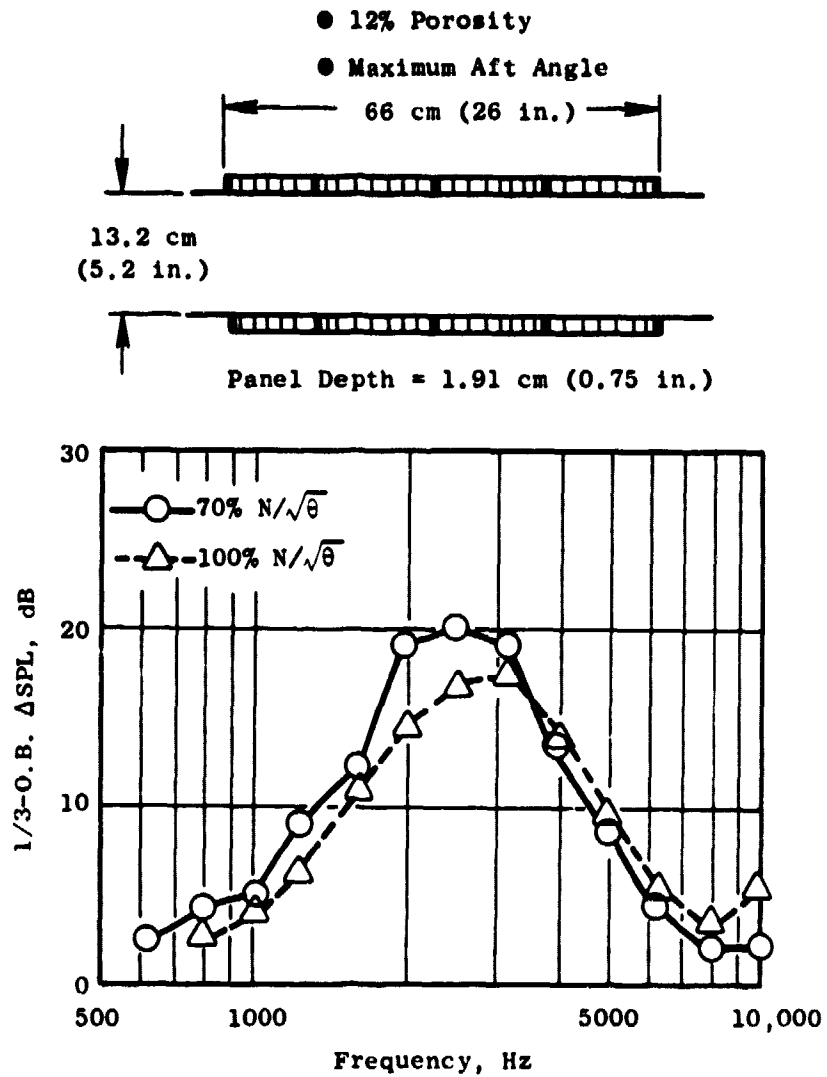


Figure 18. Measured Suppression Spectra at Two Fan Speeds - 12% Porosity.

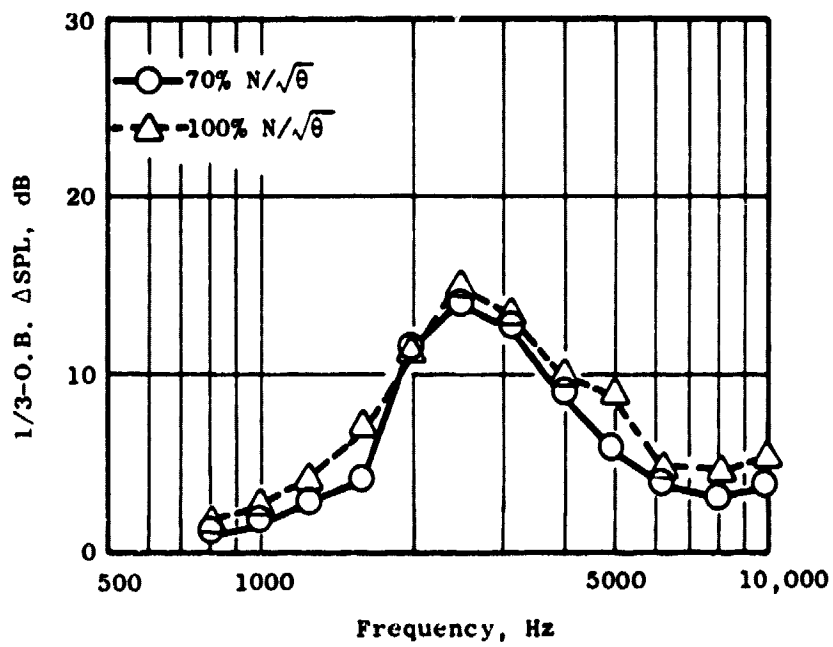
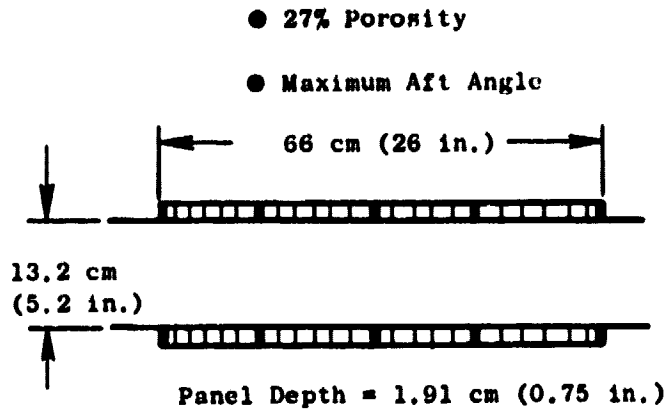
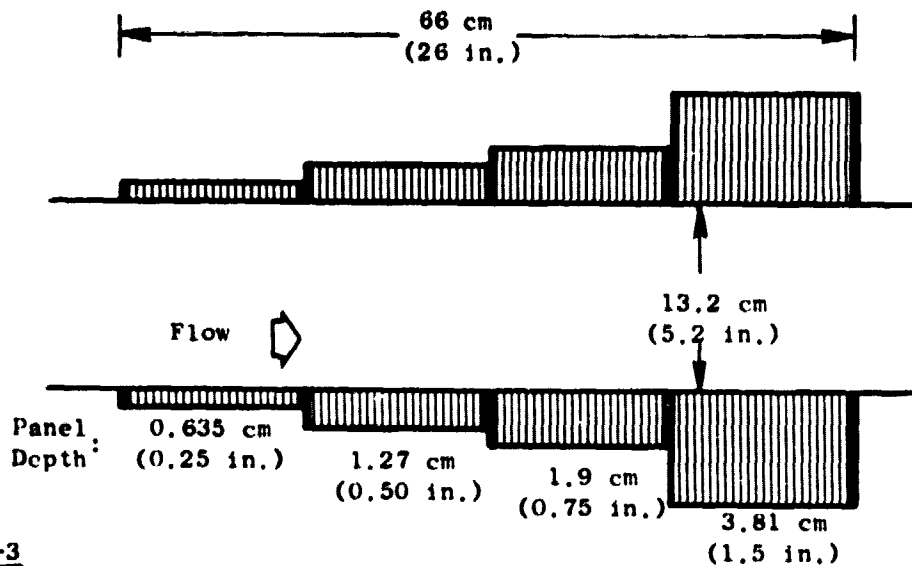


Figure 19. Measured Suppression Spectra at Two Fan Speeds - 27% Porosity.



- Configuration 7
- 12% Porosity
- Variable Depth

ORIGINAL PAGE IS  
OF POOR QUALITY



- Configuration 75-3
- 12% Porosity
- Constant Depth, 1.9 cm (0.75 in.)

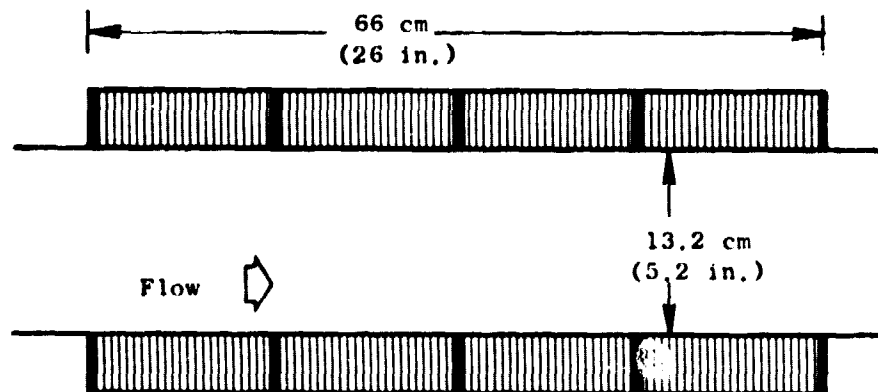


Figure 20. Constant-Depth and Variable-Depth Treatment Configurations.

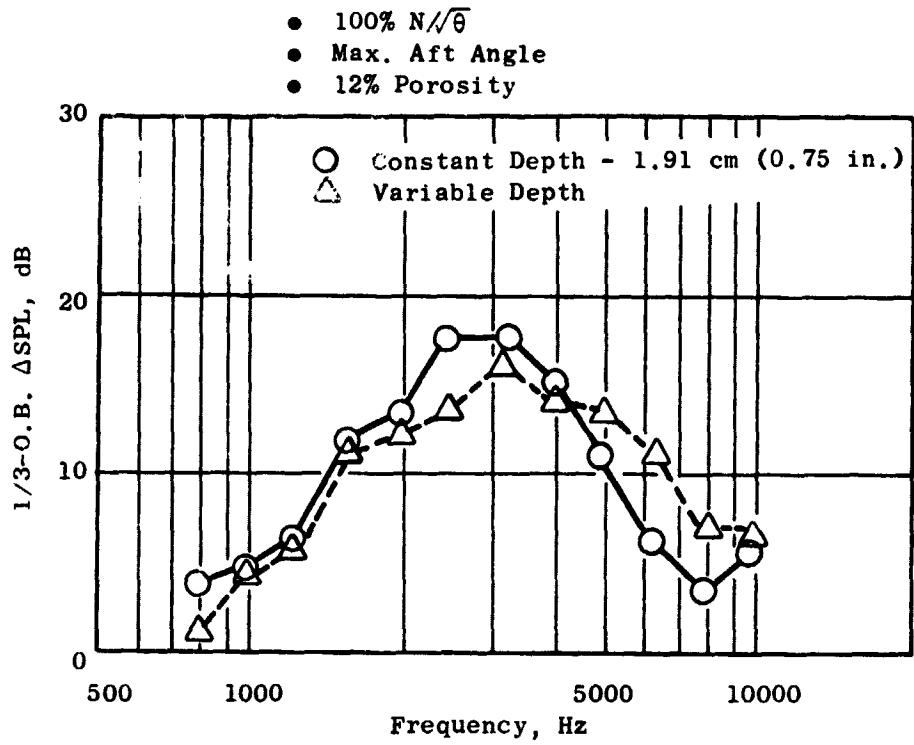


Figure 21. Measured Suppression Spectra for Constant Vs. Variable Panel Depth.

The suppression performance for these configurations can be evaluated by comparing the results with previous suppression data. Figure 22 gives a comparison of the measured and predicted suppression for the constant-depth treatment configuration. The prediction is based on a correlation developed from engine data where the treatment consisted of single-phase, constant-depth treatment designs with constant porosity. Good agreement is seen between the measured and predicted suppression bandwidth. The measured peak suppression is less than predicted. This difference could be due in part to the design frequency of the liner, which is predicted to be near the filter-split of the 2500 Hz and 3150 Hz 1/3-octave bands.

Figure 23 gives the predicted and measured suppression for a variable-depth, mixed-porosity configuration at  $100\% N/\sqrt{\theta}$ . The porosity values and the treatment orientation are indicated in the sketch shown on the figure. The predicted suppression is low, relative to the measured suppression, at all frequencies greater than 2500 Hz.

Fan exhaust suppression requirements in many cases require wall treatment plus an acoustic splitter. The thickness restriction of the splitter does not yield to a variable-depth design with the same range of treatment thicknesses that are usually available on the outer and inner flow paths. Thus, one of the treatment configurations was designed to simulate a splitter condition. A sketch depicting the treatment design is shown in Figure 24. The outer wall treatment has variable-depth panels with the inner wall treatment having a constant thickness. Also given in the figure are the predicted and the measured suppression. The splitter simulation configurations are discussed later in this report. Here, as was the case for the variable-depth treatment on both walls, the predicted suppression in the higher frequencies is less than measured. However, the difference for the splitter simulation is less than for the variable-depth, mixed-porosity design.

These results show that the suppression (at frequencies above the peak suppression frequency) obtained from these configurations is consistently higher than the average of the General Electric Company's better previous engine treatment designs, from which the prediction method was derived. Since the average Rotor 55 suppression is consistently higher than that predicted, this suggests that the difference is a result of the treatment design rather than experimental variation in the data. The increase in suppression is probably a result of an interaction effect or some phenomena introduced by the variable-depth treatment with constant- and mixed-porosity. Therefore, the data correlation needs adjusting in order to get a better relation between predicted and measured suppression bandwidths. Appropriate adjustments were made for QCSEE engine design estimates.

### C. Treatment Area Effectiveness

Treatment area losses are usually unavoidable in real engine hardware due to flanges, instrumentation, and fan sheet hole blockage. A simulation of this blockage was made by taping approximately 20% of the treated sur-

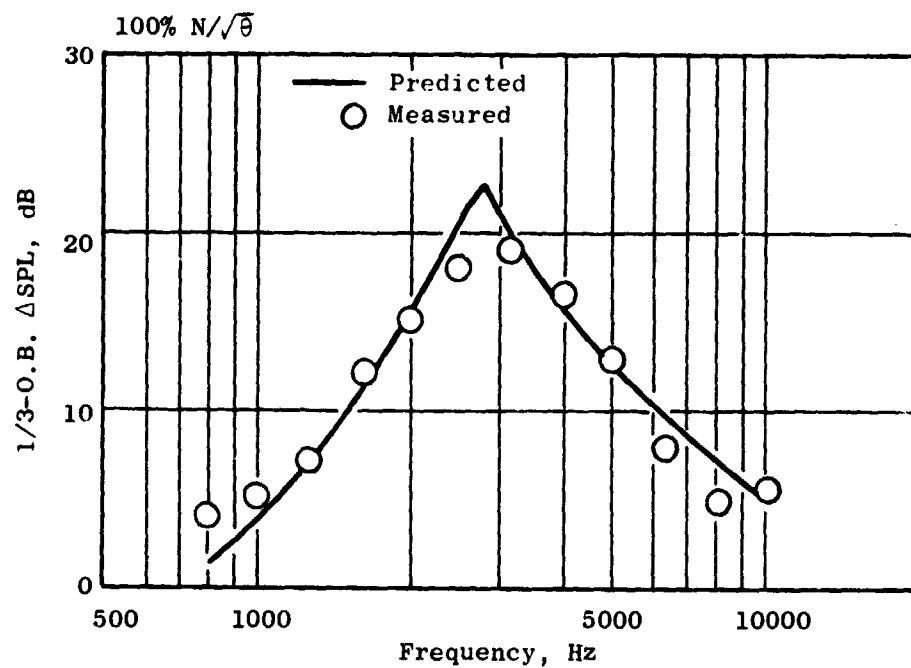
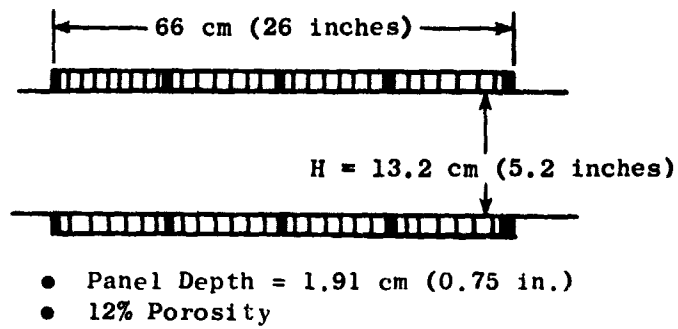


Figure 22. Predicted Vs. Measured Suppression Spectra, Constant Depth, 12% Porosity Panels.

ORIGINAL PAGE IS  
OF POOR QUALITY

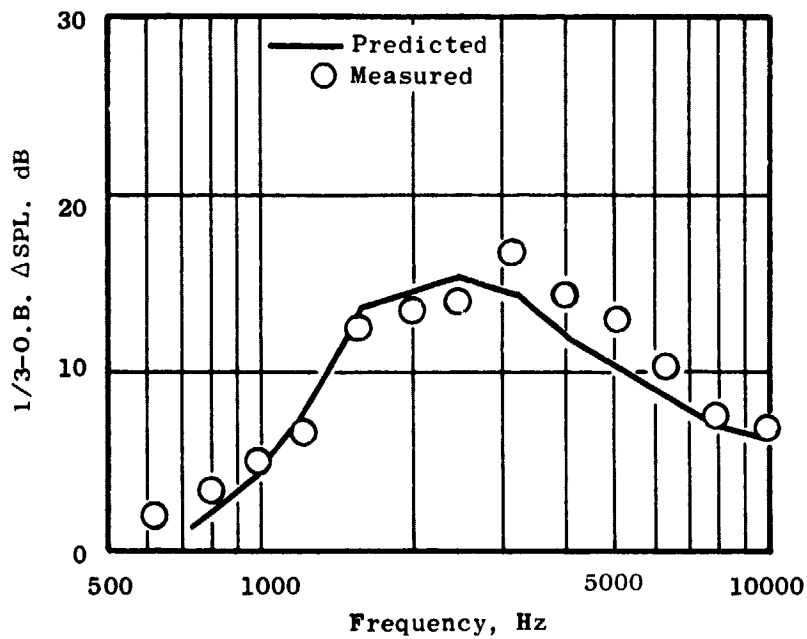
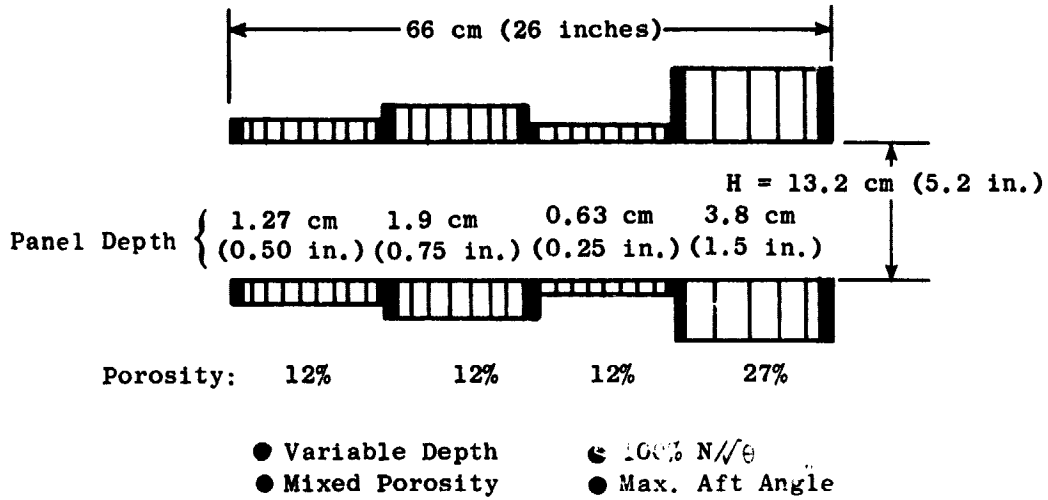


Figure 23. Predicted Vs. Measured Suppression Spectra - Variable Depth, Mixed Porosity Panels.

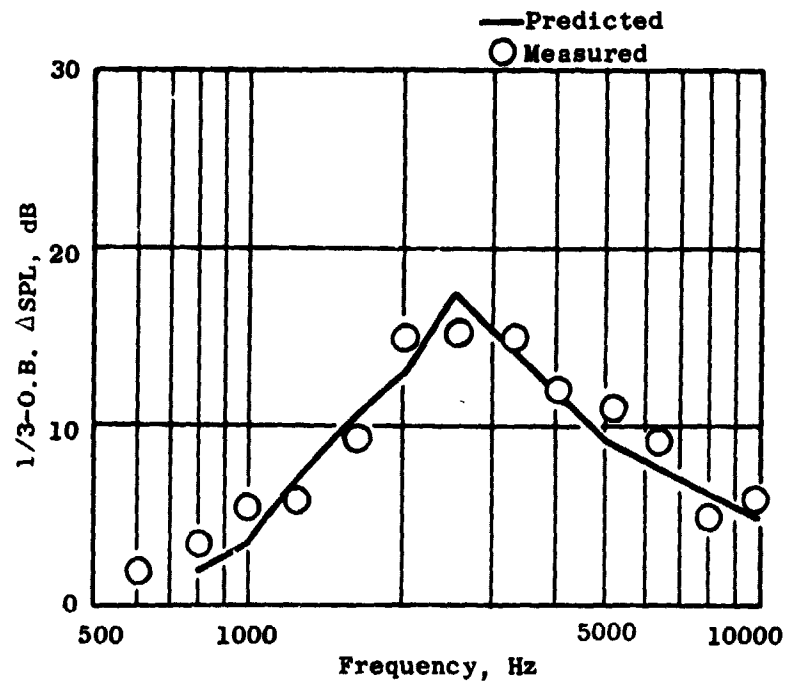
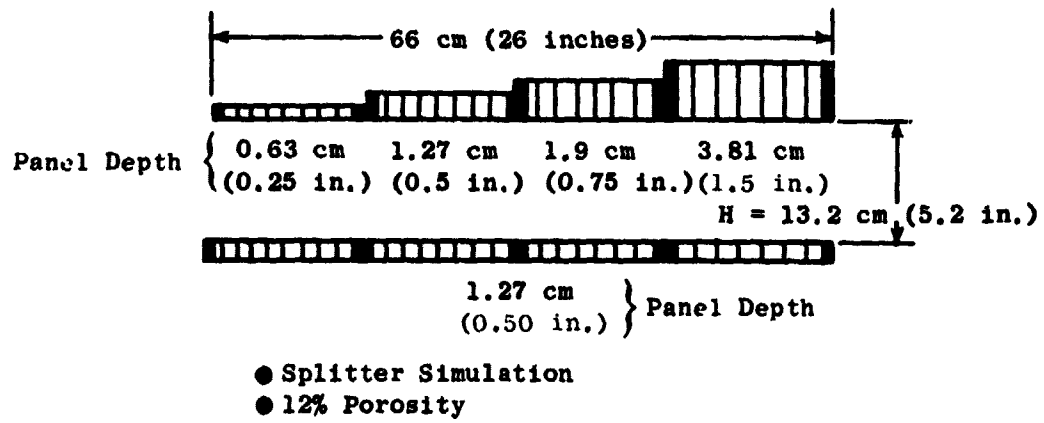


Figure 24. Predicted Vs. Measured Suppression Spectra - Splitter Simulation, 12% Porosity Panels.

face area of each of the four panels on the inner and outer walls. The fan exhaust treatment configurations tested are shown in Figure 25. The configuration without taping has an effective L/H of 4.6 and a L/H of 3.7 with taping. This would result in a predicted loss of treatment effectiveness of about 20%.

The suppression spectra for the two L/H values are shown in Figure 26 for fan speeds of  $70\% N/\sqrt{\theta}$  and  $100\% N/\sqrt{\theta}$ . Data are given at the maximum aft angle as measured on a 5.18m (17 ft) arc. Suppression is seen to decrease for each fan speed with the reduced treatment area. This reduction occurs over the 1600 Hz to 10,000 Hz frequency range. No significant change in suppression is noted at frequencies below 1600 Hz.

Figure 27 gives a comparison of the measured suppression loss with the reduced treatment area, and the suppression loss that is predicted using a linear relation between area and suppression. Approximately 1/4 to 1/2 of the predicted suppression loss was measured for the configuration with treatment blockage. This result shows that a linear relation between treatment area and suppression is not valid in the case tested.

The correlation given in Figure 28 first gives the measured peak suppression in terms of the actual L/H value while the second graph gives the peak suppression rate ( $\Delta dB/L/H$ ) versus the actual L/H value. This correlation shows that the effectiveness of the treatment decreases as the L/H parameter is increased. Also shown are the predicted suppression levels and suppression rates which were determined by using a prediction procedure that is linear with the L/H parameter. For higher L/H values, the estimated loss in suppression resulting from treatment area loss or decreased L/H using the linear model would be higher than that indicated from the measured Rotor 55 data. However, at smaller L/H values, the reverse is true. The loss in suppression due to treatment area loss would be underpredicted.

#### D. Splitter Simulation

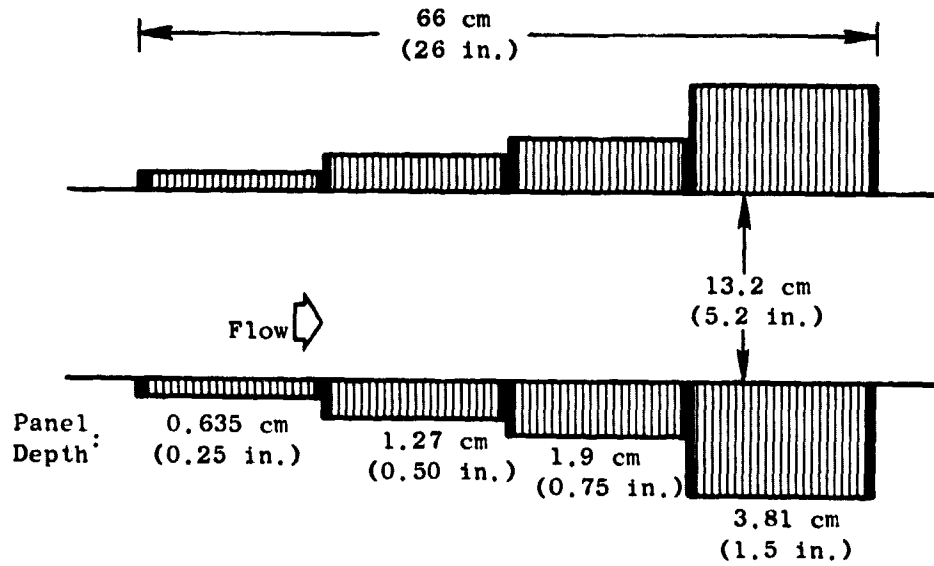
The schematic in Figure 29 shows three fan exhaust treatment configurations. The first has variable-depth treatment on both walls; the second has variable depth along the outer flowpath but constant depth on the inner flowpath. The third has constant-depth treatment on both walls. The second configuration, which was introduced in Section IV-B, represents a configuration with an acoustic splitter.

Figure 30 shows the measured suppression for the "simulated splitter" and the constant-depth configuration at fan speeds of  $70\% N/\sqrt{\theta}$  and  $100\% N/\sqrt{\theta}$ . The "splitter simulation" configuration gives a wider suppression bandwidth, although the peak suppression levels are approximately the same.

Figure 31 compares the "splitter-simulation" results with suppression levels measured for the configuration with variable-depth treatment on both walls at fan speeds of  $70\% N/\sqrt{\theta}$  and  $100\% N/\sqrt{\theta}$ . The configuration with variable depth on both walls gives somewhat better suppression bandwidth than the "splitter" case; however, it gives less peak suppression.

Configuration No. 7

- L/H = 5.0  
(Cartoon Length)
- L/H = 4.6  
(Effective Length)



Configuration No. 75-9

- L/H = 3.7  
(Effective Length)

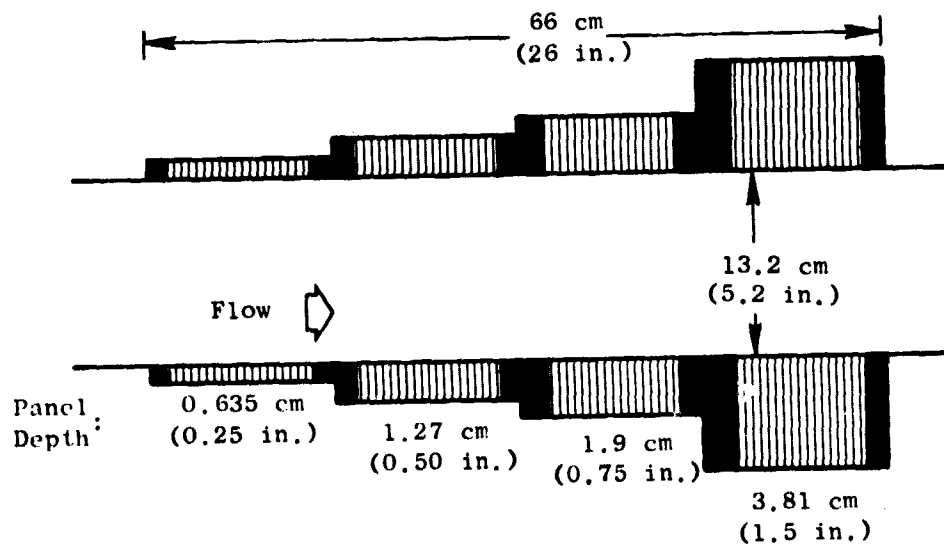


Figure 25. Configurations with and without Reduced Treatment Area.

ORIGINAL PAGE IS  
OF POOR QUALITY



ORIGINAL PAGE IS  
OF POOR QUALITY

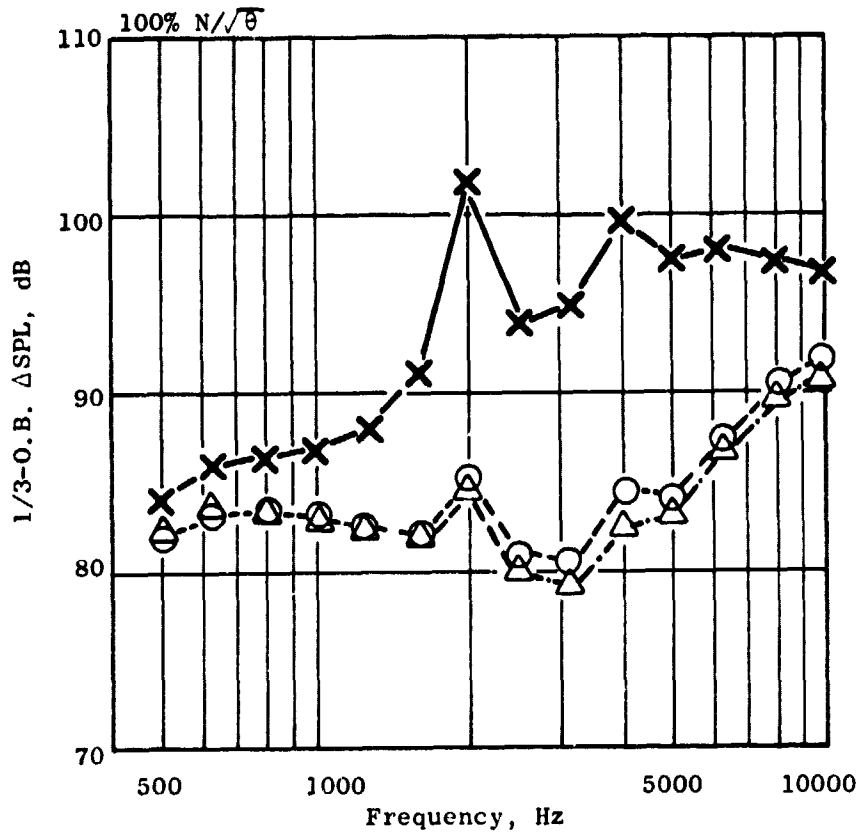
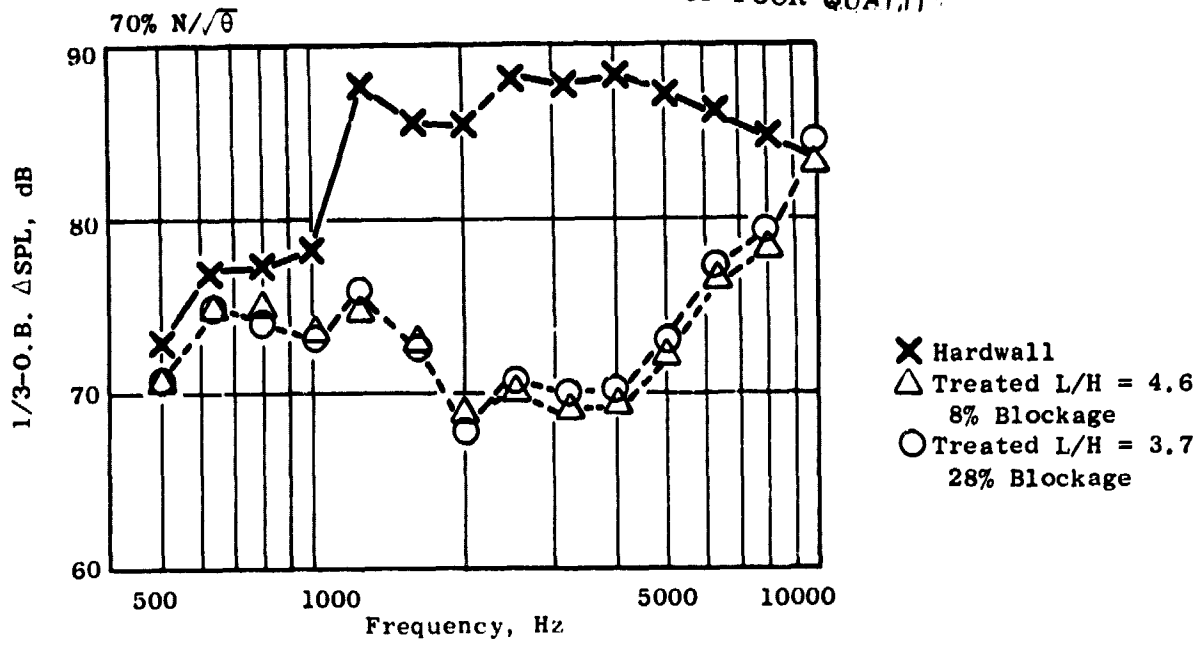


Figure 26. Suppressed and Unsuppressed Spectra for Different Treatment Areas.

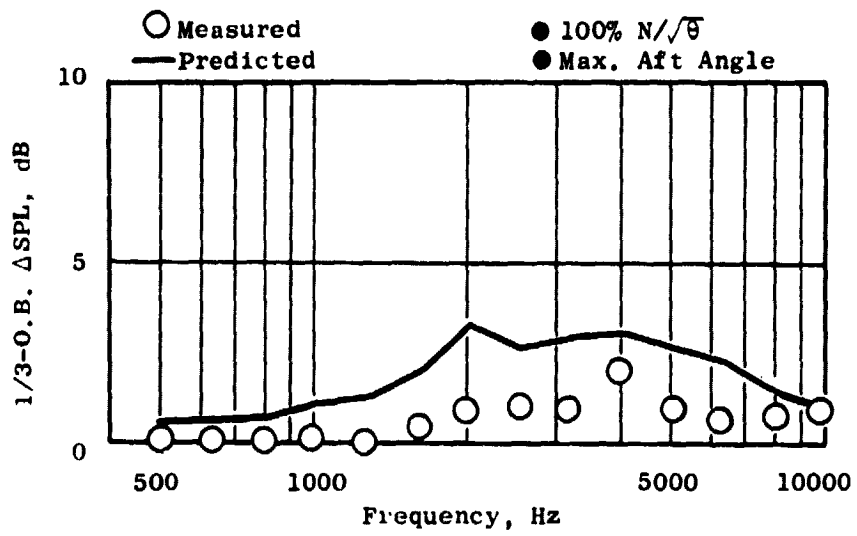


Figure 27. Predicted Vs. Measured Suppression Loss Resulting from Reduced Treatment Area.

- Predicted Suppression
- 12% Porosity - Constant-Depth Treatment
- 12% Porosity - Variable-Depth Treatment

$H/\lambda = 1.24$  for All Data

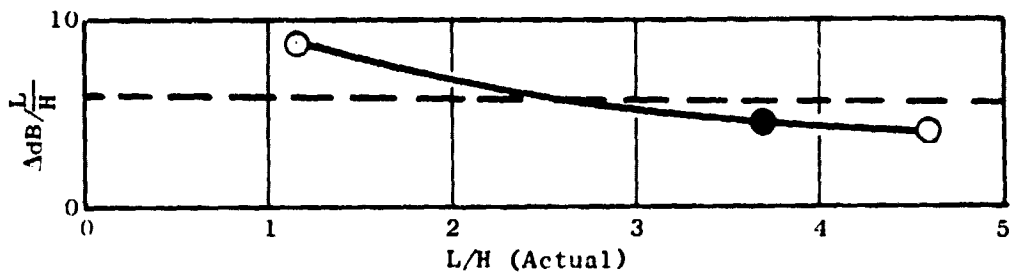
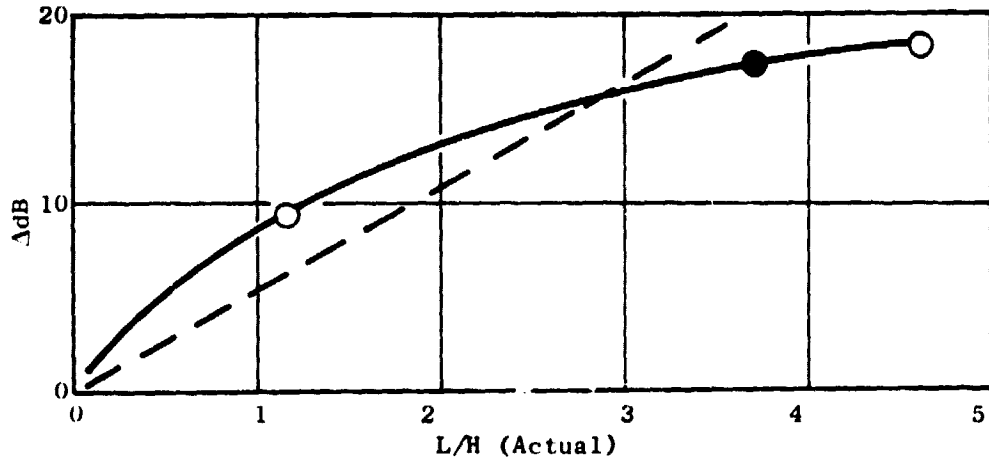
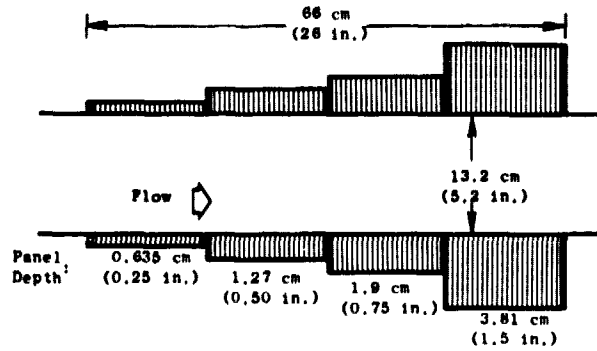


Figure 28. Suppression Vs. L/H (Actual).

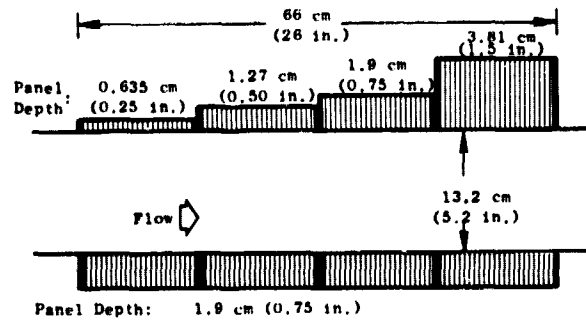
**Configuration No. 75-4**

- 12% Porosity
- Variable-Depth Treatment (Both Walls)



**Configuration No. 7**

- 12% Porosity
- Splitter Simulation



**Configuration No. 75-3**

- 12% Porosity
- Constant Depth, 1.9 cm (0.75 in.)

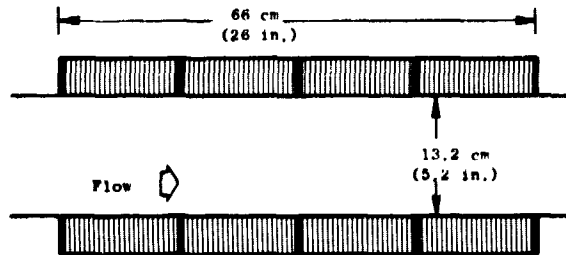


Figure 29. Variable-Depth, "Splitter Simulation", and Constant-Thickness Configurations.

ORIGINAL PAGE IS  
OF POOR QUALITY

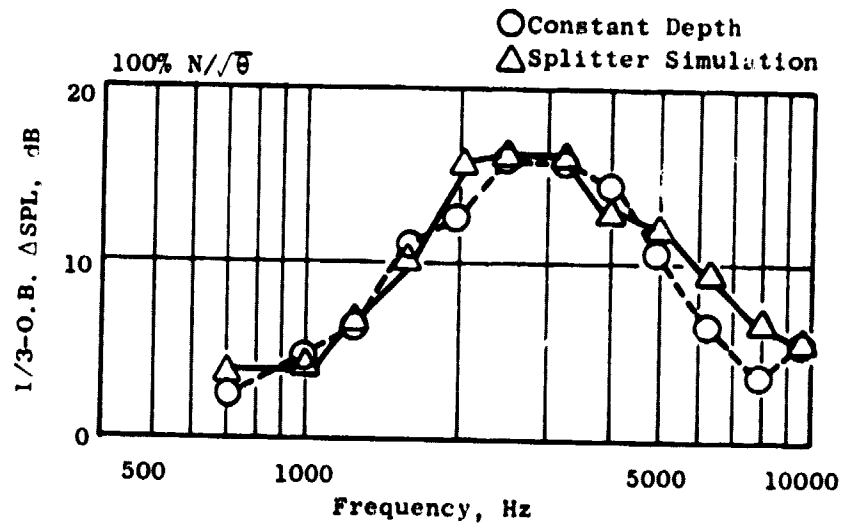
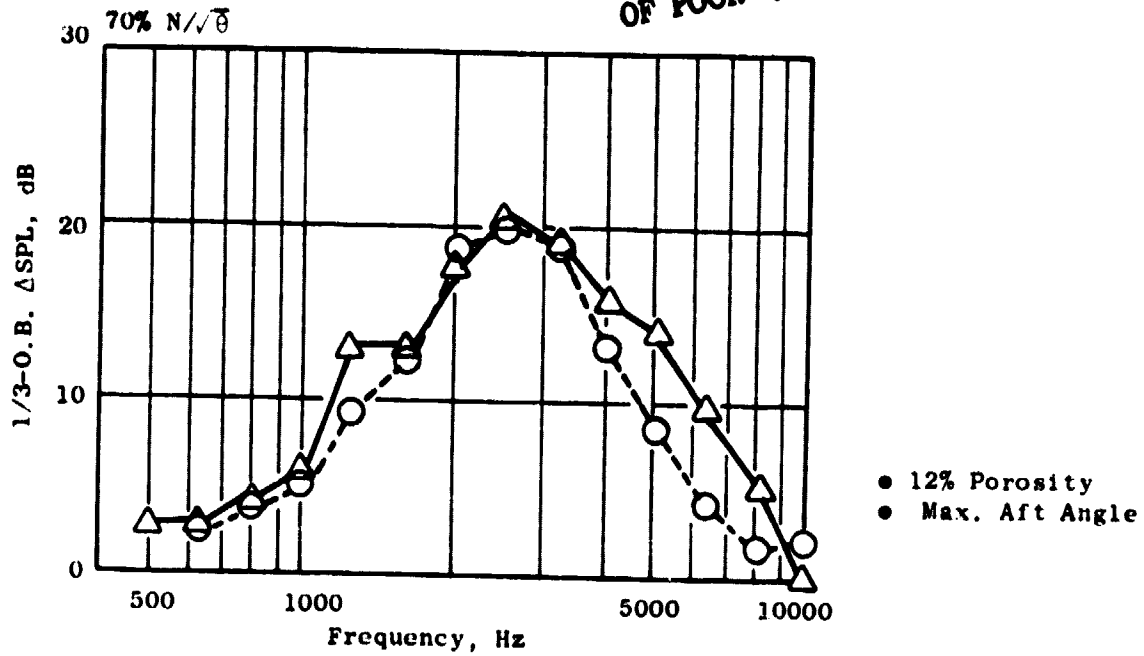
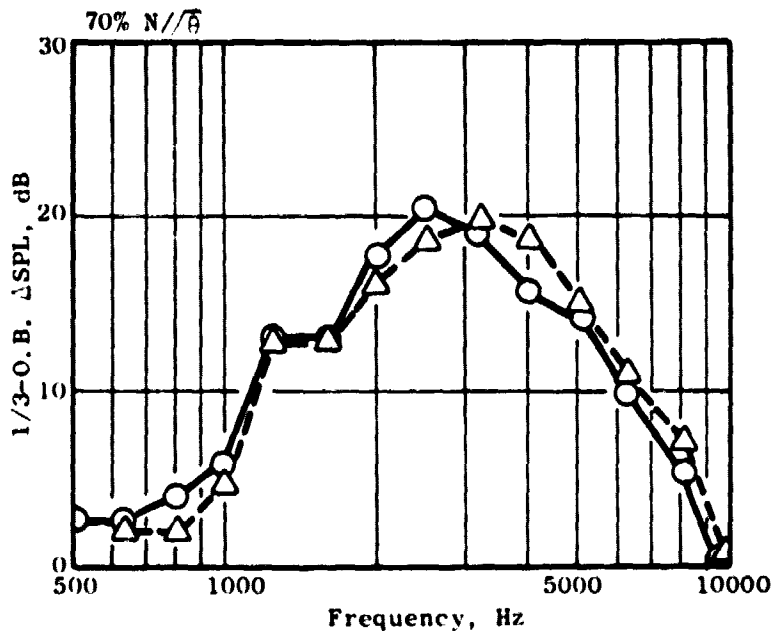


Figure 30. Splitter Simulation Vs. Constant-Depth Wall Treatment.



- Max. Aft Angle
- 12% Porosity
- Splitter Simulation
- △ Variable Depth

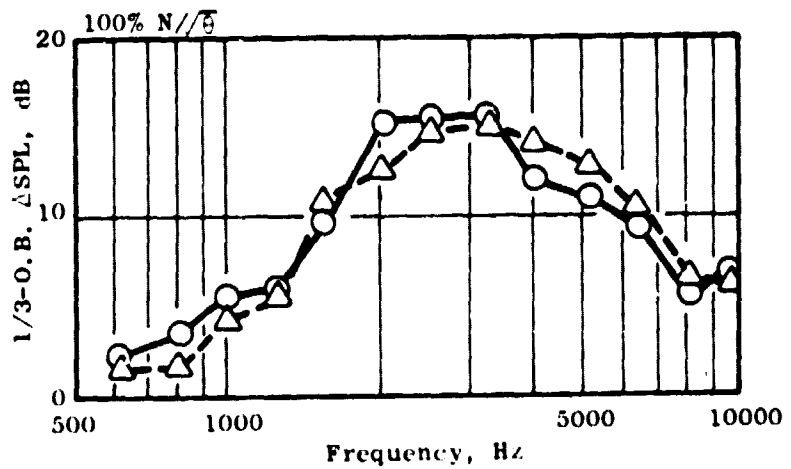


Figure 31. Splitter Simulation Compared to Treatment with Variable Depth on Both Walls.

### E. Rotor-OGV Treatment

Acoustic treatment was placed between the fan rotor and OGV's along the outer flowpath only. The type of treatment used was a single-degree-of-freedom (SDOF) resonator with the honeycomb cell slanted in the circumferential direction. The resonator cavity and faceplate dimensions of the design are as follows:

- Straight cavity depth 2.54cm (1.0 in.)
- Slant cell length 3.81cm (1.5 in.)
- 28% faceplate porosity
- Hole diameter 0.083 cm (0.033 in.)
- Faceplate thickness 0.048 cm (0.019 in.)

The panel was designed to have a tuning frequency of about 2000 Hz which is the blade passing frequency at 100%  $N/\sqrt{\theta}$ .

The rotor-OGV treatment was evaluated for two fan exhaust configurations. The first test was with an untreated fan exhaust downstream of the rotor-OGV treatment. The second was run with a fully treated fan exhaust configuration to determine if the suppression measured for the first configuration is additive with treatment in the fan exhaust.

The suppression for the configuration having rotor-OGV treatment without the fan exhaust treatment is given in Figure 32 for fan speeds of 70%  $N/\sqrt{\theta}$  and 100%  $N/\sqrt{\theta}$ . All data are for the maximum aft acoustic angle measured on a 5.18 (17 ft) arc. The data in Figure 32 show that the rotor-OGV treatment achieved both tone and broadband suppression. The tone suppression level increases from 2.5 dB at 70%  $N/\sqrt{\theta}$  to 5 dB at 100%  $N/\sqrt{\theta}$ . Broadband noise suppression varies from 0.5 to 2.0 dB over the measured frequency range for both fan speed points.

The fully treated fan exhaust configuration with rotor-OGV treatment suppression results are given in Figure 33 for 70%  $N/\sqrt{\theta}$  and 100%  $N/\sqrt{\theta}$  respectively. The fully treated fan exhaust had the following design:

- Variable-depth treatment with panel depths of 0.63 cm (0.25 in.), 1.27 cm (0.5 in.), 1.9 cm (0.75 in.), and 3.81 cm (1.5 in.) on both walls
- 12% porosity

Figure 33 gives the suppression spectra for the fully treated fan exhaust with and without the rotor-OGV treatment for 70%  $N/\sqrt{\theta}$ . The addition of the rotor-OGV treatment increased the tone broadband noise suppression levels. Broad-band suppression is from 1 to 3 dB and the tone suppression

### Honeycomb Slanted Circumferentially

● Max. Aft Angle

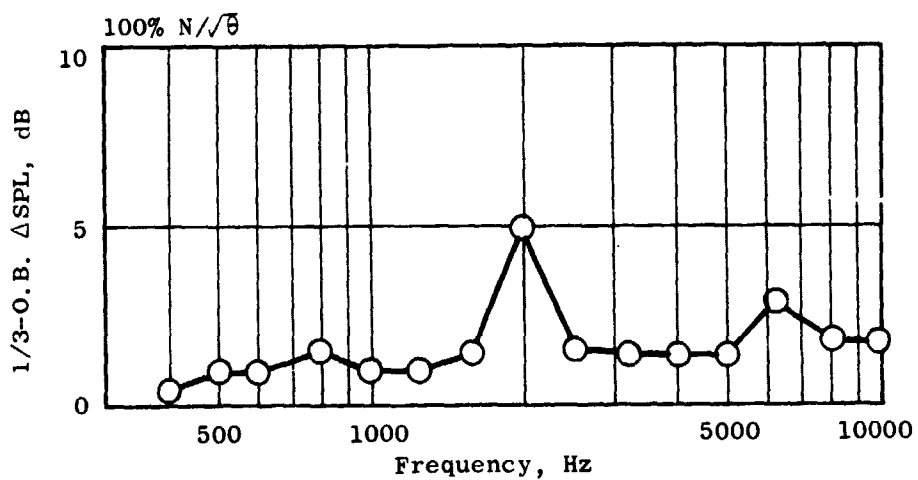
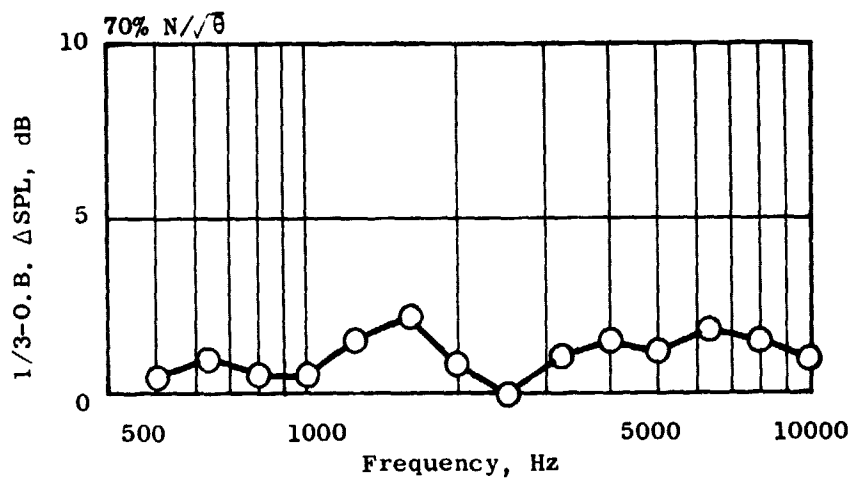
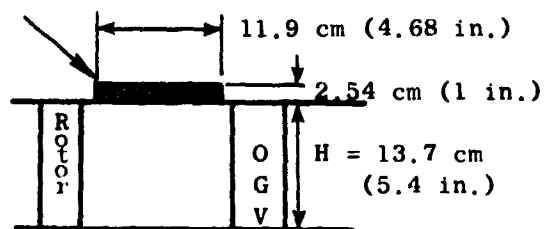


Figure 32. Measured Suppression for Rotor-OGV Treatment.



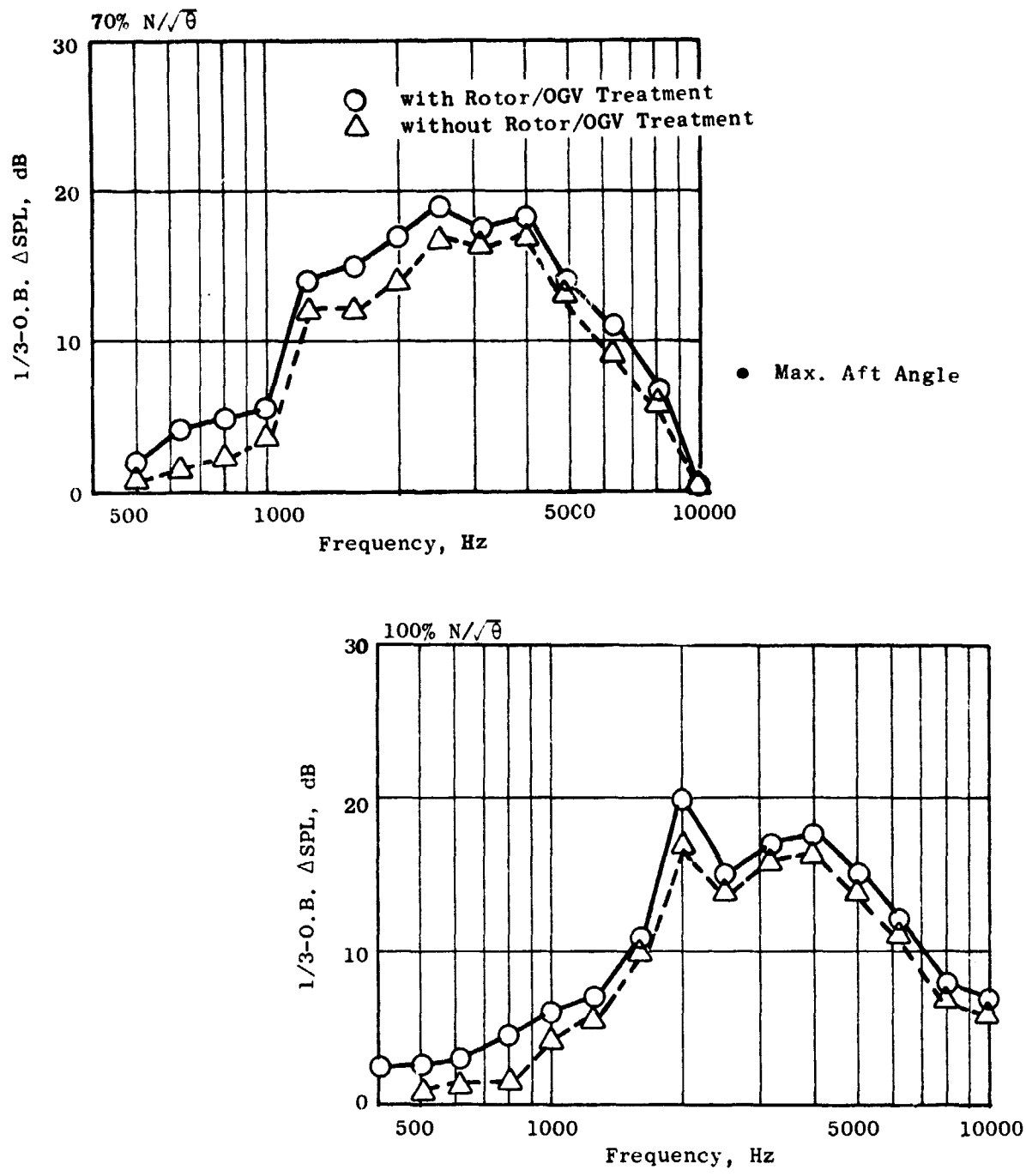


Figure 33. Measured Suppression of Fully Treated Fan Exhaust with and without Rotor-OGV Treatment.

level increased some 2 to 3 dB. Figure 33 also gives the suppression results for the 100%  $N/\sqrt{\theta}$  fan speed point. The broadband noise suppression level increased by 1 to 3 dB for the rotor-OGV treatment with about 3 dB additional tone suppression. Thus these data show the rotor-OGV treatment to be effective at both fan speeds and gives suppression even when combined with a fully treated exhaust configuration.

#### F. Variable-Depth Treatment Orientation

Rectangular duct data taken prior to the Rotor 55 fan exhaust tests gave indications that suppression levels were strongly influenced by axial treatment depth orientation for a high porosity (27%) faceplate design. The duct data showed suppression to be independent of axial orientation for a 12% faceplate.

Figure 34 shows a schematic of the variable-depth configurations that were run with thin/thick and thick/thin treatment orientation. The suppression for the configuration with 12% porosity is given in Figure 35 for 70%  $N/\sqrt{\theta}$  and 100%  $N/\sqrt{\theta}$  fan speeds. These data were taken at the maximum aft acoustic angle on a 5.18 m (17 ft) arc. The 70%  $N/\sqrt{\theta}$  fan speed point suppression results show that at frequencies greater than the peak attenuation frequency the thin/thick treatment sequence gives higher suppression. Suppression at frequencies below the peak attenuation is not influenced by the treatment sequence. The same comparison of data at 100%  $N/\sqrt{\theta}$  fan speed shows less difference in suppression over the entire frequency range.

Figure 36 gives suppression for the configuration with 27% faceplate porosity. The results are compared at fan speeds of 70% and 100%  $N/\sqrt{\theta}$ . The results in Figure 36 for 100%  $N/\sqrt{\theta}$  show a small advantage at higher frequencies for the thin/thick configuration, while at 70%  $N/\sqrt{\theta}$  the advantage is greater. The low frequencies show no difference in the suppression levels at 100%  $N/\sqrt{\theta}$  and a slight advantage to the thick/thin orientation at 70%  $N/\sqrt{\theta}$ .

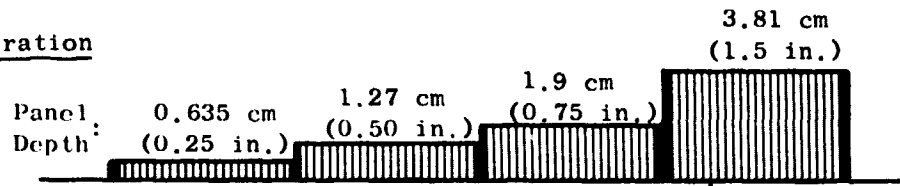
Thus the Rotor 55 data show the same trend as the duct data, in that the sensitivity in suppression with respect to treatment arrangement is more notable for the high porosity (27%) design. However, the difference in suppression level as measured in Rotor 55 is much less than prior duct data had indicated. The total suppression level obtained from the 27% porosity thin/thick configuration is poor when compared with other configurations having either constant 12% porosity, or a mixed porosity design. Thus for the optimum design of the configurations tested here, suppression seems to be independent of the treatment placement. Therefore, in the QCSEE engine design, the thick-to-thin orientation is used since the engine nacelle can accommodate this arrangement more readily.

#### G. Slant Cell Treatment

The application of slant cells in engine treatment designs is important because they act effectively in giving low frequency tuning in areas where thicker straight cell panel depths are not available. Three tests were run to demonstrate this.

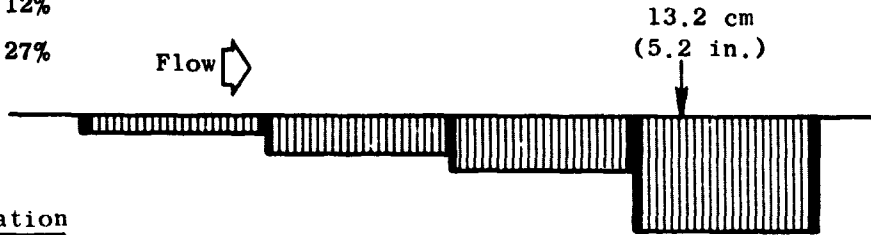
ORIGINAL PAGE IS  
OF POOR QUALITY

● Thin/Thick Configuration

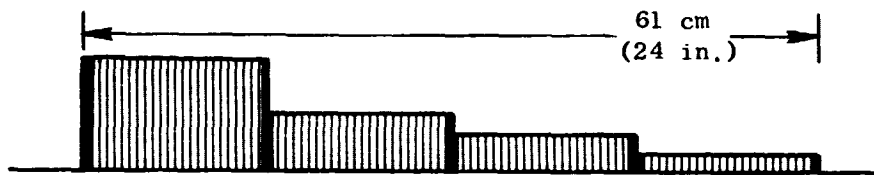


● Configuration Porosity

75-2	12%
8	27%



● Thick/Thin Configuration



● Configuration Porosity

26	12%
75-5	27%

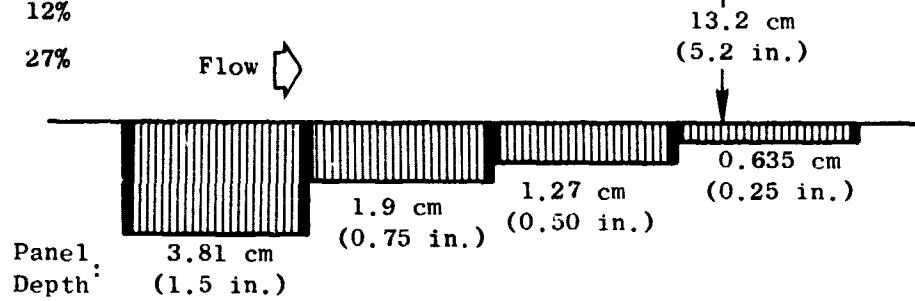


Figure 34. Thin/Thick Vs. Thick/Thin Variable-Depth Treatment Configurations.

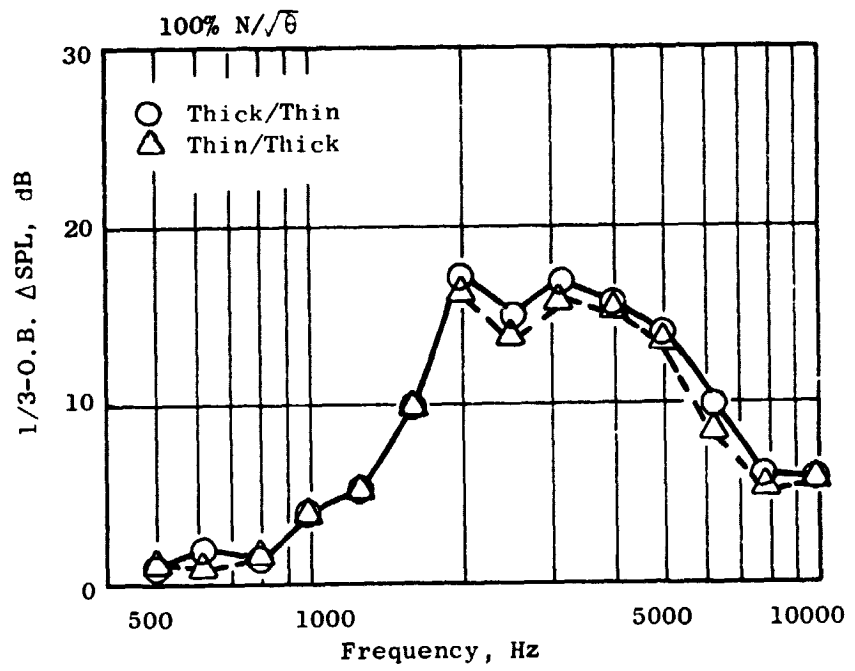
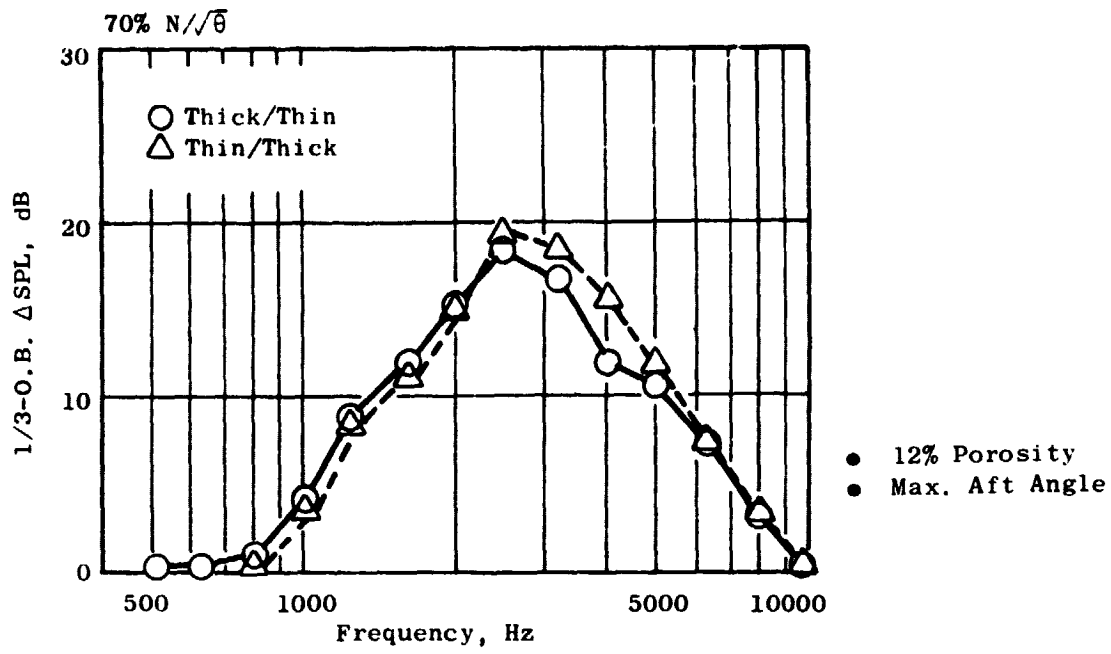
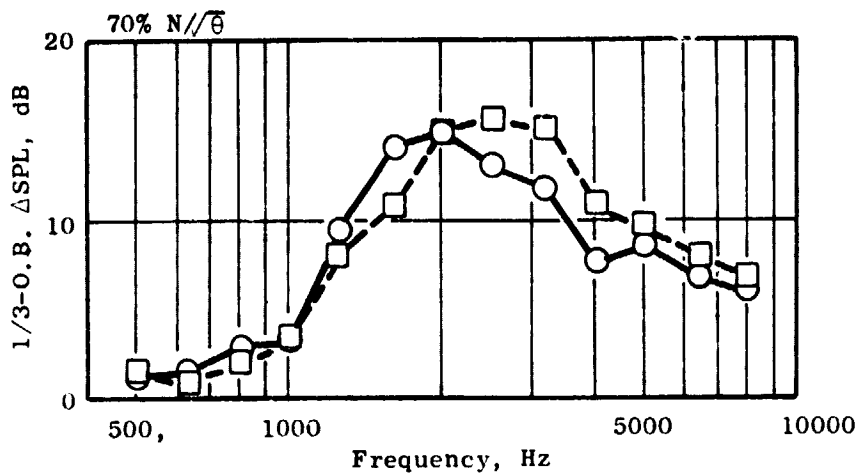


Figure 35. Effect of Treatment Orientation on Suppression.



● Max. Aft Angle  
 ● 27% Porosity

○ Thick to Thin  
 □ Thin to Thick

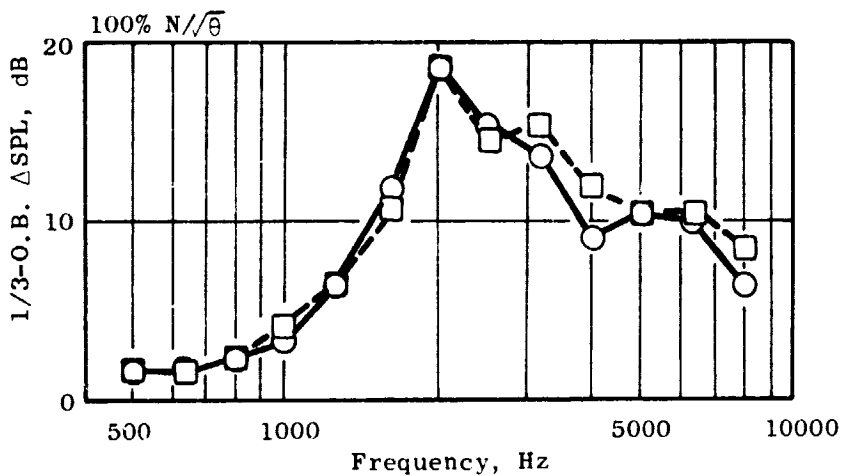


Figure 36. Suppression Spectra for Thin/Thick Vs. Thick/Thin Treatment.

- Slant cells: 2.54 cm (1.0 in.) panel depth with a slant distance of 3.86 cm (1.52 in.)
- 2.54 cm (1.0 in.) panel with a straight cell geometry
- 3.81 cm (1.5 in.) panel with a straight cell geometry

Figure 37 shows the treatment configurations. All the panels have a treatment length of 15.24 cm (6.0 in.), giving a treated L/H value of 1.15. The faceplate porosity is 27% for all configurations. The design frequencies are:

- 2000 Hz for the slant cell and 3.81 cm (1.5 in.) straight cell
- 2500 Hz for the 2.54 cm (1.0 in.) straight cell

Figure 38 gives the suppression spectra for the slant cell, and for the 2.54 cm (1.0 in.) straight cell resonator at fan speeds of 70 and 100%  $N/\sqrt{\theta}$ . At 70 and 100%  $N/\sqrt{\theta}$ , the slant cell resonator gives higher peak suppression than does the 2.54 cm (1.0 in.) straight cell treatment. The slant cell peak suppression occurs in the 2000 Hz 1/3-octave band at both fan speeds in Figure 38, and although not shown the slant cell peaks at 2000 Hz at 80 and 90%  $N/\sqrt{\theta}$ . Predicted straight cell peak suppression would be in the 2500 Hz 1/3-octave band. The measured straight cell suppression peaks at 2000 and 2500 Hz for 70 and 100%  $N/\sqrt{\theta}$ , respectively. Data at 80 and 90%  $N/\sqrt{\theta}$  indicate a broad peak at both 2000 and 2500 Hz. Why this straight cell peak does not agree with predictions at lower fan speeds is not fully understood at this time. However, the main point of the comparisons in Figure 38 is that the slant cell treatment consistently peaks at 2000 Hz.

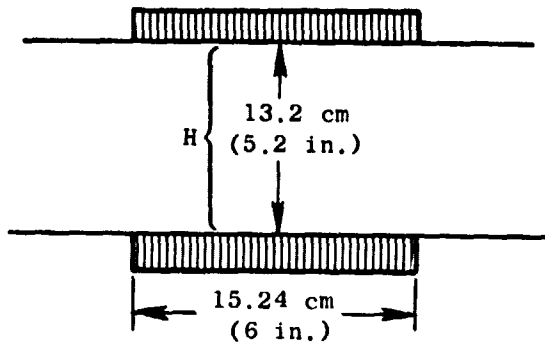
Similar data for the slant cell and the 3.81 cm (1.5 in.) straight cell are given in Figure 39. The peak attenuation for the slant and straight cell treatment occurs at 2000 Hz for the 70%  $N/\sqrt{\theta}$  fan speed. The peak suppression values are equal, each giving about 12 to 13 dB suppression. The bandwidths are essentially the same above peak frequency; however, the straight cell gives somewhat better bandwidth at lower frequencies. The peak frequency is also at 2000 Hz for both panels for the 100%  $N/\sqrt{\theta}$  fan speed. Here the peak suppression for the straight cell is  $\approx 2$  dB greater than for the slant cell.

These results indicate that the slant cell geometry enables tuning to a lower frequency for a fixed panel depth. Thus, this concept can be utilized for achieving suppression at lower frequencies where the cavity depth is limited.

The acoustic reactance for a SDOF acoustic liner is given in the following equation:

SDOF Straight Cell Treatment Configuration 75-1J

- 2.54 cm (1 in.) and 3.81 cm (1.5 in.)  
Deep Panel
- 27% Porosity
- $L/H = 1.15$



ORIGINAL PAGE IS  
OF POOR QUALITY

SDOF Slant Cell Treatment Configuration 75-1E

- 27% Porosity
- $L/H = 1.15$
- Honeycomb Slanted Circumferentially

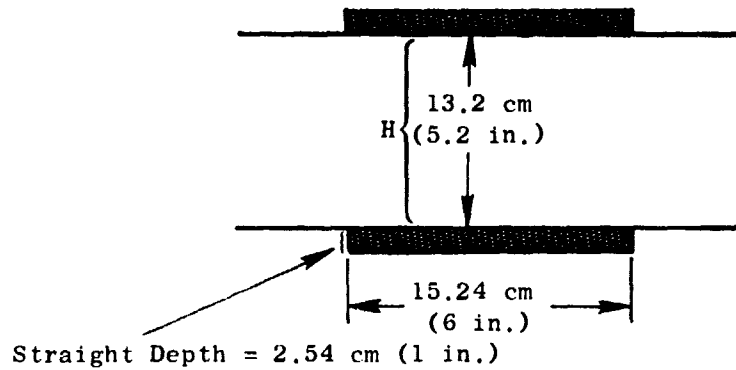
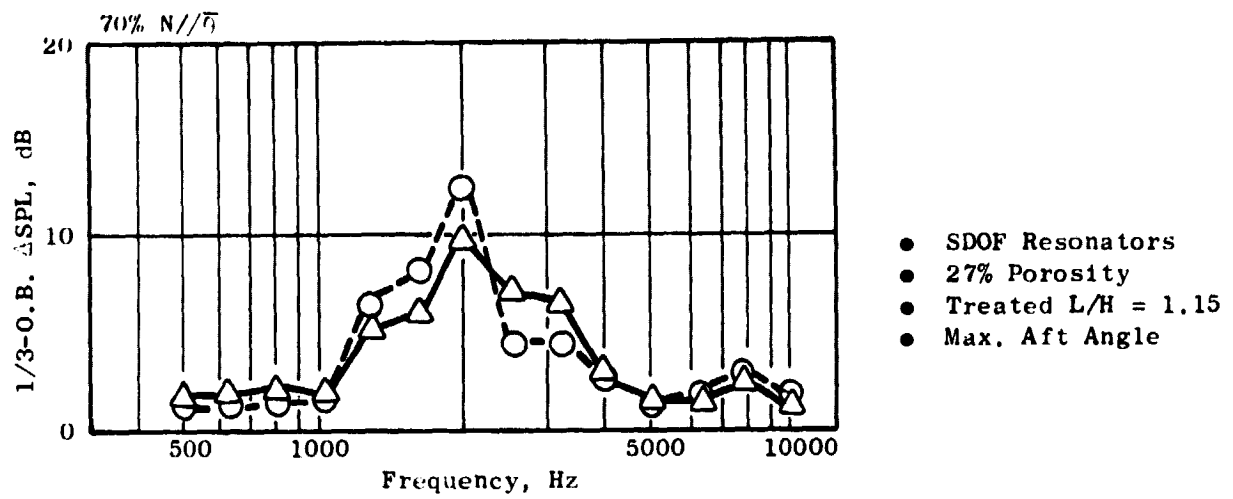


Figure 37. Straight Cell and Slant Cell Treatment Configurations.



○ 2.54 cm (1 in.) Slant Cell  
 △ 2.54 cm (1 in.) Straight Cell

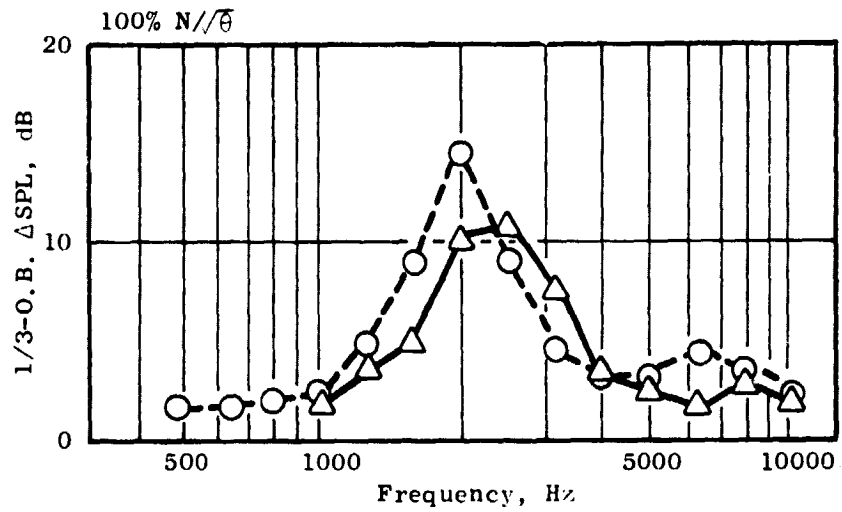
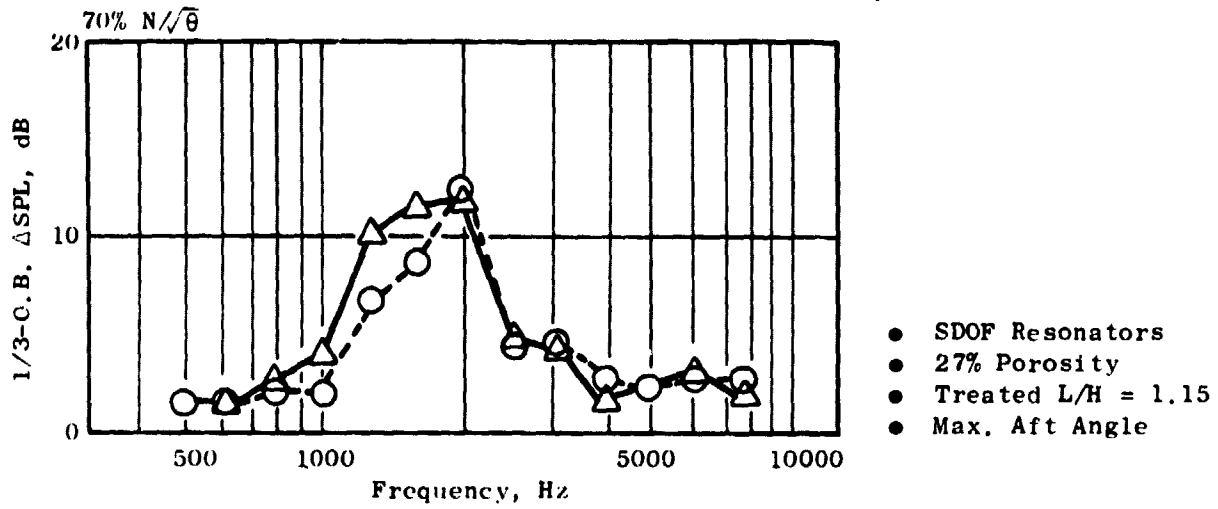


Figure 38. Suppression Spectra for Slant Cell and 2.54 cm (1 in.) Straight Cell.



ORIGINAL PAGE IS  
OF POOR QUALITY



○ 2.54 cm (1 in.) Slant Cell  
△ 3.81 cm (1.5 in.) Straight Cell

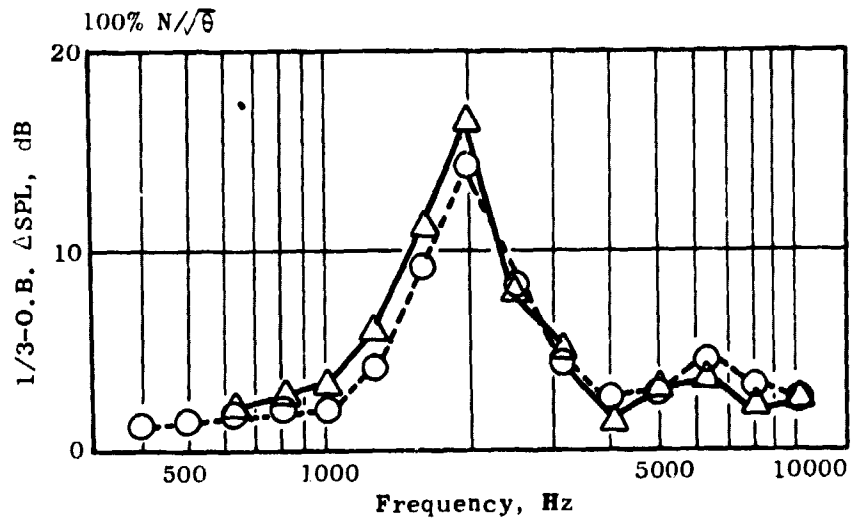


Figure 39. Suppression Spectra for Slant Cell and 3.8 cm (1.5 in.) Straight Cell.

$$\left(\frac{X}{\rho c}\right)_{\text{panel}} = \frac{2\pi t'}{\sigma \lambda} - \frac{\cot 2\pi \ell}{\lambda}$$

where  $t'$  = faceplate thickness +  $\alpha d$

$d$  = hole diameter

$\sigma$  = faceplate porosity

$\ell$  = cavity depth of honeycomb

$\lambda$  = wavelength of sound

$\alpha$  = a constant depending upon duct Mach number

For the faceplate porosity used in these tests both the slant cell and the straight cell have reactances dominated by the  $(\cot 2\pi \ell / \lambda)$  term of the reactance equation. The advantage that the slant cell treatment has is that the length term,  $\ell$ , appears to be closer to the slant height rather than the panel thickness. In the slant cell the maximum length is approximately 3.81 cm (1.5 in.). Therefore, the panel tuning frequency is the same as for the 3.81 cm (1.5 in.) straight cell configuration.

#### H. Treatment Regenerated Noise

One of the objectives in the Aft Suppression Test series was to determine levels of treatment-regenerated flow noise by varying the Mach number in the aft duct. On highly suppressed fan exhaust ducts there is a potential of meeting a noise floor which limits the achievable suppression. This floor is thought to be created by flow over the treatment surfaces and is a function of the duct Mach number. Accordingly, the duct Mach number was varied for these tests over a range representative of an engine to see if suppression decreased at Mach numbers above 0.4. The configurations involved are shown in Figure 40 and provided three Mach numbers at a given fan speed. Lowest Mach numbers were achieved with the nominal nozzle configuration without a splitter installed. Installation of the splitter increased the Mach numbers with a further increase to the highest Mach numbers achieved by opening the nozzle.

The suppression levels achieved with the three Mach number levels are shown in Figure 41 at 100% fan speed for 1.94 and 2.13 radians (111° and 122°). An average duct Mach number for the configurations is shown below:

ORIGINAL PAGE IS  
OF POOR QUALITY

- HARD ROTOR-OGV
- TREATMENT L/H = 4.6

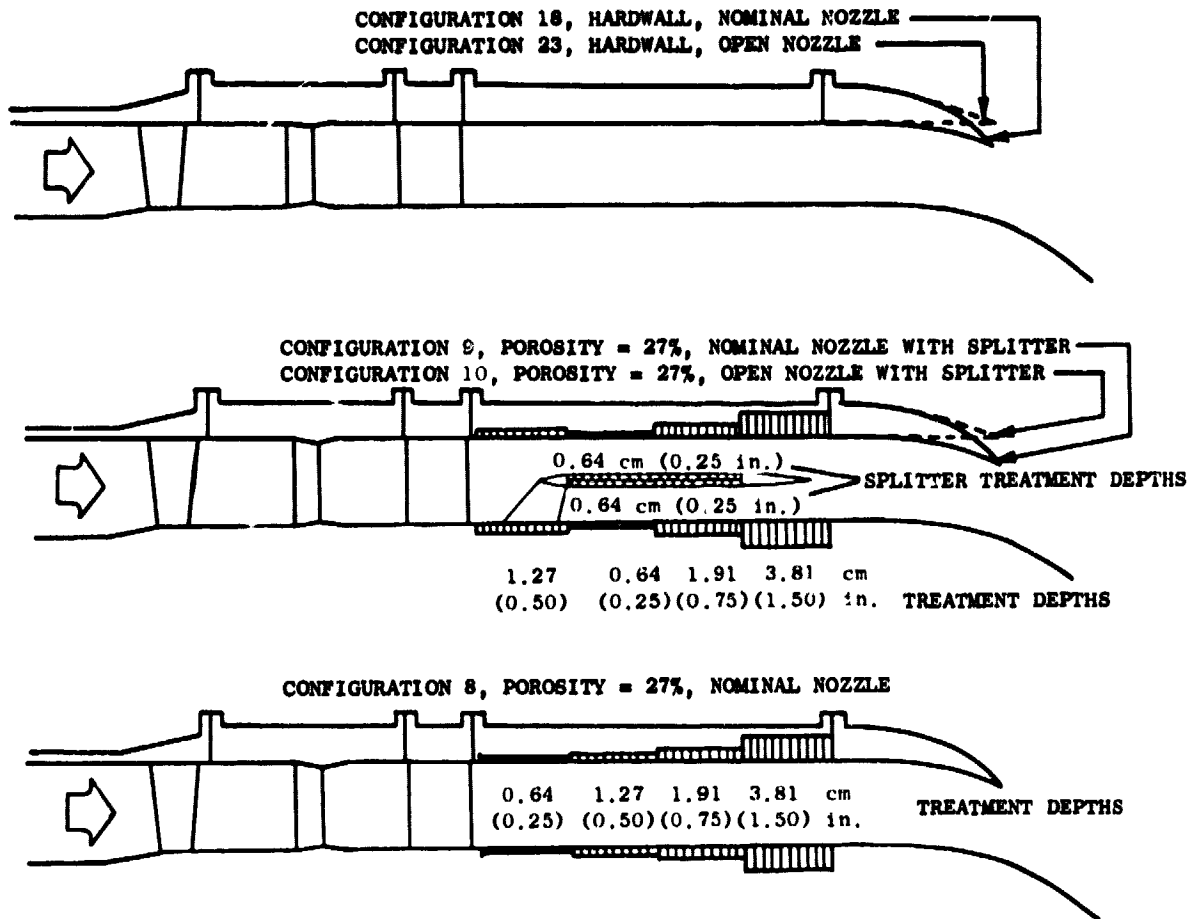
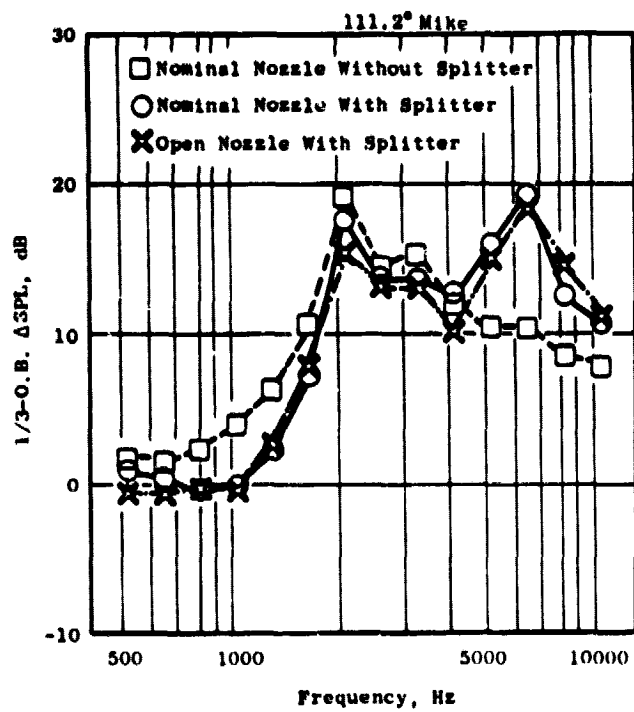


Figure 40. Treatment Regenerated Flow Noise Configurations.



● 5.2m (17 feet) Arc  
● 100% Fan Speed

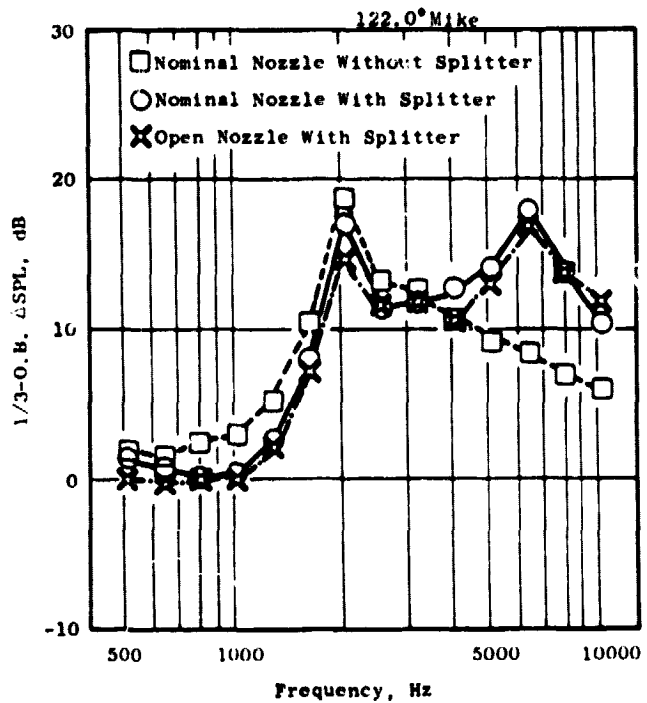


Figure 41. Aft Suppression Spectra Change with Duct Mach Number Change.

<u>Configuration</u>	<u>M<sub>Duct</sub></u>
Nominal nozzle without splitter	0.40
Nominal nozzle with splitter - outer channel	0.50
- inner channel	0.46
Open nozzle with splitter - outer channel	0.56
- inner channel	0.52

Looking at the suppression levels we see that installation of the splitter resulted in an increase in suppression peaking at 6300 Hz, which was the tuning frequency of the splitter. There is a degradation in suppression below 3150 Hz. However, whether this is due to a flow noise floor or a decrease in bandwidth cannot be established. Opening the nozzle with the splitter installed did not result in any significant change in the suppression levels. One would expect a decrease in suppression if a treatment-regenerated noise floor were being reached at higher Mach numbers.

Although no definite flow noise floor was established with these tests, they can serve to provide an upper limit on the levels estimated for a full-scale engine. By assuming that the measured suppressed level is an upper limit of the flow noise, and scaling on a 10 log (treatment area), one can estimate the impact of this assumed flow noise on a full size engine.

## SECTION V

### IN-DUCT MEASUREMENTS

In addition to the **far-field results which have been discussed, in-duct** measurements were made to aid in understanding the results. A sound separation probe which had two flush-mounted sensors was used to separate the broadband noise from turbulence noise. The same probe was used in conjunction with a wall-mounted sensor to determine radial modal characteristics of the acoustic pressure pattern propagating in the duct.

Hot film wake surveys were taken on the vehicle between the rotor and OGV to provide information on the rotor wakes.

#### A. Sound Separation Probe

General Electric is developing an acoustic discrimination technique for separation of broadband sound from turbulence in duct probe measurements. This technique incorporates a new type probe referred to as a "sound separation probe," rather than the standard waveguide probe, to acquire the data for the discrimination analysis. A photograph of the probe is shown in Figure 42.

The sound separation probe has two **flush-mounted** pressure sensors in the probe end that provide a flat frequency response as shown in **Figure 43**. As a result of the flush mounting and flat frequency response the relative phase shift between the two sensor signals can be expected to be minimal throughout the frequency range of 0 Hz to 10000 Hz.

With the probe aligned axially with the flow, cross correlation of the signals from the two sensors will provide a cross correlogram with separate peaks for each of the components of the broadband signal (see Figure 44). The slower moving turbulence provides a peak at the longest time delay (1), the faster sound moving with the flow makes a peak at the shortest time delay (2), while the sound moving against the flow gives a peak at "negative time delay" (3).

The acoustic discrimination technique is applicable to broadband random signals. This requires that the tone level be removed prior to the cross-correlation computation so that the periodicity from the tones does not contaminate the cross-correlograms as shown in Figure 45. The cross spectrum between the two sensor signals is always computed prior to Fourier transformation to the cross correlation. Interpolation of the levels in the real (co) and imaginary (quad) parts of the cross spectrum with frequency in the region of the tones leaves the broadband random portion, which transforms into the familiar **two- or three-peaked cross correlation**.

There are in general three peaks near the zero axis in the cross correlogram. For broadband measurements in a flowing duct, the peaks can be identified as (1) turbulence generated by the flowing air upstream of the

ORIGINAL PAGE IS  
OF POOR QUALITY

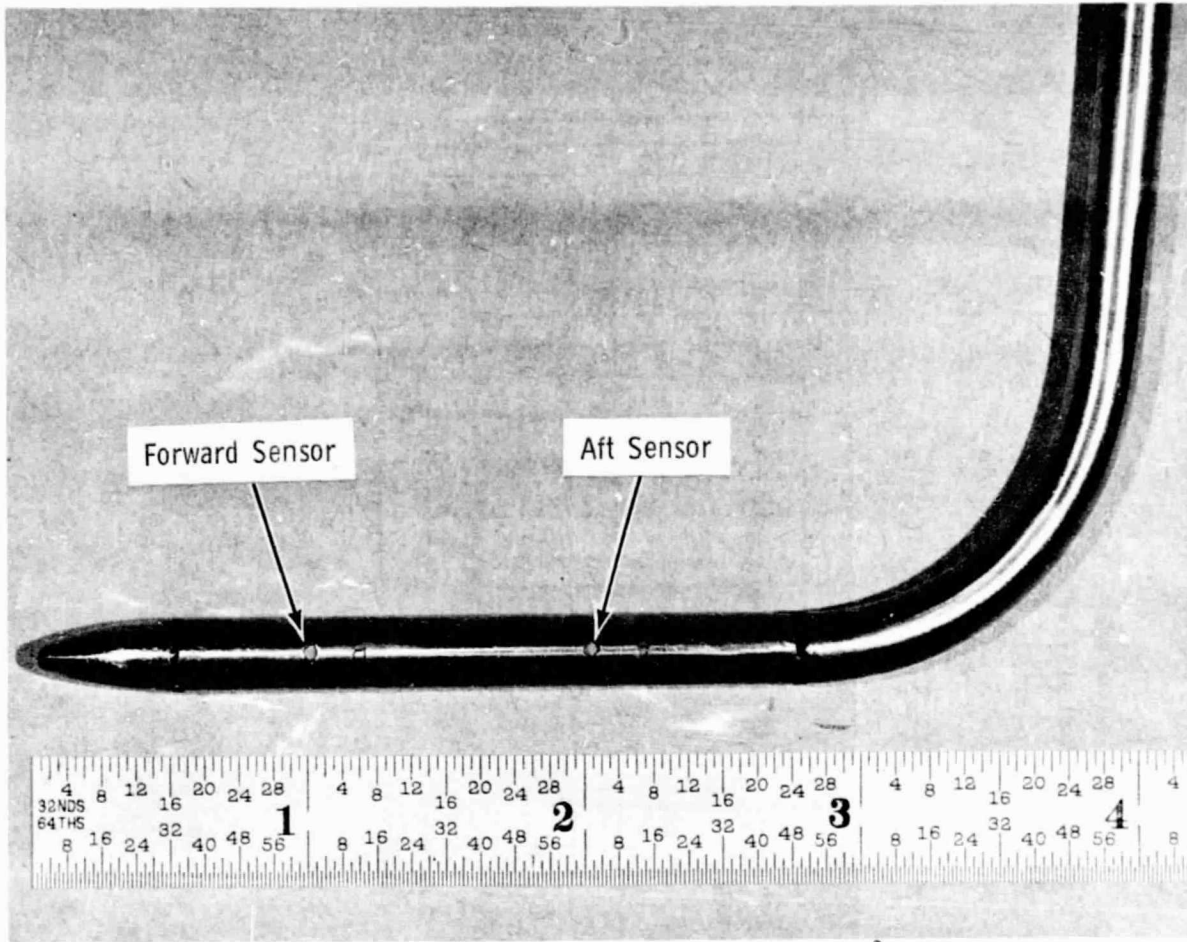


Figure 42. Sound Separation Probe (C26731).

Frequency Response  
 .64 cm (.25 in.) Acoustic Probe Dual Kulite

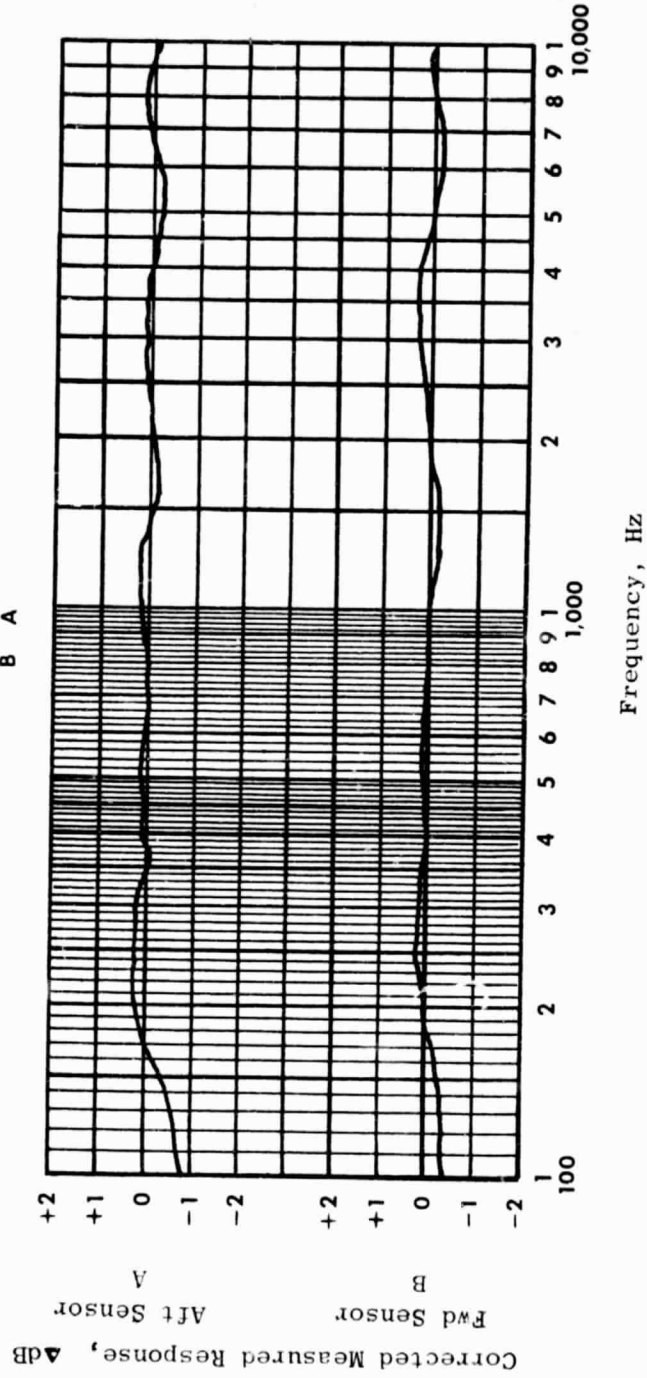
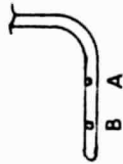


Figure 43. Frequency Response of Sensors in Sound Separation Probe.



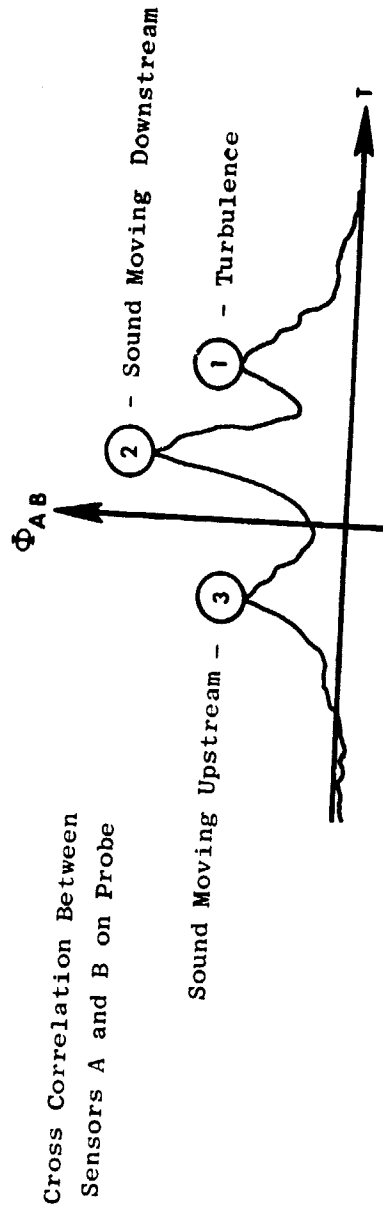
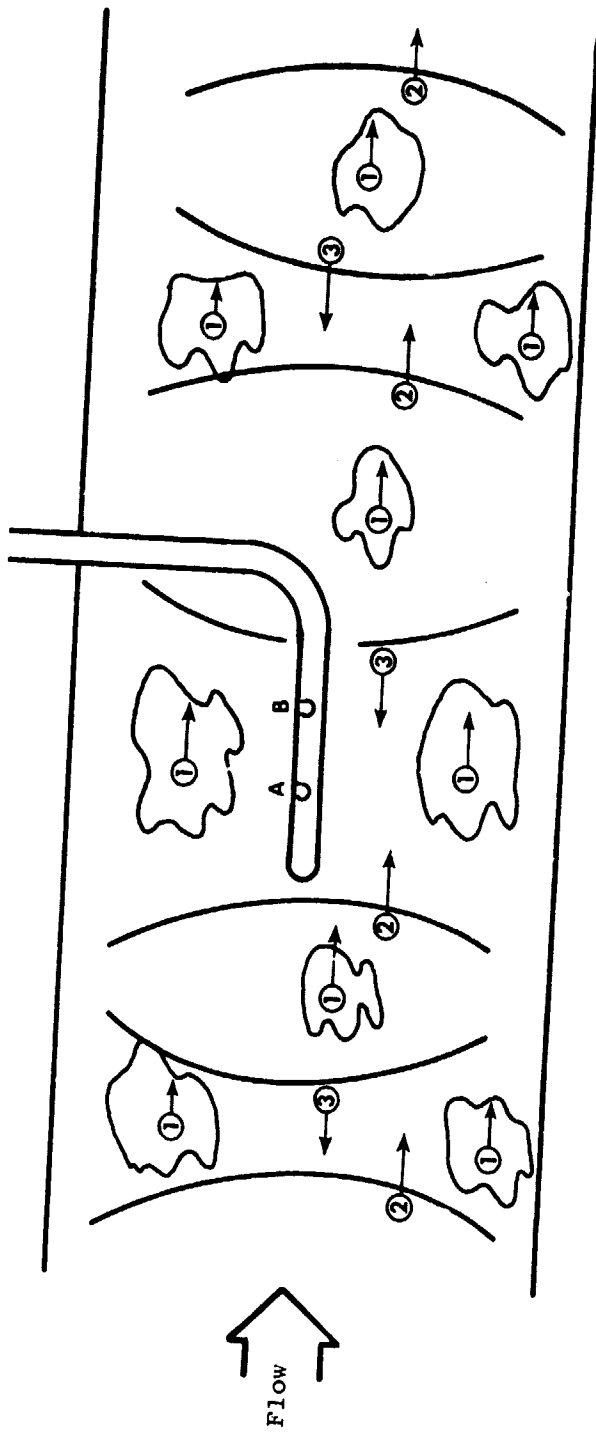


Figure 44. Typical Cross Correlation of Signals from the Sound Separation Probe.

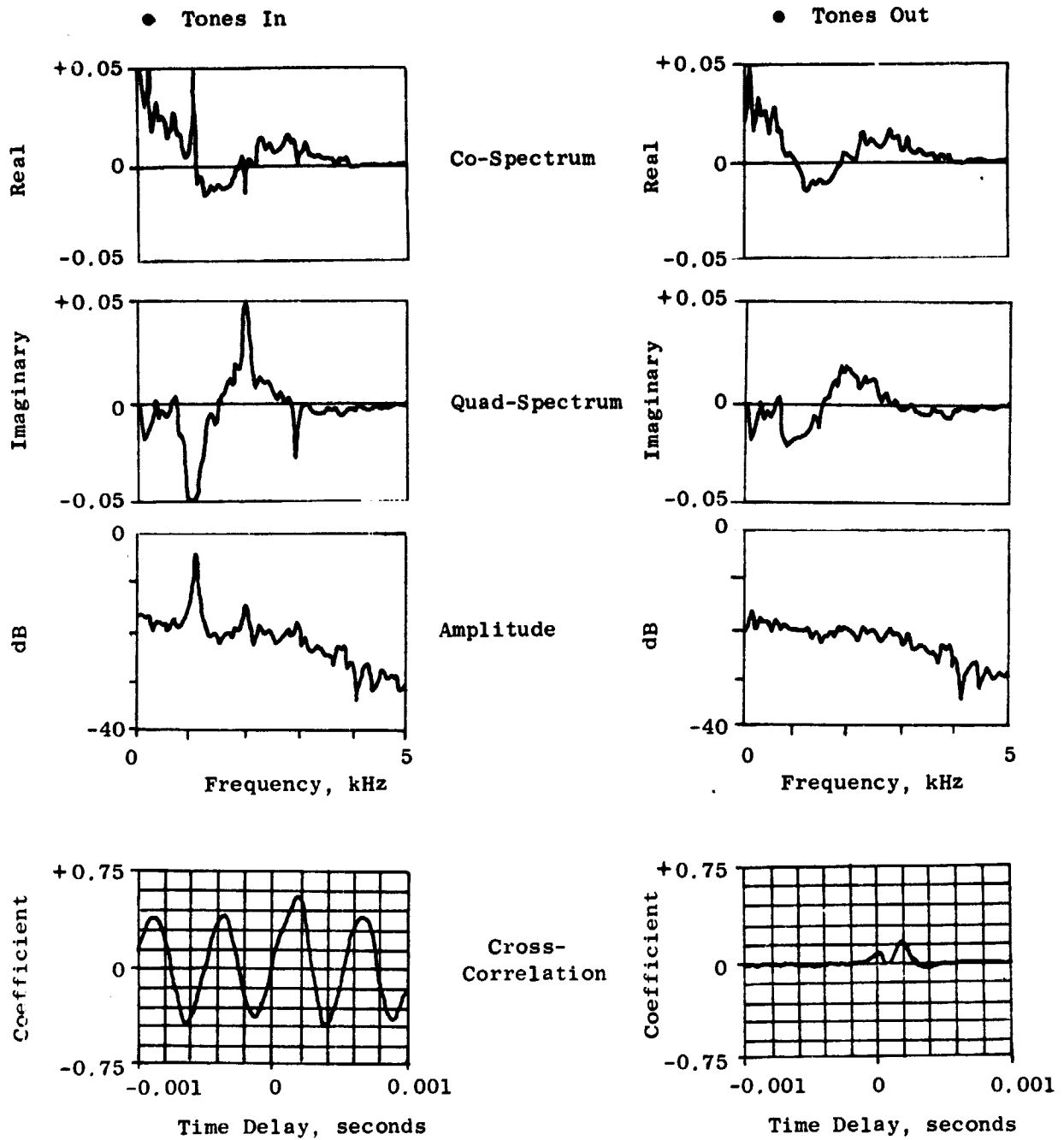


Figure 45. Tone Removal by Interpolation of Cross Spectrum.

ORIGINAL PAGE IS  
OF POOR QUALITY

probe, (2) sound generated by rotor/stator sources upstream of the probe, and (3) sound reflected from a location downstream of the probe. It is assumed the three sources of pressure fluctuations are independent, since the turbulence and sound are from different interactions and the reflected sound has lost its identity due to being broadband, random, and travelling through the turbulent medium.

In order to compute the overall level of the broadband components of the signal, use is made of the fact that the zero time delay value of the auto-correlation of any signal is equal to its mean square value. Since the sensors are close together and the time delays are small, the assumption that the mean square value of each component of the signal is equal to the peak value of the cross correlation is valid. Therefore, since the signal sources are independent, solution of the following simultaneous equations using the nomenclature of Figure 44 provides the sound level of each signal component:

$$P_1^2 + P_2^2 + P_3^2 = P^2$$

$$\frac{\phi_{AB_3}}{\phi_{AB_2}} = \frac{P_3^2}{P_2^2}, \quad \frac{\phi_{AB_2}}{\phi_{AB_1}} = \frac{P_2^2}{P_1^2}$$

$$P_2^2 = P^2 / \left[ 1 + \frac{\phi_{AB_3}}{\phi_{AB_2}} + \frac{\phi_{AB_1}}{\phi_{AB_2}} \right]$$

The sound separation technique will eventually compute the frequency spectra of the sound propagating downstream with the reflected sound and turbulence removed. The current status of the development does this for the overall level, which is useful for determining if the probe-measured data are predominately turbulence or sound. To emphasize this point the actual data from the tests will be discussed. These data were recorded for four immersions each, at the discharge of the struts ahead of the treatment sections, and at the end of the treatment sections upstream of the nozzle. The data analyzed for discussion in this report were at 100% speed from Configurations 18, 7, and 8. (See Table II.) The nozzle probe data were used to determine the treatment suppression in comparison with the far-field results.

The broadband cross-correlations for Configurations 18, 7, and 8 are shown in Figures 46, 47, and 48. The correlation levels are nondimensional and cannot be compared with one another until the fluctuating pressure level factors are applied. Care must be exercised in analysis of cross-correlograms of broadband data because the filtered data can make the cross-correlation have lobes close to the peak due to a phenomenon called "ringing". This effect is a function of the filter bandwidth (10 kHz) and the time between

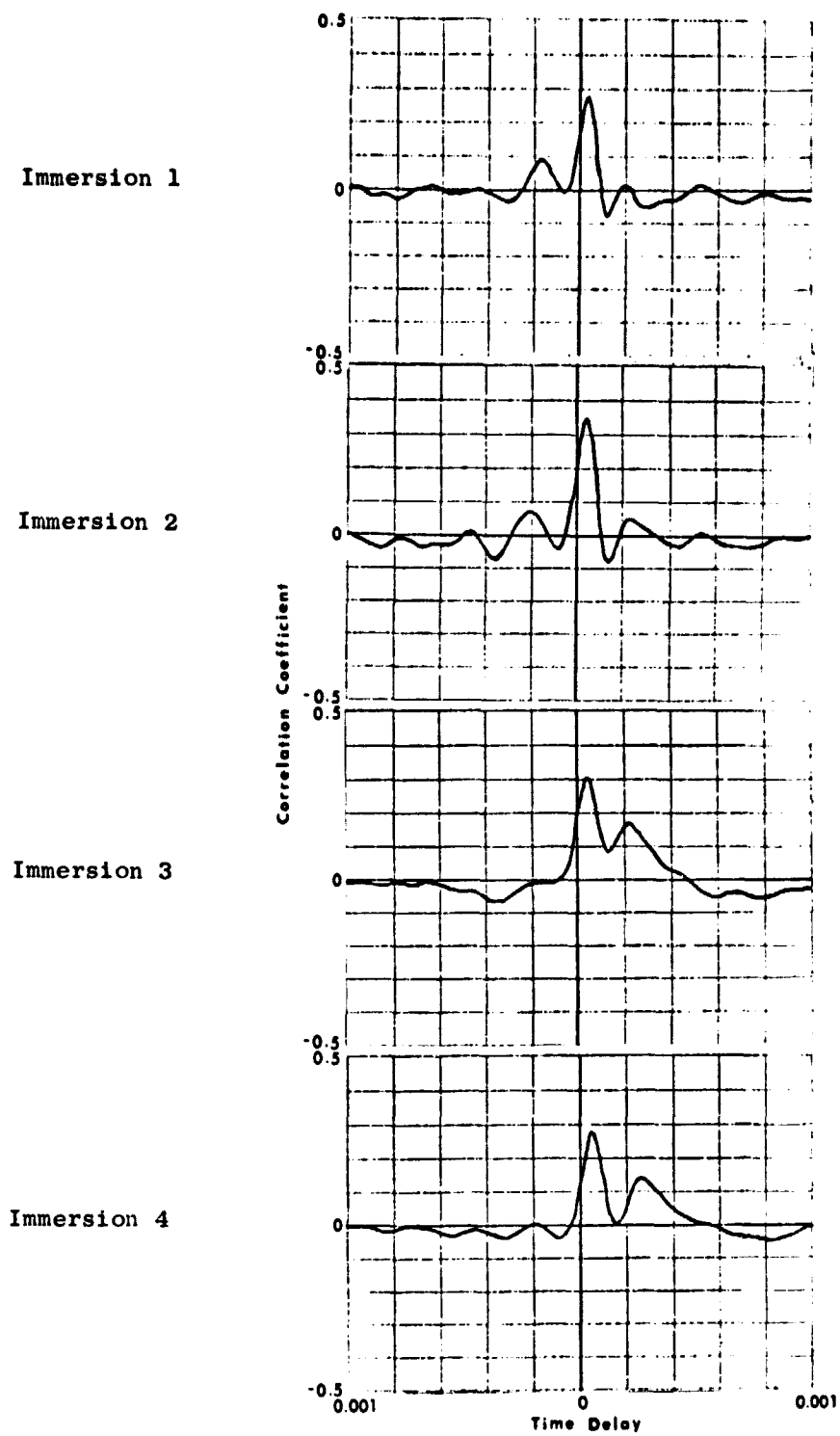


Figure 46. Correlations from Sound Separation Probe - Hardwall Configuration (18).

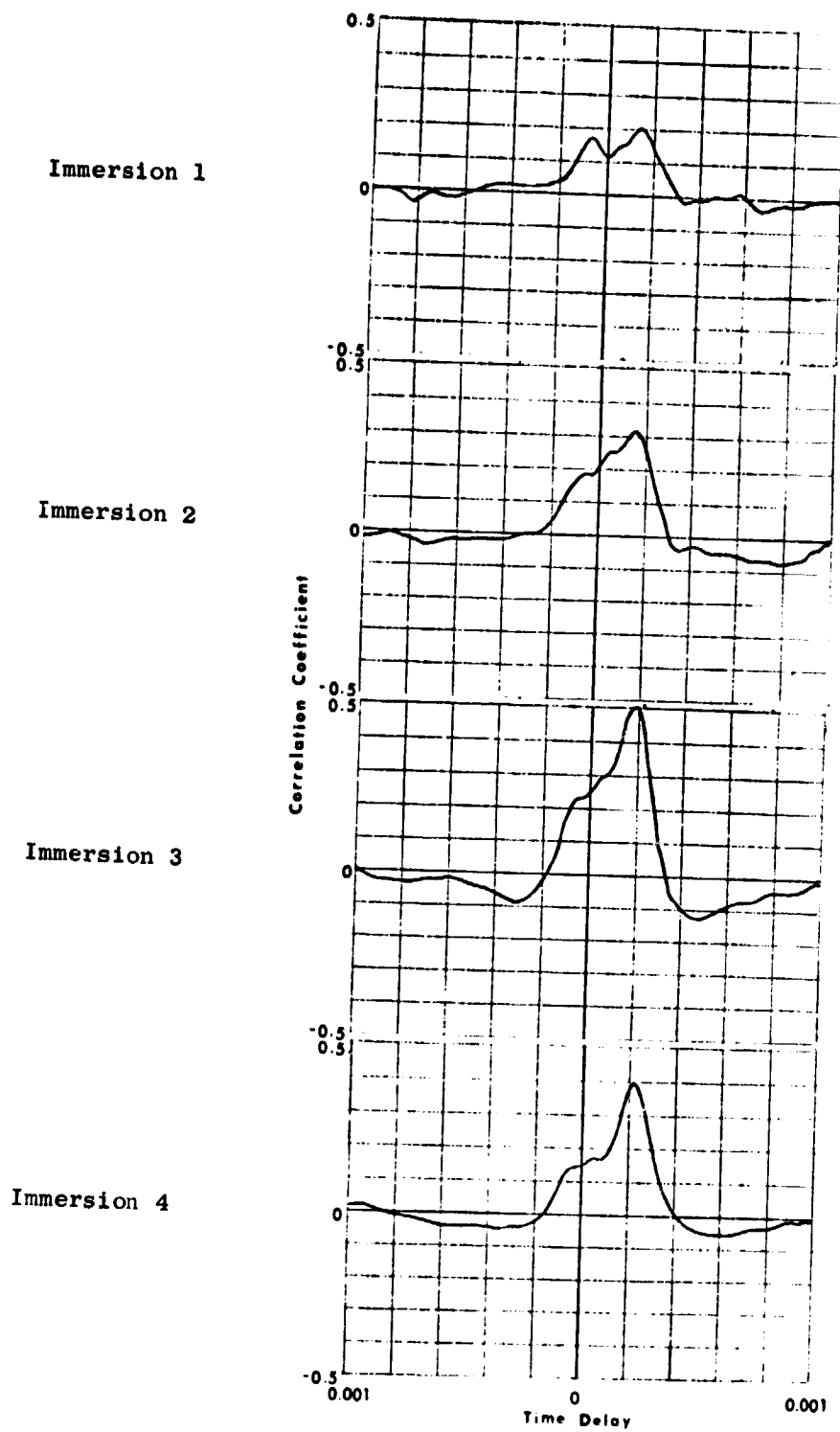


Figure 47. Correlations from Sound Separation Probe - 12 Percent Thin-to-Thick Configuration (7).

ORIGINAL PAGE IS  
OF POOR QUALITY

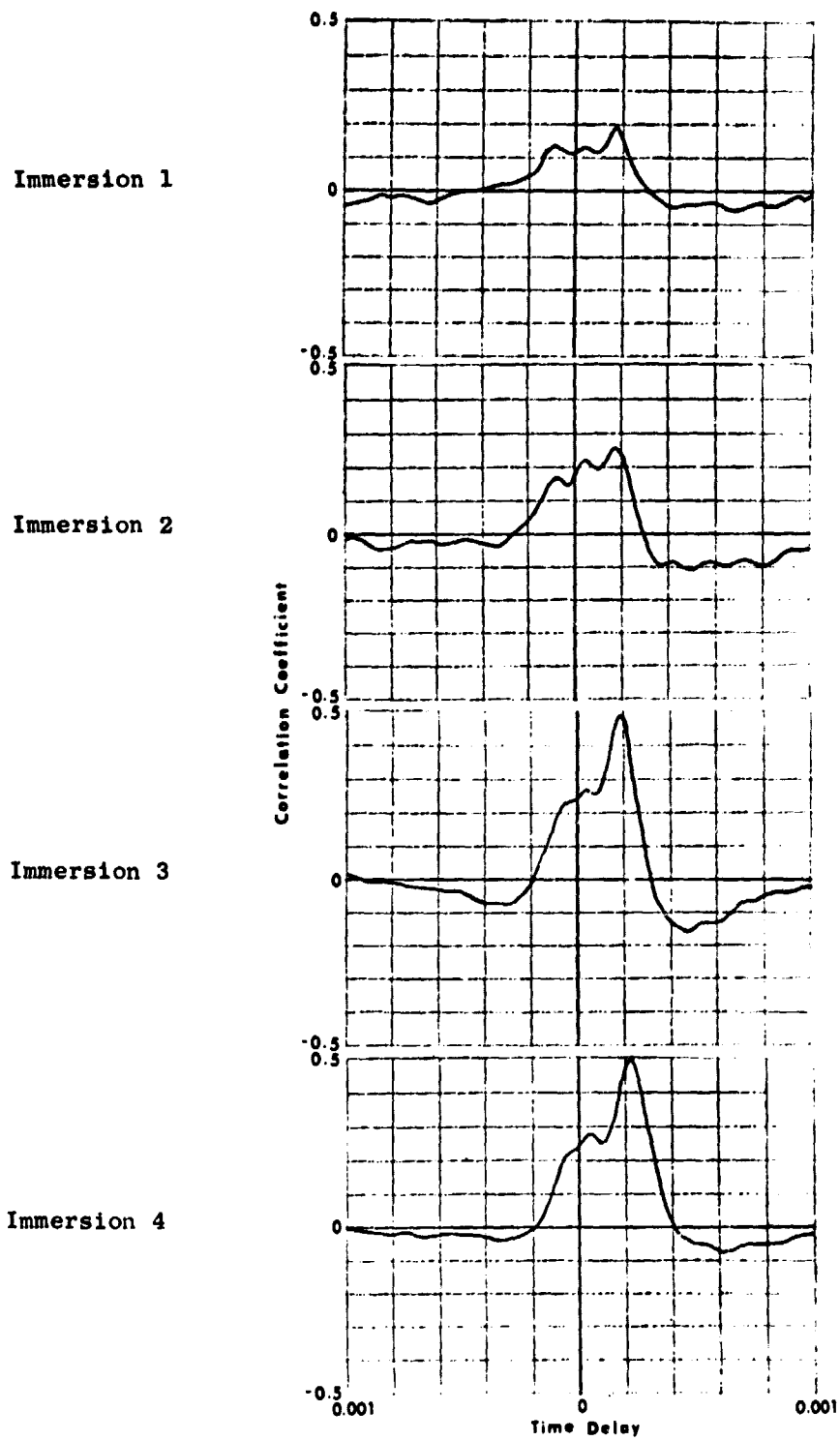


Figure 48. Correlations from Sound Separation Probe - 27 Percent Thin-to-Thick Configuration (8).

signals (Reference 11). However, when the cross-correlograms from all four immersions are compared the peaks are seen to be quite different; thereby discounting "ringing" as the source of the peaks. The hardwall case (Configuration 18) shows predominately aft-propagating sound in the data, with forward-propagating sound in the outer two immersions and turbulence in the inner two immersions making up the rest of the signals. However, the treated cases (Configurations 7 and 8) show predominately turbulence in the data with aft- and forward-propagating sound making up the rest of the signals. Furthermore, a comparison of the overall levels of the signals from the forward transducer of the probe (Figure 49) shows virtually no suppression from hardwall to treated configurations. This is due to comparison of sound in the hardwall case with turbulence in the treated case. To obtain the actual suppression of the aft-propagating sound the acoustic discrimination technique must be applied to the data.

By ratioing the peaks on the cross-correlograms to each other and applying the condition that the three peaks add to the overall level, the sound and turbulence levels can be separated. This has been done and the results are shown in Figure 50. The suppression of the aft propagating sound is shown to be approximately 10 dB which agrees very well with the far-field broadband data in the aft quadrant.

In summary, the acoustic discrimination technique using the sound separation probes will verify that probe data are sound or turbulence, and enable computation of treatment-suppression levels from the probe data. This technique was applied to this test simply by using the sound separation probes in place of the waveguide probes.

## B. Modal Measurements

### 1. Theory of Modal Measurement

Recent findings (References 12, 13, and 14) have indicated that an accurate prediction of acoustic treatment noise **suppression, and consequently** an effective design improvement of acoustic treatment, is dependent upon the knowledge of detailed modal characteristics of the acoustic pressure pattern propagating inside the duct. The existence and nature of characteristic duct modes have been known, but only since the advent of high-speed spectral analyzers and sensitive microphone-probe systems has measurement become technically feasible.

The modal content in the duct pressure signal is controlled by the rotor (or rotor/stator) noise-generating mechanism. Duct modes are either "cut-on", i.e., they propagate unattenuated in a hard-walled duct, or "cut-off", i.e., they decay exponentially. In the presence of an absorbing liner, each mode will attenuate at a specific decay rate that is a function of  $H/\lambda$  or  $\eta$ . The modes are usually ordered in terms of their decay rates. Higher order modes have higher decay rates.

Since a given pressure signal is usually composed of a number of modes, and since each of these modes usually decays at a different rate in the presence of acoustic treatment, the modal participation, and thus the overall acoustic pressure profile, will change as the wave propagates down the duct.

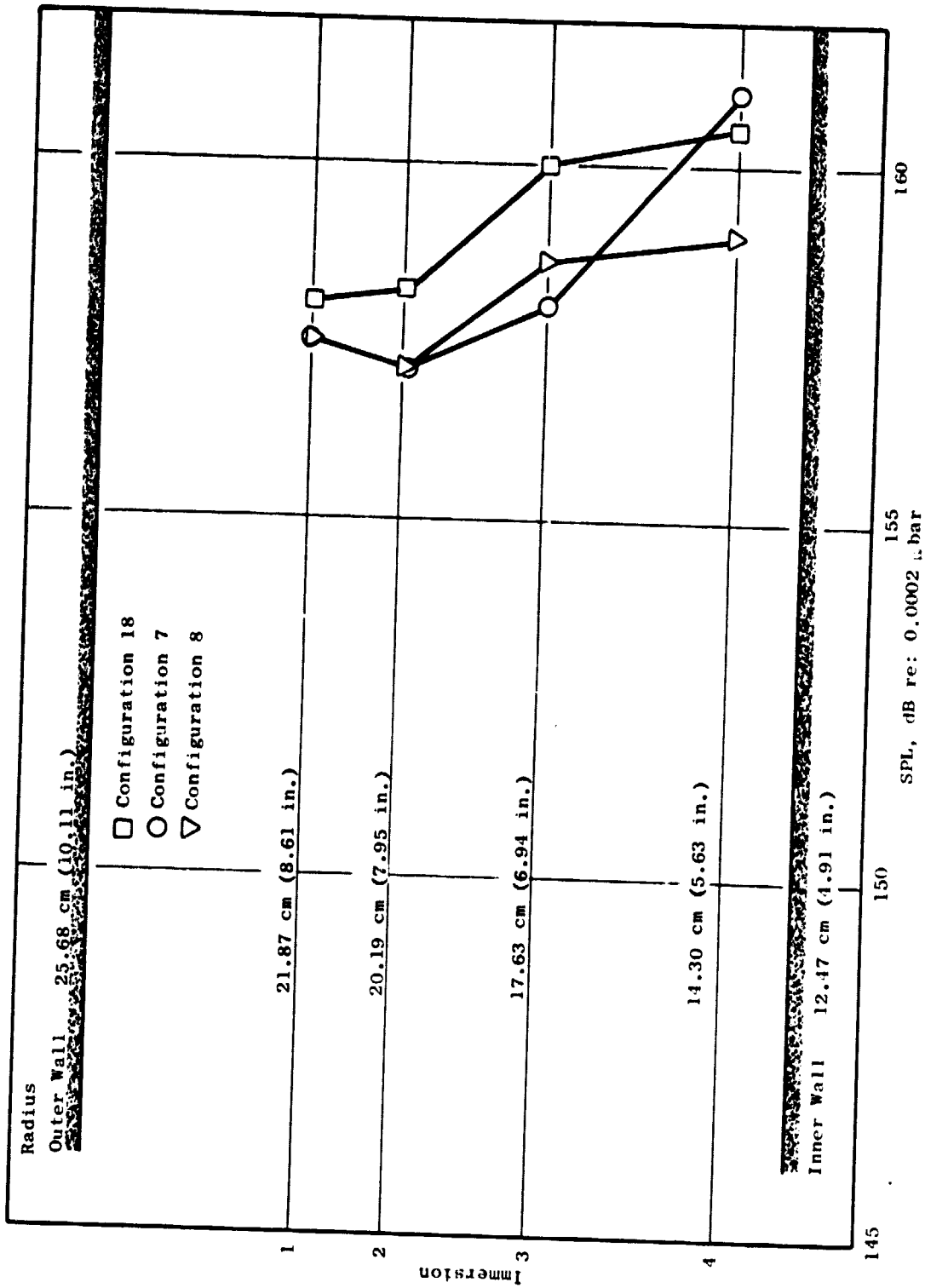


Figure 49. Total Broadband Level, 0 - 5000 Hz (Tones Removed).



ORIGINAL PAGE IS  
OF POOR QUALITY

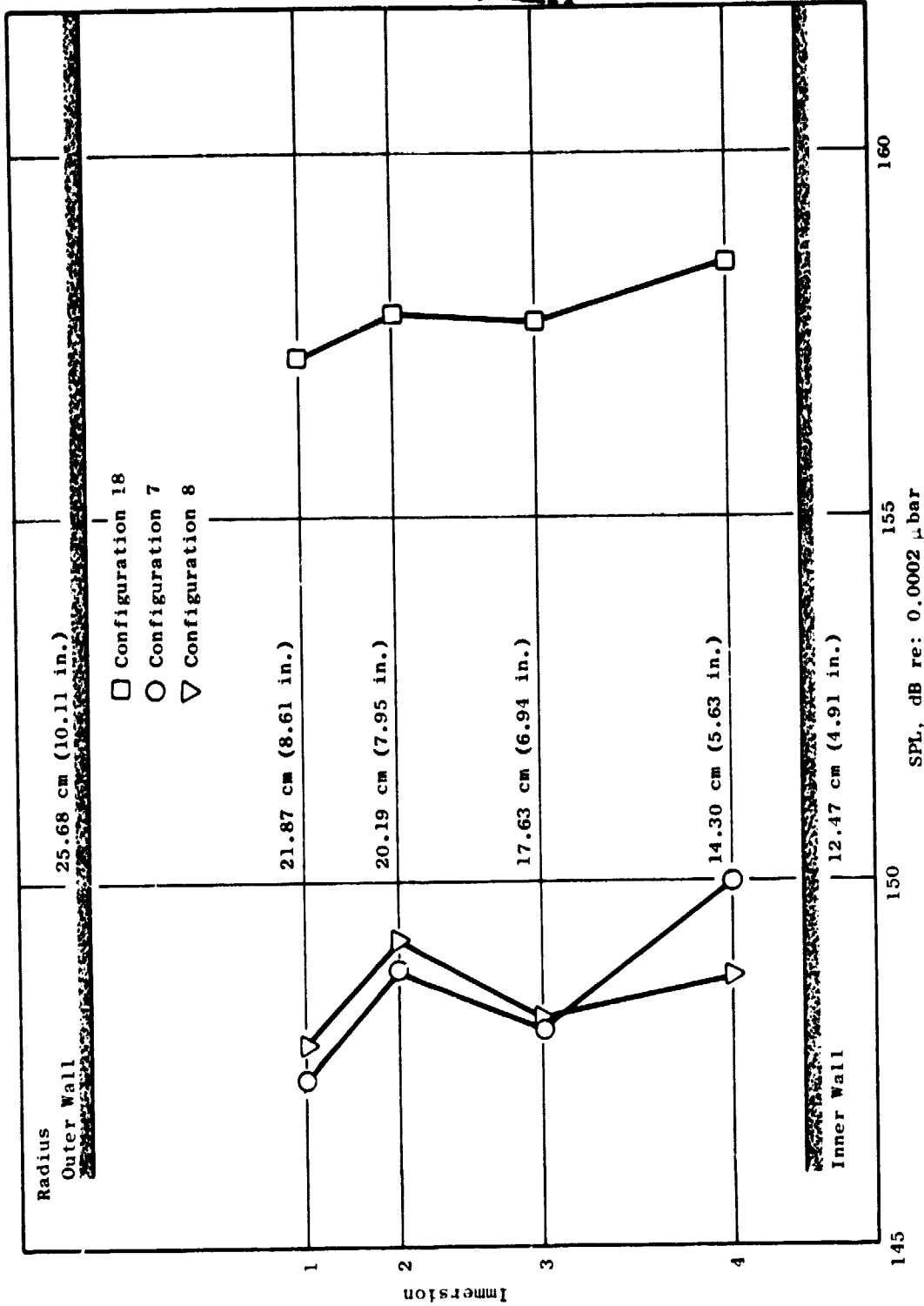


Figure 50. Separated Broadband Level, 0 - 5000 Hz (Tones Removed).

The objective of acoustic liner design is to provide treatment which maximizes the acoustic energy absorption at frequencies of interest, under the constraints of duct height and length. Since a duct liner section can be optimized to provide a maximum rate of attenuation for a given mode or combination of modes, the modal participation is an essential input to the design process.

Data were taken during this test to demonstrate the technique for measuring modal patterns and to evaluate the results with respect to the treatment suppression results.

In a duct with circular or annular cross section, two indices are required to describe the modal pattern. One index determines the order for modes with diametral nodal lines (called spinning modes). The other index determines the order for modes with circumferential nodal lines (called radial modes). These duct modes, analogous to the modes of vibration of a drum head, are illustrated figuratively in Figure 51.

For the case of high radius ratio annular ducts, an analytical simplification can be made. To a higher degree of approximation, the spinning mode content of the annular duct can be ignored and the propagation can be assumed to be the same as that in a duct of rectangular cross section with the duct height equal to the difference in radius of the annuli (Reference 15). The transverse modes in the rectangular duct become analogous to the radial modes of the annular duct, and the analysis can proceed in the rectangular coordinate system. In the rectangular duct, the characteristic acoustic pressure modes, or eigenfunctions, are given by:

$$\phi_j(x) = C_j \cos(\gamma_j x/H) + D_j \sin(\gamma_j x/H) \quad (1)$$

where:

- $\gamma_j$  = mode eigenvalue
- $x$  = transverse position in duct (immersion)
- $H$  = duct height
- $j$  = mode index
- $C_j, D_j$  = eigenfunction coefficients

An arbitrary acoustic pressure profile across the duct is analyzed in terms of its component modes by a Fourier-type series expansion of the form:

$$P(x,t) = \sum_{j=0}^{\infty} A_j(\omega) \phi_j(\gamma_j X/H) e^{-i\omega t} \quad (2)$$

where  $\omega$  is the frequency,  $t$  is time, and the  $A_j$ 's are the modal coefficients giving the participation level of each mode. The acoustic pressure, modal coefficients, eigenfunctions, and eigenvalues are all taken as complex numbers, possessing a magnitude and phase.

ORIGINAL PAGE IS  
OF POOR QUALITY

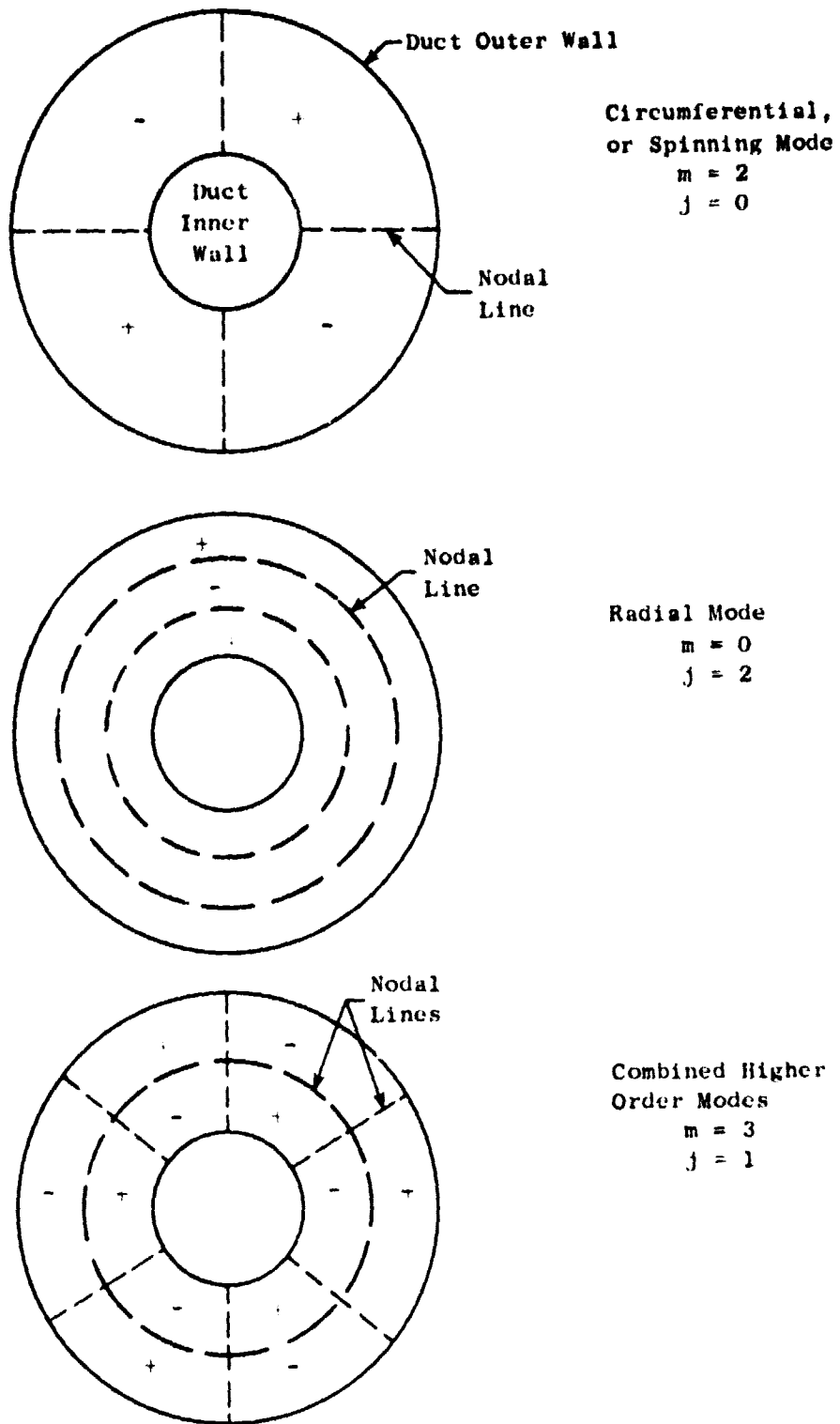


Figure 51. Illustration of Characteristic Duct Modes.

The theory behind the modal measurement requires the experimental determination of the complex acoustic pressure profile given by the left hand side of Equation (2) as a function of  $x$  across the duct at given frequencies of interest. At the given frequency, the  $A_j$  are then determined by a modal decomposition of the  $p(x)$  in Equation (2) using standard Fourier analysis-type techniques. The magnitude and phase of  $p(x)$  are determined at a number of immersions by measuring the cross-spectral density between a movable probe (see Figure 42 and description in Section V-A) in the duct and a reference microphone fixed in the wall of the duct. The experimental setup for Rotor 55 is shown schematically in Figure 52.

The cross-spectral density of two signals is the product of the Fourier (time) transforms of the two signals in the form:

$$S_{rp}(\omega, x_r, x_p) = \overline{P_r(x_r, \omega)^*} \overline{P_p(x_p, \omega)} \quad (3)$$

where:

$p_r(x_r, \omega)$  = reference microphone pressure signal  
 $p_p(x_p, \omega)$  = probe pressure signal  
 $x_r, x_p$  = positions of reference microphone, probe  
 $\omega$  = frequency

The bar denotes Fourier transform with respect to time, and the asterisk denotes complex conjugate. The Fourier transform of Equation (2) gives:

$$\overline{P(x, \omega)} = \sum_{j=0}^{\infty} A_j(\omega) P_j(\gamma_j x/H) \quad (4)$$

Combining this with Equation (3), we get:

$$S_{rp}(\omega, x) = \left[ \sum_{n=0}^{\infty} A_n^*(\omega) \right] \left[ \sum_{j=0}^{\infty} A_j(\omega) P_j(\gamma_j x/H) \right] \quad (5)$$

The first sum on the right hand side is constant with respect to  $x$ , so that, if we let:

$$B_j(\omega) = A_j(\omega) \left[ \sum_{n=0}^{\infty} A_n^*(\omega) \right] \quad (6)$$

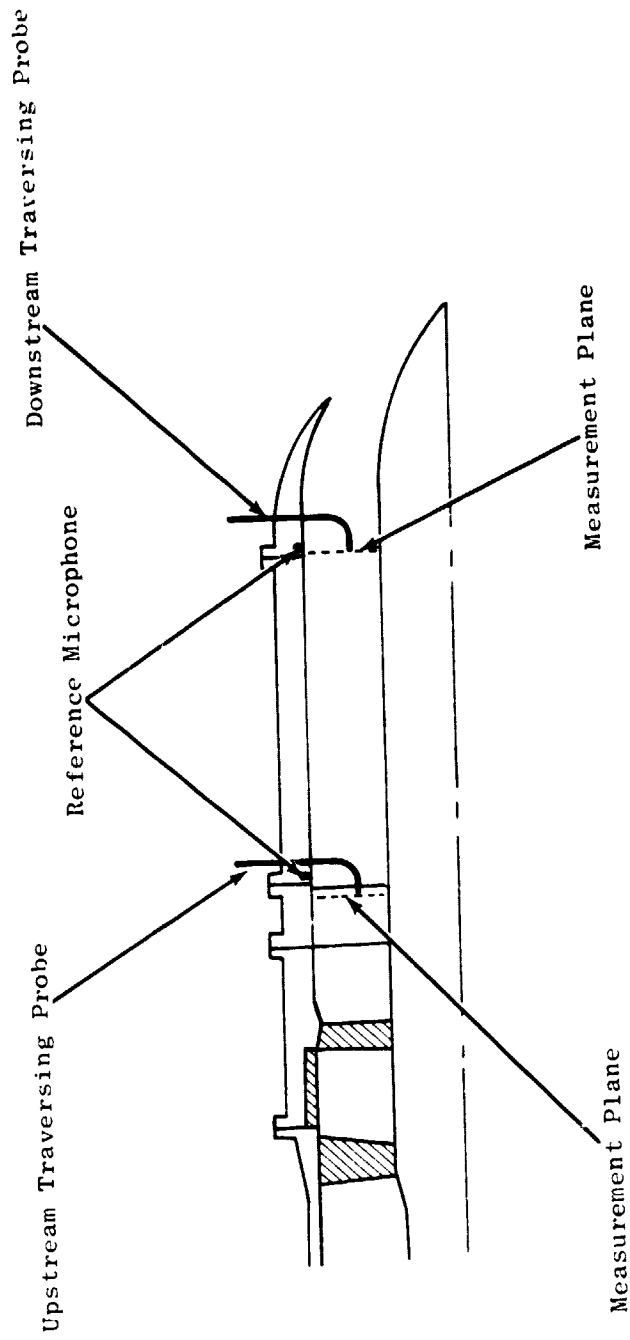


Figure 52. Schematic of Model Measurement Apparatus in Rotor 55 Vehicle.

we can write:

$$S_{rp}(\omega, x) = \sum_{j=0}^{\infty} B_j(\omega) P_j(\gamma_j x/H) \quad (7)$$

The left side of this expression is obtained from measurement, and the  $B_j$  are then obtained from analysis. Since the  $B_j$  are proportional to the  $A_j$ , the relative magnitude and phase of the modal coefficients can be obtained in this manner.

## 2. Experimental Results

At each immersion of the aft probe shown in Figure 52 a cross-spectral density was calculated between the probe microphone and the wall reference microphone using a Time/Data Fast Fourier Analyzer System. The analyzer first plots the magnitude of the cross-spectrum, then prints a tabulation of the cross-spectrum magnitude and phase for each narrowband center frequency. The calculation was made using 200 frequency averages over each data sample, with a 40 Hz bandwidth from 0 to 10,200 Hz.

Figure 53 is a plot of the logarithmic magnitude of the cross-spectrum for the probe in the downstream location for Configuration 75-1F (Hardwall) at 70% speed, at an immersion of 4.4 cm (1.715 in.) from the outer wall. Figure 54 gives tabulations of the cross-spectrum for this case. Figure 55 is a plot of the logarithmic magnitude of the cross-spectrum for the probe in the downstream location for Configuration 75-1F (Hardwall) at 100% speed, at an immersion of 4.4 cm (1.715 in.). Figure 56 gives tabulations of the cross-spectrum for this case. Similar plots were obtained at all other immersions.

## 3. Data Analysis

The frequencies of interest for the analysis are the blade passing frequency and its harmonics for both 70% and 100% speed. Complex acoustic pressure profiles for the first four harmonics of the blade passing frequency at 70% speed are shown in Figures 57 to 60. The profiles for 100% speed are Figures 61 to 64.

The circles in these figures represent measured data points at each immersion, while the solid curves resulted from the subsequent modal analysis. Note that the first immersion occurs 3.8 cm (1.5 in.) from the wall, which is the closest the gooseneck probe approaches the wall when fully withdrawn. The data between the 3.8 cm (1.5 in.) immersion point and the wall **are probably significant to the modal expansion, but could only be approximated by extrapolating the curves to the wall in the manner shown.**

The results of the modal analysis are presented in Table III, where the magnitude and phase of the modal coefficients for the first six modes are presented. The coefficients are normalized relative to the lowest order

ORIGINAL PAGE IS  
OF POOR QUALITY

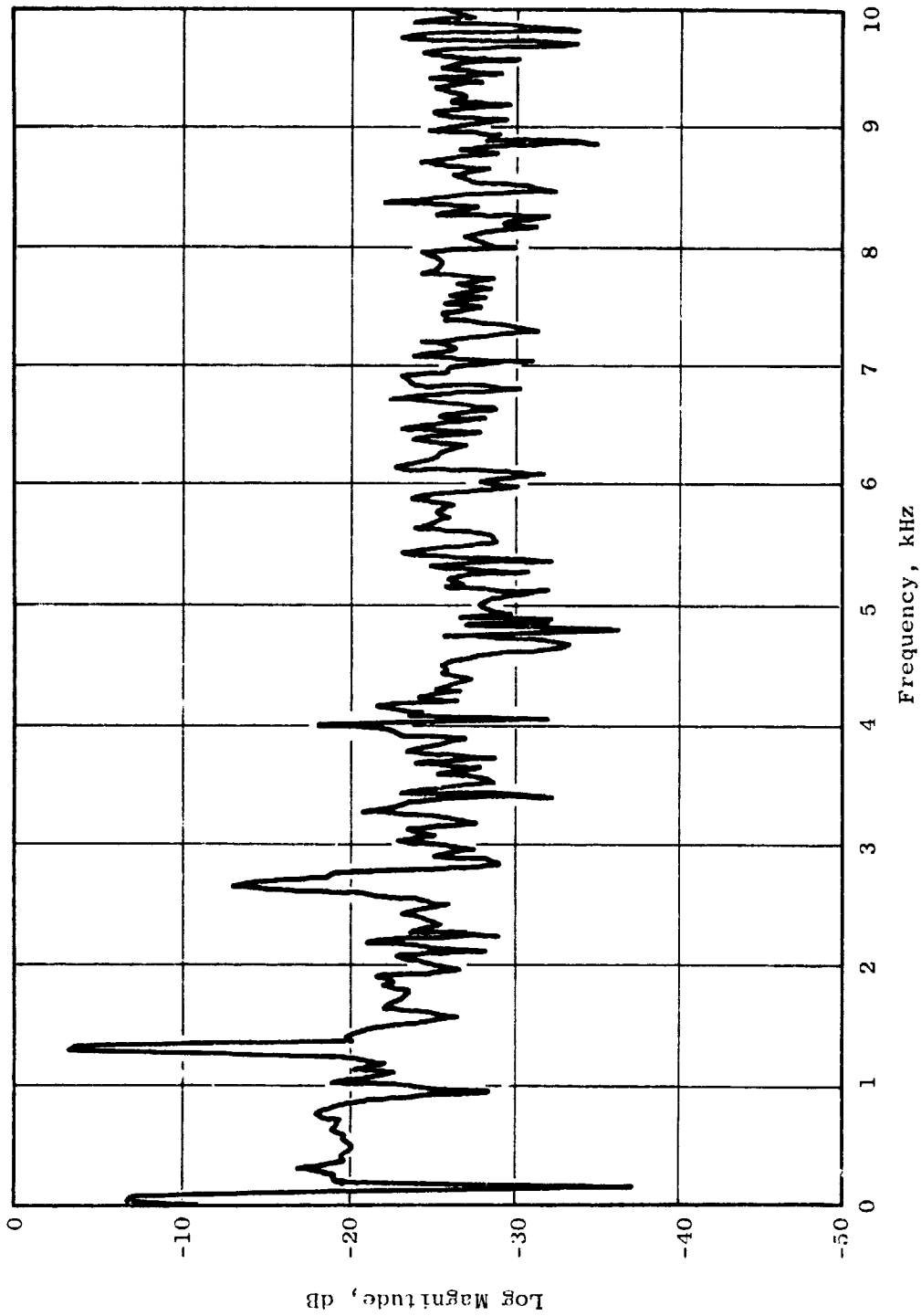


Figure 53. Relative Logarithmic Magnitude of Cross-Spectrum for Downstream Probe;  
Hardwall Configuration 75-1F, 70% Speed, Immersion 4.4 cm (1.715 in.).

FREQ=0	LOG MAG=-44	98	PHASE=0
FREQ=40	LOG MAG=-39	36	PHASE=-28 14
FREQ=80	LOG MAG=-40	4	PHASE=-27 78
FREQ=120	LOG MAG=-49	58	PHASE=-36 48
FREQ=160	LOG MAG=-70	29	PHASE=-76 95
FREQ=200	LOG MAG=-52	22	PHASE=-165 7
FREQ=240	LOG MAG=-51	56	PHASE=-160
FREQ=280	LOG MAG=-51	98	PHASE=47 54
FREQ=320	LOG MAG=-49	54	PHASE=12 02
FREQ=360	LOG MAG=-52	46	PHASE=-23 35
FREQ=400	LOG MAG=-52	67	PHASE=-18 03
FREQ=440	LOG MAG=-52	29	PHASE=15 35
FREQ=480	LOG MAG=-53	11	PHASE=42 63
FREQ=520	LOG MAG=-52	81	PHASE=24 75
FREQ=560	LOG MAG=-52	36	PHASE=36 21
FREQ=600	LOG MAG=-52	44	PHASE=43 76
FREQ=640	LOG MAG=-51	56	PHASE=15 01
FREQ=680	LOG MAG=-52	02	PHASE=2 609
FREQ=720	LOG MAG=-52	44	PHASE=-26 19
FREQ=760	LOG MAG=-50	8	PHASE=-6 914
FREQ=800	LOG MAG=-50	75	PHASE=6 195
FREQ=840	LOG MAG=-52	2	PHASE=-6 89
FREQ=880	LOG MAG=-53	55	PHASE=-20 3
FREQ=920	LOG MAG=-57	48	PHASE=6 864
FREQ=960	LOG MAG=-61	51	PHASE=-31 34
FREQ=1000	LOG MAG=-56	77	PHASE=7 637
FREQ=1040	LOG MAG=-51	68	PHASE=19 52
FREQ=1080	LOG MAG=-54	01	PHASE=25 48
FREQ=1120	LOG MAG=-55	9	PHASE=-16 03
FREQ=1160	LOG MAG=-53	05	PHASE=4 035
FREQ=1200	LOG MAG=-55	02	PHASE=-1 549
FREQ=1240	LOG MAG=-53	57	PHASE=-5 669
FREQ=1280	LOG MAG=-45	3	PHASE=-29 02
FREQ=1320	LOG MAG=-50	09	PHASE=-45 59
FREQ=1360	LOG MAG=-38	47	PHASE=-47 41
FREQ=1400	LOG MAG=-53	24	PHASE=-13 16
FREQ=1440	LOG MAG=-52	63	PHASE=-7 834
FREQ=1480	LOG MAG=-53	92	PHASE=-5 117
FREQ=1520	LOG MAG=-55	52	PHASE=-7 295
FREQ=1560	LOG MAG=-57	47	PHASE=9 777
FREQ=1600	LOG MAG=-59	58	PHASE=-61 21
FREQ=1640	LOG MAG=-54	92	PHASE=-55 78
FREQ=1680	LOG MAG=-54	97	PHASE=-25 46
FREQ=1720	LOG MAG=-55	94	PHASE=35 27
FREQ=1760	LOG MAG=-56	15	PHASE=-14 92
FREQ=1800	LOG MAG=-56	62	PHASE=-39 07
FREQ=1840	LOG MAG=-54	87	PHASE=-69 48
FREQ=1880	LOG MAG=-55	69	PHASE=-94 49
FREQ=1920	LOG MAG=-54	37	PHASE=-3 179
FREQ=1960	LOG MAG=-59	34	PHASE=83 36
FREQ=2000	LOG MAG=-59	72	PHASE=94 05
FREQ=2040	LOG MAG=-56	3	PHASE=-44 79
FREQ=2080	LOG MAG=-55	79	PHASE=-38 95
FREQ=2120	LOG MAG=-61	29	PHASE=-85 99
FREQ=2160	LOG MAG=-57	24	PHASE=68 14
FREQ=2200	LOG MAG=-53	87	PHASE=47 48
FREQ=2240	LOG MAG=-61	91	PHASE=37 06
FREQ=2280	LOG MAG=-56	43	PHASE=67 5
FREQ=2320	LOG MAG=-58	31	PHASE=110 9
FREQ=2360	LOG MAG=-58	4	PHASE=154 1
FREQ=2400	LOG MAG=-57	5	PHASE=131 6
FREQ=2440	LOG MAG=-55	89	PHASE=115 4
FREQ=2480	LOG MAG=-57	91	PHASE=131 3
FREQ=2520	LOG MAG=-59	13	PHASE=162
FREQ=2560	LOG MAG=-55	43	PHASE=177 6
FREQ=2600	LOG MAG=-53	86	PHASE=129 7
FREQ=2640	LOG MAG=-46	09	PHASE=93 38
FREQ=2680	LOG MAG=-45	9	PHASE=88 58
FREQ=2720	LOG MAG=-51	34	PHASE=130 8
FREQ=2760	LOG MAG=-52		PHASE=153 1
FREQ=2800	LOG MAG=-57	72	PHASE=149
FREQ=2840	LOG MAG=-62	2	PHASE=10 57
FREQ=2880	LOG MAG=-61	21	PHASE=93 01
FREQ=2920	LOG MAG=-57	81	PHASE=179 8
FREQ=2960	LOG MAG=-60	54	PHASE=-111 9
FREQ=3000	LOG MAG=-59	54	PHASE=-169 8
FREQ=3040	LOG MAG=-55	79	PHASE=-152 1
FREQ=3080	LOG MAG=-58	16	PHASE=163
FREQ=3120	LOG MAG=-57	63	PHASE=105 7
FREQ=3160	LOG MAG=-56	14	PHASE=108 3
FREQ=3200	LOG MAG=-60	94	PHASE=-160 5
FREQ=3240	LOG MAG=-58	51	PHASE=22 1
FREQ=3280	LOG MAG=-53	68	PHASE=55 84
FREQ=3320	LOG MAG=-55	66	PHASE=112 4
FREQ=3360	LOG MAG=-56	56	PHASE=-172 6
FREQ=3400	LOG MAG=-65	61	PHASE=154 8
FREQ=3440	LOG MAG=-55	94	PHASE=-43 65
FREQ=3480	LOG MAG=-57	96	PHASE=-146 3
FREQ=3520	LOG MAG=-61	76	PHASE=-133 5
FREQ=3560	LOG MAG=-61	27	PHASE=61 42
FREQ=3600	LOG MAG=-57	96	PHASE=29 86
FREQ=3640	LOG MAG=-60	93	PHASE=-120 6
FREQ=3680	LOG MAG=-56	88	PHASE=-173 5
FREQ=3720	LOG MAG=-62	09	PHASE=-143
FREQ=3760	LOG MAG=-58	04	PHASE=-104
FREQ=3800	LOG MAG=-56	31	PHASE=-84 32
FREQ=3840	LOG MAG=-57	8	PHASE=23 98
FREQ=3880	LOG MAG=-60	02	PHASE= 8623
FREQ=3920	LOG MAG=-56	01	PHASE=-51 56
FREQ=3960	LOG MAG=-55	41	PHASE=159 9
FREQ=4000	LOG MAG=-51		PHASE=137 8
FREQ=4040	LOG MAG=-64	93	PHASE=147 3
FREQ=4080	LOG MAG=-56	43	PHASE=-26 87
FREQ=4120	LOG MAG=-57	16	PHASE=-166 7
FREQ=4160	LOG MAG=-54	62	PHASE=-154 2
FREQ=4200	LOG MAG=-59	75	PHASE=-13 36
FREQ=4240	LOG MAG=-57	09	PHASE=40 87
FREQ=4280	LOG MAG=-59	71	PHASE=-141 2
FREQ=4320	LOG MAG=-57	96	PHASE=178 4
FREQ=4360	LOG MAG=-59	25	PHASE=101 1
FREQ=4400	LOG MAG=-60	35	PHASE=62 47
FREQ=4440	LOG MAG=-58	38	PHASE=29 81
FREQ=4480	LOG MAG=-58	97	PHASE=3 93
FREQ=4520	LOG MAG=-58	73	PHASE=88 33
FREQ=4560	LOG MAG=-59	6	PHASE=99 08
FREQ=4600	LOG MAG=-61	38	PHASE=40 96
FREQ=4640	LOG MAG=-65	81	PHASE=-12 18
FREQ=4680	LOG MAG=-66	43	PHASE=-172
FREQ=4720	LOG MAG=-64	65	PHASE=17 04
FREQ=4760	LOG MAG=-58	57	PHASE=34 01
FREQ=4800	LOG MAG=-69	49	PHASE=15 3
FREQ=4840	LOG MAG=-59	88	PHASE=-90 53
FREQ=4880	LOG MAG=-65	22	PHASE=114 2
FREQ=4920	LOG MAG=-59	56	PHASE=-110 9
FREQ=4960	LOG MAG=-62	9	PHASE=-1 22
FREQ=5000	LOG MAG=-60	89	PHASE=64 68
FREQ=5040	LOG MAG=-60	84	PHASE=169 9
FREQ=5080	LOG MAG=-62	83	PHASE=-179 8

Figure 54(a). Cross-Spectrum for Downstream Probe; Hardwall Configuration  
75-1F, 70% Speed, Immersion of 4.4 cm (1.715 in.), 0 to  
5080 Hz.



ORIGINAL PAGE IS  
OF POOR QUALITY

FREQ=5120	LOG MAG=-65	42	PHASE=26	7	FREQ=7680	LOG MAG=-59	44	PHASE=10	07
FREQ=5160	LOG MAG=-58	82	PHASE=-119	2	FREQ=7720	LOG MAG=-62	09	PHASE=127	1
FREQ=5200	LOG MAG=-59	83	PHASE=-53	41	FREQ=7760	LOG MAG=-57	29	PHASE=107	1
FREQ=5240	LOG MAG=-58	78	PHASE=52	99	FREQ=7800	LOG MAG=-57	06	PHASE=65	46
FREQ=5280	LOG MAG=-63	94	PHASE=164	8	FREQ=7840	LOG MAG=-58	4	PHASE=77	56
FREQ=5320	LOG MAG=-57	66	PHASE=-68	36	FREQ=7880	LOG MAG=-58	63	PHASE=-150	5
FREQ=5360	LOG MAG=-65	55	PHASE=-86	05	FREQ=7920	LOG MAG=-58	22	PHASE=-167	
FREQ=5400	LOG MAG=-57	83	PHASE=171	7	FREQ=7960	LOG MAG=-57	35	PHASE=145	2
FREQ=5440	LOG MAG=-56	26	PHASE=-161	7	FREQ=8000	LOG MAG=-63	33	PHASE=96	41
FREQ=5480	LOG MAG=-59	09	PHASE=110	8	FREQ=8040	LOG MAG=-61	56	PHASE=59	42
FREQ=5520	LOG MAG=-62	05	PHASE=-39	6	FREQ=8080	LOG MAG=-60	06	PHASE=98	42
FREQ=5560	LOG MAG=-61	78	PHASE=-7	012	FREQ=8120	LOG MAG=-61	21	PHASE=47	14
FREQ=5600	LOG MAG=-61	6	PHASE=-57	97	FREQ=8160	LOG MAG=-64	5	PHASE=-53	49
FREQ=5640	LOG MAG=-56	94	PHASE=-65	84	FREQ=8200	LOG MAG=-62	29	PHASE=121	6
FREQ=5680	LOG MAG=-58	78	PHASE=-96	88	FREQ=8240	LOG MAG=-65	46	PHASE=79	54
FREQ=5720	LOG MAG=-59	3	PHASE=171	3	FREQ=8280	LOG MAG=-58	32	PHASE=42	06
FREQ=5760	LOG MAG=-58	64	PHASE=-152	8	FREQ=8320	LOG MAG=-60	98	PHASE=-160	6
FREQ=5800	LOG MAG=-58	12	PHASE=-146	7	FREQ=8360	LOG MAG=-55	27	PHASE=-114	1
FREQ=5840	LOG MAG=-59	63	PHASE=-142	3	FREQ=8400	LOG MAG=-58	31	PHASE=-109	5
FREQ=5880	LOG MAG=-56	57	PHASE=-115	7	FREQ=8440	LOG MAG=-65	7	PHASE=179	2
FREQ=5920	LOG MAG=-58	64	PHASE=-80	74	FREQ=8480	LOG MAG=-64	18	PHASE=156	3
FREQ=5960	LOG MAG=-62	58	PHASE=90	1	FREQ=8520	LOG MAG=-60	57	PHASE=-13	17
FREQ=6000	LOG MAG=-63	47	PHASE=-172	5	FREQ=8560	LOG MAG=-59	93	PHASE=-110	
FREQ=6040	LOG MAG=-60	75	PHASE=-169	3	FREQ=8600	LOG MAG=-59	18	PHASE=-52	31
FREQ=6080	LOG MAG=-65	1	PHASE=-116	1	FREQ=8640	LOG MAG=-61	64	PHASE=60	8
FREQ=6120	LOG MAG=-60	8	PHASE=-73	98	FREQ=8680	LOG MAG=-57	33	PHASE=157	9
FREQ=6160	LOG MAG=-55	73	PHASE=-80	51	FREQ=8720	LOG MAG=-59	81	PHASE=152	5
FREQ=6200	LOG MAG=-56	69	PHASE=-61	71	FREQ=8760	LOG MAG=-62	41	PHASE=127	5
FREQ=6240	LOG MAG=-58	15	PHASE=-95	88	FREQ=8800	LOG MAG=-59	47	PHASE=155	8
FREQ=6280	LOG MAG=-58	32	PHASE=-135	6	FREQ=8840	LOG MAG=-68	74	PHASE=-99	95
FREQ=6320	LOG MAG=-60	24	PHASE=-68	86	FREQ=8880	LOG MAG=-61	26	PHASE=-8	737
FREQ=6360	LOG MAG=-59	76	PHASE=128	5	FREQ=8920	LOG MAG=-62	22	PHASE=-37	38
FREQ=6400	LOG MAG=-56	69	PHASE=154	6	FREQ=8960	LOG MAG=-57	7	PHASE=-71	29
FREQ=6440	LOG MAG=-61	15	PHASE=58	74	FREQ=9000	LOG MAG=-58	59	PHASE=-81	11
FREQ=6480	LOG MAG=-55	97	PHASE=44	99	FREQ=9040	LOG MAG=-63	12	PHASE=-137	7
FREQ=6520	LOG MAG=-59	2	PHASE=5	432	FREQ=9080	LOG MAG=-58	7	PHASE=-167	8
FREQ=6560	LOG MAG=-61	3	PHASE=-11	9	FREQ=9120	LOG MAG=-58	08	PHASE=-171	7
FREQ=6600	LOG MAG=-58	3	PHASE=8	221	FREQ=9160	LOG MAG=-63	1	PHASE=30	24
FREQ=6640	LOG MAG=-62	16	PHASE=149	4	FREQ=9200	LOG MAG=-58	97	PHASE=18	13
FREQ=6680	LOG MAG=-59	3	PHASE=40	93	FREQ=9240	LOG MAG=-60	18	PHASE=-1	371
FREQ=6720	LOG MAG=-55	31	PHASE=19	06	FREQ=9280	LOG MAG=-59	8	PHASE=-53	86
FREQ=6760	LOG MAG=-57	69	PHASE=58	49	FREQ=9320	LOG MAG=-58	19	PHASE=170	
FREQ=6800	LOG MAG=-63	28	PHASE=56	75	FREQ=9360	LOG MAG=-61	41	PHASE=117	8
FREQ=6840	LOG MAG=-56	97	PHASE=80	5	FREQ=9400	LOG MAG=-57	68	PHASE=146	
FREQ=6880	LOG MAG=-56	53	PHASE=113	1	FREQ=9440	LOG MAG=-62	56	PHASE=126	7
FREQ=6920	LOG MAG=-56	21	PHASE=132	6	FREQ=9480	LOG MAG=-58	62	PHASE=30	5
FREQ=6960	LOG MAG=-58	99	PHASE=162		FREQ=9520	LOG MAG=-55	56	PHASE=66	34
FREQ=7000	LOG MAG=-58	98	PHASE=81	44	FREQ=9560	LOG MAG=-63	5	PHASE=-142	4
FREQ=7040	LOG MAG=-64	41	PHASE=80	81	FREQ=9600	LOG MAG=-57	99	PHASE=-25	65
FREQ=7080	LOG MAG=-56	86	PHASE=57	81	FREQ=9640	LOG MAG=-57	42	PHASE=-11	71
FREQ=7120	LOG MAG=-58	42	PHASE=27	31	FREQ=9680	LOG MAG=-66	99	PHASE=-80	4
FREQ=7160	LOG MAG=-59	73	PHASE=22	37	FREQ=9720	LOG MAG=-57	89	PHASE=-107	2
FREQ=7200	LOG MAG=-57	36	PHASE=30	46	FREQ=9760	LOG MAG=-56	11	PHASE=-82	25
FREQ=7240	LOG MAG=-61	97	PHASE=82	69	FREQ=9800	LOG MAG=-66	98	PHASE=-49	43
FREQ=7280	LOG MAG=-64	76	PHASE=-120	7	FREQ=9840	LOG MAG=-61	87	PHASE=170	1
FREQ=7320	LOG MAG=-62	63	PHASE=9	361	FREQ=9880	LOG MAG=-56	94	PHASE=-148	4
FREQ=7360	LOG MAG=-58	79	PHASE=97	94	FREQ=9920	LOG MAG=-60	48	PHASE=105	3
FREQ=7400	LOG MAG=-59	3	PHASE=127		FREQ=9960	LOG MAG=-59	28	PHASE=56	24
FREQ=7440	LOG MAG=-58	73	PHASE=-15	58	FREQ=10000	LOG MAG=-60	95	PHASE=56	23
FREQ=7480	LOG MAG=-61	12	PHASE=-35	08	FREQ=10040	LOG MAG=-59	28	PHASE=93	05
FREQ=7520	LOG MAG=-58	77	PHASE=60	22	FREQ=10080	LOG MAG=-60	72	PHASE=46	33
FREQ=7560	LOG MAG=-61	38	PHASE=-174	8	FREQ=10120	LOG MAG=-60	47	PHASE=67	54
FREQ=7600	LOG MAG=-59	09	PHASE=-145	8	FREQ=10160	LOG MAG=-56	66	PHASE=114	7
FREQ=7640	LOG MAG=-61	73	PHASE=96	61	FREQ=10200	LOG MAG=-58	47	PHASE=110	6

Figure 54(b). Cross-Spectrum for Downstream Probe: Hardwall Configuration  
75-1F, 70% Speed, Immersion of 4.4 cm (1.715 in.), 5120 to  
10,200 Hz.

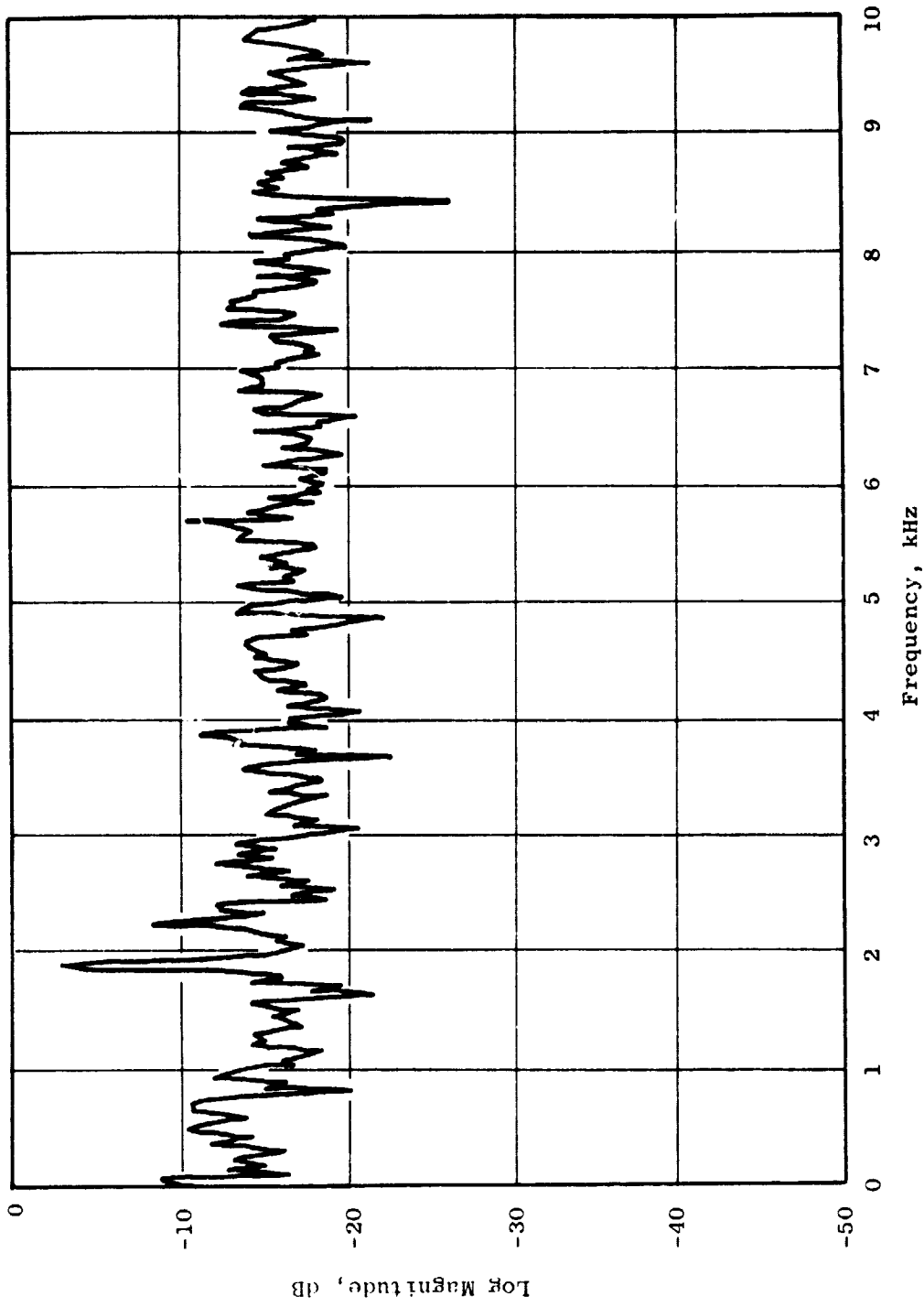


Figure 55. Relative Logarithmic Magnitude of Cross-Spectrum for Downstream Probe; Hardwall Configuration 75-1F, 100% Speed, Immersion 4.4 cm (1.715 in.).

ORIGINAL PAGE IS  
OF POOR QUALITY

FREQ=0	LOG MAG=-48	PHASE=0	FREQ=2560	LOG MAG=-56	49	PHASE=84	66		
FREQ=40	LOG MAG=-46	PHASE=6	648	FREQ=2600	LOG MAG=-52	47	PHASE=-154	3	
FREQ=50	LOG MAG=-45	37	PHASE=7	7	FREQ=2640	LOG MAG=-54	92	PHASE=-157	
FREQ=120	LOG MAG=-53	36	PHASE=-47	18	FREQ=2680	LOG MAG=-50	64	PHASE=-110	
FREQ=160	LOG MAG=-49	43	PHASE=-157	4	FREQ=2720	LOG MAG=-53	42	PHASE=-115	
FREQ=200	LOG MAG=-52	08	PHASE=177	8	FREQ=2760	LOG MAG=-52	36	PHASE=152	1
FREQ=240	LOG MAG=-49	7	PHASE=-35	21	FREQ=2800	LOG MAG=-48	63	PHASE=156	3
FREQ=280	LOG MAG=-50	87	PHASE=-73	32	FREQ=2840	LOG MAG=-52	19	PHASE=164	7
FREQ=320	LOG MAG=-53	14	PHASE=15	11	FREQ=2880	LOG MAG=-49	92	PHASE=-162	3
FREQ=360	LOG MAG=-50	43	PHASE=130	3	FREQ=2920	LOG MAG=-52	8	PHASE=151	2
FREQ=400	LOG MAG=-48	42	PHASE=111	6	FREQ=2960	LOG MAG=-49	8	PHASE=-151	8
FREQ=440	LOG MAG=-51	22	PHASE=14	62	FREQ=3000	LOG MAG=-52	22	PHASE=-144	
FREQ=480	LOG MAG=-48	7	PHASE=30	22	FREQ=3040	LOG MAG=-55	02	PHASE=177	6
FREQ=520	LOG MAG=-47	13	PHASE=21	81	FREQ=3080	LOG MAG=-57	62	PHASE=-92	63
FREQ=560	LOG MAG=-47	95	PHASE=30	03	FREQ=3120	LOG MAG=-53	35	PHASE=-114	8
FREQ=600	LOG MAG=-50	74	PHASE=-28	03	FREQ=3160	LOG MAG=-55	04	PHASE=135	5
FREQ=640	LOG MAG=-49	15	PHASE=-29	14	FREQ=3200	LOG MAG=-51	83	PHASE=133	6
FREQ=680	LOG MAG=-47	53	PHASE=7	451	FREQ=3240	LOG MAG=-52	26	PHASE=163	
FREQ=720	LOG MAG=-47	47	PHASE=6	966	FREQ=3280	LOG MAG=-52	85	PHASE=-154	8
FREQ=760	LOG MAG=-47	41	PHASE=12	8	FREQ=3320	LOG MAG=-53	66	PHASE=137	3
FREQ=800	LOG MAG=-49	03	PHASE=20	68	FREQ=3360	LOG MAG=-55	54	PHASE=135	9
FREQ=840	LOG MAG=-57	12	PHASE=-40	68	FREQ=3400	LOG MAG=-51	9	PHASE=-143	5
FREQ=880	LOG MAG=-51	45	PHASE=-64	87	FREQ=3440	LOG MAG=-53	44	PHASE=-152	9
FREQ=920	LOG MAG=-52	98	PHASE=29	83	FREQ=3480	LOG MAG=-55	34	PHASE=-63	45
FREQ=960	LOG MAG=-48	77	PHASE=33	35	FREQ=3520	LOG MAG=-55	1	PHASE=-30	14
FREQ=1000	LOG MAG=-49	19	PHASE=16	23	FREQ=3560	LOG MAG=-51	37	PHASE=94	9
FREQ=1040	LOG MAG=-50	54	PHASE=10	32	FREQ=3600	LOG MAG=-50	4	PHASE=75	25
FREQ=1080	LOG MAG=-53	68	PHASE=-30	82	FREQ=3640	LOG MAG=-52	59	PHASE=-11	84
FREQ=1120	LOG MAG=-52	85	PHASE=74	55	FREQ=3680	LOG MAG=-59	59	PHASE=-6	956
FREQ=1160	LOG MAG=-54	86	PHASE=36	11	FREQ=3720	LOG MAG=-53	7	PHASE=-142	5
FREQ=1200	LOG MAG=-55	37	PHASE=-41	88	FREQ=3760	LOG MAG=-54	68	PHASE=-87	96
FREQ=1240	LOG MAG=-50	88	PHASE=29	44	FREQ=3800	LOG MAG=-49	85	PHASE=-30	02
FREQ=1280	LOG MAG=-51	84	PHASE=61	95	FREQ=3840	LOG MAG=-50	44	PHASE=-17	83
FREQ=1320	LOG MAG=-51	3	PHASE=142						
FREQ=1360	LOG MAG=-51	05	PHASE=132	4	FREQ=3880	LOG MAG=-47	87	PHASE=-161	3
FREQ=1400	LOG MAG=-54	02	PHASE=26	23	FREQ=3920	LOG MAG=-51	26	PHASE=-125	
FREQ=1440	LOG MAG=-53	51	PHASE=-116	6	FREQ=3960	LOG MAG=-55	63	PHASE=7	877
FREQ=1480	LOG MAG=-52	09	PHASE=54	33	FREQ=4000	LOG MAG=-53	22	PHASE=-84	68
FREQ=1520	LOG MAG=-53	9	PHASE=25	84	FREQ=4040	LOG MAG=-53	3	PHASE=177	9
FREQ=1560	LOG MAG=-51	98	PHASE=-84	83	FREQ=4080	LOG MAG=-57	7	PHASE=5	588
FREQ=1600	LOG MAG=-50	94	PHASE=-104	6	FREQ=4120	LOG MAG=-53	97	PHASE=-130	9
FREQ=1640	LOG MAG=-58	39	PHASE=86	92	FREQ=4160	LOG MAG=-52	96	PHASE=-164	8
FREQ=1680	LOG MAG=-54	3	PHASE=76	8	FREQ=4200	LOG MAG=-55	56	PHASE=-88	29
FREQ=1720	LOG MAG=-56	57	PHASE=62	77	FREQ=4240	LOG MAG=-55	24	PHASE=-167	1
FREQ=1760	LOG MAG=-50	77	PHASE=31	51	FREQ=4280	LOG MAG=-52	59	PHASE=-170	3
FREQ=1800	LOG MAG=-53	PHASE=177	7	FREQ=4320	LOG MAG=-54	58	PHASE=108	2	
FREQ=1840	LOG MAG=-50	98	PHASE=54	76	FREQ=4360	LOG MAG=-52	7	PHASE=-20	92
FREQ=1880	LOG MAG=-41	46	PHASE=30	18	FREQ=4400	LOG MAG=-51	66	PHASE=-21	26
FREQ=1920	LOG MAG=-39	57	PHASE=29	29	FREQ=4440	LOG MAG=-51	3	PHASE=-67	77
FREQ=1960	LOG MAG=-46	6	PHASE=45	94	FREQ=4480	LOG MAG=-53	6	PHASE=-60	48
FREQ=2000	LOG MAG=-51	73	PHASE=-11	12	FREQ=4520	LOG MAG=-53	92	PHASE=22	62
FREQ=2040	LOG MAG=-53	18	PHASE=-19	74	FREQ=4560	LOG MAG=-51	23	PHASE=5	841
FREQ=2080	LOG MAG=-54	19	PHASE=7	524	FREQ=4600	LOG MAG=-52	02	PHASE=-34	08
FREQ=2120	LOG MAG=-52	5	PHASE=79	77	FREQ=4640	LOG MAG=-50	82	PHASE=-52	49
FREQ=2160	LOG MAG=-53	03	PHASE=158	7	FREQ=4680	LOG MAG=-50	64	PHASE=-52	12
FREQ=2200	LOG MAG=-51	24	PHASE=-149	6	FREQ=4720	LOG MAG=-51	04	PHASE=-40	43
FREQ=2240	LOG MAG=-50	PHASE=173	3	FREQ=4760	LOG MAG=-54	73	PHASE=57	75	
FREQ=2280	LOG MAG=-44	93	PHASE=152	5	FREQ=4800	LOG MAG=-53	25	PHASE=18	68
FREQ=2320	LOG MAG=-47	35	PHASE=139	7	FREQ=4840	LOG MAG=-56	57	PHASE=-106	2
FREQ=2360	LOG MAG=-51	85	PHASE=98	78	FREQ=4880	LOG MAG=-59	26	PHASE=7	713
FREQ=2400	LOG MAG=-49	08	PHASE=-177	3	FREQ=4920	LOG MAG=-49	99	PHASE=43	37
FREQ=2440	LOG MAG=-48	99	PHASE=-143	2	FREQ=4960	LOG MAG=-50	4	PHASE=-29	69
FREQ=2480	LOG MAG=-55	45	PHASE=-33	44	FREQ=5000	LOG MAG=-50	64	PHASE=-51	53
FREQ=2520	LOG MAG=-53	22	PHASE=76	34	FREQ=5040	LOG MAG=-56	89	PHASE=-85	52
				FREQ=5080	LOG MAG=-53	34	PHASE=-100	8	

Figure 56(a). Cross-Spectrum for Lownstream Probe; Hardwall Configuration  
75-1F, 100% Speed, Immersion of 4.4 cm (1.715 in.), 0 to  
5080 Hz.

FREQ=5120	LOG MAG=-51	4	PHASE=-22	84	FREQ=7680	LOG MAG=-51	67	PHASE=-20	21
FREQ=5160	LOG MAG=-50	21	PHASE=9	71	FREQ=7720	LOG MAG=-54	82	PHASE=-9	558
FREQ=5200	LOG MAG=-53	76	PHASE=45	3	FREQ=7760	LOG MAG=-55	3	PHASE=44	79
FREQ=5240	LOG MAG=-52	84	PHASE=-102	1	FREQ=7800	LOG MAG=-51	53	PHASE=58	18
FREQ=5280	LOG MAG=-54	49	PHASE=-106	8	FREQ=7840	LOG MAG=-56	05	PHASE=109	5
FREQ=5320	LOG MAG=-52	26	PHASE=-126	9	FREQ=7880	LOG MAG=-53	29	PHASE=37	72
FREQ=5360	LOG MAG=-53	35	PHASE=-59	73	FREQ=7920	LOG MAG=-51	38	PHASE=78	03
FREQ=5400	LOG MAG=-51	48	PHASE=-13	53	FREQ=7960	LOG MAG=-53	35	PHASE=27	81
FREQ=5440	LOG MAG=-52	91	PHASE=78	76	FREQ=8000	LOG MAG=-53	09	PHASE=27	72
FREQ=5480	LOG MAG=-55	27	PHASE=59	72	FREQ=8040	LOG MAG=-56	99	PHASE=70	22
FREQ=5520	LOG MAG=-53	11	PHASE=18	5	FREQ=8080	LOG MAG=-55	79	PHASE=-11	07
FREQ=5560	LOG MAG=-50	23	PHASE=-5	928	FREQ=8120	LOG MAG=-51	3	PHASE=-4	134
FREQ=5600	LOG MAG=-50	45	PHASE=-28	05	FREQ=8160	LOG MAG=-51	11	PHASE=69	32
FREQ=5640	LOG MAG=-51	28	PHASE=-35	91	FREQ=8200	LOG MAG=-56	16	PHASE=-83	61
FREQ=5680	LOG MAG=-50	05	PHASE=13	74	FREQ=8240	LOG MAG=-54	47	PHASE=161	6
FREQ=5720	LOG MAG=-47	16	PHASE=62	92	FREQ=8280	LOG MAG=-51	52	PHASE=120	5
FREQ=5760	LOG MAG=-53	6	PHASE=1	027	FREQ=8320	LOG MAG=-56	19	PHASE=44	79
FREQ=5800	LOG MAG=-50	76	PHASE=-50	83	FREQ=8360	LOG MAG=-55	16	PHASE=5	291
FREQ=5840	LOG MAG=-52	19	PHASE=-15	51	FREQ=8400	LOG MAG=-63	39	PHASE=64	11
FREQ=5880	LOG MAG=-54	95	PHASE=-39	18	FREQ=8440	LOG MAG=-56	7	PHASE=91	74
FREQ=5920	LOG MAG=-52	18	PHASE=-148	4	FREQ=8480	LOG MAG=-52	35	PHASE=27	
FREQ=5960	LOG MAG=-55	33	PHASE=92	17	FREQ=8520	LOG MAG=-51	36	PHASE=63	49
FREQ=6000	LOG MAG=-54	32	PHASE=4	828	FREQ=8560	LOG MAG=-52	72	PHASE=96	1
FREQ=6040	LOG MAG=-55	44	PHASE=-30	68	FREQ=8600	LOG MAG=-51	54	PHASE=161	5
FREQ=6080	LOG MAG=-53	83	PHASE=15	2	FREQ=8640	LOG MAG=-53	16	PHASE=-173	9
FREQ=6120	LOG MAG=-54	6	PHASE=44	08	FREQ=8680	LOG MAG=-52	03	PHASE=-109	1
FREQ=6160	LOG MAG=-55	66	PHASE=-2	357	FREQ=8720	LOG MAG=-54	99	PHASE=171	9
FREQ=6200	LOG MAG=-51	78	PHASE=-36	28	FREQ=8760	LOG MAG=-52	92	PHASE=150	8
FREQ=6240	LOG MAG=-53	34	PHASE=43	3	FREQ=8800	LOG MAG=-54	73	PHASE=-5	802
FREQ=6280	LOG MAG=-56	64	PHASE=121	4	FREQ=8840	LOG MAG=-56	41	PHASE=-33	68
FREQ=6320	LOG MAG=-55	47	PHASE=152	9	FREQ=8880	LOG MAG=-53	43	PHASE=-77	11
FREQ=6360	LOG MAG=-52	72	PHASE=42	67	FREQ=8920	LOG MAG=-56	58	PHASE=-15	25
FREQ=6400	LOG MAG=-54	31	PHASE=4	851	FREQ=8960	LOG MAG=-56	72	PHASE=-14	25
FREQ=6440	LOG MAG=-54	61	PHASE=35	33	FREQ=9000	LOG MAG=-53	34	PHASE=-70	25
FREQ=6480	LOG MAG=-51	26	PHASE=37	45	FREQ=9040	LOG MAG=-52	18	PHASE=-60	39
FREQ=6520	LOG MAG=-55	41	PHASE=55	72	FREQ=9080	LOG MAG=-54	71	PHASE=-73	09
FREQ=6560	LOG MAG=-55	09	PHASE=130		FREQ=9120	LOG MAG=-58	49	PHASE=-10	96
FREQ=6600	LOG MAG=-57	6	PHASE=140	3	FREQ=9160	LOG MAG=-53	65	PHASE=-104	9
FREQ=6640	LOG MAG=-52	3	PHASE=27	14	FREQ=9200	LOG MAG=-52	94	PHASE=-154	3
FREQ=6680	LOG MAG=-51	34	PHASE=78	25	FREQ=9240	LOG MAG=-50	52	PHASE=179	5
FREQ=6720	LOG MAG=-53	06	PHASE=94	01	FREQ=9280	LOG MAG=-51	03	PHASE=142	8
FREQ=6760	LOG MAG=-54	15	PHASE=127	2	FREQ=9320	LOG MAG=-55	16	PHASE=-50	97
FREQ=6800	LOG MAG=-55	46	PHASE=98	52	FREQ=9360	LOG MAG=-50	6	PHASE=-129	7
FREQ=6840	LOG MAG=-50	47	PHASE=-6	18	FREQ=9400	LOG MAG=-50	97	PHASE=-140	3
FREQ=6880	LOG MAG=-51	72	PHASE=4	374	FREQ=9440	LOG MAG=-54	64	PHASE=110	4
FREQ=6920	LOG MAG=-51	87	PHASE=115	8	FREQ=9480	LOG MAG=-52	75	PHASE=100	5
FREQ=6960	LOG MAG=-51	82	PHASE=111	2	FREQ=9520	LOG MAG=-52	19	PHASE=80	41
FREQ=7000	LOG MAG=-50	42	PHASE=91	94	FREQ=9560	LOG MAG=-53	78	PHASE=68	27
FREQ=7040	LOG MAG=-52	88	PHASE=80	64	FREQ=9600	LOG MAG=-58	49	PHASE=62	23
FREQ=7080	LOG MAG=-52	9	PHASE=115	4	FREQ=9640	LOG MAG=-53	57	PHASE=110	8
FREQ=7120	LOG MAG=-55	3	PHASE=107	6	FREQ=9680	LOG MAG=-55	71	PHASE=167	2
FREQ=7160	LOG MAG=-54	18	PHASE=87	2	FREQ=9720	LOG MAG=-54	04	PHASE=-143	6
FREQ=7200	LOG MAG=-54	92	PHASE=76	58	FREQ=9760	LOG MAG=-52	58	PHASE=-9	859
FREQ=7240	LOG MAG=-52	69	PHASE=147	1	FREQ=9800	LOG MAG=-50	77	PHASE=-11	58
FREQ=7280	LOG MAG=-52	37	PHASE=122	9	FREQ=9840	LOG MAG=-51	07	PHASE=-35	22
FREQ=7320	LOG MAG=-56	5	PHASE=-144	6	FREQ=9880	LOG MAG=-51	31	PHASE=-23	52
FREQ=7360	LOG MAG=-51	89	PHASE=-28	11	FREQ=9920	LOG MAG=-53	72	PHASE=-8	656
FREQ=7400	LOG MAG=-49	33	PHASE=-19	08	FREQ=9960	LOG MAG=-54	73	PHASE=138	1
FREQ=7440	LOG MAG=-53	05	PHASE=-22	38	FREQ=10000	LOG MAG=-56	22	PHASE=48	39
FREQ=7480	LOG MAG=-53	93	PHASE=103	3	FREQ=10040	LOG MAG=-55	76	PHASE=165	1
FREQ=7520	LOG MAG=-49	72	PHASE=71	19	FREQ=10080	LOG MAG=-55	95	PHASE=-175	5
FREQ=7560	LOG MAG=-50	3	PHASE=56	91	FREQ=10120	LOG MAG=-55	6	PHASE=150	1
FREQ=7600	LOG MAG=-49	95	PHASE=81	45	FREQ=10160	LOG MAG=-54	37	PHASE=164	7
FREQ=7640	LOG MAG=-51	34	PHASE=61	14	FREQ=10200	LOG MAG=-55	03	PHASE=-42	23

Figure 56(b). Cross-Spectrum for Downstream Probe; Hardwall Configuration 75-1F, 100% Speed, Immersion of 4.4 cm (1.715 in.), 5120 to 10,200 Hz.

ORIGINAL PAGE IS  
OF POOR QUALITY

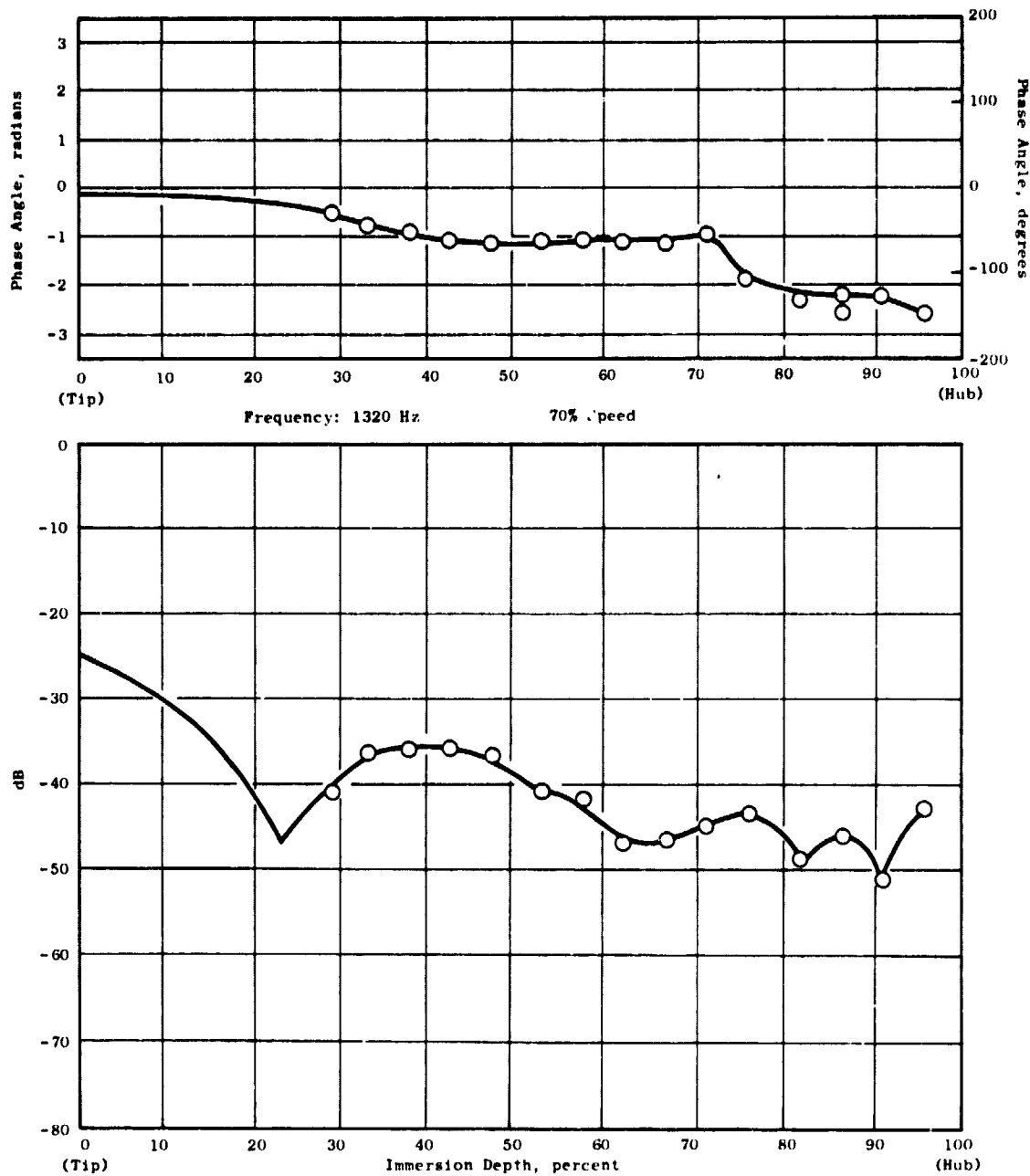


Figure 57. Complex Acoustic Pressure Profile for Hardwall Configuration  
75-1F; 1320 Hz, 70% Speed.

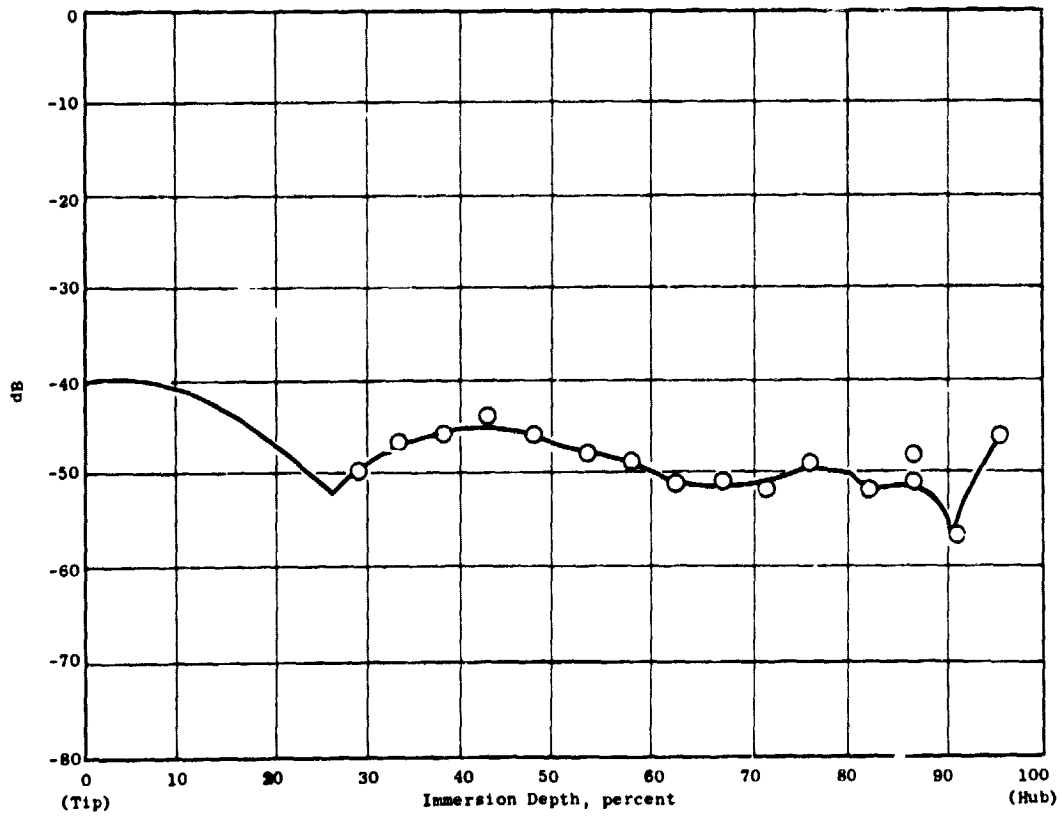
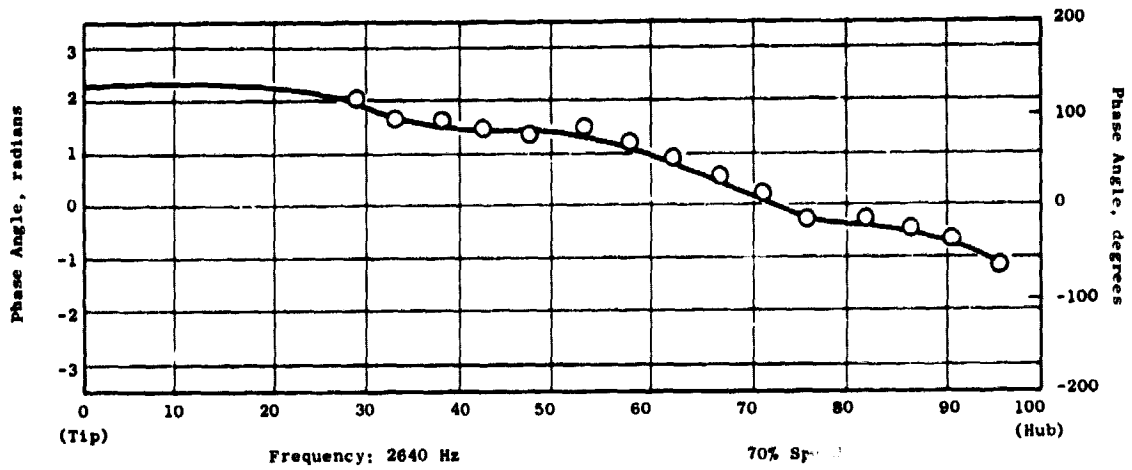


Figure 58. Complex Acoustic Pressure Profile for Hardwall Configuration 75-1F; 2640 Hz, 70% Speed.

ORIGINAL PAGE IS  
OF POOR QUALITY

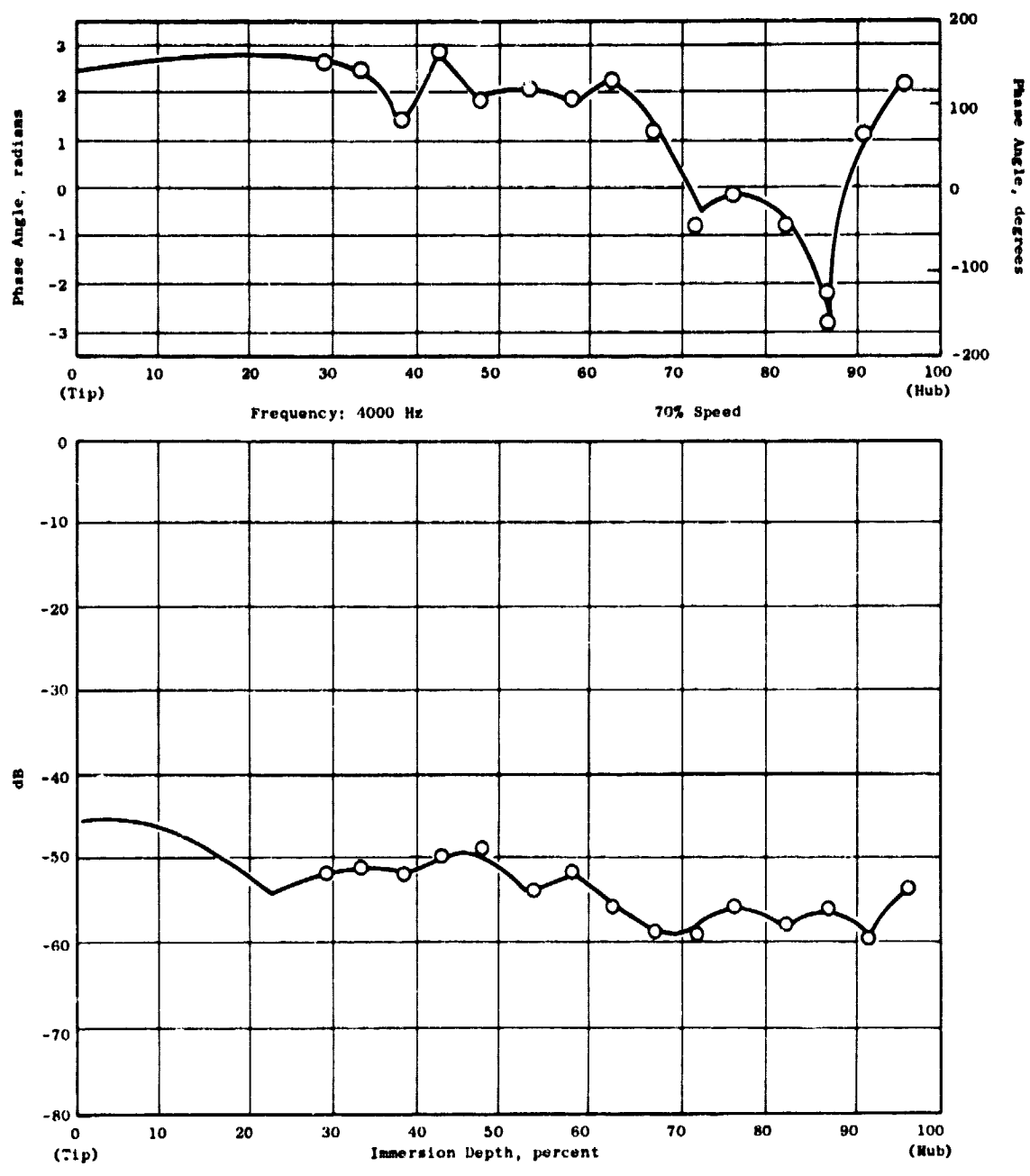


Figure 59. Complex Acoustic Pressure Profile for Hardwall Configuration  
75-1F; 4000 Hz, 70% Speed.

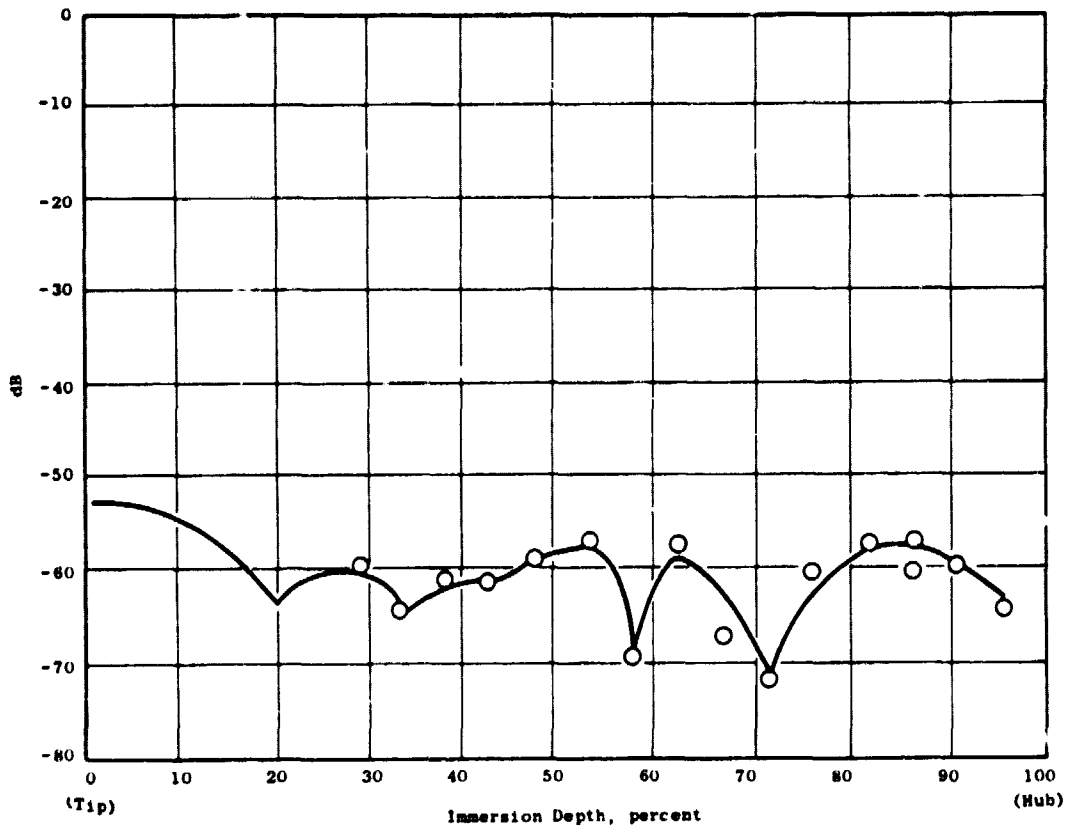
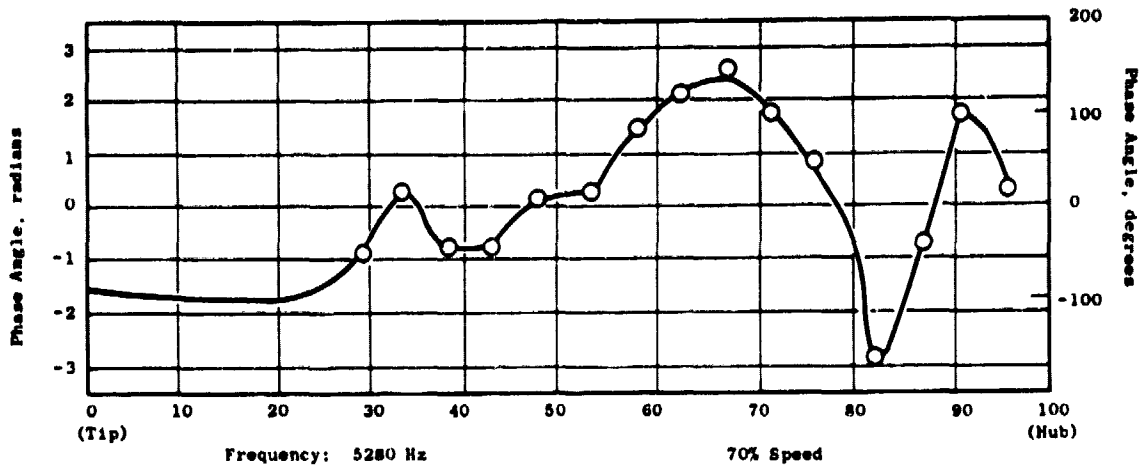


Figure 60. Complex Acoustic Pressure Profile for Hardwall Configuration 75-1F; 5280 Hz, 70% Speed.



ORIGINAL PAGE IS  
OF POOR QUALITY

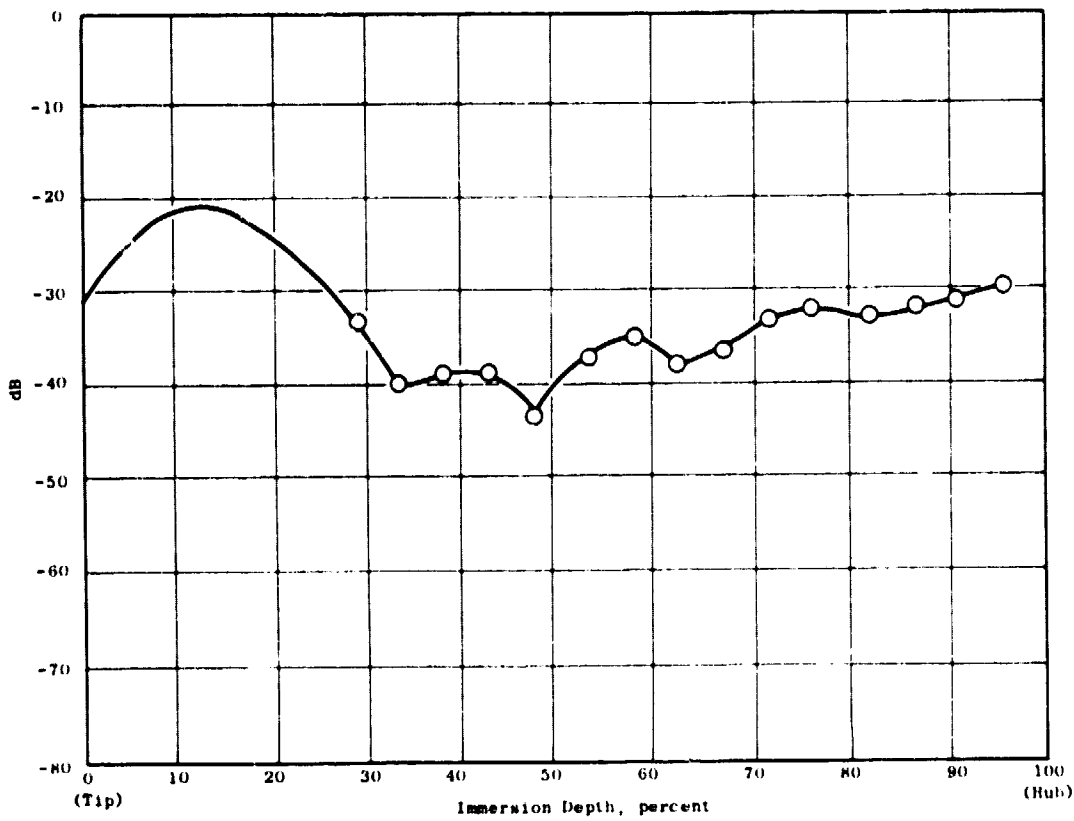
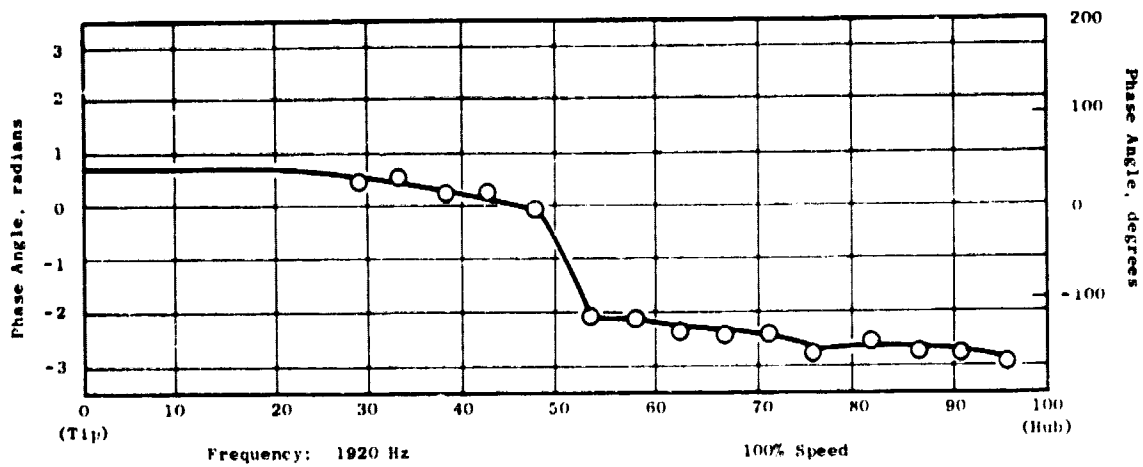


Figure 61. Complex Acoustic Pressure Profile for Hardwall Configuration  
75-1F; 1920 Hz, 100% Speed.

C-2

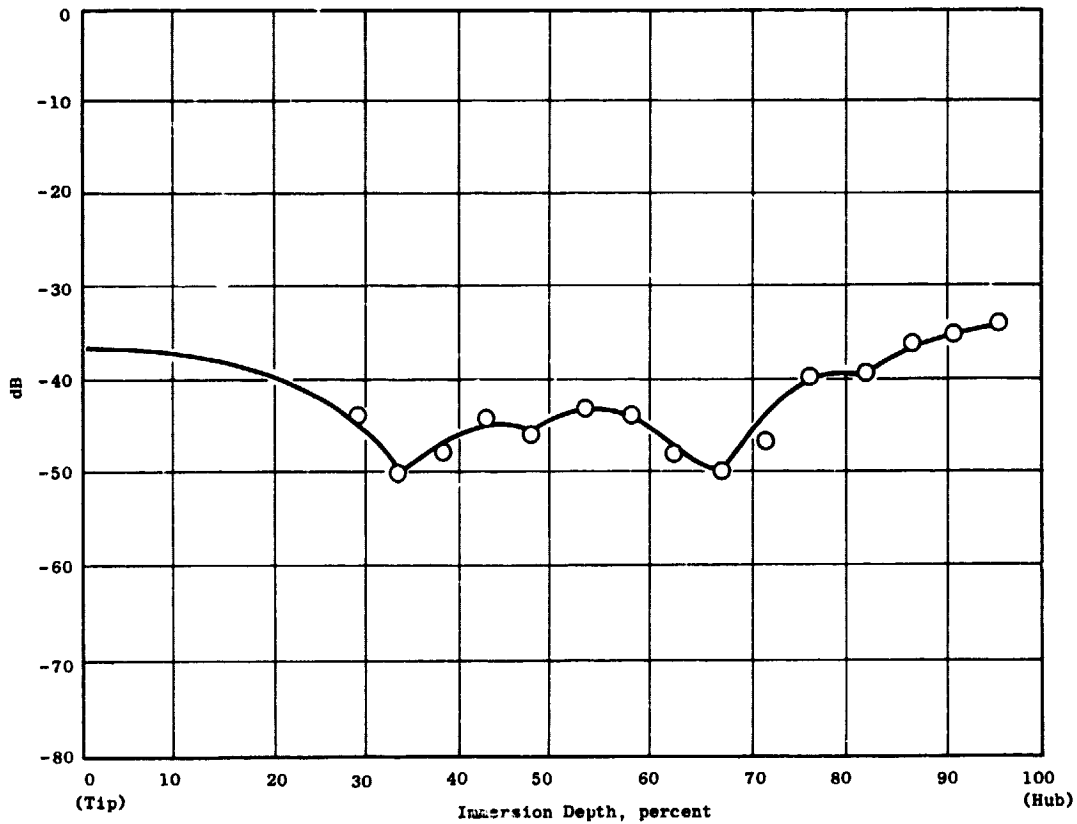
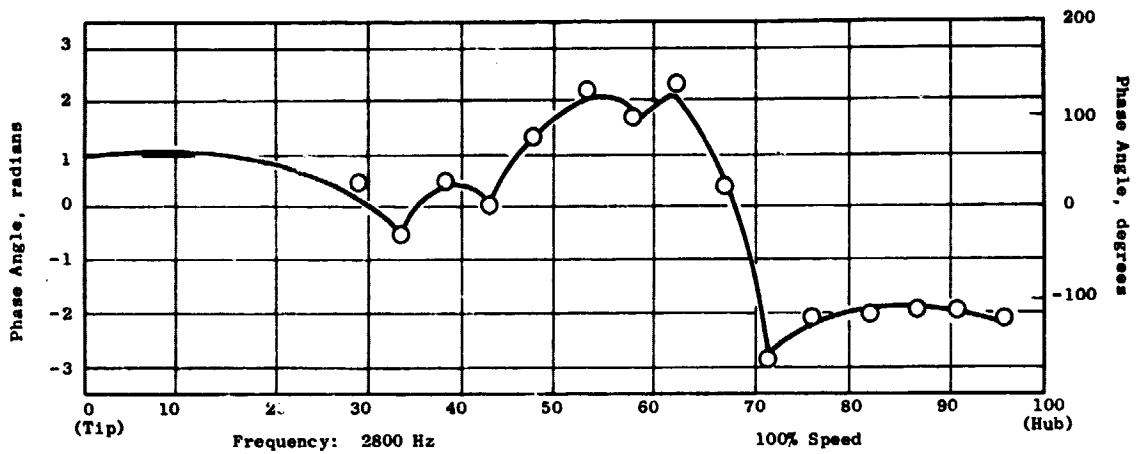


Figure 62. Complex Acoustic Pressure Profile for Hardwall Configuration 75-1F; 3800 Hz, 100% Speed.

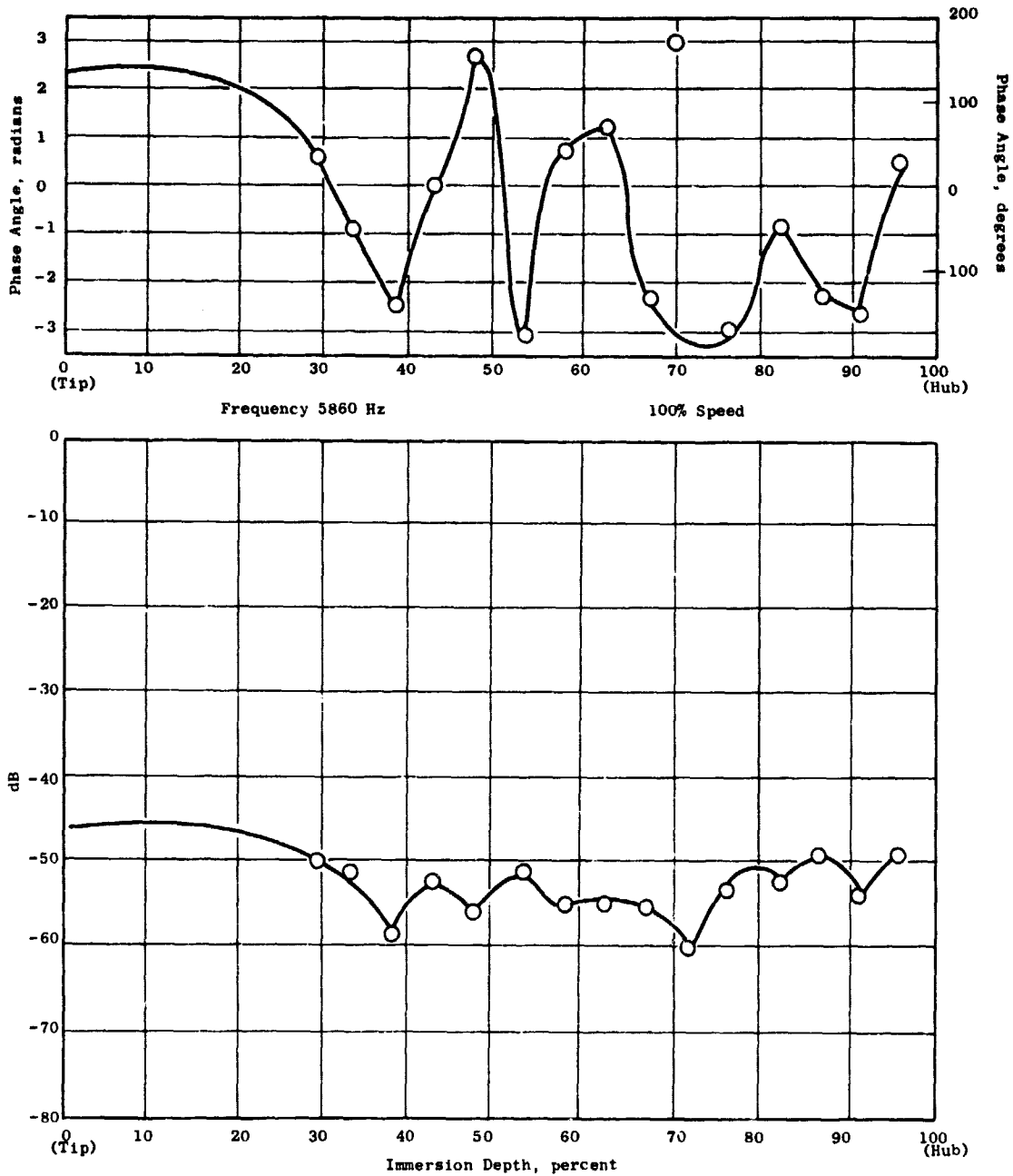


Figure 63. Complex Acoustic Pressure Profile for Hardwall Configuration 75-1F; 5860 Hz, 100% Speed.

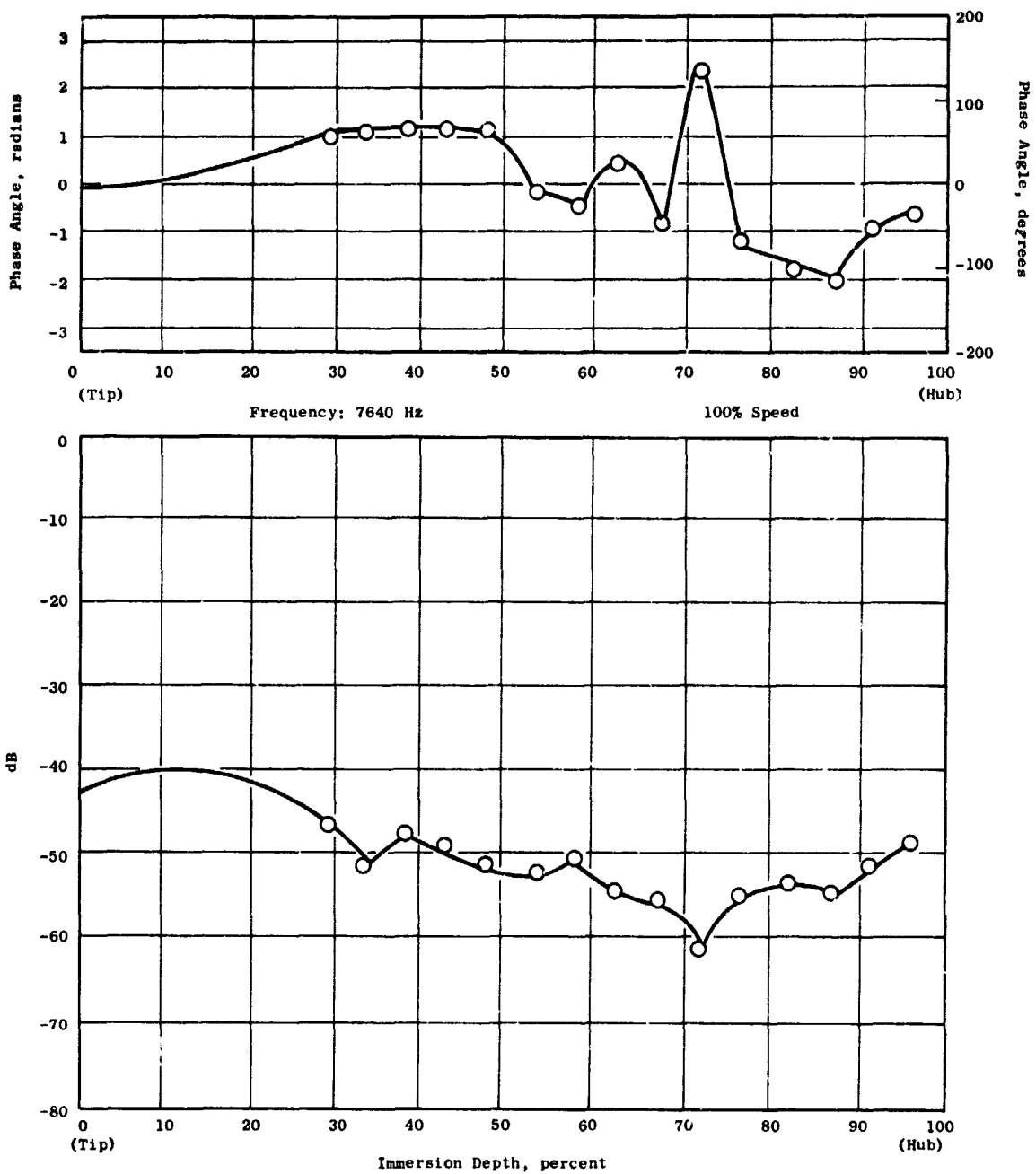


Figure 64. Complex Acoustic Pressure Profile for Hardwall Configuration 75-1F; 7640 Hz, 100% Speed.

Table III. Rotor 55 Modal Analysis.

Configuration 75-1F, 70% Speed												
Mode	Frequency 1320 Hz		Frequency 2640 Hz		Frequency 4000 Hz		Frequency 5280 Hz		Relative Magnitude	Phase, deg.	Relative Magnitude	Phase, deg.
	Relative Magnitude	Phase, rad.	Relative Magnitude	Phase, rad.	Relative Magnitude	Phase, rad.	Relative Magnitude	Phase, rad.				
	deg.	deg.	deg.	deg.	deg.	deg.	deg.	deg.				
1	1.000	0.00	1.000	0.00	1.000	0.00	1.000	0.00	1.000	0.00	1.000	0.00
2	0.896	0.17	0.926	0.41	0.685	0.21	1.100	12.0	1.100	-0.35	1.100	-20.1
3	0.721	0.34	0.413	1.08	0.336	0.67	1.013	38.6	1.013	-0.62	1.013	-35.5
4	0.654	0.29	0.361	0.50	0.254	0.22	0.461	12.6	0.461	-0.84	0.461	-47.9
5	0.585	0.13	0.360	0.24	0.382	-0.02	0.441	-1.3	0.441	0.38	0.441	21.8
6	0.499	0.12	0.246	0.08	0.108	0.25	0.520	14.4	0.520	-0.24	0.520	-13.7

Configuration 75-1F, 100% Speed												
Mode	Frequency 1920 Hz		Frequency 3800 Hz		Frequency 5800 Hz		Frequency 7640 Hz		Relative Magnitude	Phase, deg.	Relative Magnitude	Phase, deg.
	Relative Magnitude	Phase, rad.	Relative Magnitude	Phase, rad.	Relative Magnitude	Phase, rad.	Relative Magnitude	Phase, rad.				
	deg.	deg.	deg.	deg.	deg.	deg.	deg.	deg.				
1	1.000	0.00	1.000	0.00	1.000	0.00	1.000	0.00	1.000	0.00	1.000	0.00
2	1.175	-0.03	8.784	1.92	1.160	-0.16	0.788	-9.3	0.788	0.04	0.788	2.1
3	0.763	0.06	1.963	-0.86	0.623	0.23	0.535	13.0	0.535	-0.31	0.535	-18.0
4	0.546	0.02	4.949	2.09	0.586	0.41	0.260	23.7	0.260	-0.64	0.260	-36.4
5	0.252	0.21	1.072	-1.46	0.187	-4.86	0.128	-278.7	0.128	-1.45	0.128	-83.0
6	0.076	0.50	1.140	1.69	0.319	-3.84	0.193	-220.3	0.193	-3.02	0.193	-172.8

mode; that is, the lowest order modal coefficient has an amplitude of one, and a phase angle of zero radians (0 degrees) in each case. The most interesting result is the relative participation of the modes. This can be better visualized when shown in bar graph form, in Figures 65 to 72.

The ability of the modal expansion to converge to the desired acoustic pressure profile is evidenced by reexpanding the profile in a series of eigenfunctions as given by Equation (2). Samples of the reexpansion of two cases are shown in Figures 73 and 74. In all cases, the modal expansion was performed assuming the measurement was done in a hardwall section of duct.

#### 4. The Use of Modal Measurements in Prediction of Suppression

The most likely place to perform a modal measurement to characterize the source would be in a plane upstream of the treated section. It was discovered by using the sound separation technique discussed in Section V-A that this signal contained "hydrodynamic" pressure pulsation due to the turbulent wakes of the rotor passing the probe. These wakes cause a nonacoustic signal which is correlated between the wall and probe microphone, thus contaminating the acoustic signal. For this reason, the modal measurements made at the downstream probe location in the hardwall duct configuration were assumed to be representative of the source modal distribution. It was further assumed that the source modal distribution would not change appreciably between the hardwall and the treated configurations.

General Electric (Reference 12) has developed a rectangular flow duct acoustic propagation program which calculates wave propagation in ducts with multiple treatment sections and uniform mean flow. The required input to the program consists of the duct dimensions, the flow Mach number, the modal participation at the source plane, and the acoustic impedance of the wall treatment at the given frequency. The calculation is based on a narrowband assumption, and reflections at the duct termination are neglected. Inherent also is the assumption that the annular duct can be represented as a rectangular duct for purposes of analysis.

Using the source modal measurements, acoustic PWL suppression was calculated for several Rotor 55 treatment configurations. These configurations are listed in Figure 75. The predicted results are presented in Table IV.

The calculations have been compared to both narrowband and 1/3-octave band far-field  $\Delta$ PWL measurements. Table V lists the measured PWL suppressions for the six treated configurations for 1/3-octaves which contain the pure tone frequencies of the analysis. Since the 1320 Hz blade passing frequency at 70% speed is near the cutoff frequency between the 1250 and 1600 Hz 1/3-octaves, both are tabulated. Table VI lists the measured PWL suppressions for the 20 Hz bandwidth narrowbands.

Before considering the correlation between the analytical and measured data, it should be noted that several sources of error are present which could adversely affect the agreement. First, one would normally expect a

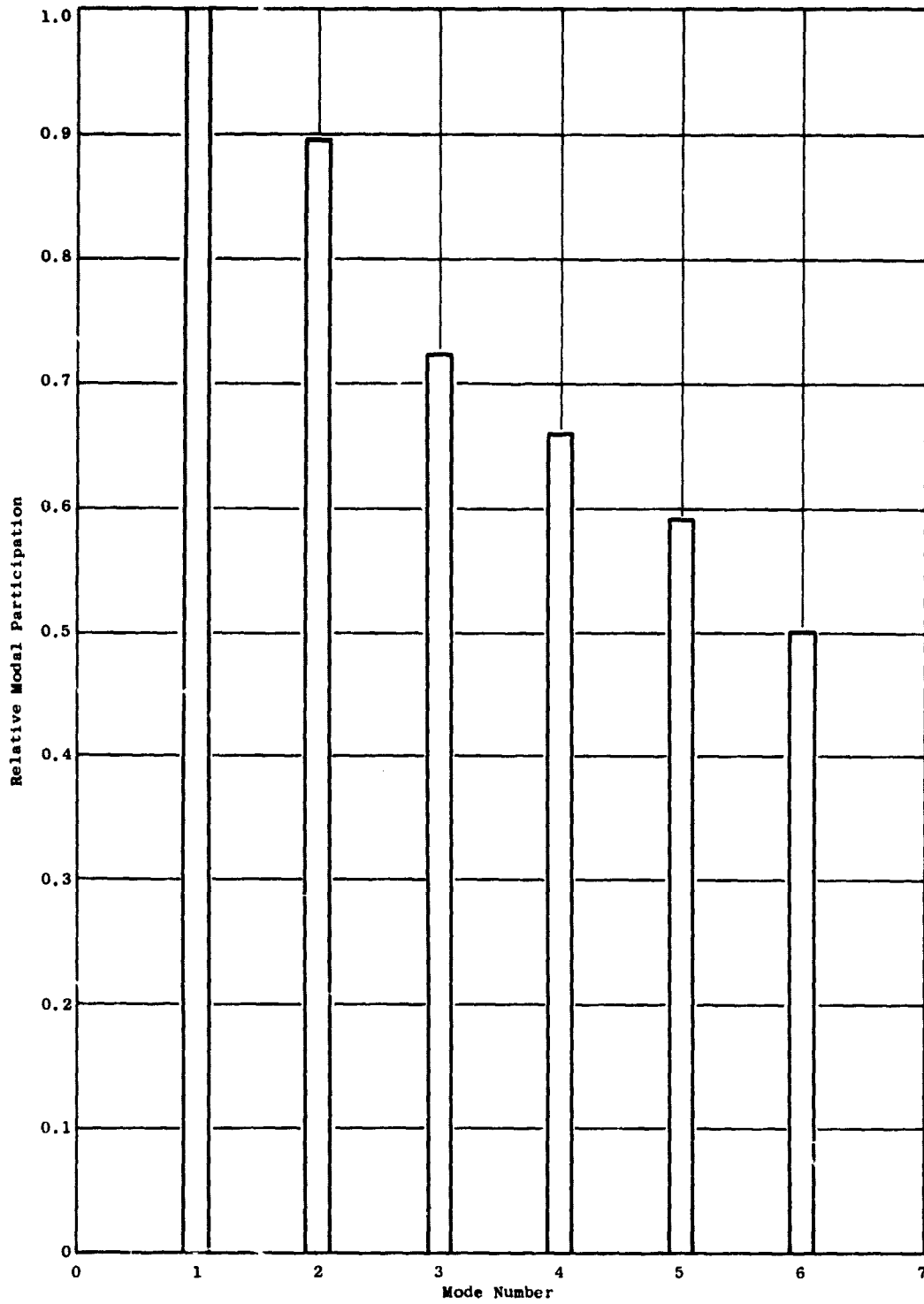


Figure 65. Relative Modal Participation for Hardwall Configuration  
75-1F; 70% Speed, 1320 Hz.

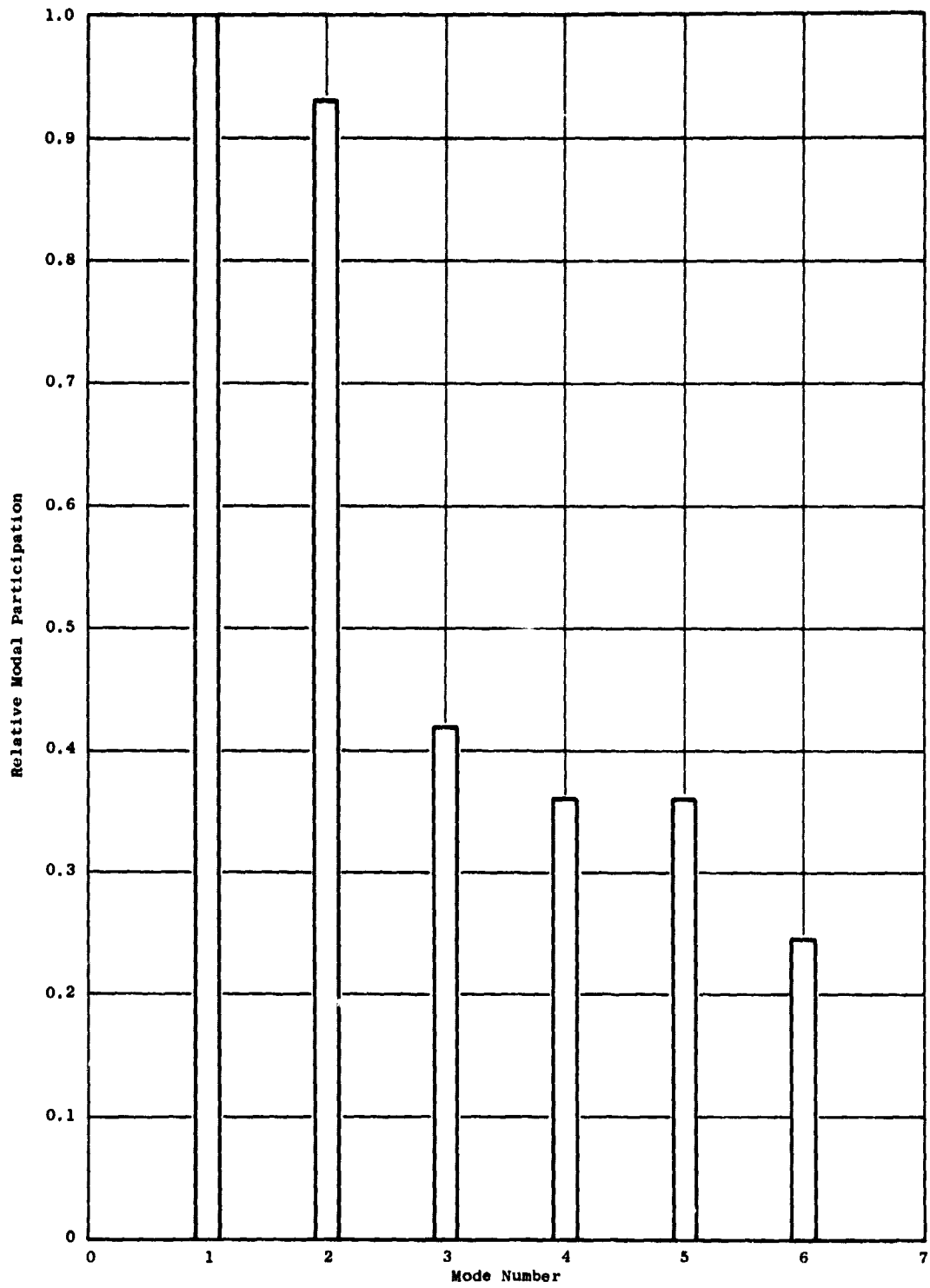


Figure 66. Relative Modal Participation for Hardwall Configuration  
75-1F; 70% Speed, 2640 Hz.



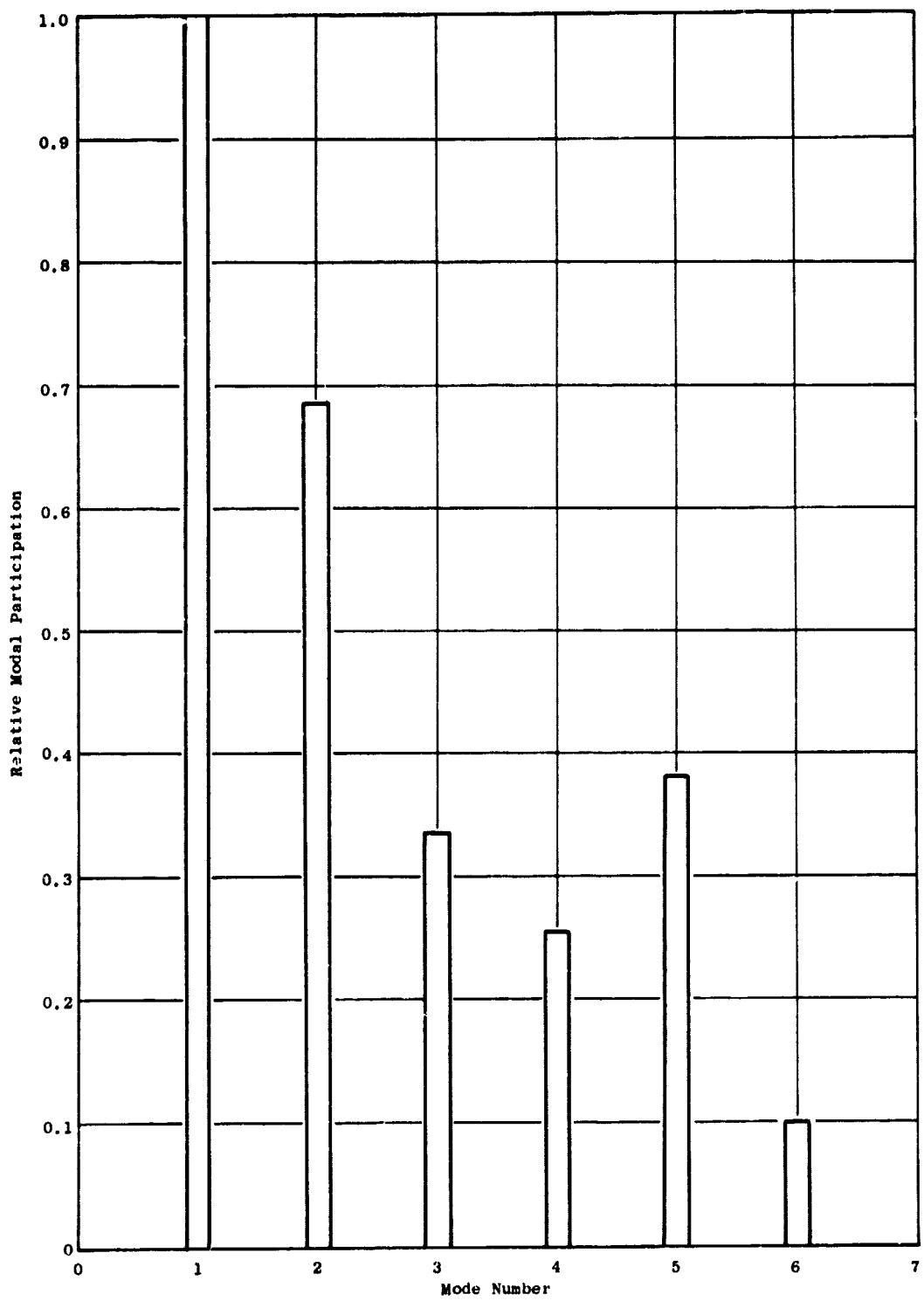


Figure 67. Relative Modal Participation for Hardwall Configuration 75-1F; 70% Speed, 4000 Hz.

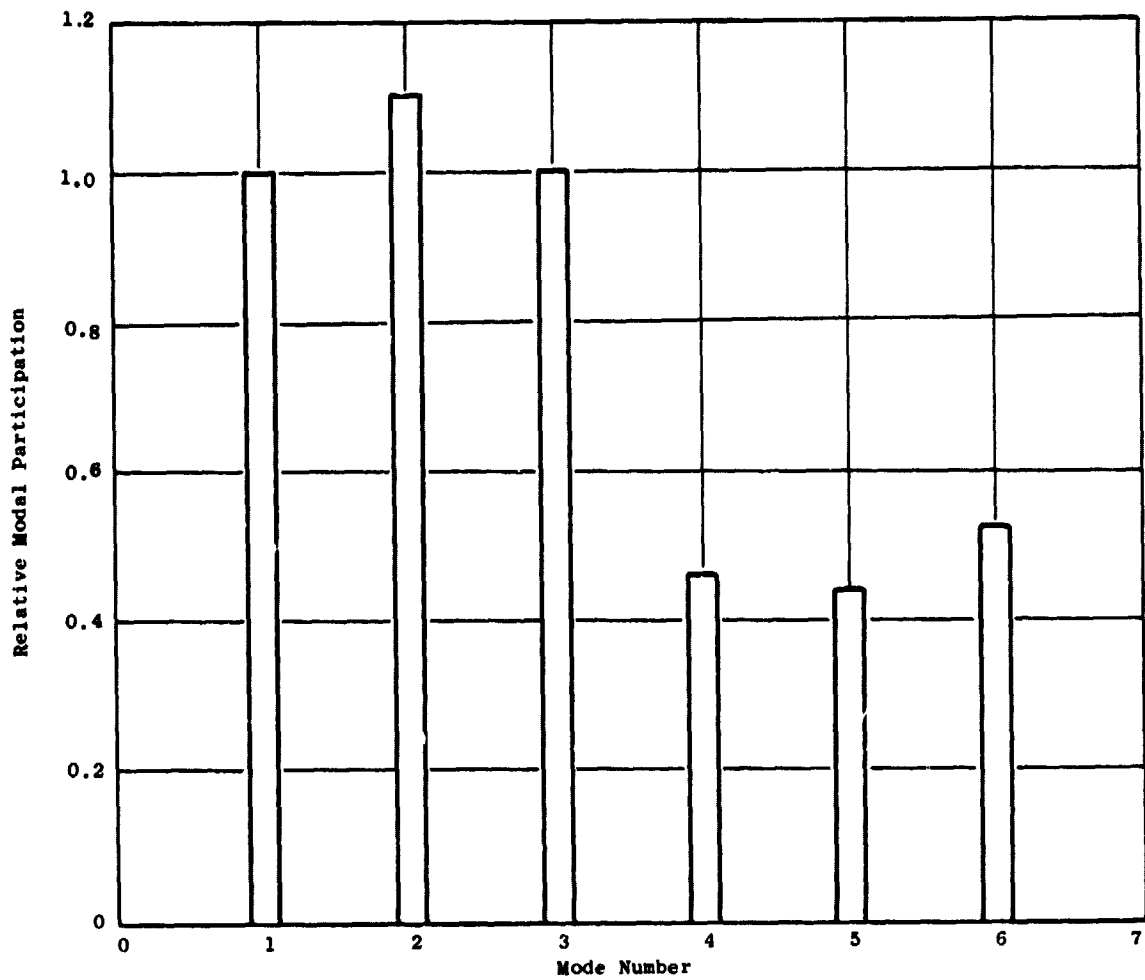


Figure 68. Relative Modal Participation for Hardwall Configuration 75-1F; 70% Speed, 5280 Hz.

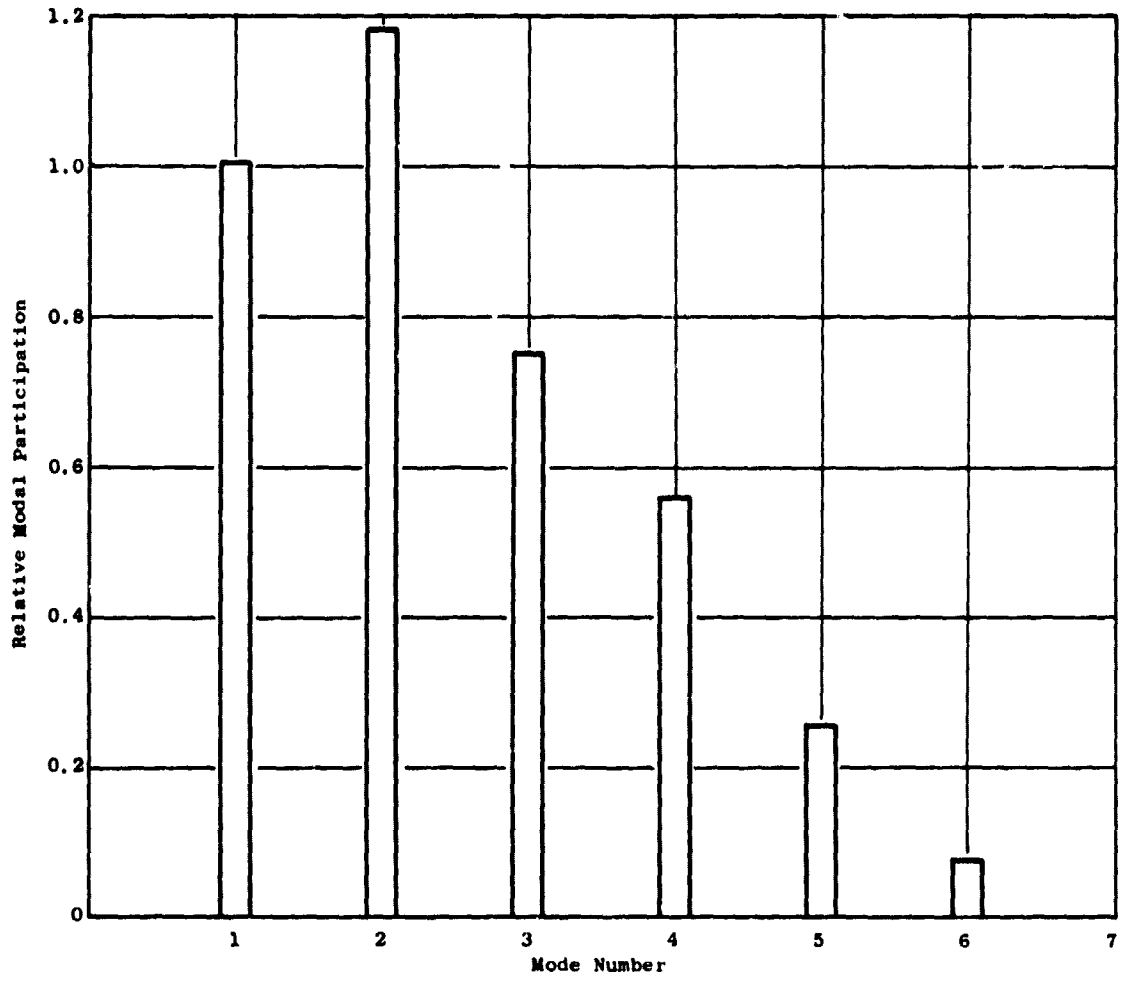


Figure 69. Relative Modal Participation for Hardwall Configuration  
75-1F; 100% Speed, 1920 Hz.

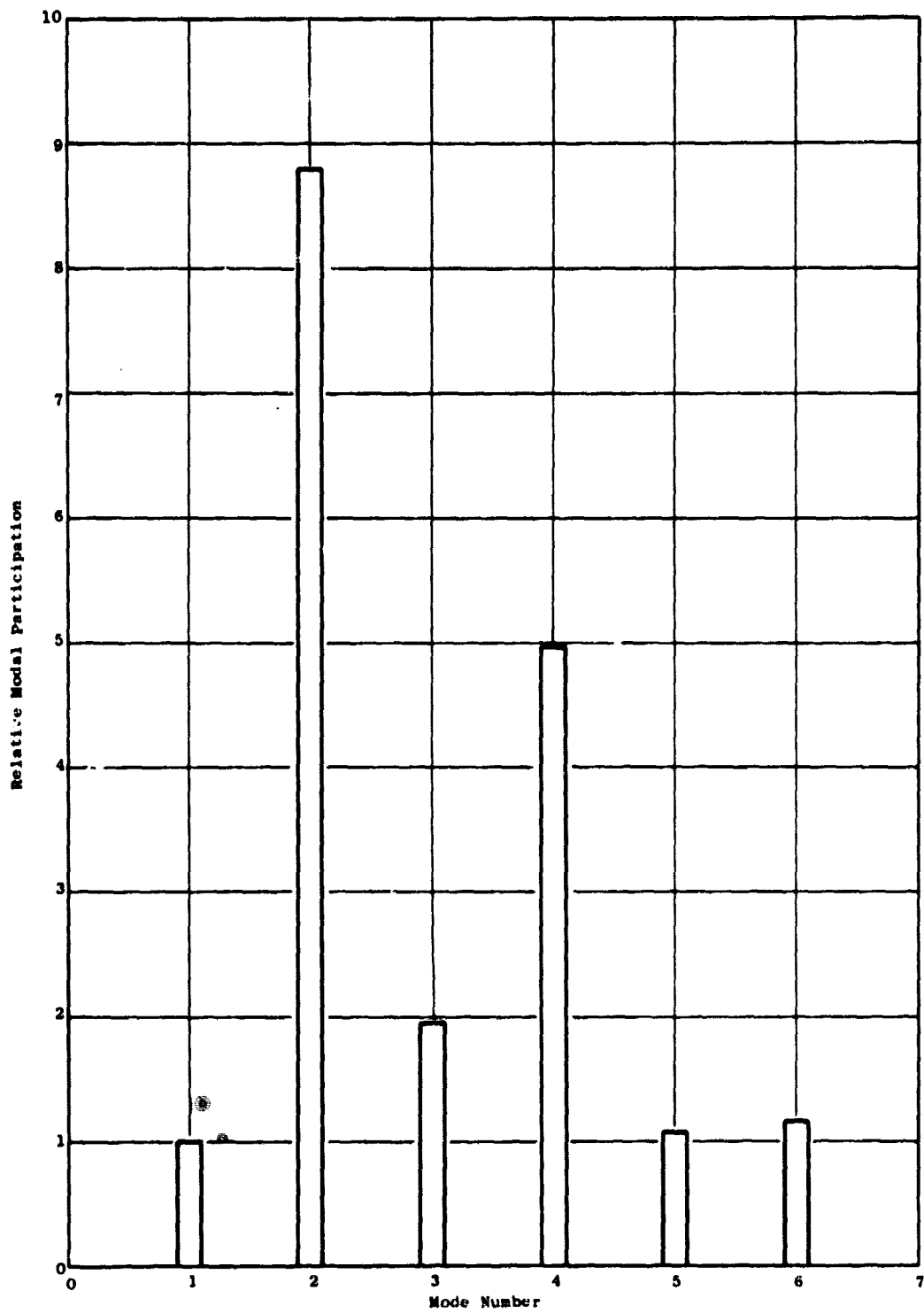


Figure 70. Relative Modal Participation for Hardwall Configuration  
75-1F; 100% Speed, 3800 Hz.

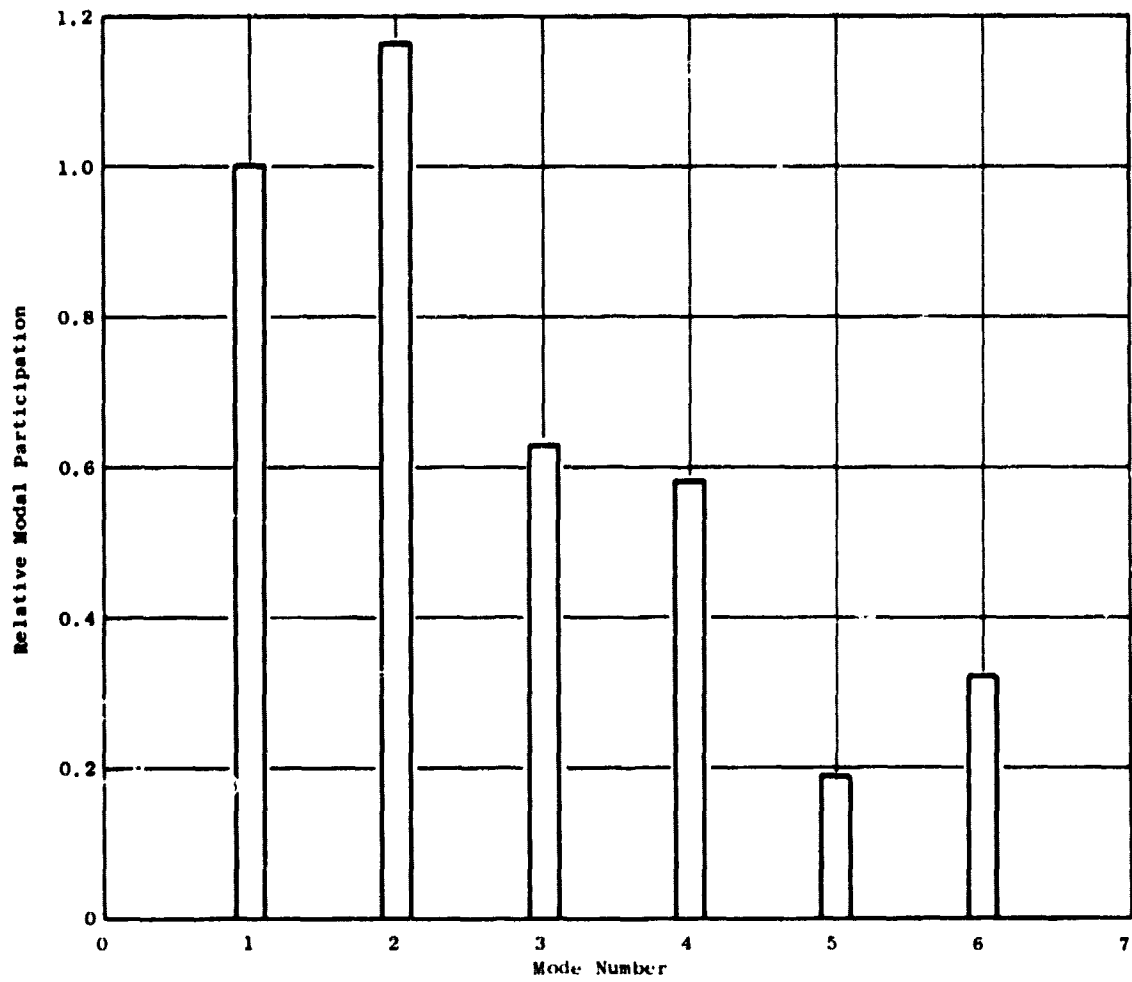


Figure 71. Relative Modal Participation for Hardwall Configuration  
75-1F; 100% Speed, 5800 Hz.

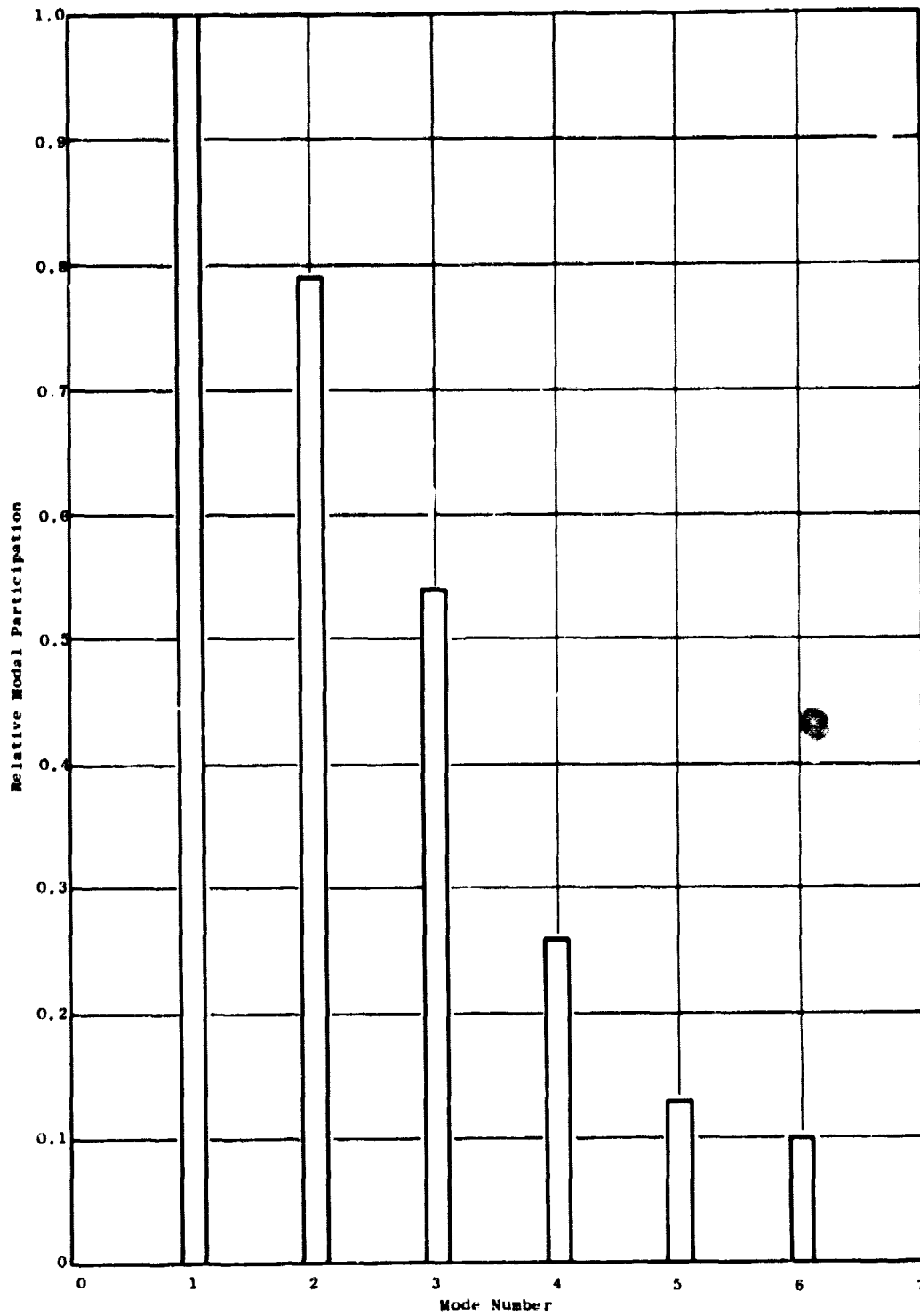


Figure 72. Relative Modal Participation for Hardwall Configuration 75-1F; 100% Speed, 7640 Hz.

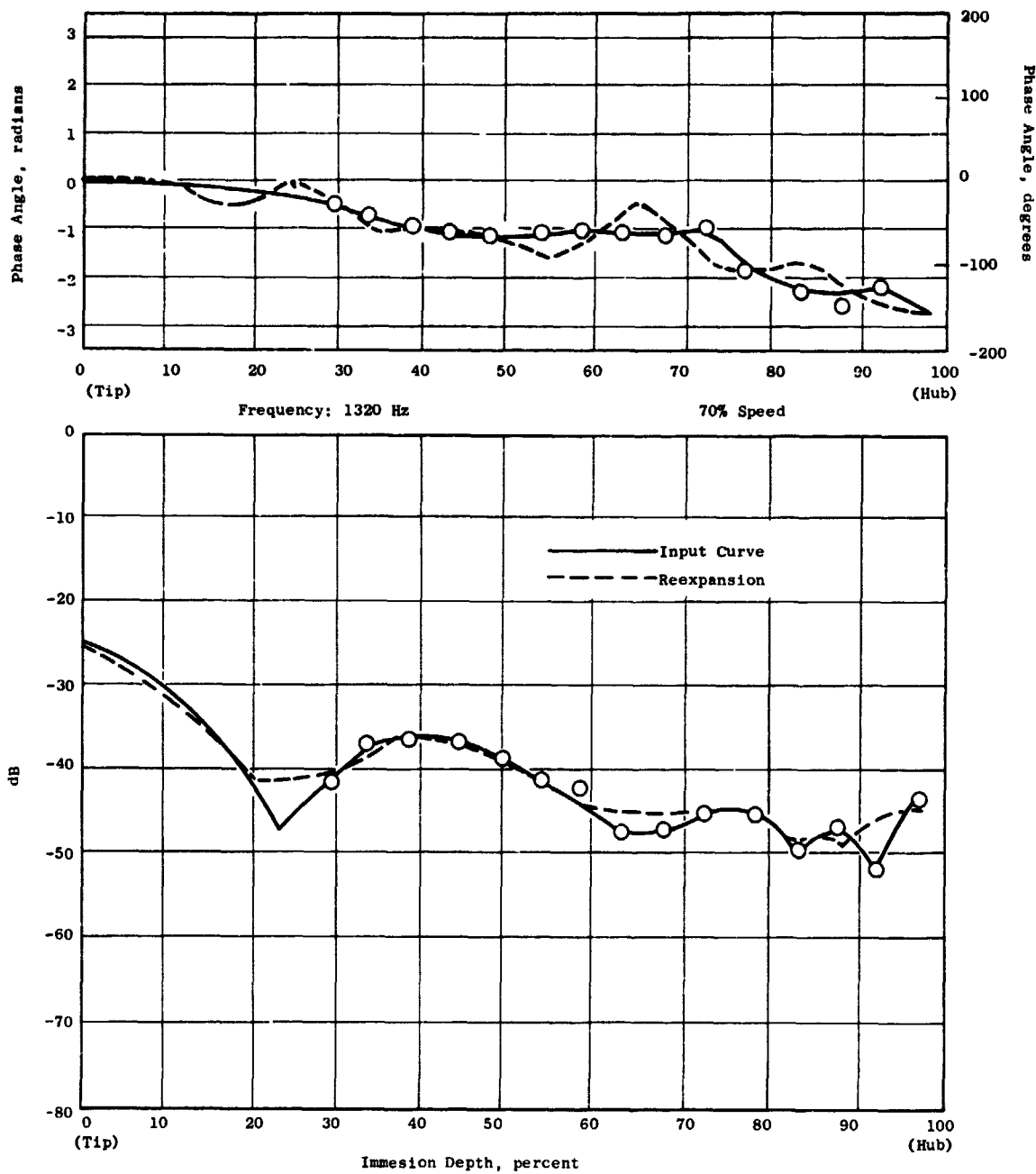


Figure 73. Reexpansion of Complex Acoustic Pressure Profile; 1320 Hz, 70% Speed.

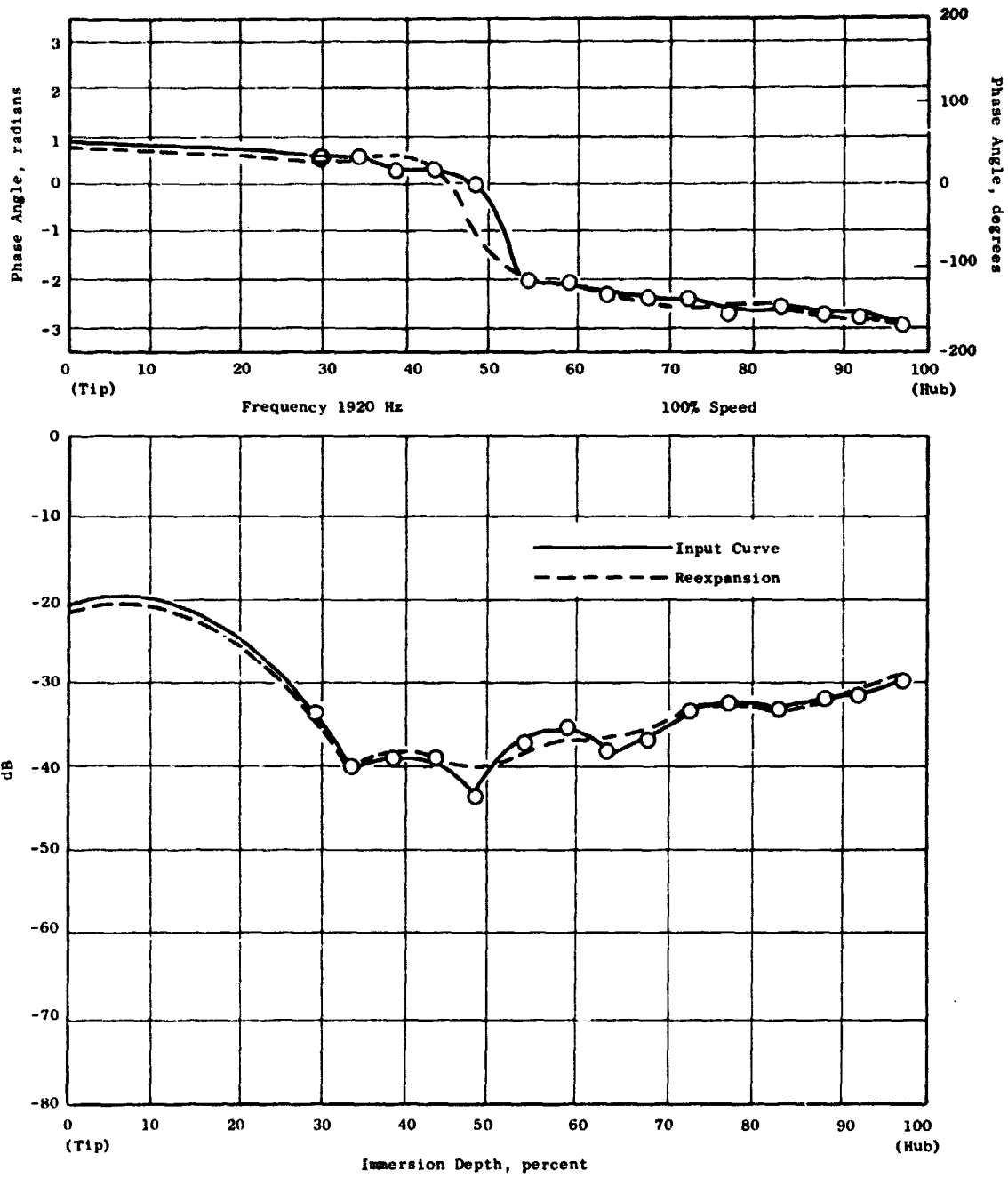
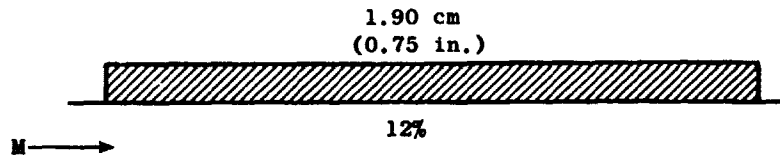


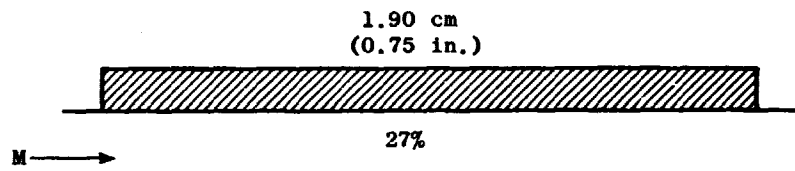
Figure 74. Reexpansion of Complex Acoustic Pressure Profile; 1920 Hz, 100% Speed.



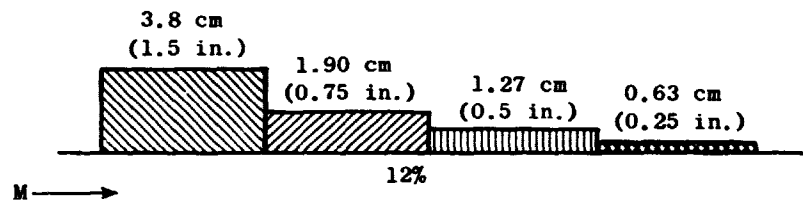
ORIGINAL PAGE IS  
OF POOR QUALITY



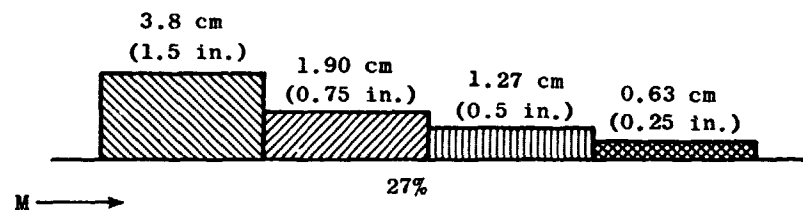
Configuration 75-3 12% Single Phase



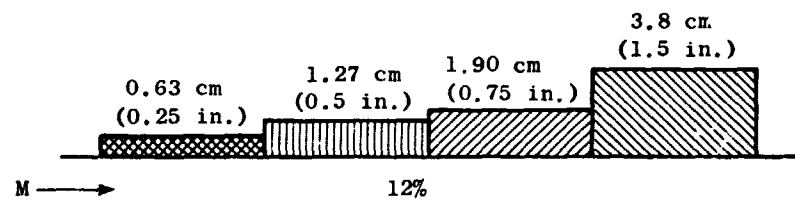
Configuration 17 27% Single Phase



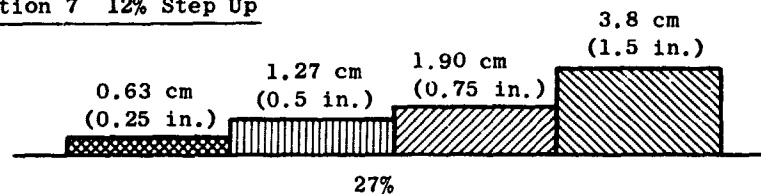
Configuration 26 12% Step Down



Configuration 75-5 27% Step Down



Configuration 7 12% Step Up



Configuration 8 27% Step Up

Figure 75. Designation of Configurations Used for Analytical Predictions.

Table IV. Calculated Narrowband  $\Delta$ PWL Suppressions, Rotor 55.

Configuration		70% Speed $\Delta$ PWL, dB			
		1320 Hz	2640 Hz	4000 Hz	5280 Hz
75-3	12% Single Phase	3.3	41.9	9.3	6.6
17	27% Single Phase	0.5	25.5	7.8	6.6
26	12% Step Down	6.9	18.1	9.0	9.5
75-5	27% Step Down	2.5	*	6.1	*
7	12% Step Up	6.9	18.4	13.3	10.6
8	27% Step Up	4.0	15.8	*	*

Configuration		100% Speed $\Delta$ PWL, dB			
		1920 Hz	3800 Hz	5800 Hz	7640 Hz
75-3	12% Single Phase	13.3	28.0	6.2	1.8
17	27% Single Phase	6.3	26.5	5.8	1.5
26	12% Step Down	11.4	23.6	10.4	4.6
75-5	27% Step Down	16.9	21.7	13.2	4.5
7	12% Step Up	10.1	20.2	10.8	5.2
8	27% Step Up	12.6	18.1	14.5	5.5

\* Program Experienced Numerical Difficulties

Table V. Measured 1/3-Octave  $\Delta$ PWL Suppressions, Rotor 55.

Configuration		70% Speed $\Delta$ PWL, dB				
		1250 Hz	1600 Hz	2500 Hz	4000 Hz	5000 Hz
75-3	12% Single Phase	9.1	10.9	20.8	10.8	7.4
17	27% Single Phase	3.1	4.6	16.9	7.6	5.8
26	12% Step Down	10.3	11.6	16.7	12.2	11.3
75-5	27% Step Down	6.3	11.2	14.0	8.0	8.4
7	12% Step Up	10.2	11.3	17.9	13.0	10.3
8	27% Step Up	6.4	9.7	13.7	8.7	8.3

Configuration		100% Speed $\Delta$ PWL, dB			
		2000 Hz	4000 Hz	6300 Hz	8000 Hz
75-3	12% Single Phase	17.1	14.5	5.4	3.4
17	27% Single Phase	13.6	9.4	5.6	3.7
26	12% Step Down	17.0	15.3	11.0	7.3
75-5	27% Step Down	15.6	9.5	7.5	5.3
7	12% Step UP	15.3	15.3	10.9	6.6
8	27% Step Up	16.7	10.0	9.0	6.2

Table VI. Measured Narrowband  $\Delta$ PWL Suppressions, Rotor 55.

Configuration		70% Speed $\Delta$ PWL, dB			
		1320 Hz	2640 Hz	4000 Hz	5280 Hz
75-3	12% Single Phase	9	27.8	8.5	8.4
17	27% Single Phase	2.7	21.8	8.8	7.2
26	12% Step Down	12.7	24.5	12.2	12.3
75-5	27% Step Down	5.7	16.1	7.8	9.4
7	12% Step Up	12.5	24.7	16	13.3
8	27% Step Up	10.3	15.3	12.2	9.3

Configuration		100% Speed $\Delta$ PWL, dB			
		1920 Hz	3800 Hz	5800 Hz	7640 Hz
75-3	12% Single Phase	21.7	18	7.3	6.3
17	27% Single Phase	17.1	12	8.7	8.7
26	12% Step Down	20.5	17	12.8	5.9
75-5	27% Step Down	20.8	11	12.2	7.2
7	12% Step Up	19.7	19.7	16.5	7.1
8	27% Step Up	23.2	15.7	15.2	11

different attenuation rate for a tone spike which falls within a certain 1/3-octave band than for the overall 1/3-octave band attenuation, depending on how much the tone level exceeds the broadband noise. Second, for both 1/3-octave band and narrowband comparisons the analytical prediction is quite sensitive to variations in impedance of the liners. The impedance for the calculations was obtained from simplified analytical models and may contain substantial errors. Third, the rectangular duct analogy is assumed. If higher order spinning modes are present in the vehicle, the measured attenuations might tend to be higher than the calculated values. Fourth, the incomplete radial modal traverse and estimated extrapolation may cause the modal expansion to be in error. This may be the dominant effect as the prediction is quite sensitive to modal content.

In comparing Tables IV and V, several observations can be made. First, the analytical program underpredicts the suppression at the blade passing frequency. Considering the four possible sources of error, a possible cause of this would be that higher order spinning modes contribute substantially to the source energy at this frequency. No spinning mode measurements were attempted in this program, so this cannot be quantitatively determined from the present data. Since this is the only harmonic at which the suppression levels were underpredicted, it would also require that coherent higher order spinning modes be produced most effectively at blade passing frequency. It should be noted that Yurkovich (Reference 15) suggests that only the radial modes need be considered in the annular exhaust duct.

At the second harmonic, the calculations overpredict the suppression for both the third octave and narrowband data. These frequencies are near the tuning frequencies of the single-phase liners, where the attenuation is quite sensitive to the impedance. Slight errors in determining the impedance for the analytical prediction could have caused the overprediction in these cases.

At all frequencies, substantial errors could have been introduced by the extrapolation of the pressure profile to the outer wall. The 25% of the profile at the outer wall which was missed is very likely the most important part of the profile as far as energy content of the propagating signal is concerned. The extrapolation of the profile over this region was only a rough guess at the shape of the waveform. The modal participation is dependent on the profile shape, and the prediction, in turn, is very sensitive to the modal content.

The measured and predicted suppressions at the third and fourth harmonics yield reasonably good quantitative correlation.

Ignoring the quantitative aspect of the data for a moment, qualitative correlation can be obtained by ranking the treatment configurations in order of suppression effectiveness, from best to worst, at each speed and frequency. Tables VII and VIII show this type of comparison for the measured and calculated results. It is obvious that, with some exceptions, the agreement in ranking between measured and calculated configurations is quite close. For the considered duct and condition, the analytical program definitely predicts the trend which indicates the 12% porosity liners to be more

Table VII. Comparison of Measured and Calculated Suppression Effectiveness Rankings of Rotor 55 Treatment Configurations, 70% Speed.

Measured			Calculated			Measured		
Rank	Configuration	ΔPWL	Rank	Configuration	ΔPWL	Rank	Configuration	ΔPWL
<u>1250 Hz 1/3-Octave</u>								
1	26	10.3	1	26	6.9	1	1320 Hz Narrowband	12.7
2	7	10.2	2	7	6.9	2	12% Step Down	12.5
3	75-3	9.1	3	8	4.0	3	12% Step Up	10.3
4	75-5	6.3	4	75-3	3.3	4	27% Step Up	9.0
5	8	6.4	5	75-5	2.5	5	12% Single Phase	5.7
6	17	3.1	6	17	0.5	6	27% Step Down	2.7
<u>2500 Hz 1/3-Octave</u>								
1	75-3	20.8	1	75-3	41.9	1	2640 Hz Narrowband	27.8
2	7	17.9	2	17	25.5	2	12% Single Phase	24.7
3	17	16.9	3	7	18.4	3	12% Step Up	24.5
4	26	16.7	4	26	18.1	4	12% Step Down	21.8
5	8	13.7	5	8	15.8	5	27% Single Phase	15.3
<u>4000 Hz 1/3-Octave</u>								
1	7	13.0	1	7	13.3	1	4000 Hz Narrowband	16.0
2	26	12.2	2	75-3	9.3	2	12% Step Up	12.2
3	75-3	10.8	3	26	9.0	3	12% Step Down	8.8
4	75-5	8.0	4	17	7.8	4	27% Single Phase	8.5
5	17	7.6	5	75-5	6.1	5	12% Single Phase	7.8
<u>5000 Hz 1/3-Octave</u>								
1	26	11.3	1	7	10.6	1	5280 Hz Narrowband	13.3
2	7	10.3	2	26	9.5	2	12% Step Up	12.3
3	75-3	7.4	3	75-3	6.6	3	12% Step Down	8.4
4	17	5.8	4	17	6.6	4	12% Single Phase	7.2

ORIGINAL PAGE IS  
OF POOR QUALITY

Table VIII. Comparison of Measured and Calculated Suppression Effectiveness Rankings of Rotor 55 Treatment Configurations, 100% Speed.

Measured			Calculated			Measured		
Rank	Configuration	ΔPWL	Rank	Configuration	ΔPWL	Rank	Configuration	ΔPWL
<u>2000 Hz 1/3-Octave</u>								
1	75-3	17.1	1	75-5	16.9	1	8	23.2
2	26	17.0	2	75-3	13.3	2	75-3	21.7
3	8	16.7	3	8	12.6	3	75-5	20.8
4	75-5	15.6	4	26	11.4	4	26	20.5
5	7	15.3	5	7	10.1	5	7	19.7
6	17	13.6	6	17	6.3	6	17	17.1
<u>4000 Hz 1/3-Octave</u>								
1	26	15.3	1	75-3	28.0	1	7	19.2
2	7	15.3	2	17	26.5	2	75-3	18.0
3	75-3	9.4	3	26	23.6	3	26	17.0
4	8	10.0	4	75-5	21.7	4	8	15.7
5	75-5	9.5	5	7	20.2	5	17	12.0
6	17	9.4	6	8	18.1	6	75-5	11.0
<u>6300 Hz 1/3-Octave</u>								
1	26	11.0	1	8	14.5	1	7	16.5
2	7	10.9	2	75-5	13.2	2	8	15.2
3	8	9.0	3	7	10.8	3	26	12.8
4	75-5	7.5	4	26	10.4	4	75-5	12.2
5	17	5.6	5	75-3	6.2	5	17	8.9
6	75-3	5.4	6	17	5.8	6	75-3	7.3
<u>8000 Hz 1/3-Octave</u>								
1	26	7.3	1	8	5.5	1	8	11.0
2	7	6.6	2	7	5.2	2	17	8.7
3	8	6.2	3	26	4.6	3	75-5	7.2
4	75-5	5.3	4	75-5	4.5	4	7	7.1
5	17	3.7	5	75-3	1.8	5	75-3	6.3
6	75-3	3.4	6	17	1.5	6	26	5.9
<u>1920 Hz Narrowband</u>								
<u>3800 Hz Narrowband</u>								
<u>5800 Hz Narrowband</u>								
<u>7640 Hz Narrowband</u>								

effective than the 27% porosity liners. As this technique becomes more definitive it may be applied to engine designs when the modal content of the source and duct is known. While the check on an absolute basis was not as good in this case as needed for predicting suppression levels, other experience suggests that significantly improved correlation might have been obtained if (1) the radial modal measurement had been made across the entire annulus height (~50% of the area was not traversed because of a goose-neck used on the sound-separation probe used in this program), and (2) the acoustic impedance of the treatment had been determined experimentally in the grazing flow impedance tube.

### C. Rotor Wake Analysis

Interaction of fan blade wakes with downstream blade rows has long been recognized as an important generation mechanism for fan noise. In fact, with today's larger rotor-stator spacings, viscous wake interaction and turbulence-rotor interaction are the two dominant factors in the production of fan noise. Traditionally, viscous wake interaction has been associated mainly with pure tones, but more recently (Reference 10) this mechanism has also been identified as a source of fan broadband noise. Over the years, much effort has been expended on the analytical prediction of wake interaction noise, but one major flaw in all these analyses has been the lack of a good mathematical wake description. Presently used models have been derived using stationary isolated airfoil data or cascade data, but these models do not appear to provide complete representations of the wakes shed from a fan rotor.

Wake modulations have recently been postulated as a source of fan broadband noise. Analytical work has been done on this problem but detailed experimental data on the type and extent of wake modulation which exists behind a fan rotor are almost nonexistent. Hence, we are forced in our analytical work to use wake models derived from comparatively smooth flow over stationary blades, and to guess at the behavior of these wakes as a function of time and space for a moving blade row. The need for aerodynamic investigations of fan rotor wakes is thus clearly indicated.

A step toward the solution of this problem was taken when hot film wake survey data were acquired on Rotor 55. This type of data provides velocity information directly rather than requiring the transformation of pressure to velocity, as is necessary with conventional aerodynamic data. This allows a more direct comparison of our analytical wake models with experiment.

#### 1. Basics of Hot Film Anemometry

Hot film probes consist of a temperature-sensitive metallic coating deposited on a cylindrical ceramic substrate. The coating is heated electrically and placed in an electronic Wheatstone bridge similar to that used with strain gages. When this heated metallic element is immersed in a flowing field, the sensor is cooled an amount proportional to the mass flux ( $\rho V$ ) of the flow. The resulting sensor temperature change alters the probe's electrical resistance, which is, in turn, measured by the bridge circuit.



By calibrating this probe system over a known range of  $\rho V$ , the mass flux in any flow can be measured. Then by measuring or computing the flow density, the velocity can be extracted from the mass flux.

Many different styles and types of hot film probes are available. In this case the two-dimensional "x" array probe such as illustrated in Figure 76 was used. The two elements of the probe are electrically and mechanically isolated from each other and each has its own electronics package for measuring the sensor resistance. The probe is oriented so that the incoming flow vector is at or near the bisector of the right angle between the sensors as indicated in Figure 77. Then, denoting the voltage signal from one sensor as "A" and the other as "B", the longitudinal velocity is proportional to  $\overline{A + B}$ ; and the transverse velocity is proportional to  $\overline{A - B}$ .

## 2. Probe Calibration

Probe calibration is accomplished by immersing the probe in a free air jet of known velocity and thermodynamic properties. By directing the jet along the probe "x" bisector the probe was calibrated for longitudinal velocity alone since  $\overline{A - B}$  should be zero. Varying the jet Mach number then produces the longitudinal calibration curve of Figure 78. Note that the  $\overline{A - B}$  voltage is virtually zero ( $\leq .1$  volt) as it should be for zero yaw angle. Simple conversion of jet Mach number and gas properties to mass flux converts Figure 78 to the more useful Figure 79.

Calibration for flow directionality is obtained by simply yawing the probe to several angles at various fixed jet Mach numbers. This calibration is presented as  $\overline{(A - B) / (A + B)}$  versus yaw angle in Figure 80. Use of the directionality calibration in this ratio form is advantageous since any gas temperature change effects are automatically cancelled out. The probe calibrations shown in Figures 78, 79, and 80 are those obtained on the probe used to take wake data on Rotor 55. These curves are by no means universal for all "x" array hot film probes, nor even for the same probe from test to test. The probe tips must be recalibrated before each job to assure reasonable accuracy.

Calibration curves of Figures 79 and 80 have been curve fit by fourth-order polynomials to allow use of computerized data reduction techniques. The following equations represent these curves within a reasonable accuracy band.

$$\rho V_{\text{long}} = 0.8567084 + 8.577701 \overline{(A + B)} - 0.20490007 \overline{(A + B)}^2 \\ + 0.021138243 \overline{(A + B)}^3 - 0.00070591945 \overline{(A + B)}^4$$

$$\text{Yaw Angle (rad)} = - 0.0090939458 + 1.9812846 (R) - 0.49972652R^2 \\ - 3.7908338R^3 + 7.4028571R^4$$

$$R = \frac{A - B}{A + B}$$

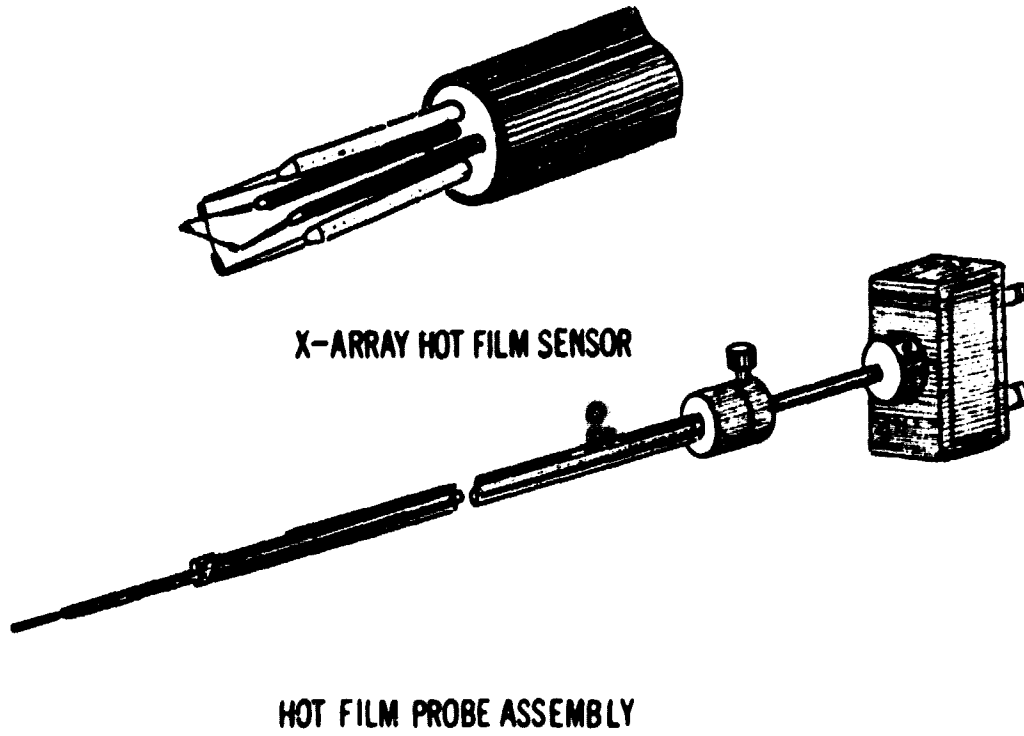
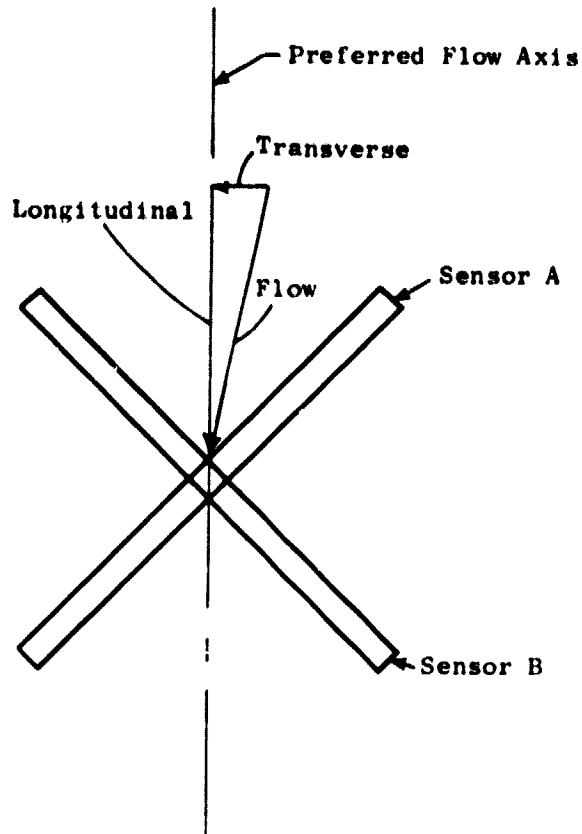


Figure 76. Velocity-Sensitive, Hot Film Probe.

ORIGINAL PAGE IS  
OF POOR QUALITY



$$\left\{ \begin{array}{l} v_{\text{long}} \propto \overline{A + B} \\ v_{\text{trans}} \propto \overline{A - B} \end{array} \right\}$$

Figure 77. Basic Operation of Hot Film Probe.

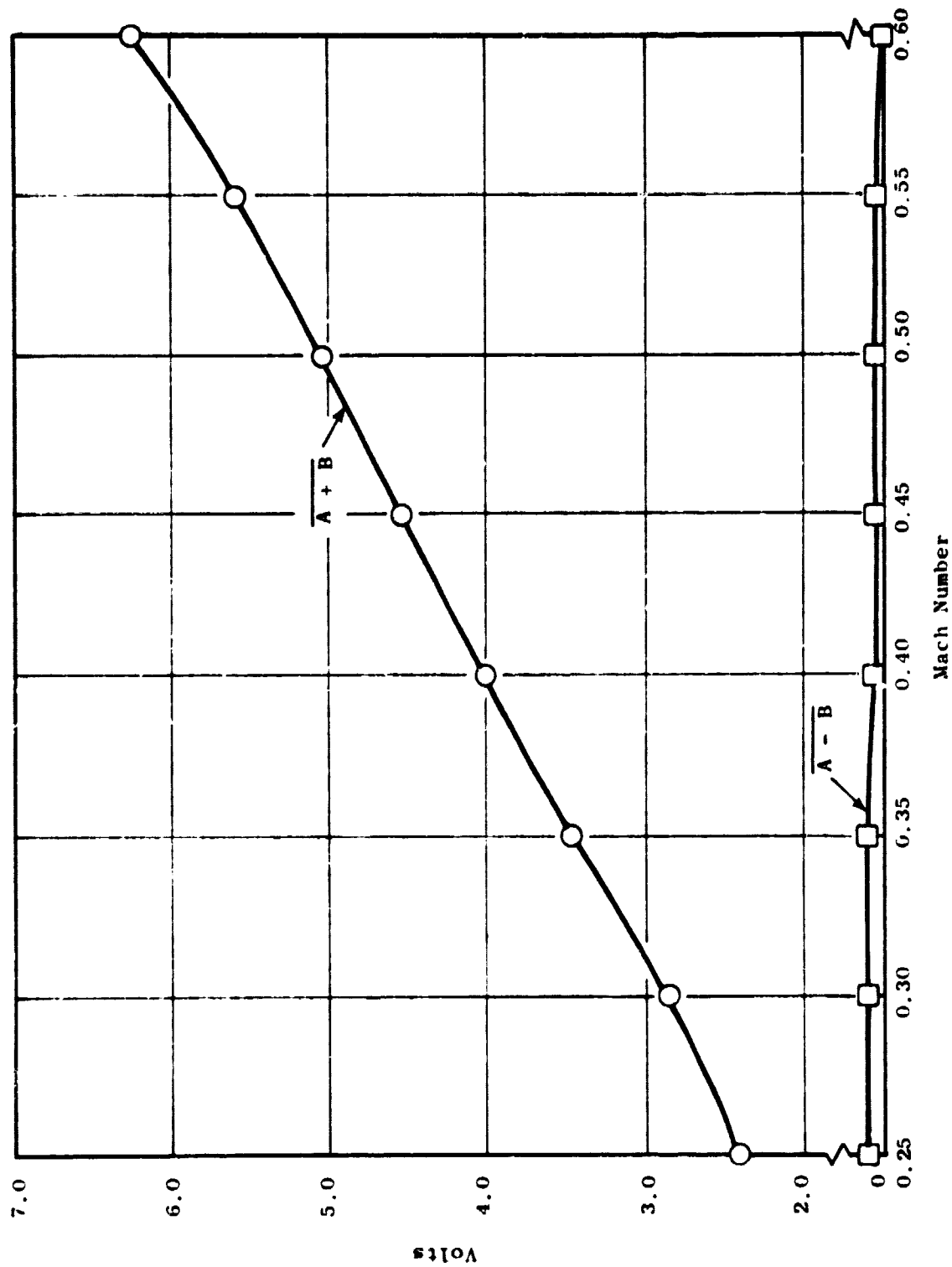
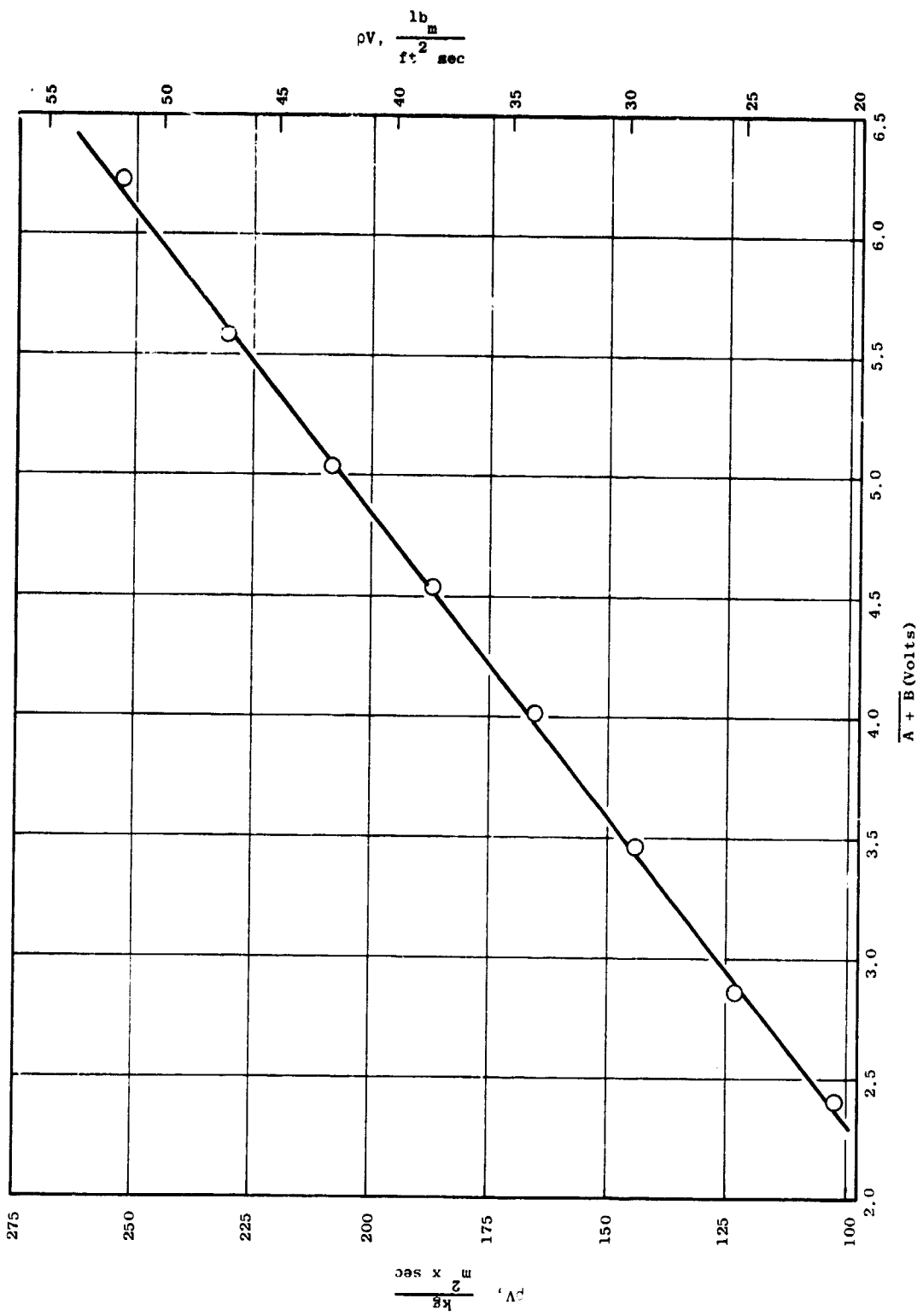


Figure 78. Hot Film Probe Calibration.



$$\rho V, \frac{lb}{ft^2 \cdot sec}$$

Figure 79. Hot Film Probe Calibration for Rotor 55 Wake Survey.

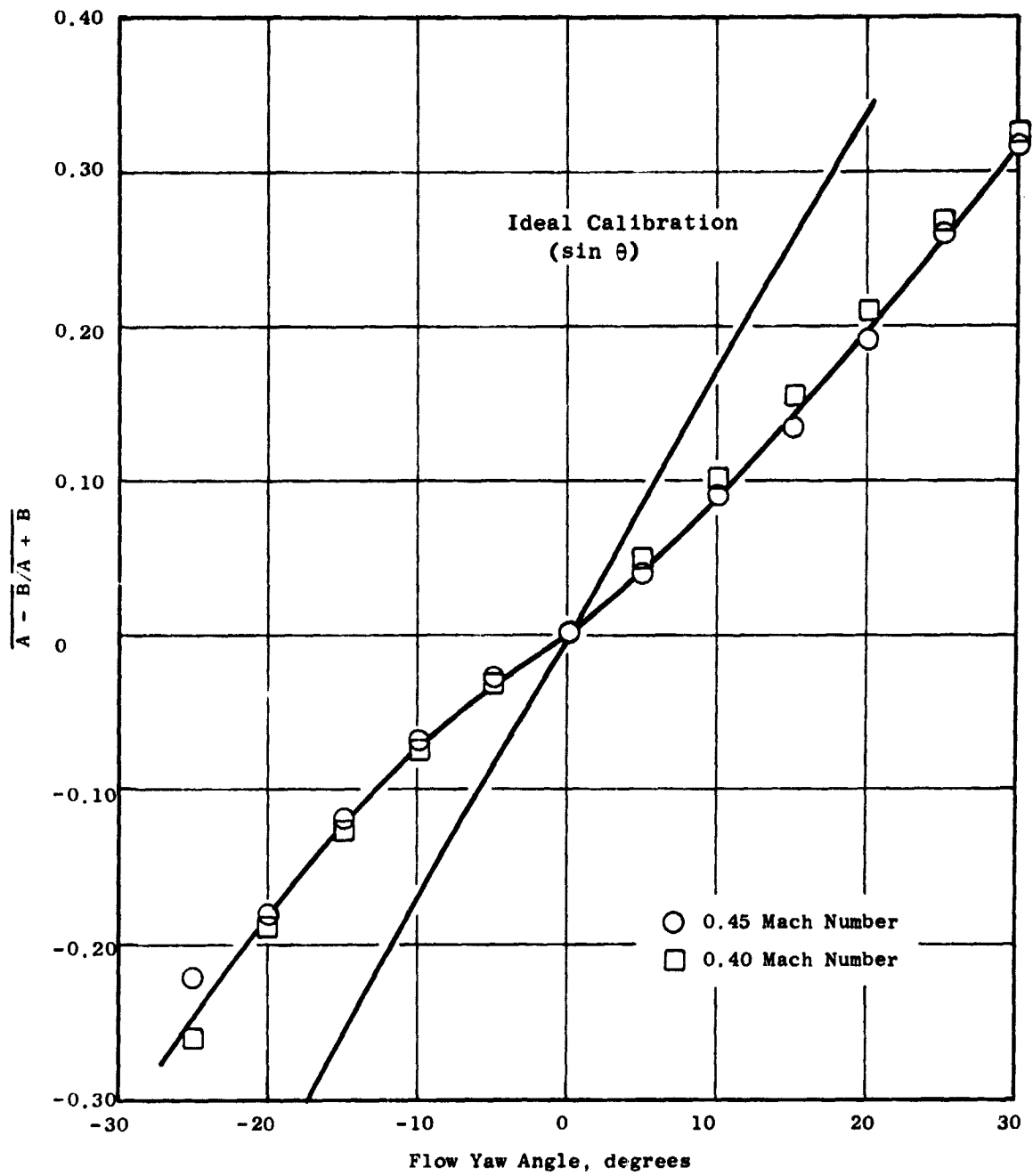


Figure 80. Directionality Calibration.

### 3. Data Acquisition

Wake survey data obtained on Rotor 55 was taken one rotor tip chord downstream of the rotor trailing edge. The probe was traversed to five radial stations as indicated in Figure 81. Both the outermost and innermost immersions were chosen at locations which were felt to lie outside of the hub and casing boundary layers. At design speed, the rotor exit absolute air angle averaged around 0.56 radians (32 degrees) from hub to tip. The hot film probe was thus set at this nominal 0.56 radians (32 degrees) angle from axial.

For the 100% speed points, this approach probably gave reasonably accurate results. Accuracy at the low speeds, however, may be somewhat less.

### 4. Data Filtering

Preliminary analysis of the Rotor 55 wake data revealed that although the blade wakes were clearly visible, the data were somewhat muddled by high-frequency, small-amplitude random fluctuations. When the data were plotted as waveforms, this high frequency signal made the data quite difficult to digitize. In order to overcome this problem, the data were passed through a low-pass filter with a sufficiently high cutoff frequency to prevent significant modification of the primary wake information but low enough to filter out the unwanted high frequency signals.

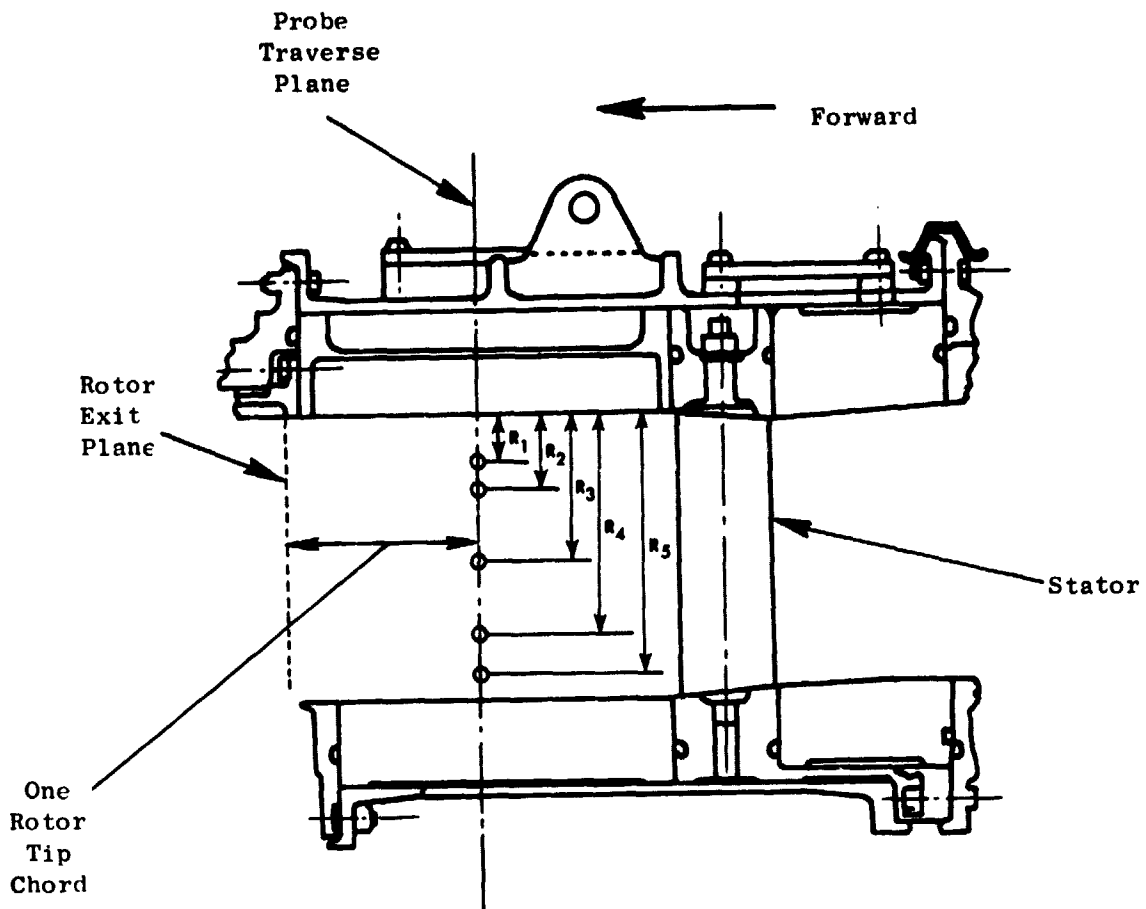
Figure 82 shows representative wave form plots of the data comparing the filtered and unfiltered signals. The 12,800 Hz filter successfully removed the high frequency random signal without seriously affecting the primary information.

Examination of the data in Figure 82 reveals a secondary, medium amplitude signal which is apparently quite regular. The frequency of this signal appears to be approximately four times BPF or  $\approx 8$  kHz. Further investigation of this situation revealed that at other fan speeds, the signal frequency does not change appreciably. This indicates the signal is not generated by the fan at all but is instead a resonance in the instrumentation system. Similar electronic "ring" has been noted sporadically during previous hot film data acquisition.

Existence of this electronic resonance has degraded the quality of the data somewhat. However, while the widths and shapes of the wakes have probably suffered some distortion, the wake signal amplitude appears to be affected only minimally.

### 5. Reduction to Velocity

The raw data consist of voltage measurements which are proportional to velocity in the absolute frame of reference. That is, the velocity vector marked  $C_2$  on the rotor exit velocity triangle of Figure 83 is measured. We are interested, however, in the rotor relative velocity  $W_2$  since the wakes are shed from the moving rotor.  $W_2$  is obtained by simply subtracting the wheel speed  $U$  vectorially from  $C_2$  as shown.



Immersion Point	Radius	
	cm	in.
R <sub>1</sub>	2.2	0.85
R <sub>2</sub>	3.6	1.40
R <sub>3</sub>	7.0	2.75
R <sub>4</sub>	10.4	4.10
R <sub>5</sub>	12.3	4.85

Figure 81. Rotor 55 Hot Film Probe Measurement Points.



ORIGINAL PAGE IS  
OF POOR QUALITY

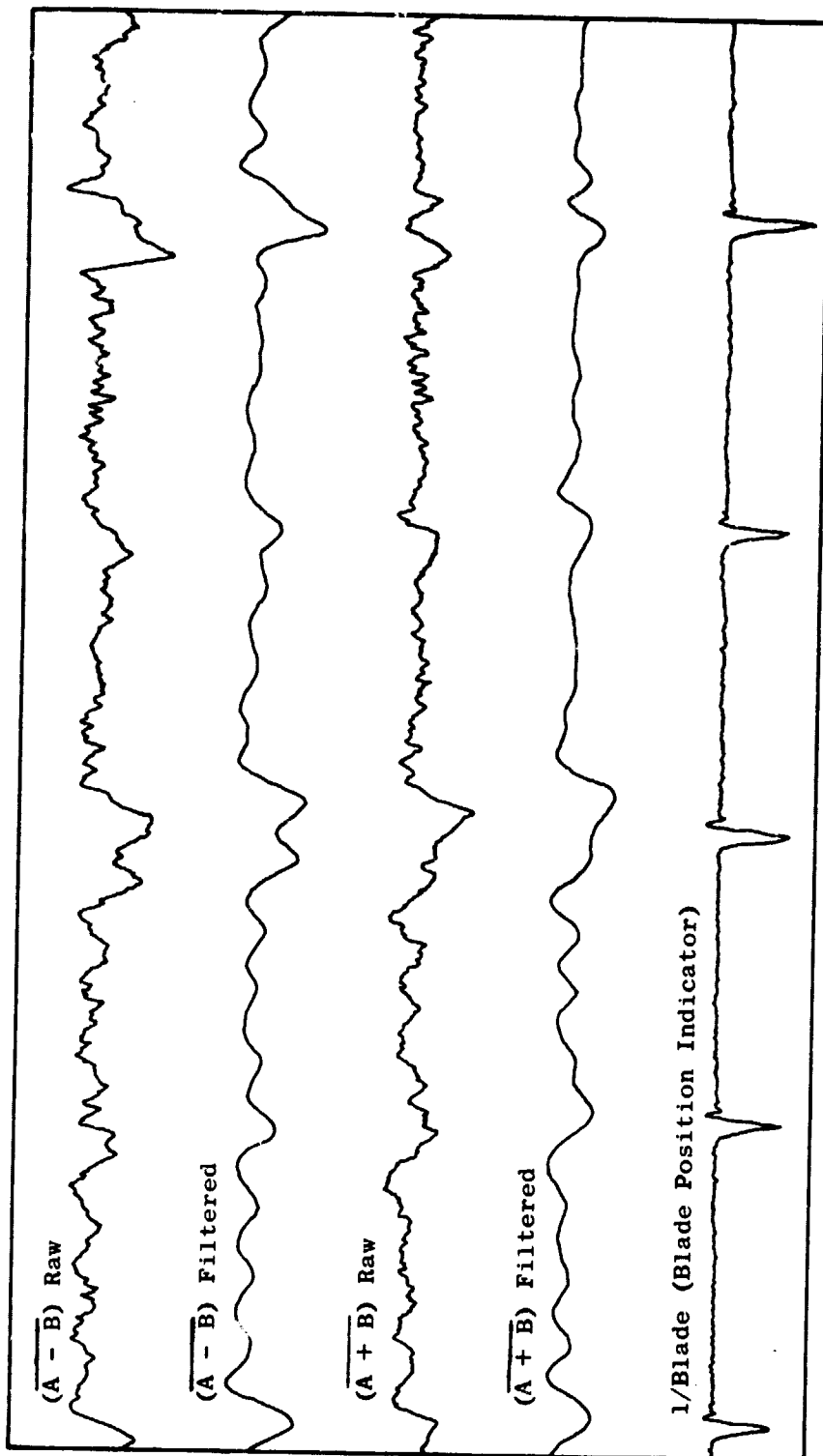


Figure 82. Hot Film Wake Data, Filtered at 12800 Hz.

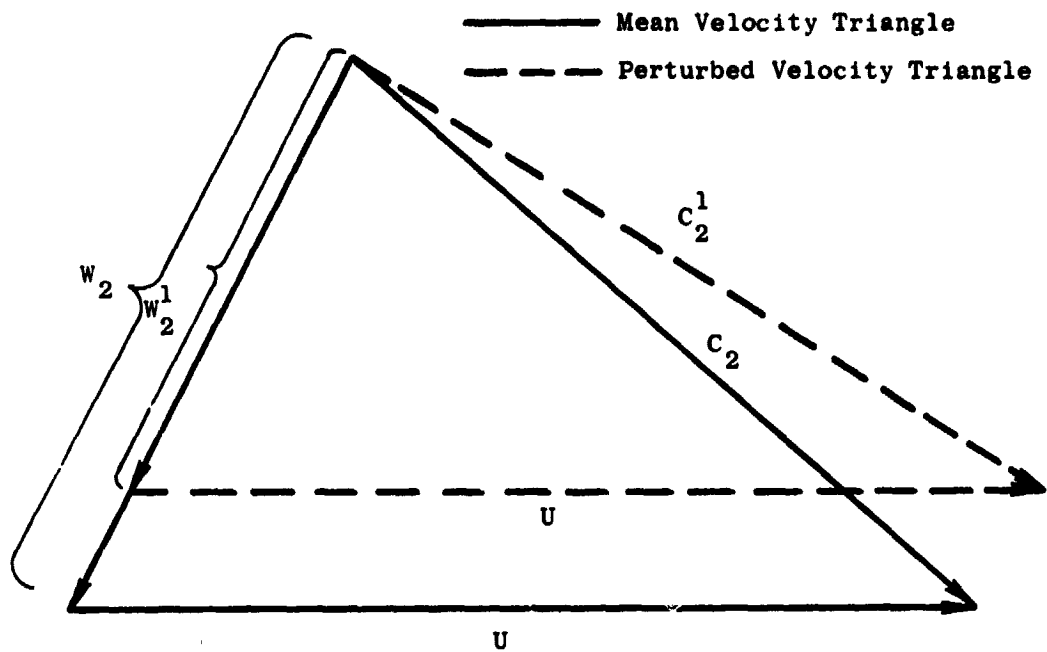


Figure 83. Typical Rotor Exit Velocity Triangle.

As the wake sweeps past the sensor, a simple magnitude decrease in rotor relative velocity  $W_2$  due to the wake velocity defect will be reflected as both a magnitude and angle change in  $C_2$  which is the velocity that the probe measures. Hence, two-dimensional data are required to resolve a one-dimensional change in  $W_2$ . The (A - B) and (A + B) probe voltages, along with their corresponding calibration curves provide all the necessary information. Rotor 55 hot film data were recorded both d.c. and a.c. coupled. The reason for this was that the a.c. coupled signal would give good resolution of the velocity fluctuations while the d.c. signals would provide the mean velocities to be added to the fluctuations. Unfortunately, the (A + B) d.c. levels were obscured by a noise problem in that channel of data acquisition equipment. Hence, no measured mean velocity was available for addition to the a.c. signal to resurrect the total velocity. This situation prevents defining the magnitude of  $C_2$  and, in turn, would not allow the determination of  $W_2$ . Therefore, a computed rather than measured mean value of  $C_2$  was used in conjunction with the experimental measurements. Figure 84 shows the design velocity triangle for Rotor 55 at the radial point corresponding to the tip-most data point. Using this computed velocity information, along with the probe orientation sketch of Figure 84, it was possible to obtain the following mean velocities:

$$\text{Longitudinal Velocity} = 180.3 \text{ m/sec (591.7 ft/sec)}$$

$$\text{Transverse Velocity} = 14.5 \text{ m/sec (47.6 ft/sec)}$$

Assuming then that the probe had measured these velocities, the probe voltages as obtained from the calibration curves would have been  $A - B = 0.747$  volts and  $A + B = 5.38$  volts.

These mean voltages were then added to the measured a.c. voltages to give the time history of the  $C_2$  velocity.

A time-sharing computer program was written to carry out the vector transformation from  $C_2$  to  $W_2$ . The raw hot film wave form data filtered at 12,800 Hz shown in Figure 85 were digitized and converted to rotor relative exit velocity  $W_2$ . Figure 86 shows the results of this calculation where  $W_2$  is plotted versus blade travel circumferentially. Notice that the electronic ringing signal is clearly visible in the Figure 85 plots. At times, the ringing signal amplitude approaches 50% of the wake amplitude, indicating that the ring could have an effect on the wake signals on these occasions.

## 6. Modulation

Disregarding, for now, the apparent electronic resonance, inspection of Figure 86 shows that the wake defect amplitudes vary from about 17% of the free stream value to 28%, which corresponds roughly to 30% amplitude modulation. This is a very substantial wake-to-wake amplitude modulation which, according to theory, could produce a significant level of broadband noise when impacting on the stator. It should be noted however that Hanson (Reference 10) assumed 100% maximum variation between wake amplitudes (amplitude

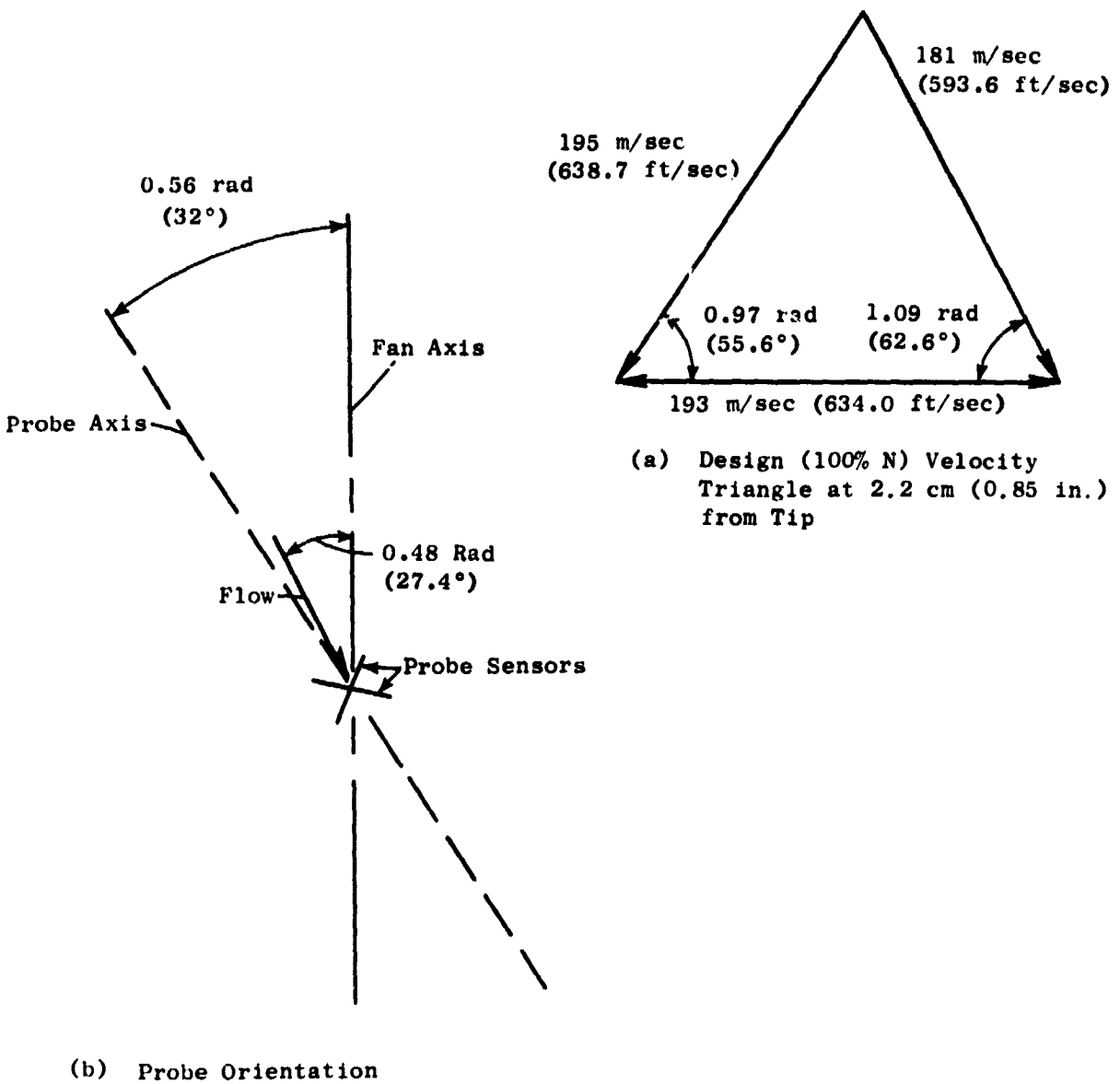


Figure 84. Design Velocity Triangle and Probe Orientation.

ORIGINAL PAGE IS  
OF POOR QUALITY

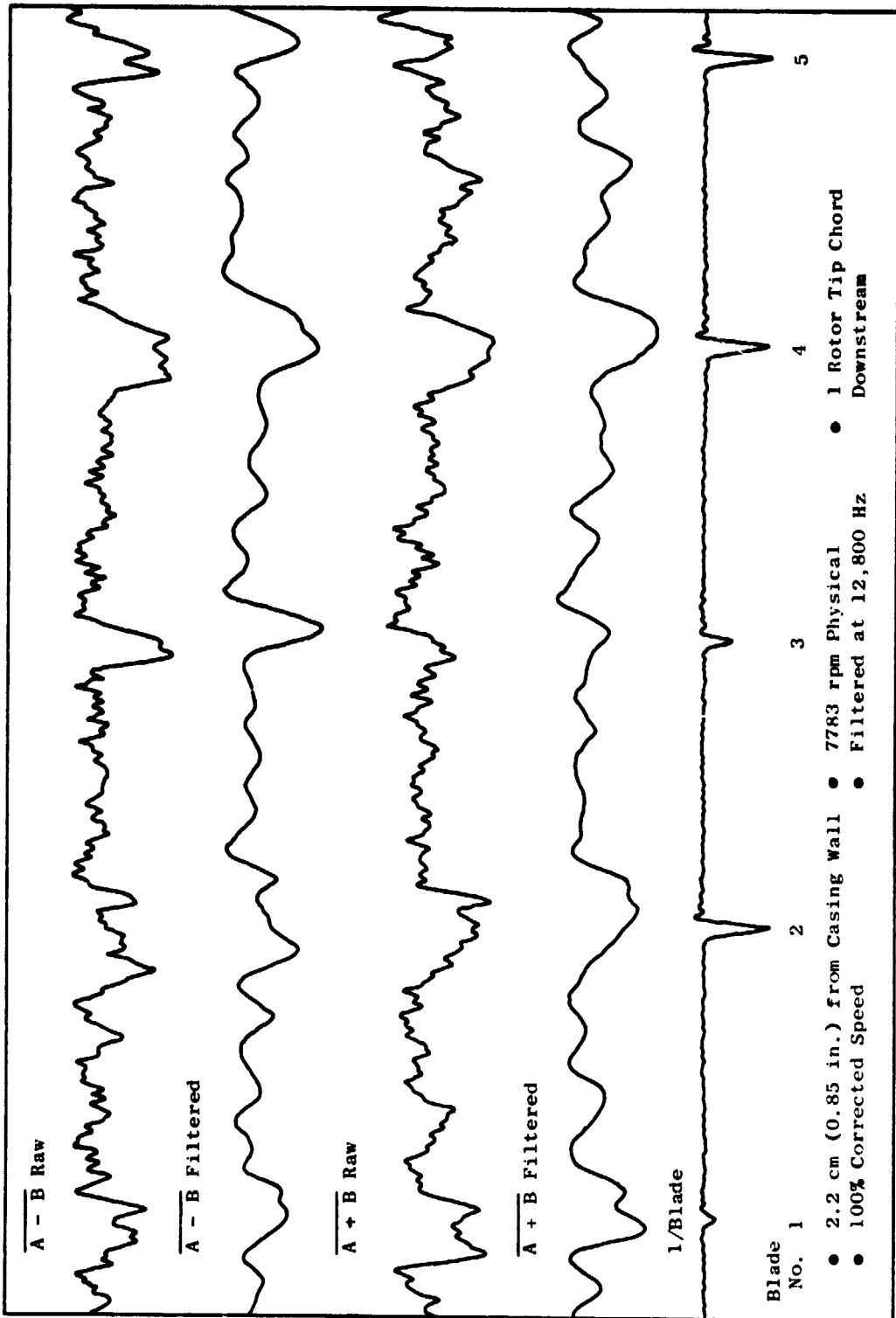


Figure 85(a). Rotor 55 Hot Film Wake Survey Data, Blades 1 through 5.

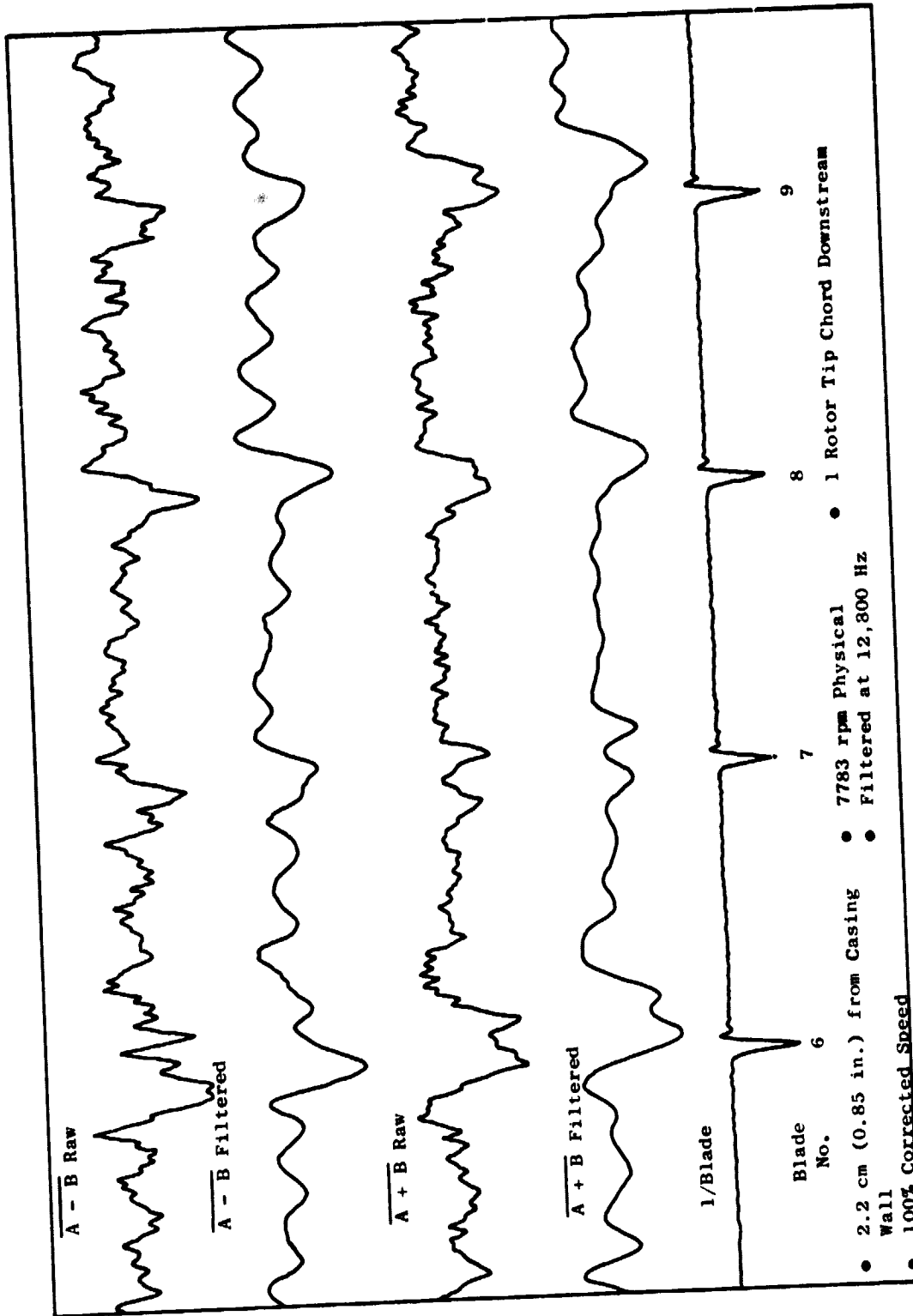


Figure 85(b). Rotor 55 Hot Film Wake Survey Data, Blades 6 through 9.

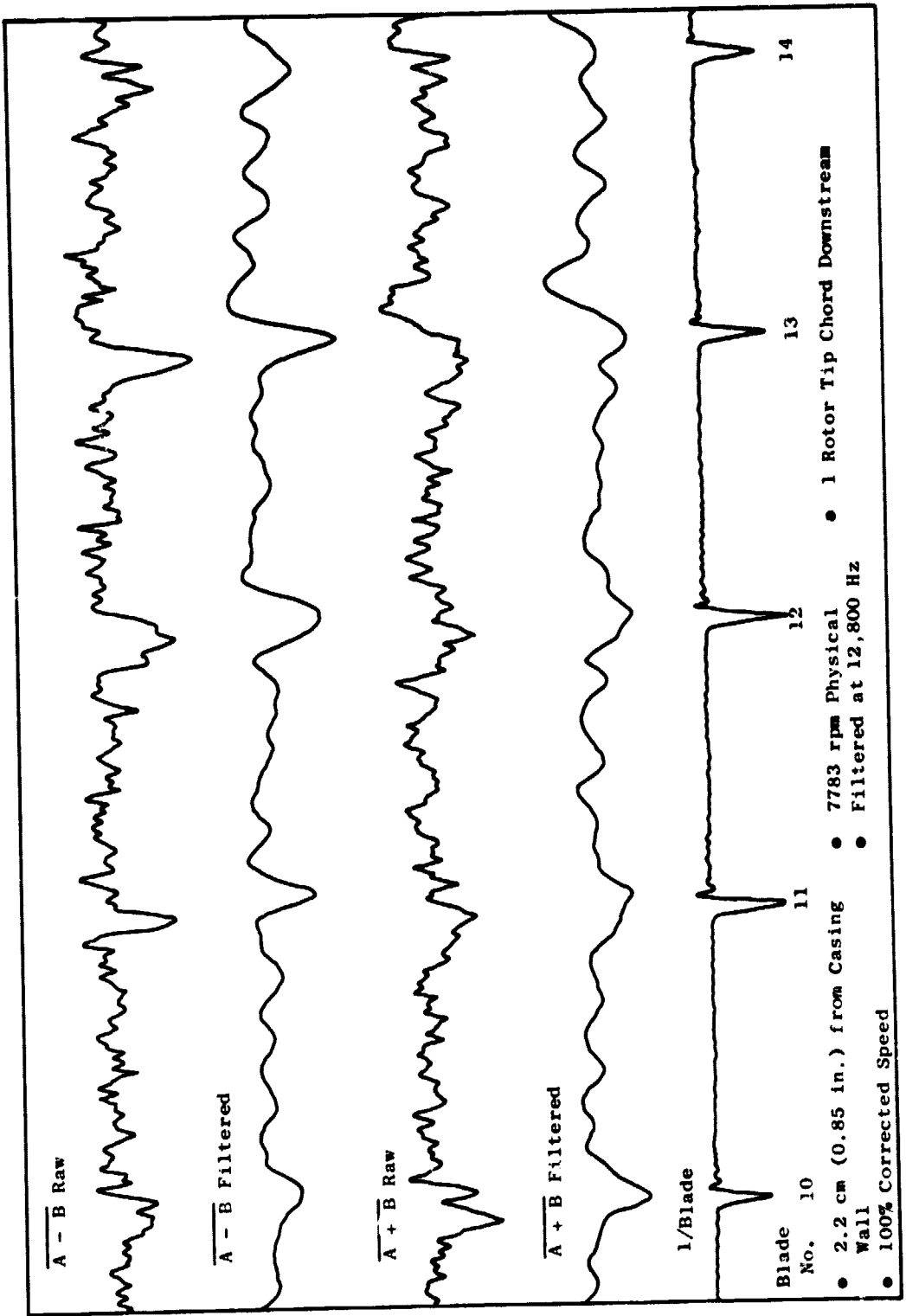
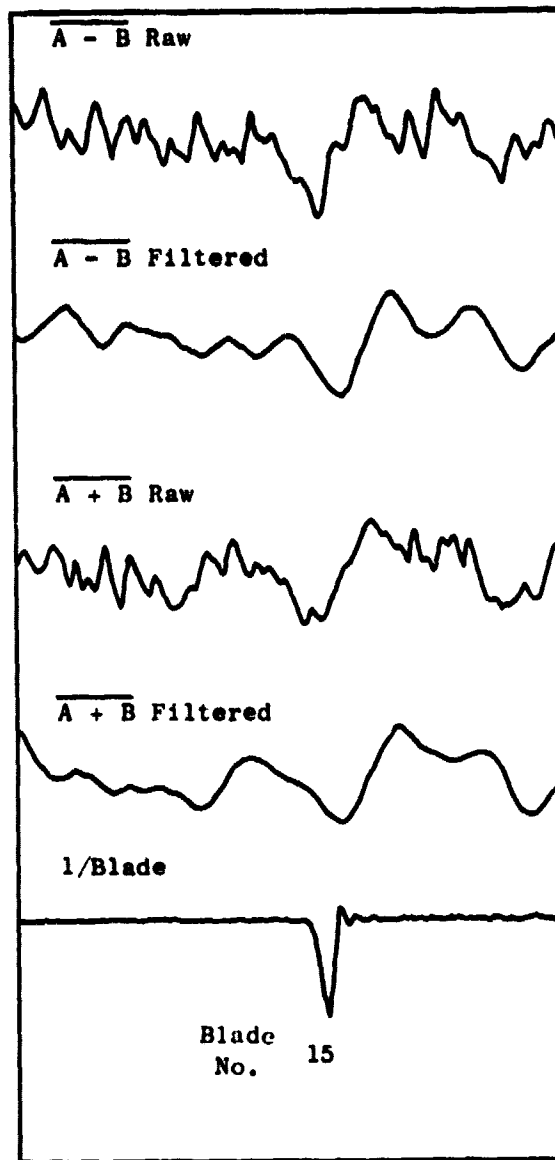


Figure 85(c). Rotor 55 Hot Film Wake Survey Data, Blades 10 through 14.



- 2.2 cm (0.85 in.) from Casing Wall
- 100% Corrected Speed
- 7783 rpm Physical
- Filtered at 12,800 Hz
- 1 Rotor Tip Chord Downstream

Figure 85(d). Rotor 55 Hot Film Wake Survey Data, Blade 15. .



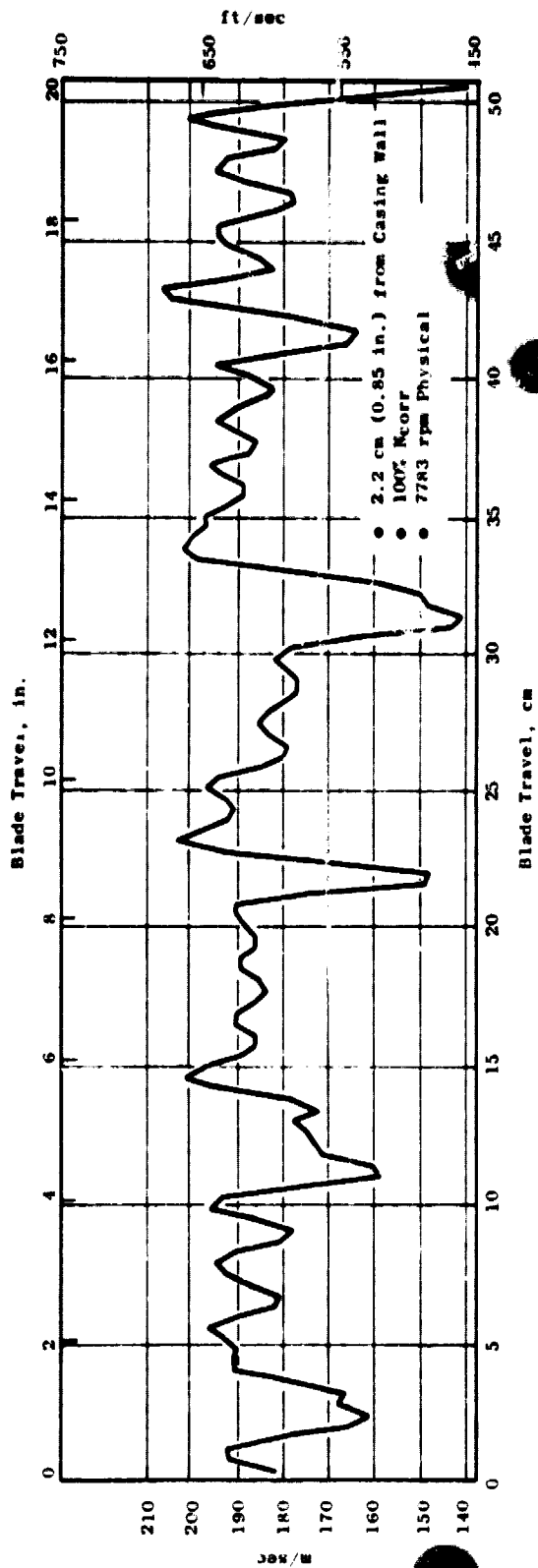


Figure 86(a). Rotor 55 Wake Trace.

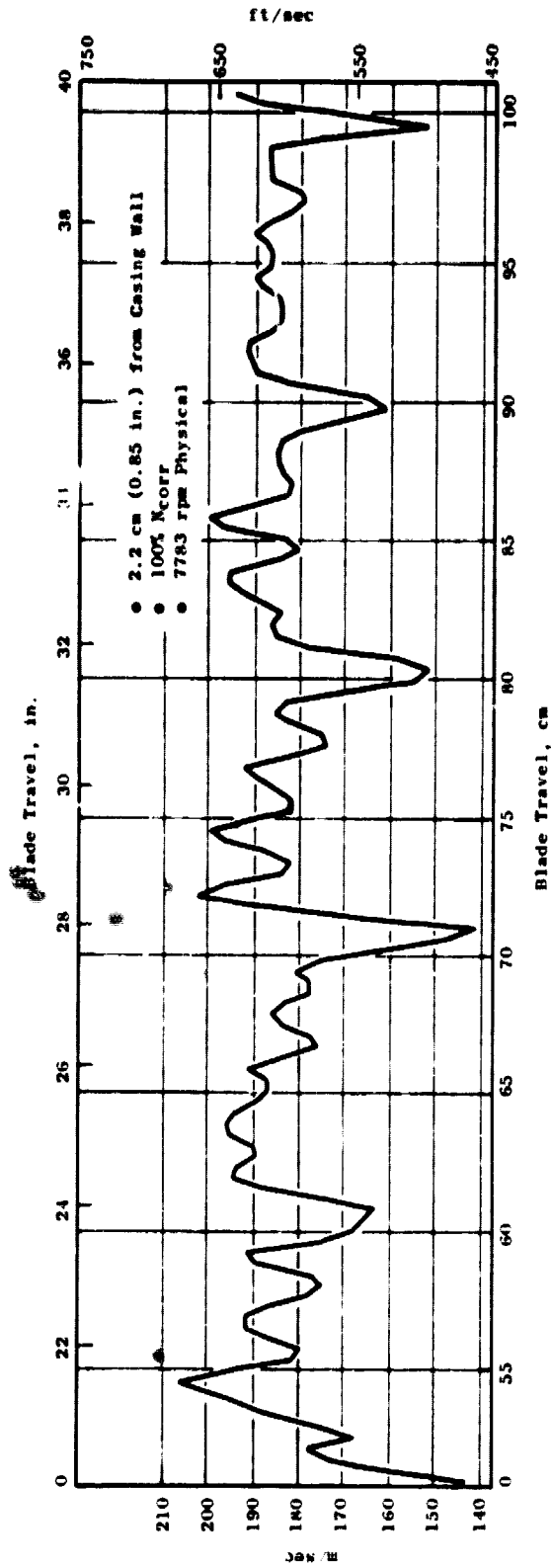


Figure 86(b). Rotor 55 Wake Trace.

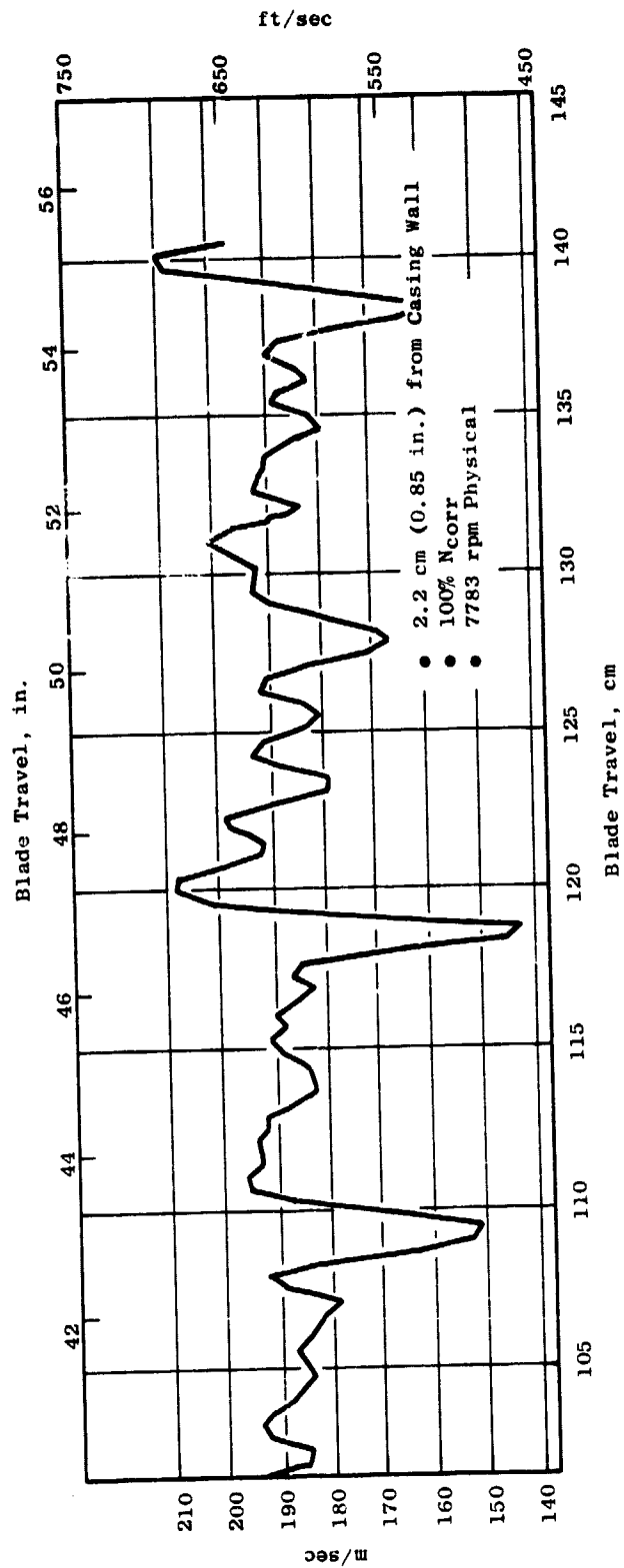


Figure 86(c). Rotor 55 Wake Trace.

modulation) in his analysis. Maximum wake spacing variation (spacing modulation) appears to be on the order of 0 to 5% and should be fairly insignificant in the production of broadband noise. Hanson (Reference 10) used 3% spacing modulation in his study.

Wake shape and width modulation are two variables which are not taken into account in some present theories. The hot film data, however, indicate that there are fairly large modulations in these two quantities. It is believed that the wake width modulations would also have an effect on broadband noise production; however, the quantitative impact remains to be determined. In any case the width modulation would most certainly affect the discrete frequency noise, as analytic experience has shown that narrow wakes cause higher tones and slower dropoff in the harmonics as compared to wide wakes.

Presently, there are two different wake models used in General Electric analytical prediction models. One, the Silverstein model in Reference 9 was developed from data taken on isolated airfoils while the other, Mugridge's, in Reference 16, was based on a combination of isolated airfoil and cascade data. Neither, however, had the benefit of rotor data such as presented above.

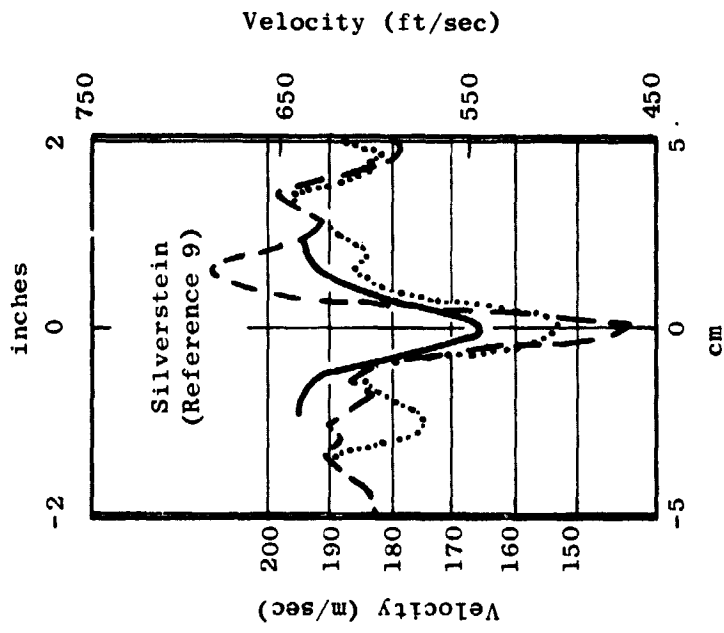
Shown in Figure 87 are the Silverstein and Mugridge model predictions for the Rotor 55 wakes at the measuring point of Figure 87. Note that, at this location, the two predictions differ by only small amounts, with Silverstein being slightly wider and weaker than Mugridge. These differences do have important effects on noise predictions. If the model wakes of Figure 87 are compared with the experimental ones of Figure 86, it can be shown that on the average, the experimental wakes are wider and stronger by a substantial amount than either of the mathematical models. Errors of this magnitude in our analytical wake models would definitely have an important effect on our noise predictions. The "ringing" problem discussed earlier had a definite but unknown effect on the accuracy of the data, hence the absolute difference between the theoretical and experimental wakes cannot be determined.

## 7. Summary and Conclusions

A semiautomated computer reduction technique for hot film probe wake survey data has been developed and demonstrated. One set of Rotor 55 wake data has been reduced and shown to contain large amounts of wake amplitude modulation and only small period modulation, as expected. Substantial wake shape and width modulation were also present in the data, which could have large effects on broadband viscous wake interaction noise generation. Comparison of the current viscous wake models with the reduced Rotor 55 data showed large differences in width shape and velocity-defect amplitude.

Consideration of the results shown here points out the potential benefit to be gained from this type of wake data. New, more realistic wake models can be developed from velocity measurements on a rotor, rather than pressure measurements on a cascade as done almost exclusively in the past. Problems with presently available mathematical wake models are well known. The above-

..... Rotor 55 Wake Trace  
 - - - Rotor 55 Wake Trace  
 — Silverstein Math. Model



..... Rotor 55 Wake Trace  
 - - - Rotor 55 Wake Trace  
 — Mugridge Math. Model

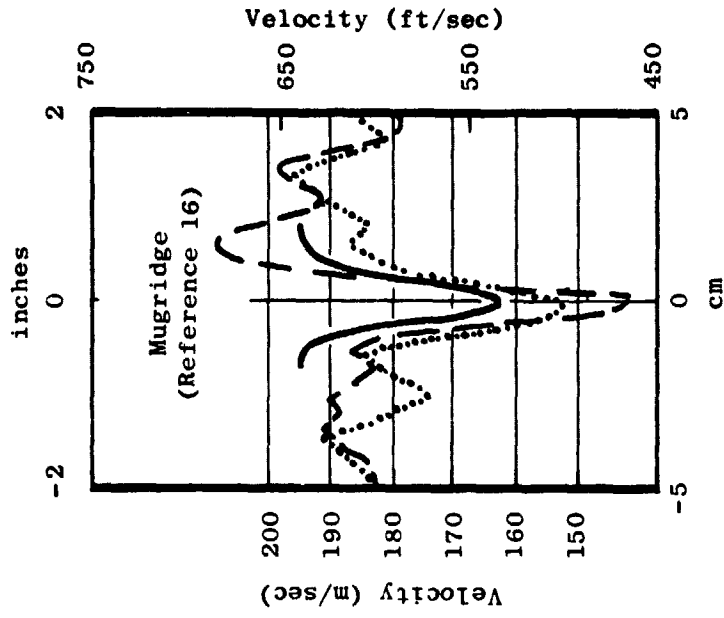


Figure 87. Comparison of Experimental and Mathematical Wake Shapes.

demonstrated technique provides the means to substantially improve these models and should be pursued further.

In addition to providing a means for developing a better mathematical model for the mean wake, this new type of data also provides an excellent picture of the time history of wake modulations, which are important to fan broadband noise generation. For the Rotor 55 case, the existence of these variations from wake to wake was clearly demonstrated. Moreover, the amplitude modulation appeared to be significantly less than that used in Reference 9.

## SECTION VI

### CONCLUSIONS

1. For a range of vane-blade ratios from 1.67 to 2.07, second harmonic tone propagation in the aft duct tended to minimize at a vane-blade ratio of 1.87 at a rotor-stator spacing of 0.5. No significant differences in second harmonic noise level were observed at 1.5 chord spacing.
2. Analysis of the rotor-stator spacing results indicated that a second noise source (most likely rotor-turbulence noise) was controlling at spacings of 1.5 to 2.0 rotor-tip chords. Wide spacings of 1.5 to 2.0 rotor-tip chords offer potential benefit in actual flight where lower rotor-turbulence noise levels are expected.
3. No significant change in fan broadband noise was observed by lowering the Mach number through the vane row; however, any changes may be masked by rotor-turbulence noise. Further testing on low-Mach vanes should be considered, but should be conducted in a facility where the levels and eddy sizes of inlet turbulence are controlled and monitored.
4. Tests of acoustic treatment panels with various porosities and backing depths showed that to increase suppression, variable-depth treatment panels should be used with porosities that optimize the acoustic resistance for each panel. Variable depth treatment configurations with either constant or mixed porosity faceplate achieved suppression at frequencies higher than the peak frequency that consistently exceeded predictions based upon the best previous designs of the General Electric Company.
5. Tests of 12 percent porosity acoustic panels with  $H/\lambda_0 = 1.24$ , showed that the measured suppression loss due to treatment area blockage did not vary linearly with L/H (actual).
6. The splitter simulation configuration with variable-depth treatment on the outer wall and constant depth treatment on the inner wall had better peak suppression than the configuration with variable-depth treatment on both sides with somewhat less suppression bandwidth. The splitter simulation configuration gave wider suppression bandwidth than a configuration with constant depth treatment on both walls.
7. Rotor-OGV treatment gives suppression (2 to 5 dB tone and 0.5 to 3 broadband) which is observed both with and without fan exhaust duct treatment.

8. Suppression was found to be independent of treatment orientation for variable-depth configurations with 12 percent faceplate porosity. The thin/thick treatment gives a somewhat better suppression bandwidth than the thick/thin for the 27 percent porosity configuration - primarily at lower fan speeds.
9. Slant cell treatment can be tuned to a lower frequency, relative to a straight cell resonator geometry for a given treatment thickness.
10. An increase in average aft duct Mach number from 0.48 to 0.54 did not result in any significant degradation of suppression. This indicates that no flow noise floor was reached.
11. An acoustic discrimination technique using the sound separation probe can separate sound from turbulence in probe data.
12. Hot film probe measurements between the fan rotor and stators showed that substantial modulation of blade wake shape, width, and strength exist on the Rotor 55 fan blades. A viable method utilizing hot film measurements between the rotor and stator has been demonstrated for obtaining velocity data behind a rotor, with which an improved analytical fan blade wake model could be developed.
13. Exhaust duct suppression predicted by means of duct-mode acoustic propagation theory for several pertinent test configurations which included radial modal measurements, is shown to correspond qualitatively with the measured effectiveness; rank-ordering corresponded well enough to encourage further intensive effort to develop the analytical method.



SECTION VII  
NOMENCLATURE

<u>Symbol or Abbreviation</u>	<u>Definition</u>	<u>Units</u>
$A_j$	Modal coefficient	-
BPF	Blade passing frequency	Hz
$B_j(\omega)$	Modal coefficient	-
C	Absolute velocity	m/sec (ft/sec)
c	Speed of sound	m/sec (ft/sec)
$C_j$	Eigenfunction coefficients	-
$D_j$	Eigenfunction coefficients	-
d	Hole diameter	cm (in.)
H	Duct height	m (ft)
i	$\sqrt{-1}$	-
j	Modal index	-
l	Cavity depth of honeycomb	cm (in.)
L	Duct length	m (ft)
m	Spinning mode index	-
M	Mach number	-
$M_t$	Tip Mach number	-
N	Fan speed	rpm
OGV	Outlet guide vane	-
PNL	Perceived noise level	PNdB
PWL	Sound power level re: $10^{-13}$ watts	dB
$p(x,t)$	Acoustic pressure	$N/m^2$ (psia)

<u>Symbol or Abbreviation</u>	<u>Definition</u>	<u>Units</u>
P	Pressure	N/m <sup>2</sup> (psia)
P <sub>1</sub>	Turbulence pressure	N/m <sup>2</sup> (psia)
P <sub>2</sub>	Pressure from downstream moving sound wave	N/m <sup>2</sup> (psia)
P <sub>3</sub>	Pressure from upstream moving sound wave	N/m <sup>2</sup> (psia)
P <sub>p</sub> (x <sub>p</sub> , ω)	Probe microphone pressure signal	N/m <sup>2</sup> (psia)
P <sub>r</sub> (x <sub>r</sub> , ω)	Reference microphone pressure signal	N/m <sup>2</sup> (psia)
S <sub>rp</sub> (ω, x <sub>r</sub> , x <sub>p</sub> )	Cross-spectral density	$\frac{(N/m^2)^2}{\text{rad/sec}} \left[ \frac{(\text{psia})^2}{\text{rad/sec}} \right]$
SPL	Sound pressure level re 0.0002 microbars	dB
x	Panel depth	cm (in.)
t	Time	sec
t'	Effective thickness of faceplate	cm (in.)
U	Wheel speed	m/sec (ft/sec)
V	Velocity	m/sec (ft/sec)
W	Rotor relative velocity	m/sec (ft/sec)
X	Duct transverse length	m (ft)
X	Acoustic reactance	rayls
X <sub>p</sub>	Probe microphone position	m (ft)
X <sub>r</sub>	Reference microphone position	m (ft)
α	Mach number constant	-
γ <sub>j</sub>	Duct eigenvalue	-
η	Duct height divided by wavelength	-
θ	Relative absolute temperature	-
θ	Yaw Angle	rad (degrees)

<u>Symbol or Abbreviation</u>	<u>Definition</u>	<u>Units</u>
$\lambda$	Wavelength of sound	m (ft)
$\lambda_0$	Tuning frequency wavelength	m (ft)
$\pi$	3.14159	-
$\rho$	Density	kg/m <sup>3</sup> (lbm/ft)
$\sigma$	Faceplate porosity	-
$\phi_j (x)$	Characteristic duct pressure mode	-
$\phi$	Cross correlation	-
$\omega$	Circular frequency	rad/sec
$( )^*$	Denotes complex conjugate	-
$\overline{(\ )}$	Denotes Fourier Time Transform	-

## SECTION VIII

### REFERENCES

1. Adamson, A.P., "Quiet Clean Short-Haul Experimental Engine (QCSEE) Design Rationale," Society of Automotive Engineers, Air Transportation Meeting, Hartford, Conn., May 6-8, 1975, Paper No. 750605.
2. Anon., "Quiet Clean Short-Haul Experimental Engine (QCSEE) Aerodynamic and Mechanical Design of the QCSEE Under-the-Wing Fan," NASA Contractor Report 134847, March 1976.
3. Lewis, Jr., G.W., and Tysl, E.R., "Overall and Blade-Element Performance of a 1.20 Pressure Ratio Fan Stage at Design Blade Setting Angle," NASA TM X-3101, September 1974.
4. Glaser, F.W., Wazyniak, J.A., Friedman, R., "Noise Data from Tests of a 1.83 m (6 ft) Diameter Variable Pitch, 1.2 Pressure Ratio Fan (QF9)," NASA TM X-3181, March 1975.
5. Stimpert, D.L., McFalls, R.A., "Demonstration of Short-Haul Aircraft Aft Noise Reduction Techniques on a Twenty Inch (50.8 cm) Diameter Fan." 3 Volumes, NASA Contractor Report Numbers 134849, 134850 and 134851, April 1975.
6. Mani, R., "Discrete Frequency Noise Generation from an Axial Flow Fan Blade Row," Paper 69-GE-12, ASME, presented at Applied Mechanics and Fluids Engineering Conference, June 16-18, 1969.
7. Cumpsty, N.A. and Lowrie, B.W., "The Cause of Tone Generation by Aero-Engines at High Subsonic Tip Speeds and the Effect of Forward Speed," ASME Paper 73-WA/GT-4, November 1973.
8. Hanson, D.B., "Spectrum of Rotor Noise Caused by Atmospheric Turbulence," J. Acoust. Soc., Am. 56, 1, July 1974.
9. Silverstein, A., Katzoff, S., and Bullivant, W.K., "Downwash and Wake Flow Behind Plain and Flapped Airfoils," NACA Tech Report No. 651 (1939).
10. Hanson, D.B., "A Unified Analysis of Fan Stator Noise," ASA Paper, 12-1-1972. J. Acoustic Soc., Am. Volume 54, Number 6, 1976.
11. Anon., "Cross-Correlation and Cross-Spectrum Analysis," Bruel & Kjaer Technical Review Number 4, 1970.
12. Motsinger, R.E., Kraft, R.E., and Zwick, J.W., "Design of Optimum Acoustic Treatment for Rectangular Ducts with Flow," ASME Paper 76-GT-113, March 1976.
13. Kraft, R.E., Paas, J.E., and Clark, L.R., "Effects of Multi-Element Acoustic Treatment on Compressor Inlet Noise," AIAA Paper No. 76-515, July 1976.

14. Kraft, R.E. and Motsinger, R.E., "Practical Considerations for the Design of Two-Element Duct Liner Noise Suppressors," AIAA Paper No. 76-517, July 1976.
15. Yurkovich, R., "Attenuation of Acoustic Modes in Circular and Annular Ducts," AIAA Paper Number 74-552, June 1974.
16. Mugridge, B.D., and Norfey, C.L., "Sources of Noise in Axial Flow Fans," Paper presented at 31st Meeting of Acoustical Society of America, April 23, 1971, J. Acoust. Soc., Am. Volume 51, Number 5, 1972.